

*This is a manuscript of the book sent to the  
Nova Science Publishers*

**(Submitted 9 May 2014; published 20 August 2014)**

# **High-Power Ultrasound Phased Arrays for Medical Applications**

**LEONID R. GAVRILOV  
JEFFREY W. HAND**

## Contents

<b>Introduction</b>		<b>4</b>
<b>Chapter 1</b>	<b>Linear Phased Arrays</b>	<b>6</b>
	1.1. Advantages and Shortcomings of Linear Phased Arrays; Elimination of Grating Lobes	6
	1.2. Design and Experimental Evaluation of an Endocavitary Linear Phased Array	14
	1.3. Other Constructions of Powerful Linear Phased Arrays	19
<b>Chapter 2</b>	<b>Two-Dimensional Phased Arrays with a Regular Distribution of Elements</b>	<b>22</b>
	2.1. General Comments	22
	2.2. Designs	23
	2.3. Possibilities to Generate and Steer Simultaneous Multiple Foci	30
	2.4. Research	32
<b>Chapter 3</b>	<b>Two-Dimensional Phased Arrays with a Random Distribution of Elements</b>	<b>34</b>
	3.1. The Basis of the Method	34
	3.2. Methods of Calculating of Ultrasound Fields Generated by the Arrays	35
	3.3. Generation and Steering of a Single Focus, Data from Modeling	39
	3.4. Generation and Steering of Multiple Foci, Data from Modeling	48
	3.5. Generation of Focal Regions of Complex Configurations	56
	3.6. Ability to Focus Ultrasound Energy behind Acoustic Obstacles	59
	3.7. Real Constructions of 2D- Random Powerful Phased Arrays and Methods of Measuring Their Acoustic Parameters	65
	3.8. Studies of Randomized Arrays	72

<b>Chapter 4 Potential Medical Applications of Powerful Phased Arrays</b>	<b>80</b>
4.1. Surgery of Deep Brain Structures by Sonication through the Intact Skull	80
4.2. Neurological Disorders	86
4.3. Prostate	91
4.4. Tissue Ablation in the Presence of Ribs	93
4.5. Surgery	98
4.6. Hyperthermia	99
4.7. Cardiac Ablation	100
4.8. Stimulation of Neural Structures	102
4.9. Uterine Fibroids	105
4.10. Other Applications	106
<b>Concluding Comments</b>	<b>109</b>
<b>References</b>	<b>111</b>

## Introduction

Over the past 7 decades there have been many developments in medical applications of ultrasound. Diagnostic techniques which typically use frequencies in the range from 1 to 50 MHz are ubiquitous in today's healthcare with on the order of  $10^9$  imaging procedures carried out globally per year. Less well known, but attracting considerable research attention and ever increasing clinical interest over the past 3 decades, are the therapeutic applications of ultrasound referred to as hyperthermia and surgery (also known as high intensity focused ultrasound – HIFU). Hyperthermia (or thermal therapy or thermotherapy), in which body tissue is exposed to temperatures of around 41 to 45 °C, is used as an adjuvant to radiotherapy or chemotherapy in the treatment of some cancers. In contrast, HIFU involves the use of focused ultrasound beams to create acoustic intensities in excess of  $1000 \text{ W cm}^{-2}$  and temperatures greater than 50 °C in the focal region(s) resulting in tissue ablation through thermal and cavitation processes. These therapeutic applications typically use ultrasound at a frequency in the range from 0.5 to 3 MHz where the acoustic properties of tissues are such that penetration, transfer of energy to the tissue and the wavelength are such that the desired acoustic intensity and temperature can be achieved locally at depth in the body to make non-invasive organ targeted therapy a reality. At much lower intensities and durations than are required for ablation, more subtle biological effects such as stimulation of neural structures, changes in membrane permeability, and release of drugs from liposomes are possible. In 2011 Time magazine heralded focused ultrasound therapy as “one of the 50 most inspired ideas, innovations and revolutions of 2011” and commented that “once the medical community understands that focused ultrasound can destroy tumours, dissolve clots, relieve pain and deliver medicines to precise targets without damaging incisions, this remarkable technology will become a standard of care for many of today's most deadly and debilitating conditions.”

The benefit of adding hyperthermia to radiation therapy and/or chemotherapy for the treatment of recurrent breast cancer, melanoma, head and neck cancer, and other sites of locally advanced or recurrent cancers has been demonstrated in clinical trials. HIFU techniques have been used not only in the treatment of cancers of the prostate, breast, pancreas, kidney, liver and uterus but also in the treatment of uterine fibroids. Evaluations of such approaches are being undertaken worldwide. In China alone more than 50,000 treatments have been carried out. Examples of other applications of focused ultrasound include stopping bleeding, the targeted delivery of drugs to predetermined parts of the body, liposuction (i.e. the removal of unwanted fat), neurosurgery to target specific brain tissues by sonication through the intact skull, ablation of tissues located behind acoustic obstacles such as the rib cage, and in cardiology.

Until recently the main tools used in these medical applications have been single focusing transducers with a surface shaped as part of a spherical shell. Attractive features of these transducers are the relative simplicity of their design and practical application. However, a significant drawback of these systems is that they are able to focus ultrasound energy only at a fixed focal distance. Since the volume of the focal region of the transducer is usually much smaller than the volume of targeted tissue, a means for mechanical movement of the transducer relative the targeted volume such as an automated positioning system must be provided. However, practical experience shows that using a single element focused transducer to destroy a  $2 \text{ cm}^3$  volume of tissue takes approximately 1 hour since time must be allowed for cooling of tissue in the path of the ultrasound propagation; to destroy a relatively small clinically relevant volume of, say,  $10 \text{ cm}^3$ , requires several hours of sonication. Whilst these relatively simple single transducer systems continue to be used, it is clear that if the dimensions of the site for ultrasonic treatment are sufficiently large, the use of mechanically scanned focused transducers with a fixed focal length is not always the best choice. A much more promising and flexible solution to such problems is to use a phased array capable of electronically controlled dynamic

focusing. Such systems can not only steer a single focus without movement of an array itself, but also generate several foci simultaneously and create focal regions with complex configurations.

There are two kinds of arrays for ultrasound surgery and therapy: extracorporeal arrays positioned outside a patient's body and intracavitary arrays that can be inserted into natural body cavities such as the rectum. The former are not restricted in size and typically have dimensions on the order of 10 cm or more. Such arrays consist of a 2-dimensional distribution of discrete radiating elements. The latter type of array are restricted in size such that transverse dimensions are about 25 mm or less; they consist of a 1 dimensional distribution of discrete elements and are referred to as linear arrays. Both types of array must be capable of delivering considerable acoustic power.

The main content of this book addresses the design, research and development, and medical applications of linear and two-dimensional high-intensity focused ultrasound phased arrays. In particular, sparse phased arrays with a random distribution of elements are discussed, as well as methods for calculating ultrasound fields generated by different phased arrays including the generation of multiple simultaneous foci and focal regions with complex geometrical shapes.

The book is aimed at a wide circle of readers including specialists in the field of physical and medical acoustics who are interested in the study of the biological effects of ultrasound and the search for new physical methods to use in various fields of physiology and medicine, engineers who are interested in developing new devices and systems for medical applications, physicians interested in applying these devices to various fields of clinical and experimental medicine, and physiologists who use various physical methods to study the origin, development and modification of different functions. The information provided in this book will also be of interest to undergraduate and graduate students of all of these specialties.

*Dr. Leonid R. Gavrilov,*  
Principal Research Scientist,  
Acoustics Institute,  
Moscow, 117036, Russia  
[gavrilov@akin.ru](mailto:gavrilov@akin.ru)

*Prof. Jeffrey W. Hand*  
Professor of Imaging Physics  
Division of Imaging Sciences and Biomedical Engineering  
King's College London  
St Thomas' Hospital  
London SE1 7EH, UK  
[jeffrey.hand@kcl.ac.uk](mailto:jeffrey.hand@kcl.ac.uk)

## Chapter I

### Linear Phased Arrays

This chapter considers practical aspects of the use of planar linear ultrasound phased arrays for transrectal thermotherapy and surgery of prostate diseases. Several regimens for driving the array are investigated and spatial distributions of measured and numerically simulated ultrasound intensities are compared. Practical recommendations for suppressing grating lobes based, for example, on the use of subsets of elements and the deactivation of several elements in the array are given.

#### 1.1. Advantages and Shortcomings of Linear Phased Arrays; Elimination of Grating Lobes

There is an interest in developing minimally invasive therapeutic ultrasound techniques for surgery (tissue ablation) since these may offer potential benefits compared with conventional approaches in terms of reduced morbidity, increased patient acceptability and reduced in-patient time. Much of the work previously reported has involved the use of a single or a few piezoceramic transducers with spherical curved surfaces (Fry et al. 1954; Fry 1978; Hill and ter Haar 1995; Rivens et al. 1996; Hill et al. 2005), lenses (Yoon et al. 1990; Lalonde et al. 1993; Fjfield et al. 1997, 1999) and phased arrays; the latter is the topic to be addressed in this book.

Phased arrays which offer electronically controlled dynamic focusing and the ability to vary and control precisely the range, location and size of the focus during treatment without moving the array are particularly useful in these clinical applications.

The principle of action of a linear phased array is illustrated in Figure 1 (NCRP Report № 74, 1983). The delays of the electrical signals to the elements are adjusted in such a way that the ultrasonic signals reach a predetermined point in the acoustic field of the array at the same time. Thus the array focuses ultrasound energy at this point located at the distance  $F$  from the array. By varying the delays, it is possible to steer the focal region in both distance and azimuth.

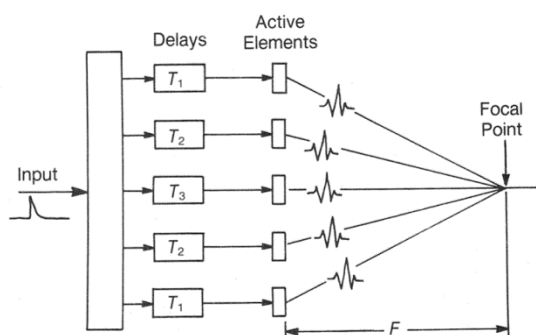


Figure 1. Principle of action of linear phased array based on the use of electrical delays at the elements of the array (NCRP Report № 74, 1983). Reproduced with permission from NCRP.

The structure of the acoustical field generated by a phased array contains a main lobe, so called grating lobes, and smaller side lobes as shown in Figure 2 (NCRP Report № 74, 1983). Excluding the main lobe, the most significant and simultaneously the most dangerous factor for

possible clinical applications is the appearance of grating lobes which are absent in the field of a single element transducer.

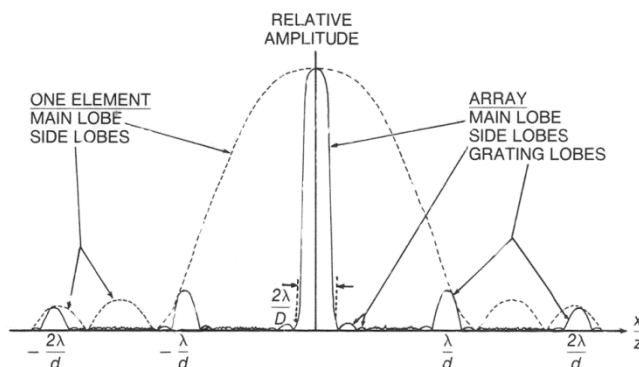


Figure 2. The structure of the acoustical field generated by a linear phased array (NCRP Report № 74, 1983). Reproduced with permission from NCRP.

A simple explanation of how grating lobes occur in the field of a phased array is to draw an analogy with a discrete array of elements being equivalent to placing a grating in front of a transducer with a continuous radiating surface (NCRP Report № 74, 1983).

It is seen from Figure 2 that the amplitude of the grating lobes is determined by the single-element directivity. When the beam is steered, the amplitude of the grating lobes may become as large as, or even exceed, that of the main lobe.

As shown in Figure 2, for linear phased arrays the grating lobes are located at a distance of  $\frac{x}{z} = \frac{\lambda}{d}$ , where  $x$  is the lateral distance from the centre of the beam,  $z$  is the range from the transducer,  $\lambda$  is the wavelength, and  $d$  is the spacing between the centres of the elements.  $D$  is the length of entire array, i.e.  $D=nd$ , where  $n$  is the number of elements.

The most widely used and effective application of linear arrays in medicine is in thermotherapy of prostate disease and surgical treatment for prostate cancer. Chronic prostatitis, i.e., inflammation of the prostate is one of the most common diseases in men. Medical aspects of these problems are discussed in more detail in Chapter 4, Section 4.3. From a technical point of view, the problem is to destroy prostate tumour, or at least significantly reduce its volume. Ideally a focused system (e.g., a linear phased array) is inserted into the rectum, and good acoustic contact between it and tissues can be achieved by containing the device within a thin-walled rubber balloon filled with water. A normal prostate gland is about 3-4 cm long and about 3-5 cm in width. Thus, steering of the focus (or foci) within the prostatic tissue must comply with these constraints.

Ultrasound ablation of prostate tissues is quite feasible because the physical parameters characterizing the propagation of ultrasound in soft tissues (wavelength, attenuation and absorption) in the frequency range from fractions of to several MHz are highly favorable for performing local ablations of specified dimensions in deep tissues. The wavelength of ultrasound in soft tissue (1.5 mm at 1 MHz) is sufficiently small to ensure effective focusing of the ultrasonic energy at a distance of several centimeters. Furthermore, the attenuation coefficient of ultrasound in prostatic tissue (approximately  $5-10 \text{ Np m}^{-1} \text{ MHz}^{-1}$ ) is not too great, and the absorption coefficient (of the same order of magnitude) is not too small. Thus it is possible to thermally ablate appropriate volumes of tissue within the constraints referred to above using an endocavitary transrectal focused ultrasonic system.

One approach to this problem is to use a small sized single element focused transducer and move it mechanically within the rectum so that it traverses across the prostate. Devices

based on this principle have been developed by two groups in the USA and France. The first of these is the commercially available Sonablate<sup>®</sup> device (Focus Surgery, Indianapolis, IN, USA) (Foster et al. 1993; Bihrlle et al. 1994; Sanghvi et al. 1999; Illing and Emberton 2006). The device includes two single element focusing radiators with different focal distances (usually 30 and 40 mm) mounted back-to back, and mechanically movable relative the prostate. Probes are also available with a longer focal distance of 45 or 50 mm to accommodate larger glands (Illing and Emberton 2006). A second commercial device is the Ablatherm<sup>®</sup> (EDAP-TMS SA, Vaulx-en-Velin, France) (Gelet et al. 1993, 1999). In this system a treatment transducer with a focal distance of 35 mm is driven at 3 MHz and a 7.5 MHz imaging probe is also incorporated. A disadvantage of both these approaches is that they are based on the use of single focused transducers having fixed focal distances. Thus, if the depth of sonication in the prostate tissue needs to be changed, it is necessary to use a transducer with a different focal distance, and to retune the focusing system. The use of phased arrays is a more flexible approach since these allow electronic steering of the focus over the prostatic tissue. An additional advantage is that several, spatially distinct foci can be created simultaneously if necessary.

The feasibility of using a cylindrical array for intracavitary hyperthermia of the prostate (but not for surgery) was first suggested on both theoretical and experimental grounds by Diederich and Hynynen (1991). The 0.5 MHz array consisted of 16 semi-cylindrical segments with centre to centre spacings of 2.5 mm, an external diameter of 15 mm, and a total length of 40 mm. Each of the elements was connected to a 16-channel power amplifier with digital adjustment of the signal phase. Experimental and theoretical data showed that the concentration of energy through focusing could overcome the losses due to the cylindrical geometry (in accordance with the expression  $1/r$ , where  $r$  is the distance) and that hyperthermic temperatures in tissues at a depth of 20-50 mm from the array could be achieved.

Somewhat later, the focusing properties of such a system were significantly improved by the application of a 64- element array of semi-cylindrical 500 kHz elements with centre to centre spacing of 1.73 mm (Buchanan and Hynynen 1994). Further details of linear arrays developed for hyperthermia are given in the review paper by Diederich and Hynynen (1999).

The rationale for using an intracavitary linear phased array to achieve higher temperatures with the aim of delivering surgical treatment to the prostate was given in the theoretical work by Hand et al. (1993). This approach was based on the use of energy emitted by all elements of the array to generate one, or (less commonly) several, foci steered over the given space electronically.

Subsequently the application of an intracavitary linear phased array for surgical treatment of the prostate was implemented in practice independently by two groups - Hynynen and his colleagues at the Harvard Medical School (Boston, USA) (Hutchinson et al. 1996; Hutchinson, Hynynen 1996; Sokka and Hynynen 2000), and Gavrilo and Hand and their colleagues in London and Moscow (Gavrilo et al. 1996, 1997; Gavrilo and Hand 1997, 2000c). The first description of a design of a linear array for prostate surgery was published in 1996 (Hutchinson et al. 1996; Hutchinson and Hynynen 1996).

As mentioned previously, a serious practical problem associated with a phased array (be it linear or two-dimensional) is the possibility of generating secondary intensity maxima (grating lobes) located in the tissue at considerable distances from the focus (foci). The appearance of such uncontrolled regions in which relatively high levels of acoustic field are present gives rise to a significant risk of thermal damage to non-targeted tissues.

Figure 3 (Gavrilo and Hand 2000c) illustrates the presence of these secondary maxima of the ultrasound intensity. Here the results of a calculation of the acoustic field of a 35-element linear phased array in which the centres of the elements are spaced at 2.5 mm, a distance approximately equal to the wavelength at the operating frequency of 585 kHz. The calculation is based on methods described in Ocheltree and Frizzell (1989) and Ebbini and Cain (1989). It is assumed that propagation is in a biological tissue with sound velocity  $1500 \text{ m s}^{-1}$ , tissue density

$1000 \text{ kg m}^{-3}$ , and attenuation coefficient of  $10 \text{ Np m}^{-1} \text{ MHz}^{-1}$ , values which correspond approximately to the acoustic parameters of prostate tissue (Duck 1990). Such calculations are discussed further in Chapter 2. It is seen that, along with the main intensity maximum, there are secondary maxima of intensity (grating lobes) whose amplitude at a distance of 40-50 mm from the array surface can reach up to 20% of that at the focus. In practice, such a distribution is unacceptable.

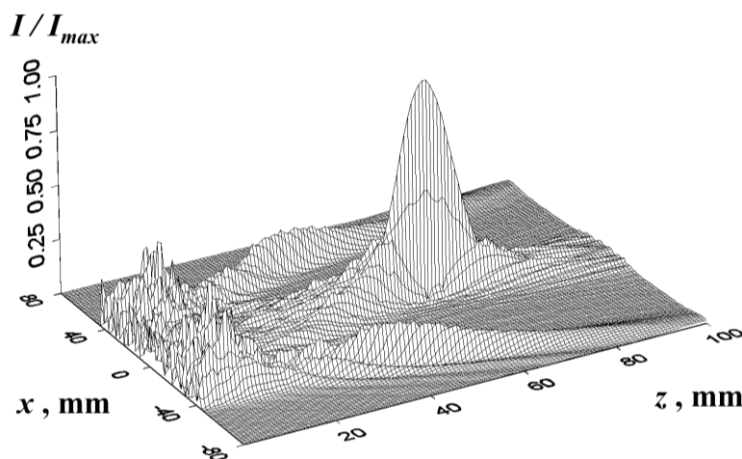


Figure 3. Calculated distribution of the relative intensity of ultrasound in the acoustical field of a 585 kHz linear array consisting of 35 elements of width 2 mm, length 16 mm, and with centre to centre distance of 2.5 mm. The array is focused at the point (0, 0, 60 mm);  $x$  is the co-ordinate along the array aperture and  $z$  is the co-ordinate along the acoustic axis. The intensity is normalized to the maximum at the centre of the focal region (Gavrilov and Hand 2000c).

The physical nature of grating lobes is related to the presence of discrete elements and some spatial regularity in the array. We shall use the term grating lobes in relation to these factors in contrast to other secondary intensity maxima that can exist in the field of any focused transducer. Comparison of theoretical and experimental intensity distributions produced by arrays shows that, in practice, the actual level of the grating lobes can exceed the predicted value, in particular, due to the acoustic interaction between the array elements (Gavrilov et al. 1997). Thus, reducing the level of grating lobes in the acoustic field produced by the array is of prime importance for safety of ultrasound surgery of the prostate.

To achieve a considerable decrease in the level of grating lobes in the acoustic field of an array, the distance between the array elements should be less than  $\lambda/2$  (Skolnik 1962; Radar Handbook 1970), i.e. for example, less than 0.75 mm at 1 MHz. However, to create an array with such small elements and a sufficiently large aperture and, in addition, to provide the required acoustic power (for instance, 200 W), it would be necessary to use a very large number of elements and electronic channels, which complicates the system and increases its cost. A further difficulty is that, a "dead zone" is formed due to the spaces between the elements, decreasing the efficiency of an array of fixed overall size. Moreover, for transrectal applications, the transverse dimensions of the array should be approximately no greater than about 25 mm to comply with physiological limits. Thus, the design of real arrays intended for transrectal prostate surgery involves a compromise between a number of contradictory requirements.

There are several methods that can be used to reduce the levels of grating lobes in the acoustic field of an array. One approach is to taper the oscillation amplitude such that it is greatest in the central part of the array and decreases toward its periphery (Skolnik 1962; Radar Handbook 1970). However, this is not practicable in the present application because of the requirement for the array to produce high levels of acoustic power. Another method of decreasing the influence of grating lobes is based on the use of arrays with unequal distances

between their elements (Skolnik 1962; Radar Handbook 1970) to break up the periodicity of the element positions. This was suggested and investigated by Hynynen and his colleagues (Hutchinson et al. 1996; Hutchinson and Hynynen 1996). They described a 0.83 MHz linear phased array for prostate surgery that consisted of 57 elements of equal length (15 mm) but with different widths (1.6 and 1.2 mm). The elements were randomly arranged and spaced at intervals of 0.13 mm to achieve centre to centre spacings ranging from 0.71 to  $0.96\lambda$ . These authors predicted that the reduction in the level of grating lobes due to the aperiodicity of the elements was around 30-45% (Hutchinson et al. 1996).

Another simple but effective method for suppressing grating lobes based on the use of subsets of elements and deactivation of several elements in the array was described by Gavrilov, Hand and co-authors (Gavrilov et al. 1997).

Experiments to investigate the effect of deactivating array elements on the suppression of grating lobes were carried out using a linear array, constructed from 25 individual elements, each 3 mm wide and 16 mm long, cut from a single piece of piezoceramic material PZT-4D 2.6 mm thick and driven at 475 kHz. The number and size of elements and the operating frequency were chosen on the basis of simulations (Hand et al. 1993); some of these parameters are similar to those reported for arrays with different geometry (Diederich and Hynynen 1991). The elements were separated from each other by 0.4-mm thick sections of rubber and fixed by silicone adhesive using a similar technique for acoustical and electrical insulation as described in (Diederich and Hynynen 1987). The resulting centre to centre spacing was 3.5 mm. The array was located within a cylindrical housing 25 mm in diameter and the space between the surface of the array and the tissue was occupied by temperature controlled degassed water contained within a thin rubber sheath.

A modular system supporting up to 64 channels and developed by Cain and his colleagues in the Bioengineering Program at the University of Michigan provided RF power and digital control of the frequency, phases and magnitudes of the signals applied to the array elements. For the experiments described here a digital board generated 25 square wave signals with specified phases and magnitudes (8 bit resolution) and provided the inputs to 25 amplifiers. The output of each amplifier provided up to approximately 20 W of RF power over the frequency range 100 kHz to 1.5 MHz. Acoustic fields produced by the array were measured in a water tank lined with ultrasound-absorbing material. A miniature piezoceramic hydrophone 0.6 mm in diameter (angular response better than 1 dB over  $\pm 30$  degrees) and a wide frequency band (1 kHz-50 MHz) amplifier were used to measure the spatial distribution of the sound pressure field produced by the array. The hydrophone was held in a gantry that enabled its position to be adjusted in three orthogonal directions. Measurements of the acoustic power radiated by the array were carried out using a radiation pressure balance method.

Experiments were performed to evaluate the array's ability to produce a single focus at different ranges (30-60 mm) both on and up to 20 mm off the central axis. The driving regimens used were (i) an iterative implementation of the pseudo-inverse technique (Ebbini and Cain 1989) that resulted in all elements being driven at the same power; (ii) a contiguous subset of elements such that the number used was dependent on the range and displacement of the focus from the central axis. The experimental results were compared with computer simulations reported by Hand et al. (1993). The sound pressure and  $(\text{sound pressure})^2$  were calculated at the nodes of a 3-dimensional array with inter-node spacing of 1 mm using the rectangular radiator method (Ocheltree and Frizzell 1989) as a numerical solution to the Rayleigh-Sommerfeld diffraction integral. The complex pressure  $p(x,y,z)$  at the node  $(x,y,z)$  due to all  $N$  elements of the array is given by:

$$p(x, y, z) = \sum_{n=1}^N u_n \cdot h_n(x, y, z) \quad (1)$$

where  $u_n$  is the velocity at the surface of the  $n$ th element and  $h_n(x,y,z)$  is of the form:

$$h_n(x, y, z) = \frac{j\rho c}{\lambda} \int_S \frac{e^{jkr_m}}{r_m} dS \quad (2)$$

$\rho$  is the density of tissue;  $c$ ,  $k=2\pi/\lambda+j\alpha$ ,  $\lambda$  and  $\alpha$  are the speed of sound, the propagation constant, the wavelength and the attenuation constant within the tissue;  $S$  is the surface area of the  $n$ th array element (assumed to be comprised of elemental rectangular areas  $dS$  with dimensions 0.5 mm x 0.5 mm such that position vector of the  $m$ th is  $r_m$ ). The attenuation coefficient for water was taken to be  $0.025 \text{ Np m}^{-1} \text{ MHz}^{-2}$  (Duck 1990).

The experimentally determined and theoretically predicted spatial distributions of intensity when uniform power was applied to all 25 elements and phases were adjusted to produce a focus at a range of 60 mm (i) along on the central axis (0, 0, 60 mm) and (ii) displaced by 20 mm from the central axis (20, 0, 60 mm) are shown in Figures 4 and 5 (Gavrilov et al. 1997), respectively. The relative intensity values are normalized with respect to the maximum values in the focus. When the focus was at (20, 0, 60 mm), the maximum relative intensity of the grating lobe in the focal plane was about 0.2 (Figure 4a) but the maximum intensity in the lobes closer to the array (at ranges of 20 and 30 mm) was as high as 0.5 and clearly is unacceptable, especially in practice when the attenuation in tissue (approximately  $10 \text{ Np m}^{-1} \text{ MHz}^{-1}$ ) will accentuate this problem. The relatively high intensities measured in regions near to the array's surface are greater than those predicted (Figure 4b).

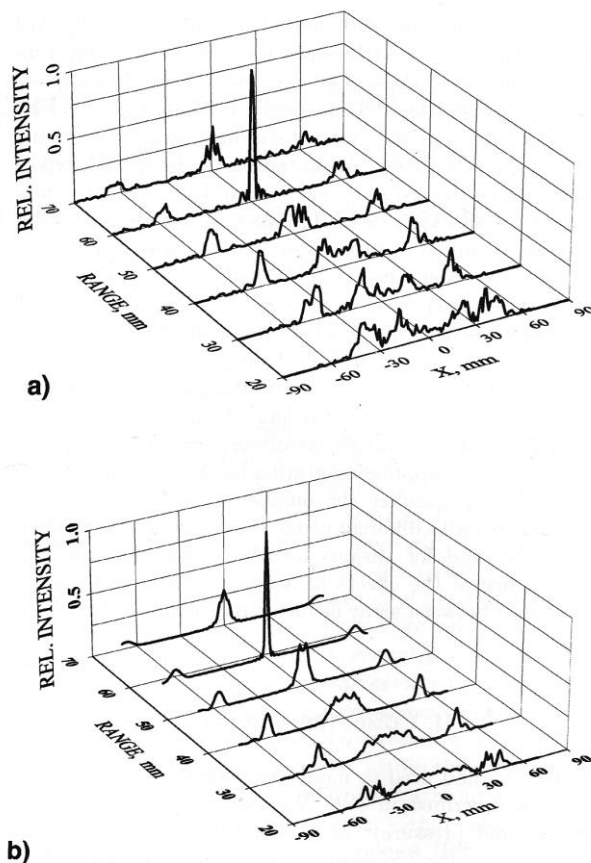


Figure 4. Relative intensity profiles at ranges of 20, 30, 40, 50, 60 and 70 mm for 25 element array focused at a range of 60 mm along the central axis: experimental data obtained in water (a); theoretical model (b) (Gavrilov et al. 1997).

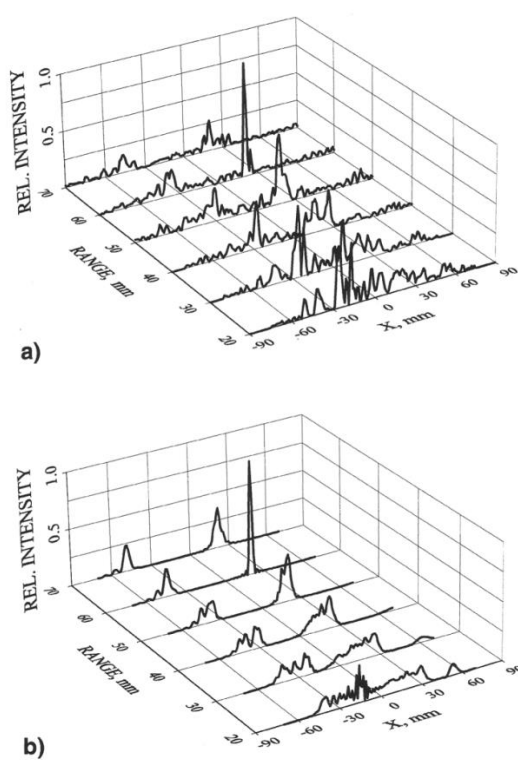


Figure 5. Relative intensity profiles at ranges of 20, 30, 40, 50, 60 and 70 mm for 25 element array focused at a range of 60 mm and displacement of 20 mm from the central axis: experimental data obtained in water (a); theoretical model (b) (Gavrilov et al. 1997).

A method of improving this situation by activating only an optimum (at least for this array) subset of elements is illustrated quantitatively in Table 1 (Gavrilov et al. 1997). This Table shows a value for the relative power in the “worst” grating lobe in Figure 5a (range 30 mm) (relative intensity integrated along that part of the profile in the mid-plane of the transducer at range 30 mm over which the grating lobe was present). This experiment suggests that use of 19 elements results in an improved intensity distribution with only 4% (Table 1) reduction in the maximum intensity in the focus, a reduction of 24% in the ultrasound energy introduced into the tissues, and of 44% in the amplitude and 60% of the relative power in the “worst” section of the grating lobe.

**Table 1. Effect of varying the number of active elements when focusing at (20, 0, 60 mm)**  
(Gavrilov et al. 1997)

No. of active elements	1-25	1-21	1-19	1-16	1-13
Max. rel. intensity in focus	1	0.96	0.96	0.82	0.69
Max. rel. intensity in grating lobe at range 30 mm	0.5	0.39	0.28	0.25	0.12
Relative power in grating lobe at range 30 mm	1	0.7	0.4	0.35	0.29
Length of active array, mm	87	73	66	55.5	45
Relative length of active array	1	0.84	0.76	0.64	0.52
Decrease of irradiated ultrasound power, %	0	16	24	36	48

The results of another experiment in which the array was focused at (0, 0, 30 mm) whilst the number of active elements was varied from 25 through 21 and 17 to 13 are illustrated in Figure 6 and Table 2. The use of more than 17 elements did not add significantly to the intensity at the focus but instead resulted in a less desirable acoustic field and led to an additional unwanted load on the sonicated tissue of up to 32% of the radiated ultrasound energy (Table 2). From results such as these it was determined empirically that the active aperture of this array should be no more than approximately 1.9 times the focal distance.

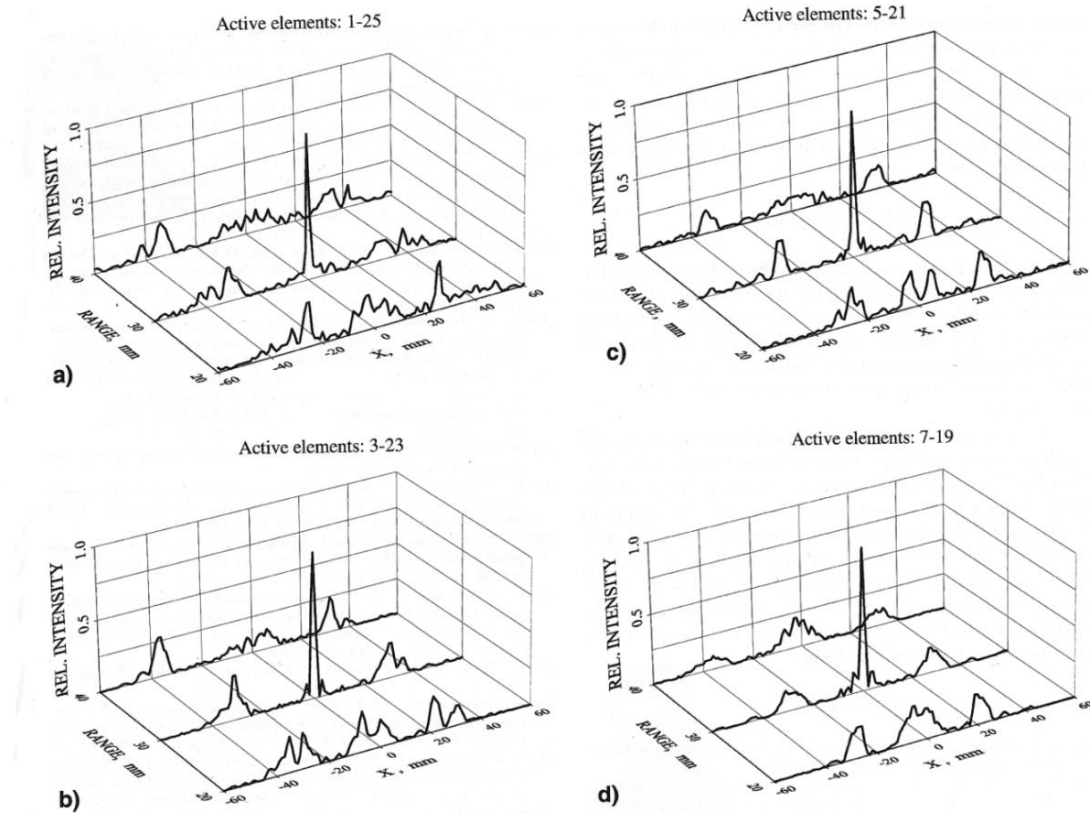


Figure 6. Relative intensity profiles measured at ranges of 20, 30 and 40 mm in water for arrays focused at a range of 30 mm along the central axis. The numbers of contiguous active elements are 25 (a), 21 (b), 17 (c), and 13 (d). The profiles are normalized to the respective maximum intensities (Gavrilov et al. 1997).

**Table 2. Effect of varying the number of active elements when focusing at (0, 0, 30 mm)**  
(Gavrilov et al. 1997)

No. of active elements	1-25	3-23	5-21	7-19
Max. rel. intensity in focus	1	0.985	0.97	0.79
Max. rel. intensity in grating lobes in focal plane	0.24	0.28	0.15	0.15
Max. rel. intensity in grating lobes at range 20 mm	0.3	0.24	0.22	0.21
Relative power in grating lobes in focal plane	0.9	0.81	0.61	0.55
Relative power in grating lobe at range 20 mm	1	0.98	0.77	0.61

Length of active array, mm	87	73	59	45
Relative length of active array	1	0.84	0.68	0.52
Decrease of irradiated ultrasound power, %	0	16	32	48

This study showed that using subsets of active elements resulted in a significant reduction of the maximum intensity and power in the grating lobes compared with the case when all array elements were driven at full power. There was also a reduction in the amount of the ultrasound energy introduced into the tissues. The optimum number of active elements which should be used in various practical situations was strongly dependent on the effective sizes of the elements and their actual directivities.

It was also suggested that the difference between theoretically simulated and experimentally measured acoustic field distributions induced by the array is likely to be related to the interaction between array elements. One of the consequences of the inevitable acoustic interaction between the elements is that the "effective" width of the elements may be considerably greater than their real geometric dimensions (e.g. 1.5 times greater for the array described in Gavrilov et al. (1997) resulting in a narrower radiation pattern associated with each element.

The safety of treatment is likely to be increased by the use of subsets of active elements since the relative intensity and power in the grating lobes and other secondary intensity maxima near the array may be decreased, as can the overall ultrasound energy introduced into the body without significant reduction in the maximum power at the focus.

It has been found empirically for the particular array used in this work that the maximum aperture of the active part of the array should not exceed approximately 1.2-3.3 times the focal distance when the focus is located on the central axis of the array. If the aperture of the array is larger, then the "extra" elements should be switched off. If the focus is shifted off the central axis, it is useful to switch off some elements on the contralateral side of the array; so that the total length of the deactivated elements is equal to the distance the focus is shifted.

It was shown that the effectiveness of this approach decreases with (i) increasing focal distance and (ii) increasing the ratio centre to centre distance/ wavelength. Although the quantitative results relate specifically to the device(s) investigated, the general nature of these recommendations is valid for other array configurations.

## **1.2. Design and Experimental Evaluation of an Endocavitary Linear Phased Array**

The design and results of an experimental evaluation of a 70-element linear phased ultrasonic array intended for endocavitary (transrectal) surgical treatment for chronic prostatic disease (see Figure 7) are presented in Gavrilov and Hand (2000c). The 70 elements were 1 mm wide, 15 mm long, and 1.73 mm thick corresponding to an operating frequency of 1 MHz. A contiguous subset of 63 elements was active at any one time. The elements were insulated electrically and acoustically by a double-sided adhesive tape of approximate thickness 0.1 mm. The length of the array was 77 mm and the distance between the centres of the elements corresponded to  $0.73\lambda$ .

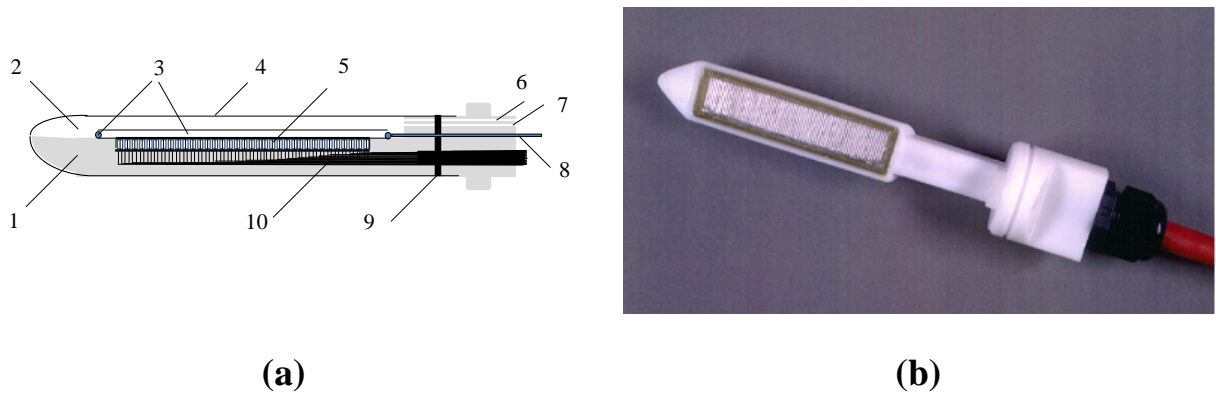


Figure 7. a): Schematic sketch of a linear array operating at the frequency of 1 MHz and consisting of 70 elements with dimensions of 1 x 15 mm: (1) housing of the array, (2) space filled with degassed cold water, (3) coil of the receiving NMR antenna, (4) membrane made of thin rubber, (5) 70-element array, (6) inlet water, (7) outlet water, (8) cable connected to the receiving coil, (9) seal, and (10) cable for driving the array elements (Gavrilov and Hand 2000c). b): A photograph of the linear phased array for transrectal surgery of prostate.

The array was enclosed in a housing *1* (Figure 7a) made of Delrin the widest part of which was 26 mm, and the minimum transverse dimension was 16 mm. The array and housing were enclosed in a rubber membrane *4*, the distance between the array surface and membrane being approximately 10 mm. The acoustic contact between the array and the biological tissue was provided through degassed cold water (for cooling both the array and the adjacent tissue). Water flowed into the space *2* between the housing and the membrane through hole *6* and drained through hole *7*. The conductors of a shielded cable *10* were soldered to the elements of the array. A photograph of the array is shown in Figure 7b.

The frequency, amplitude, and phase of the signals at the elements of the array were controlled by an 8-bit digital waveform generator and a 64-channel power amplifier.

The acoustic field generated by the array was measured in a water-filled tank with sound-absorbing walls. A miniature piezoceramic hydrophone was used to measure the spatial distribution of acoustic pressure. This was mounted on a positioner providing movement and the ability to monitor the position of the hydrophone relative to the array in three mutually perpendicular directions.

In the development and subsequent use of the array, attention was given to the reduction of grating lobes in the generated acoustic field. In previous attempts at developing such arrays (Gavrilov and Hand 1997, Gavrilov et al. 1997), a method was proposed based on the use of a subset of activated elements which was determined by the required focusing (see Section 1.1); that particular method was also used for this array.

Another approach aimed at decreasing grating lobes, discussed in detail in Chapter 3, is to introduce randomization of elements in the array construction. Since the physical nature of the grating lobes is related to the spatially periodic structure of the array, this method is expected to result in a reduction of grating lobe level at the expense of some broadening of the main diffraction maximum. Drawbacks of a laboratory-made array include the facts that its surface cannot be fabricated ideally flat, and there are likely to be some differences in the heights of the elements, giving rise to some phase shift, i.e. to some irregularity.

Table 3 characterizes the dependence of the relative intensity measured in the focus and in grating lobes in the focal plane at a distance of 10 mm from the surface of the array on the number of active elements when the array was focused at a distance of 30 mm along its acoustic axis (0, 0, 30 mm), corresponding to a depth of the focus in tissues of 20 mm. The voltages at all

active elements were constant to maximize the acoustic power of the array. Also listed are the length of the active part of the array and the reduction in the radiated ultrasound energy.

**Table 3. Influence of the number of active elements of the array on the level of the main lobe and grating lobes; focusing at the point (0, 0, 30 mm) (Gavrilov and Hand 2000c)**

Numbers of active elements/Total number of active elements	1-62/62	6-57/52	11-52/42	16-47/32
Maximum relative intensity at the focus	1.0	1.0	0.98	0.9
Maximum relative intensity of the grating lobe in the focal plane	0.06	0.03	0.02	0.01
Maximum relative intensity of the highest secondary maximum at a distance of 10 mm from the array	0.11	0.11	0.11	0.12
Length of the active part of the array (mm)	62	52	2	32
Reduction of the radiated ultrasonic energy (%)	0	16	32	48

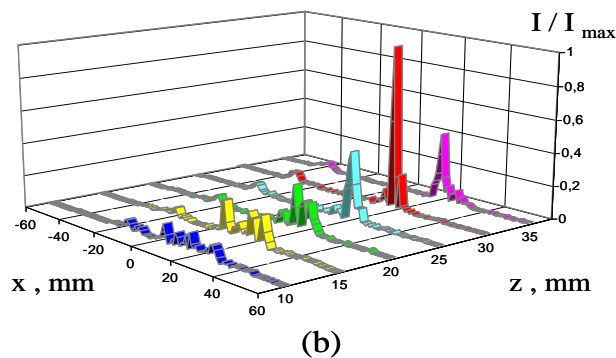
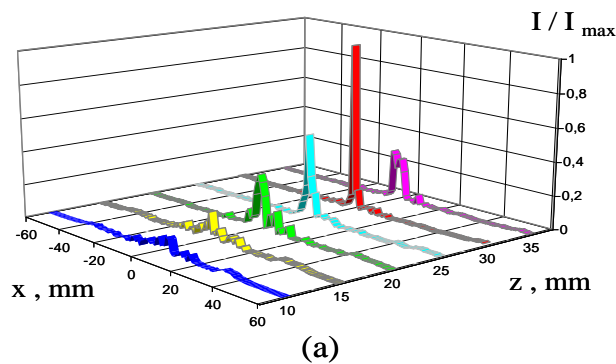


Figure 8. Experimental spatial distribution of the relative intensity of the array field: (a) for focusing at the point (0, 0, 30 mm) with the use of 42 active elements out of 62 (10 elements at each end of the array were switched off); (b) for focusing at the point (20, 0, 30 mm) with the use of 42 active elements and with 20 elements on the side of the array opposite to the direction of the focus shift switched off;  $x$  is the co-ordinate along the array aperture and  $z$  is the co-ordinate along the acoustic axis (Gavrilov and Hand 2000c).

Figure 8a shows the experimentally obtained intensity distribution for the location of focus at (0, 0, 30 mm) for the case of using 42 active elements out of 62. From Table 3 and Figure 8a, it follows that the reduction in the number of active elements resulted in an acceptable distribution of intensity, with a decrease in the maximum intensity at the focus by only 2%. Simultaneously, the total radiated power was reduced by 32%, and the level of the grating lobes

in the focal plane dropped by a factor of 3 (down to 2% of the maximum intensity at the focus). The level of the maximum intensity of the highest secondary maximum observed at a distance of 10 mm from the array remained the same. Under these conditions of focusing, the ratio between the length of the active part of the array (42 mm) and the focal length (30 mm) was 1.4.

Similar data for the case of the array being focused at the same distance, but with a shift of 20 mm from acoustic axis (20, 0, 30 mm), are presented in Table 4 (Gavrilov and Hand 2000c).

**Table 4. Influence of the number of active elements of the array on the level of the main and secondary intensity peaks; focusing on the point (20, 0, 30 mm)**

Numbers of active elements/Total number of active elements	1-62/62	21-62/42
Maximum relative intensity at the focus	1.0	1.0
Maximum relative intensity of the grating lobes in the focal plane	0.19	0.07
Maximum relative intensity of the highest secondary maximum at a distance of 10 mm from the array	0.12	0.12
Reduction of the radiated ultrasonic energy (%)	0	32

Figure 8b illustrates the intensity distribution obtained in the experiment for the mentioned location of the focus when 20 elements of the array on the side opposite to the direction of the focus shift were switched off. From Table 4 and Figure 8b, it follows that the reduction in the number of active elements from 62 to 42 resulted in an acceptable distribution of intensity without a decrease in the maximum intensity at the focus. The total radiated power was reduced by 32%, and the level of the secondary maximum in focal plane dropped from 19% of the maximum intensity at the focus to 7% of this value. The level of the maximum intensity of the highest secondary maximum located at a distance of 10 mm from the array remained invariable. However, when the focus was shifted by 30 mm off the acoustic axis, then, for 62, 42, and 32 active elements, the maximum intensity at the focus was essentially unchanged; the maximum relative intensity of the grating lobes in the focal plane was 0.7, 0.3, and 0.1, respectively; the maximum relative intensity of the highest secondary maximum at a distance of 10 mm from the array was 0.65, 0.5 and 0.45, respectively. It is clear that such a high level of secondary maxima observed for this focus shift is unacceptable from the point of view of safety.

Similar field measurements were carried out for focusing at a distance of 60 mm from the array (which corresponding to a focus in tissue 50 mm deep), both without a shift of the focus relative to the acoustic axis of the array (0, 0, 60 mm) and with a shift of 20 mm from the axis (20, 0, 60 mm). In the first case for 62, 56, 52, and 42 active elements, the maximum relative intensities at the focus were 1.0, 0.97, 0.94, and 0.76, respectively, which means that in this specific case it was better to use all 62 elements. Figure 9a presents the measured spatial distribution of intensity for this case. The ratio of the active part of the array aperture to the focal length for these conditions of focusing was 1.03. Figure 9b shows a similar distribution with the focus shifted by 20 mm off the acoustic axis (20, 0, 60 mm). In this case, the use of 42 active elements (20 elements on the side opposite to the direction of the focus shift were switched off) resulted in a reduction of the maximum intensity at the focus by only 2.5%, whereas the radiated acoustic power decreased by 32%, and the maximum relative intensity of the highest grating lobe in the focal plane dropped to 2% of the maximum intensity at the focus, compared to 5% for 62 active elements. However, when the focus was shifted by 30 mm from the acoustic axis, the maximum relative intensity at the focus for 62, 52, and 42 active elements was 1.0, 0.97, and 0.72, respectively; the maximum relative intensity of the grating lobes in the focal plane was 0.15, 0.08, and 0.06 whilst the maximum relative intensity of the highest secondary maximum at a distance of 10 mm from the array was 0.35, 0.2, and 0.2, respectively. These data are much

better than those for the similar focus shift in the case of the 30-mm focal length (see above), but the level of the secondary maxima for this shift is also excessively high.

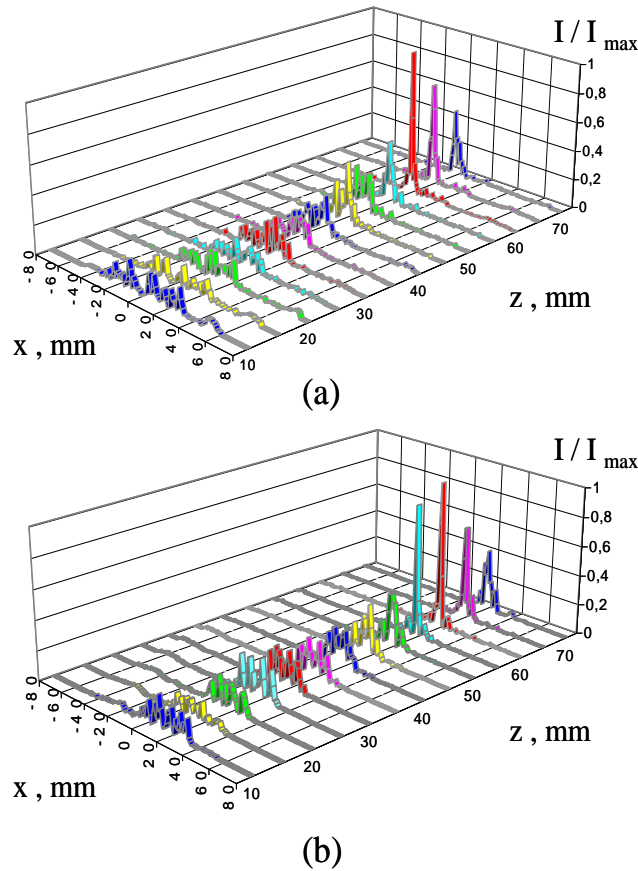


Figure 9. Experimental spatial distribution of the relative intensity of the array field: (a) for focusing at the point (0, 0, 60 mm) with the use of 62 active elements; (b) for focusing at the point (20, 0, 60 mm) with the use of 42 active elements and with 20 elements on the side of the array opposite to the direction of the focus shift being switched off (Gavrilov and Hand 2000c).

Measurements of the acoustic power radiated by the array were performed using a purpose made 18-element array with the same elements and design as the 70-element array. The aperture of this array was about 20 mm (cf 77 mm aperture of the main array). The power was determined by measuring the radiation force with a target in the form of an absorber of sufficiently large dimensions (90 x 180 mm) to span the whole ultrasonic beam. The basic error of measurements was about  $\pm 10\%$ . The acoustic power of the array was 55 W in a continuous mode of operation during 5 s; the limiting near-destructive operation mode of the array was not investigated because of the risk of damaging the circuits driving the array. According to Hutchinson et al. (1996) an acoustic power of approximately 28 W per cm of a linear array is more than sufficient for thermotherapy and thermosurgery of prostate tissue. The results of Hutchinson and Hynynen (1996), as well as those of our experiments, suggest that arrays delivering such power levels can easily create local thermal ablations in specimens of biological tissues (liver, beef). The results of measurements with the additional array indicated that the maximum acoustic power of the main 70 element array at least 200 W.

Evidently, the wide clinical use of linear phased arrays for prostate surgery depends on the development of a means for monitoring the location of the focal region in prostate both before and after the ablation. The use of conventional ultrasonic diagnostic equipment intended for imaging the prostate tissue does not provide reliable monitoring of the location of the focus,

since even a slight error in the rotation of the array about its axis may result in a considerable shifting of the focus location from the required zone of ablation. MRI can be used to monitor temperature changes due to low level sonication prior to ablation as well as imaging tissue changes due to ablation within the HIFU focal region. In this way the location of the focus can be verified immediately prior to high power sonication (e.g., Cline et al. 1994, 1995; Hynynen et al. 1996).

Although the development of a MRI system for control and assessment of the ablated volume created by the linear phased array was not a particular objective of Gavrilov and Hand (2000c) the design was MRI compatible. Moreover, a simple removable rectangular receive coil (86.5 x 24 mm) was located in the array housing (see Figure 5, #3). This was similar to the receive coil described by de Sousa (1996). The laboratory evaluation of the developed device showed that the use of a linear array with the parameters specified above enabled the focus to be scanned within 30-60 mm along the array axis and  $\pm 20$  mm in the perpendicular direction (which corresponds to the dimensions of prostate) with an acceptable level of grating lobes in the focal plane (considerably less than 10% of the maximum intensity at the focus) and secondary intensity maxima near the surface of the array (no greater than 10%). Measurements of the acoustic power radiated by the array showed that it was sufficient for ablation of prostate tissue. The spatial distributions of intensity created by the array were comparable with the distributions produced by the arrays described elsewhere (Hutchinson and Hynynen 1996; Hutchinson et al. 1996).

This array design is a promising for prostate surgery; however, the possibility of extensive clinical use of the ultrasound linear phase arrays depends on the subsequent development of combined systems providing not only ultrasonic ablation of prostate tissue but verification of the location of the focal region in the prostate prior to ablation and verification of the post treatment results.

### 1.3. Other Constructions of Powerful Linear Phased Arrays

Over the past 15-20 years, research on the development of linear phased arrays has been very active. Key players include Hynynen and his colleagues from his former laboratory (Boston, USA). The results of their first *in vivo* experiments on rabbit thigh muscles were presented in Hutchinson and Hynynen (1998). Subsequently array design was improved through the use of an ultrasonic motor that provided controlled mechanical rotation of the array around its axis (Sokka and Hynynen 2000), an action carried out manually in previous designs. Hence it became possible to accurately move the focus not only in depth and along the prostate but in the transverse direction too. The 62 elements of their 1.1 MHz array were fabricated from piezoelectric ceramics PZT- 4. Half of them had dimensions 15 mm x 1 mm, and the other half had dimensions 15 mm x 1.15 mm. The distance between the elements was 0.11 mm and this space was filled with silicone. The elements were arranged in a random manner, and the total size of the active part of the array was 15 mm x 75 mm. An ultrasonic motor provided rotation of the array up to  $\pm 50^\circ$  in increments of  $0.09^\circ$ . Verification of the resulting ablation was made using MRI. The maximum acoustic power was 150 W, and the estimated time for the destruction of the entire prostate was up to 40 min. The results obtained in rabbit tissues *in vivo* are presented in Section 4.3.

There has also been commercial development and manufacture of devices for prostate surgery based on the use of single focusing transducers with fixed focal length in recent years. The foremost companies in this area are Focus Surgery, Indianapolis, IN, USA and EDAP-TMS, France. Having accumulated years of practical experience in the use of such devices, both companies began to investigate the possibility of replacing their single-element focusing systems by phased array transducers. For example Focus Surgery together with Frizzell from the University of Illinois published two articles (Tan et al. 2000, 2001) on the effects of array

geometry on its ability to move the focus in a manner appropriate for the destruction of the prostate. Figure 10 (Tan et al. 2001) shows the configuration of the arrays investigated. Of all configurations studied by the authors, the greatest ability to steer the focus both along the axis of the array, i.e. at various depths into tissue, and along the prostate, was demonstrated for a cylindrical concave array with the curvature along its length (Figure 10e).

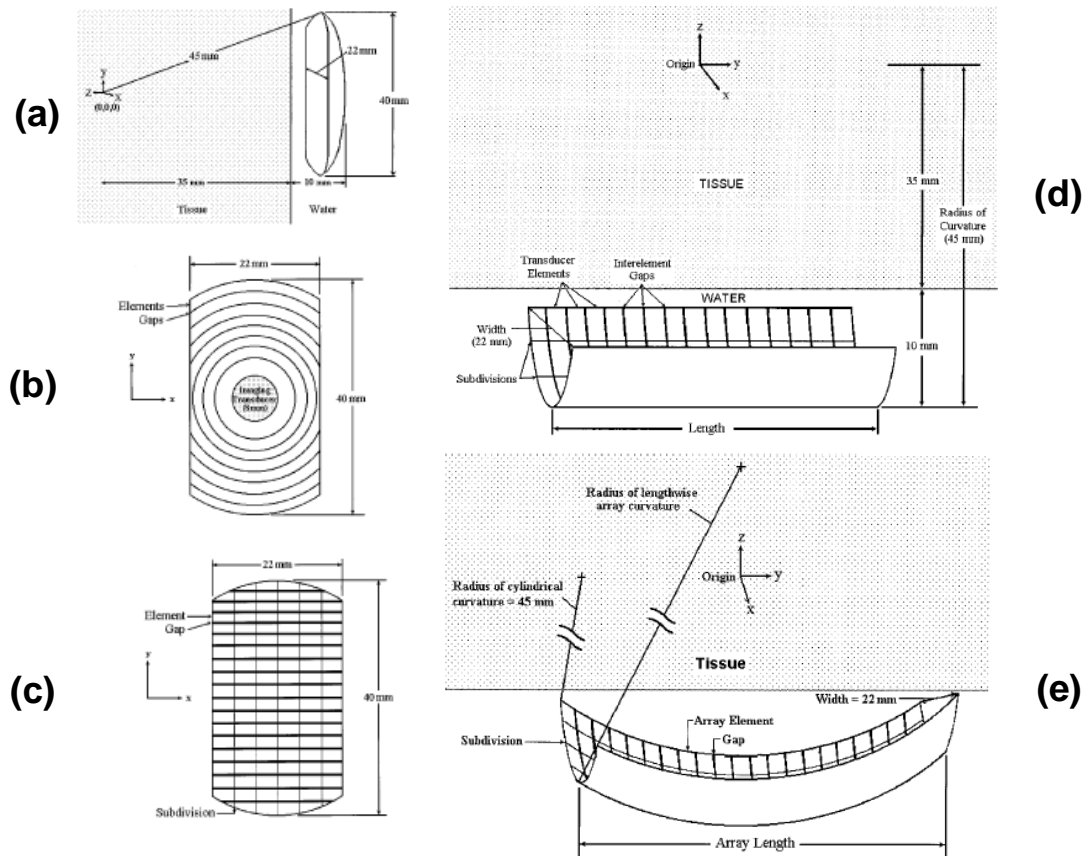


Figure 10. Configuration of the studied arrays for the surgical treatment for prostate, a - a truncated spherical array, side view, b - a truncated spherical annular array, top view, c - a truncated spherical linear array, top view; d - a cylindrical array, e – a cylindrical concave array. Reproduced with permission from Tan, J. S. et al (2001) Ultrasound phased array for prostate treatment. *J. Acoust. Soc. Am.* 109, 6, 3055-3064. Copyright 2001, Acoustical Society of America

Shortly thereafter EDAP- TMS, France proposed a multi- element 1.5-dimensional array for use in prostate surgery (Curiel et al. 2002). This consisted of a part of a spherical shell of radius of curvature 40 mm, truncated on both sides to a size of 36 mm. The array was made of 1-3 piezocomposite material (Imasonic, France) and consisted of 6 strips, each of which contained 42 elements. The elements were symmetrical relative the central axis of the array and were connected electrically with each other. The total number of channels driving the array was 126 and the centre frequency was 2.5 MHz with a bandwidth of 1.3 MHz.

Experiments performed by the authors on pig liver samples showed that a tissue volume  $20 \times 20 \times 20 \text{ mm}^3$  could be destroyed using a single fixed position of the focusing system. Sonication was implemented at a certain distance from the array (e.g., 40 mm) by scanning the focus over the focal plane within  $\pm 9.6 \text{ mm}$ . However, the criteria characterizing the quality of acoustic fields, as measured by the amplitude of the secondary maxima, selected by the authors, were significantly less stringent compared with the criteria selected using random two-dimensional arrays (see Chapter 3). Although intended for transrectal use, the large transverse dimension of the array housing (up to 36 mm), was also a potential problem.

In 1999 a collaboration between Hitachi, and Focus Surgery resulted in the idea of using two focused radiators with shifted foci (Umemura et al. 1999). They replaced fixed foci radiators with two miniature, 3.6 MHz linear arrays, each consisting of 48 elements, that were slightly tilted relative to each other (Ishida et al. 2003). To change the depth of the focus in the tissues, cylindrical lenses were used. Experiments were performed on dogs *in vivo* and demonstrated the possibility of destruction of prostate tissue at a depth of 30 to 50 mm without changing the system of transducers.

In a simpler modification of the system for the treatment for the prostate, a device consisting of eight concave (radius of curvature of 35 mm) sectors with a rectangular aperture of 40 x 20 mm was described by Umemura et al. (2000). This device achieved an order of magnitude increase in the volume of tissue coagulation in comparison with that associated with the use of a single focus.

Focus Surgery suggested new designs for arrays for intracavitary prostate surgery (Seip et al. 2005). One of them was a 20 element annular array, capable of focusing 4 MHz ultrasound at a depth from 25 to 50 mm. A second design was based on the use of a cylindrical array consisting of 422 elements (211 channels), allowing ultrasound focusing not only to a depth from 25 to 50 mm, but also to steer the focus to  $\pm 20$  mm along the axis of the array. These limits correspond to the maximum size of the prostate. Both arrays have been successfully tested in experiments *in vitro* and even *in vivo* (dogs prostate).

Held and colleagues (Held et al. 2006) developed and investigated a 3 MHz annular array designed for intracavitary surgery of uterine fibroids (benign tumors of the uterus, see also Section 4.9). The concave array consisted of 11 elements of equal area, made of 1-3 piezocomposite. The dimensions of the array in the form of a truncated spherical segment were 60 mm long and 35 mm wide. The geometric focus was located at a depth of 50 mm and could be steered electronically from 30 to 60 mm. A probe for visualizing tissues and focus was a part of the device. Experimental verification of the device was carried out on gels and porcine liver tissues (see Section 4.9).

To conclude this Section, it is worth noting that not all intracavitary ultrasonic devices for surgery and hyperthermia are based on the use of focusing transducers, i.e. the systems in which the maximum intensity is realized at some distance from the radiator. Devices in which high-intensity ultrasound radiates superficial tissues have also found practical use. Various modifications of prostate hyperthermia devices in which the transducer has a cylindrical shape and consists of several (e.g., 16) sections, each of which can be driven individually, have been developed. In these cases ultrasound is propagated radially, and the intensity is maximal on the surface of tissues and decreases with depth (Diederich and Hynynen 1989, 1990; Smith et al. 1999, 2001).

A device was designed in which a miniature, but sufficiently powerful flat radiator revolved around its axis and could be used for the treatment for esophageal cancer (Melodelima et al. 2003). Subsequently this design was modified (Melodelima et al. 2004). A 16- element 4.55 MHz array, representing a  $\frac{1}{4}$  part of a cylinder was used; the diameter of the emitter was 10.6 mm. The phases of signals on the elements of the array could be adjusted in two regimens, namely to create a plane wave when sonication at a relatively large depth (17 mm) was required, or to generate a cylindrical wave when the required depth of exposure did not exceed 6 mm. Destruction in the tissues up to these depths were obtained with the intensity on the elements of  $17 \text{ W cm}^{-2}$  and exposure time of 20 seconds. The number of active elements could be reduced in the case of small volumes of tumor.

Summarizing the results of work on the design of powerful linear phased arrays for intracavitary surgery, it may be noted that there is tendency to replace the linear arrays by small two-dimensional multiple-element arrays. Such arrays for intracavitary prostate surgery will be discussed in the next Chapter.

## Two-Dimensional Phased Arrays with a Regular Distribution of Elements

There is an interest in the development of minimally invasive therapeutic ultrasound techniques for surgery (tissue ablation) since these may offer potential benefits compared with conventional approaches in terms of reduced morbidity, increased patient acceptability and reduced in-patient time. This chapter discusses two-dimensional phased arrays in which elements are distributed on their surface in a spatially regular and repetitive manner.

### 2.1. General Comments

In Chapter 1 it was shown that linear arrays are often used in cases when they can be inserted into a body cavity (e.g., the rectum). Typically, these arrays permit scanning of the focus electronically in the lateral and axial directions; mechanical movement is required to shift the focus in the third direction. If the array can be accommodated outside the patient's body then the opportunity to use two-dimensional arrays arises. These permit steering of the focus electronically in three orthogonal directions. Furthermore, they have the potential to create multiple simultaneous foci and thereby can increase significantly the size of the targeted region. These advantages over the performance of linear arrays come with the cost of a significantly increase in the number of elements and electronic channels.

To ablate a clinically relevant tissue volume, say  $\geq 10 \text{ cm}^3$ , at depth in the human body, a device should be capable of steering the focus at the required distances in three orthogonal directions and have an acoustic power of at least 300-400 W. In addition, it is necessary that the intensity in undesirable grating lobes and other secondary intensity maxima are at a level appropriate for clinical practice. The realization of such an array is a compromise between several contradictory requirements. In order to increase the distance for the focus scanning, and therefore to extend the volume of the destruction region, it is necessary to reduce the size of elements, i.e., make them less directional. On the other hand, it is necessary that the active area of the array be not smaller than  $50 \text{ cm}^2$  to meet the requirements for the radiated power with realistic values of intensity at the surface of the elements. These considerations lead to the designing arrays containing excessively large numbers of elements, and therefore, to an increase in the complexity and costs of an array driving system.

Safety of the ultrasonic technique must be the determining factor in the design of phased arrays intended for surgical applications. Therefore, the minimum level of grating lobes and other secondary intensity maxima of ultrasound beyond the focal region become basic criteria for the estimation of the quality of acoustic fields produced by an array. The presence of such maxima can lead to undesirable overheating in non-targeted regions and even to the destruction of structures beyond the preset region of action. As mentioned in Chapter 1, in order to reduce the influence of the grating lobes of a directivity pattern, the distance between the centres of the array elements must be less than  $< \lambda/2$  (Skolnik 1962), where  $\lambda$  is the wavelength, i.e., for example, less than 0.5 mm at a frequency of 1.5 MHz.

However, with such small elements, it is necessary to use a large number of elements and electronic channels in order to produce an array with a large enough aperture and to obtain the acoustic power needed for a therapeutic array. In addition, the "dead" space between elements increases. The methods for reducing the level of grating lobes in the array directivity pattern discussed in the previous Chapter are not always applicable for two-dimensional phased arrays because of the need for significantly greater acoustic power.

It is worth noting that until recently practically all two-dimensional phased arrays for medical applications had elements that were distributed over the surface of the array in a regular spatial manner, for example, in square (see Figure 11), annular or hexagonal patterns. The most popular was a square configuration (e.g. Ebbini and Cain 1991a; Wan et al, 1996; Daum and Hynynen 1998, Fan and Hynynen 1996a; Mc Gough et al. 1996).

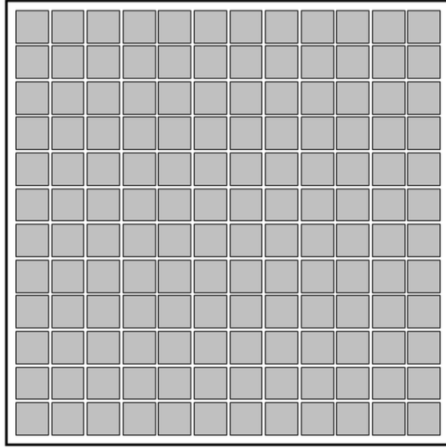


Figure 11. A generic array of elements positioned in a regular manner on a rectangular grid. In practice, the elements are often distributed in this manner on a spherical bowl. In another common configuration some centrally located elements may be replaced by an ultrasound imaging transducer.

## 2.2. Designs

As for the history of two-dimensional phased arrays, research related to the development of devices for hyperthermic therapy of tumours, and then for surgical purposes, began in the mid 1980s under the guidance of Charles Cain, Head of the Bioacoustic Research Laboratory in the University of Michigan, USA. There were many designs proposed for the early arrays. In some geometric focusing was used, and in others electronic focusing. Some of them were intended to steer a single focus, others were designed to synthesize more complex fields with a specific configuration to cover the required volume of the tumour. At first, to simplify the electronics and reduce size, the number of channels was minimized. For example, the available electronic channels were connected to the first particular set of elements arranged along one line (for example,  $n-1, n, n+1$ ), then to the next set ( $n, n+1, n+2$ ), *etc.*, which provided a substantial savings compared to the simultaneous excitation of all elements (Ocheltree et al. 1984).

In another design (Benkeser et al. 1987) elements of different thicknesses were used. The focal region was moved in two directions by changing the phases on the elements, and in the third direction - by changing the frequency, i.e. by the use the part of the element for which this frequency is close to the resonance one. Thus the number of channels  $N$  was reduced compared to  $N^2$  channels which are necessary in an array consisting of  $N \times N$  elements. In subsequent studies all  $N \times N$  elements were used in arrays with a flat, spherical or cylindrical geometry (Ibbini and Cain 1990; Ibbini et al. 1990; Ebbini and Cain 1991b; McGough et al. 1996).

The design of a sector- vortex array was first proposed in the works of Cain and Umemura (Cain and Umemura 1986; Umemura and Cain 1989, 1992; Umemura et al. 1992). This array permitted the creation of an annular focus at a depth corresponding to the radius of curvature of the array whose diameter was determined by the selected mode excitation of array elements.

An array design with elements mounted on a spherical surface was proposed for the first time in the work of Ebbini and Cain (1991a,b) and has subsequently become the most popular of all available arrays.

A significant role in the development and practical realization of two-dimensional therapeutic arrays played the Laboratory in the Department of Radiology, Harvard Medical School, Brigham and Women's Hospital, Boston, led at those times by Hynynen.

The sketch of the simplest spherical two-dimensional array consisting of 16 elements is presented in Figure 12 (Fan and Hynynen 1996b).

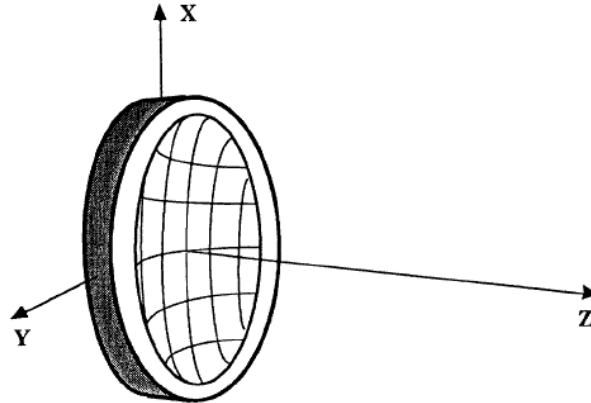


Figure 12. The sketch of the simplest two-dimensional array consisted of 16 elements (from Fan, X. and Hynynen, K. (1996). A study of various parameters of spherically curved phased arrays for noninvasive ultrasound surgery. *Phys. Med. Biol.* **41**(4), 591-608. © Institute of Physics and Engineering in Medicine. Published on behalf of IPeM by IOP Publishing Ltd. All rights reserved).

In this laboratory a 1.1 MHz array in the shape of a spherical shell with radius of curvature 10 cm and diameter 12 cm consisting of 256 elements of piezocomposite 1-3 was designed, manufactured and tested under *in vivo* conditions (Daum and Hynynen 1999; Daum et al. 1999; Diederich and Hynynen 1999). Photos of the array (front and rear view) are shown in Figure 13 (Diederich and Hynynen 1999).

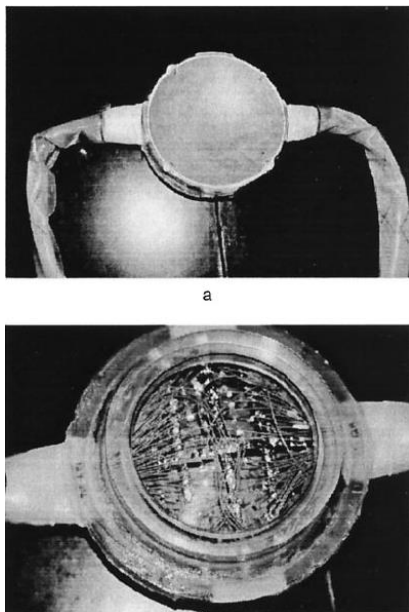


Figure 13. An array consisting of 256 elements (frequency of 1.1 MHz) Reprinted from *Ultrasound in Med. and Biol.* Diederich, C. J. & Hynynen, K, *Ultrasound technology for hyperthermia* **25**(6), 871-887, copyright (1999) with permission from Elsevier.

The size of the projection element was  $6.5 \times 6.5 \text{ mm}^2$ , equal to 4.78 wavelengths. Unlike earlier designs of spherical two-dimensional arrays (Ebbini and Cain 1991a), the array was made from a single piece of piezocomposite 1-3 (Imasonic, France) rather than individual elements and the elements were separated from each other by an engraving on the convex surface of the array.

It was shown that the array parameters permitted lesions with an area of  $1 \times 1 \text{ cm}^2$  to be created at a distance of approximately 7 cm from the tissue surface. The side lobe levels did not exceed 10 % of the intensity in the main maximum. The maximum acoustic power was 350 W.

From difficulties and problems discovered during the laboratory tests of the 256 element array, Daum and Hynynen noted the existence of significant interaction between the elements, despite the fact that the array was made of piezocomposite material. The use of a quarter-element matching layer on the surface enhanced this interaction. At the same time, it appeared that the piezocomposite material was extremely resistant and could withstand more than 100 hours of immersion in water during the treatment sessions.

Clement et al. (2000b) considered the possibility of a substantial reduction of the number of array elements and their driving channels by using relatively simple arrays rotated about an imaginary axis of symmetry of an object (in this particular paper the object was the skull). Constructions of two such arrays are shown in Figure 14. The first (Figure 14a) consisted of 11 equal area 0.665 MHz elements on a shell 10 cm in diameter and with radius of curvature 8 cm. The second (Figure 14b), operating at 0.51 MHz, consisted of 64 square elements of  $1 \text{ cm}^2$ , of which only 40 (shaded in the Figure) were active elements.

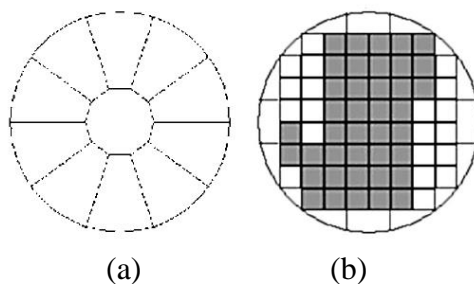


Figure 14. A simple geometry of the arrays proposed to use instead of multiple element arrays of a large area. On the left is an array consisted of 11 equal area elements, on the right is an array consisted of 64 elements, of which only 40 darkened elements were active (from Clement, G. T., White, J. P. & Hynynen, K.. (2000). Investigation of a large area phased array for focused ultrasound surgery through the skull *Phys. Med. Biol.* **45**, 1071-1083. © Institute of Physics and Engineering in Medicine. Published on behalf of IPEM by IOP Publishing Ltd. All rights reserved).

To reproduce the effect of the array with a large area, these arrays were set relative to the skull on the hemisphere in four positions at a  $45^\circ$  polar angle and at  $90^\circ$  azimuth interval (Figure 15).

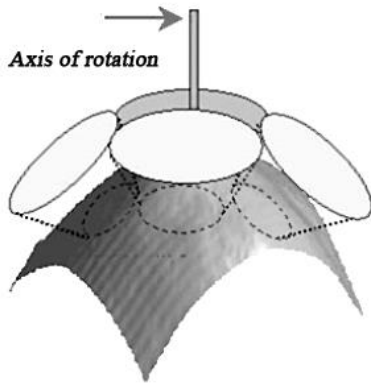


Figure 15. The array consisting of small number of elements is set to four positions relative to the skull (from Clement, G. T., White, J. P. & Hynynen, K. (2000). Investigation of a large area phased array for focused ultrasound surgery through the skull. *Phys. Med. Biol.* **45**, 1071-1083. © Institute of Physics and Engineering in Medicine. Published on behalf of IPEM by IOP Publishing Ltd. All rights reserved).

In reality it was more convenient to rotate the skull relative to the array. As a result the research was carried out for two virtual arrays with 44 and 160 elements, respectively. Field measurements were carried out using a miniature hydrophone. After an appropriate correction of the phases, an acceptable quality of the focusing was observed even for the array of 44 elements. Sound pressure after correction of the phases was from 26 % to 42 % in comparison with the value obtained in water without propagation through the skull. The maximum mechanical displacement of the array relative to the skull parallel to the surface was  $\pm 15$  mm. The authors evaluated the extent of electronic scanning of the focus using the 160 element array to be  $\pm 10$  mm.

In the work of Clement et al. (2000a) the 0.665 MHz array developed by the authors having the form of a hemisphere with a radius of curvature of 15 cm was investigated and described. It consisted of 64 elements of equal size, each with an area of  $\sim 22$  cm<sup>2</sup>. Photographs of the array are presented in Figure 16 and its design is shown schematically in Figure 17. At level 1 one element is contained, at level 2 - 7 elements, at 3 - 13, at 4 - 20, at 5 - 23 elements. The supporting rings are designated as 6.

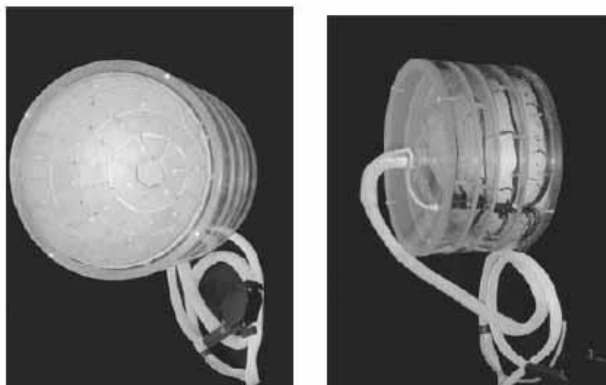


Figure 16. Photographs of the array of the hemispherical form, consisting of 64 elements (from Clement, G. T., Sun, J., Giesecke, T. & Hynynen, K. (2000). A hemisphere array for non invasive ultrasound surgery and therapy. *Phys. Med. Biol.* **45**, 3707-3719. © Institute of Physics and Engineering in Medicine. Published on behalf of IPEM by IOP Publishing Ltd. All rights reserved).

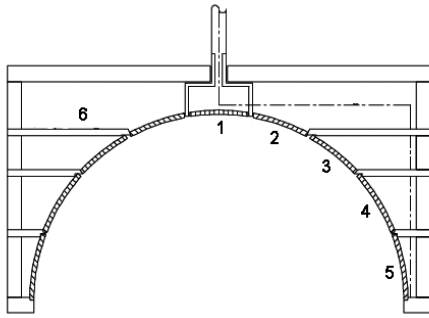


Figure 17. The design of the array of the hemispherical form, consisting of 64 elements (from Clement, G. T., Sun, J., Giesecke, T. & Hynynen, K. (2000). A hemisphere array for non invasive ultrasound surgery and therapy. *Phys. Med. Biol.* **45**, 3707-3719. © Institute of Physics and Engineering in Medicine. Published on behalf of IPEM by IOP Publishing Ltd. All rights reserved).

The acoustic field was measured by miniature hydrophone (diameter 0.2 mm), which was also used for correction of the phases. Ablations after the propagation of ultrasound through a human skull were created in the muscle tissue of the rabbit only with maximum possible power of 2624 W (at 41 W per channel) and an exposure of 8 seconds. The temperature increases on the surface of the skull ranged from 12.4 °C to 18.6 °C.

Furthermore Clement et al. (2000a) carried out a calculation of the sound pressures in the geometric centres of arrays of the same size, but differing only in the number of elements, i.e. 8, 11, 64, 228 or 501. The results are shown in Figure 18. It follows from the graph that the values of the square of the sound pressure for these arrays normalized to the corresponding value for the real 64 element array were 0.52, 0.56, 1.0, 1.4, and 1.52, respectively. This implies that the 64 element array significantly exceeded the performance the array with a small number of elements, but was not greatly inferior to more expensive and complicated arrays consisting of 200-500 elements.

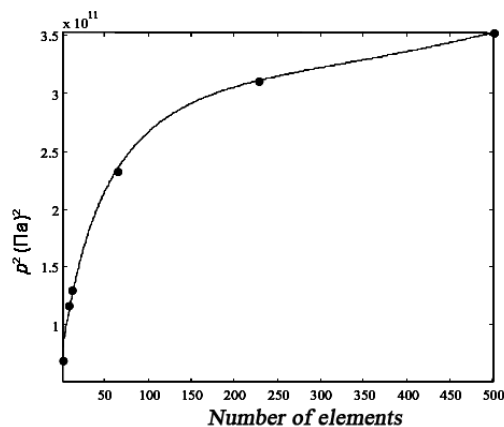


Figure 18. Dependence of the squared sound pressure after the propagation of ultrasound through the skull on the number of array elements (from Clement, G. T., Sun, J., Giesecke, T. & Hynynen, K. (2000). A hemisphere array for non invasive ultrasound surgery and therapy. *Phys. Med. Biol.* **45**, 3707-3719. © Institute of Physics and Engineering in Medicine. Published on behalf of IPEM by IOP Publishing Ltd. All rights reserved).

Regarding this conclusion it is worth noting that although the value of the intensity at the focus is very important, it is not the sole criterion for assessing the optimal characteristics and quality of the array. An almost equally important criterion is the level of grating lobes and other secondary intensity maxima when the focus is steered electronically off the geometrical focus. It

is this criterion which, to a large extent, determines the safe use of the array. As is shown in Chapter 3, it is necessary that the size of elements does not exceed a few wavelengths if the influence of the grating lobes is to be reduced. This inevitably leads to an increase in the number of elements.

Clement and Hynynen (2000) developed the concept of a noninvasive ultrasound transducer array for trans-skull ultrasound surgery and therapy and criteria for the design and characterization of large-area arrays for therapeutic and surgical procedures in the brain. The primary aim of their approach was to produce an array that can correct for the distortion of a focused beam caused by propagation through the skull bone and at the same time avoid significant skull heating during high power sonications. The number of array elements must be sufficient to correct for ultrasound diffraction and scattering, permit steering of the beam whether mechanically or electronically, and possess the ability to deliver therapeutic power levels. The surface area of the array must be large enough to minimize levels of skull heating to the point where it is safe for the patient as well as insignificant to cause severe changes in the acoustic properties of the bone. Further, the frequency must be optimized to allow for the maximum gain between the skull surface and the transducer. Two phased arrays of different design were developed. One of them was a hemisphere-shaped 64 element array with inner radius of 150 mm, and optimized in frequency ( $f = 0.67$  MHz). A second transducer was a 500-element PZT 1-3 composite array ( $f = 0.81$  MHz), designed to both restore the focus through the skull as well as electronically shift the beam. For this particular array an ability to steer beam electronically was evaluated. An effective range of steering approximately  $30 \times 30 \times 26$  mm was observed as bounded by the  $-6$  dB decrease of its maximum acoustic intensity. The level of grating lobes and side lobes related with steering of the focus was not reported in this paper. This array was also described in Clement et al. (2000a).

Studying the propagation of focused ultrasound through an intact skull, Clement and Hynynen (2002c) used a two-dimensional, 30 cm diameter, 0.74 MHz array consisting of 500 elements made of 1-3 piezocomposite (Imasonic, Lyon, France); of these 320 were active at any one time. To drive the elements a 500-channel amplifier (InSightec, Haifa, Israel) with a total power of 1800 W was used. Calculation of the set of phases and amplitudes, taking into account all data regarding the thickness and internal structure of bones, took about 5 hours on a personal computer (1 GHz, 256 MB RAM). To control the quality of focusing after the propagation of focused ultrasound through the skull, a PVDF- 0.2mm diameter hydrophone was used, which was moved by a 3D-positioner in a water tank. Measurements with a hydrophone allowed optimal tuning of the two-dimensional array and comparison of this method with the results of the calculation of phases. Calculations predicted intensities of approximately 45% of the intensity when setting of the phases were made using a hydrophone. According to the authors, the results of their studies demonstrated the feasibility of the proposed method for completely non-invasive neurosurgery and therapy by exposing the brain tissues through the intact skull.

Subsequently a hemispherical 500-element ultrasound phased array operating at a frequency in the range 700–800 kHz was used to investigate trans-skull brain tissue ablation (Hynynen et al. 2004; White et al. 2005; Clement et al. 2005).

White et al. (2005) developed a 448-element, 1-3 composite spherically focused array of diameter 120 mm and radius of curvature 120 mm (Imasonic, Lyon, France), operated at 1.1 MHz. The array consisted of elements distributed in a regular manner within 12 rings. The array was driven by a 256-channel phase-and-amplitude controllable amplifier system. The array was driven in two separate stages (channels 1–256, then channels 257–448) for each field measurement; the resulting scans were superimposed numerically to create the composite scan (Clement et al. 2000b). It will be shown in Chapter 3 that the annular array is the best choice of all two-dimensional regular arrays.

Liu et al. (2008) described hemispherical arrays operating at 270 kHz consisting of 22, 31 and 80 circular piezoceramic elements each of diameter 25 mm and carried out experiments *in vivo* in rats to investigate transcranial sonication to disrupt the blood-brain barrier.

Beginning in 2006, research was carried out using a clinical prototype ultrasound system ExAblate® 3000 manufactured by InSightec, Haifa, Israel (Hynynen et al. 2006). The basis of this system is a hemispherical ultrasound array with 512 equal area elements, a radius of curvature of 15 cm and operating at 670 kHz, manufactured by Imasonic, Besancon, France. Each of the array elements was driven with a separate RF line with independent amplitude and phase control. The multi-channel RF driver was computer controlled. The hemispherical array was positioned on a three dimensional manual positioning device that allowed it to be aimed at the target volume. The system was integrated within a 1.5-T MR-scanner. Initial trials in three glioblastoma patients were carried out recently using this system (McDannold et al. 2010), see Section 4.2.

Modifications to the InSightec system – namely the ExAblate 4000 TcMRgFUS, consisting of 1024 elements, have been described. The low-frequency variant operates at 220-230 kHz, and the high frequency one operates at 650-660 kHz. For example, the high-frequency modification was used in a hospital in Zurich for the treatment of chronic neuropathic pain (Martin et al. 2009) (see the details in Section 4.2). A thorough analysis of the low-frequency version of the ExAblate 4000 was reported by Hynynen and his colleagues (Pulkkinen et al. 2011). Their findings offered operators of therapeutic ultrasound devices an understanding of the potential dangers of base of the skull heating and suggested safety limits for thermal treatments operated at the frequency of 230 kHz.

Hynynen and his co-workers also proposed a new approach to the design of powerful arrays for ultrasound surgery (Hynynen and Yin 2009; Song and Hynynen 2010). This was based on the use of radially polarized cylinders as the array elements which were excited in their length resonant mode rather than a thickness resonance. The electrical impedance of elements defined by the wall thickness of the cylinder can be almost an order of magnitude lower than that for standard approaches. These workers designed and constructed a large hemispherical array consisting of 1372 cylindrical elements having an outer diameter of 10 mm and a height of 6 mm and a wall thickness of 1.24 mm. Operating frequencies of the array were 306 kHz and 840 kHz, and the maximum intensity on the array surface reached  $27 \text{ W cm}^{-2}$ . The matching of the elements was not required. The array allowed a single focus to be scanned within a cylindrical volume of diameter 10 cm, and height 6 cm at a frequency of 306 kHz, and a diameter of 3 cm and a height of 3 cm at 840 kHz. The lower frequency is more suitable for targeted drug delivery, and to modify the blood brain barrier, whilst the higher frequency is more appropriate when better quality focusing is required, for example, for thermotherapy.

In a study by another group (McGough et al. 2001), a calibration technique for two-dimensional arrays for which the location of centres of elements was not rigidly fixed, and for cases in which the uncertainty of the element centre locations was known, was described. Such a situation may arise, for example, if the array elements are mounted on a flexible base, which permits the geometry of the array to be changed. The calibration procedure proved to be very time-consuming, and it was concluded not to create variable configuration arrays. As a result of this research the authors fabricated an array consisting of 96 elements, each 7 x 7 mm (frequency 617 kHz), arranged on a square grid and driven at 617 kHz.

Evidence of the popularity of regular two-dimensional arrays is seen in the published work of Chinese researchers (Lu et al. 2005) in which the simulation of the distribution of acoustic fields created by a regular array was performed using a combination of known methods of calculation and an optimization algorithm proposed by the authors. The array consisted of 256 0.7 x 0.7 cm square elements, mounted on a regular square grid. The operating frequency was 1.1 MHz and the diameter of the array was 14 cm. A central hole 3.4 cm in diameter was provided in the array to accommodate an ultrasound imaging probe. A subsequent study by the

same authors (Lu et al. 2006) tested this array in a transparent tissue-like phantom (acrylamide/BSA) and in bovine eye and porcine liver tissues *in vitro*.

The arrangement of elements on a square grid was the most popular approach for several years (Ebbini and Cain 1991a; Fan and Hynynen 1996b; Wan et al. 1996; McGough et al. 1996; Daum and Hynynen 1998; Saleh and Smith 2004). However, as will be shown in the next Chapter, this distribution of elements on the array surface is associated with high levels of grating lobes. For example, in the last of the cited papers Saleh and Smith (2004) made and tested a two-dimensional array for the surgical treatment of benign prostatic hyperplasia. The frequency was 1.2 MHz. The array was 20 x 20 mm in size and consisted of 64 square elements, installed in a regular manner in the form of squares. The centre to centre distance was 2.5 mm, i.e. about  $3\lambda$ . When focused at a depth of 30 mm, and steered 6 mm laterally from the array axis, the intensity in the grating lobes exceeded 0.3 of the maximum intensity in the main focus. Increasing the lateral shift of the focus to 9 mm resulted in the intensities at the primary and secondary maxima being almost equal. Chapter 3 shows how using random arrays with similar characteristics would significantly improve the acoustic field

### 2.3. Possibilities to Generate and Steer Simultaneous Multiple Foci

Ebbini et al. (1988) were first to show the ability of a phased array to create two or more foci simultaneously. The feasibility of forming a region of heating or destruction by means of a customized set of synthesized foci led to a substantial interest in the potential use of high-power two-dimensional arrays in surgery and hyperthermia. Naturally, the calculation of the phase and amplitude of excitation signals on the elements, the number of which in modern therapeutic arrays can exceed 1000, became a challenge and required special calculation algorithms.

Ebbini and Cain (1989) developed a method for the synthesis of multifocal ultrasonic fields using therapeutic arrays. It enabled the phase and amplitude of signals necessary to generate a certain level of acoustic field in several "control points" in a given volume to be determined. In this method, called "pseudo-inverse",  $M$  foci are presented as a set of imaginary sound sources located on some plane, and then the total amplitude-phase distribution on the array elements switched on simultaneously are calculated. If we now apply the signals with the calculated amplitude and phase distribution, but changing the sign of the phases, to the array elements, we obtain in this plane the desired  $M$  foci. In principle, by using the "pseudo-inverse" method it is possible to create a region of impact of any predetermined size and configuration.

The ability of ultrasonic phased arrays to synthesize multiple foci in predetermined regions has been the subject of many studies (Ebbini and Cain 1989, 1991a,b; Damianou and Hynynen 1993; Fan and Hynynen 1996a,b; Wan et al. 1996; Daum and Hynynen 1998; Fjield et al. 1996). This feature is of considerable interest to applications in surgery, particularly, when the target is deep-seated tissue of relatively large volume. This mode of using arrays provides an opportunity to significantly reduce the duration of such a procedure as compared to the use of simpler focusing systems forming a single focus at a fixed focal distance (Fan and Hynynen 1996a,b).

Techniques for minimising overheating of tissues in the propagation path between ultrasound transducer and the intended treatment area have been discussed by many researchers (Ebbini and Cain 1991b; Damianou and Hynynen 1993; Fan and Hynynen 1996b; Wan et al. 1996; Daum and Hynynen 1998).

One method proposed by Ebbini and Cain (1991b) and later developed by others (Daum and Hynynen 1998, 1999; Fan and Hynynen 1996a,b) involved the following. Instead of a static field with a certain set of secondary maxima ("hot points"), fields of several configurations with a smaller number of foci switched electronically at a frequency of 10-20 Hz were generated. For example, a pattern of 25 foci can be synthesized using six configurations consisting of 1+4+4+4+8+4 foci, respectively (Figure 19).

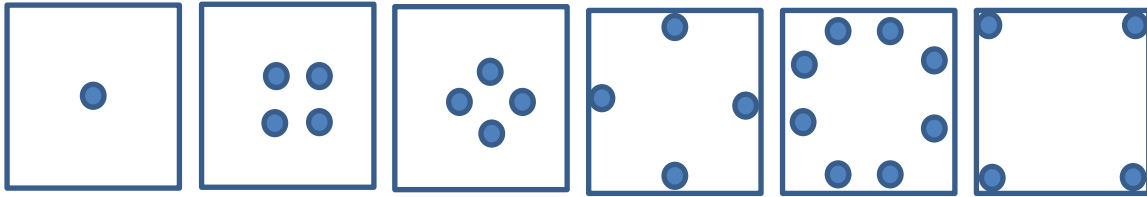


Figure 19. Six configurations consisting of 1+4+4+4+8+4 foci switching between which results in the formation of 25 foci.

However, keeping in mind that one of the major requirements for high-power therapeutic arrays is to achieve a sufficiently high intensity at the foci, the choice of this configuration cannot be considered successful. In one case, the acoustic power must be distributed among eight foci, and in another it must be released in only one of them. Since the intensities at all 25 foci must be approximately equal, the maximum intensity in the set of foci is finally determined by the intensity for the set of eight foci. Thus, the use of arrays with such a set of foci is inefficient.

Experiments in which multiple foci were generated were carried out both in water and in tissues *in vivo*. Referring to the original paper of Daum and Hynynen (1999), their figure 4 compares the calculated and measured (in water using a hydrophone) intensity distributions for 16 foci spaced at 5 mm and 25 foci spaced at 4 mm in the focal plane of the 256 element array. The authors noted excellent agreement between calculations and measurements and that the amplitude at the foci varied within 20% for 16 foci and more than 50% for 25 foci. However, these data demonstrated that even within a very limited area of the field in which the calculations and measurements were performed ( $\pm 15$  mm in both directions X and Y) there were significant grating lobes even in the absence of steering of these sets of foci off the axis of the array.

The optimal distance between the individual foci required to obtain uniform temperature distributions is dependent on the maximum temperature, duration of exposure, the size of the focus and volume of blood flow in the tissues and for this particular array was equal to 2-3 mm. Electrical switching of several groups of foci forming a predetermined set consisting of a large number of foci (e.g. 25 or 36), can reduce unwanted heating of the tissue in the pre-focal region.

This issue was addressed in more detail in Daum and Hynynen (1998). It was shown that switching groups of foci, each of which consists of a relatively small number of foci (usually 4-5 foci) can, in some cases, not only reduce the duration of the procedure, but also reduce the required average power and the unwanted heating of tissue.

The phases and amplitudes in the control points significantly influence on the spatial distribution of the acoustic field. The method of determining the phases and amplitudes in the control points was proposed by Fan and Hynynen (1995, 1996b). Normally the control points selected on a plane at a desired focal distance were evenly distributed on circles or squares with centres on the central axis. The phases of the control points on each circle or square were chosen out of phase such that the phase rotated around the central axis (this is similar to the phase rotation used in the sector-vortex array by Cain and Umemura (1986)). The amplitudes in the control points were chosen to be the same for all the points, which were equidistant from the central axis. This method of phase and amplitude selection produces destructive interference on the central axis and minimizes undesired peaks on the central axis. In the following studies the control points usually were selected on a square grid in the focal plane. Any four adjacent points forming a square and having a  $90^\circ$  phase difference between adjacent points were used for the phase rotation method.

The methods of calculations of acoustic fields created by two-dimensional array of different design will be discussed in detail in the next Chapter.

## 2.4. Research

To conclude this chapter we present a brief summary of some of the many research activities involving the use of regular two-dimensional phased arrays. A number of papers discuss the application of phased arrays to different strategies of ultrasonic hyperthermia and surgery. One example is that by McGough et al. (1996) which considers hyperthermia of the prostate. The hyperthermia procedure is discussed, including the use of computer tomography data of the heated object and the surrounding tissues, optimization of the exposure parameters, as well as the evaluation of data generated by computer modeling of acoustic and thermal fields to maximize therapeutic efficacy while minimizing the harmful side-effects.

In another theoretical study, Wan et al. (1996) investigated the problem of reducing the time required for a medical procedure to destroy a relatively large volume of tissue. Calculations were performed for a virtual array consisting of 1225 3 mm x 3 mm square elements distributed in a 35 x 35 pattern, driven at 1 MHz, and mounted on a surface of a sphere of radius of curvature 100 mm. The task was to ablate the volume of tissue of 10 x 10 x 10 mm<sup>3</sup> at a depth of several centimeters in the minimum time while avoiding tissue damage along ultrasound propagation path. It was assumed that the heating of the tissue volume was implemented by means of 41 foci. In the same work authors theoretically studied and compared several possible techniques for obtaining a large area of concentration of ultrasonic energy in tissues with the use of phased arrays. These included (1) successive scanning of the whole volume of a tissue with a single focus; (2) scanning by an "array" of several foci; and (3) simultaneous formation of multiple foci in tissue (without scanning) within the co-ordinates of the area of the tissue to be destroyed. Despite the differences between these approaches, they have the same "side effect," namely, the possibility of overheating the tissues outside the targeted region of sonication due to the appearance of secondary intensity maxima. The analysis showed that from this point of view, the worst results were obtained with the first method, commonly applied with the use of a single element focused radiator with a fixed focal distance. The best results (lowest dose, minimum intensity of side lobes, and the most uniform temperature distribution) were obtained using case 3. Thus, the simultaneous creation of many foci may lead to significant reduction in the time required for the surgical procedure, together with an acceptable level of tissue heating in the pre-focal region.

Fan and Hynynen (1996a) investigated the relationship between the duration of the ultrasonic pulse, acoustic power and the time required to minimize unwanted heating of tissues outside the targeted region. Using a single element focused transducer to ablate a large volume of tissue requires a large number of sonications and hence a long time to cool the normal tissues surrounding the irradiated volume. To shorten the procedure it is necessary to decrease the total number of pulses. This can be done by increasing the acoustic power and/or pulse duration. However, an upper limit to the increase of power is avoidance of boiling in the tissues and the formation of gas bubbles. At the same time, with increasing exposure duration, the cooling effect of blood flow increases. Thus, the only alternative is the formation of a larger and more homogeneous distribution of the temperature field in the tissue, which can be achieved using phased arrays. In this study it was shown that the use of even a relatively simple array (e.g., a 16-element array in the form of a part of a spherical shell) leads to a considerable saving in time required to ablate relatively large tissue volumes in comparison with single element focused transducers.

Experiments *in vivo*, carried out in tissues of 30-40 kg pigs, demonstrated that it was possible to thermally coagulate a tissue volume of 25 cm<sup>3</sup> in 90 min using a powerful two-dimensional array (Daum and Hynynen 1999).

Methods for determining the optimal amplitude correction to apply to the array elements that providing the best quality of focusing following ultrasound propagation through the skull were described by White et al. (2005). In principle, two approaches are possible. The essence of

the first of them is that if the attenuation in some site of the skull is large, the amplitude of the signal at the element located above it should be increased (or *vice versa*). The logic of the second method, which is quite different, is necessary to choose the amplitude on the elements so that the absorbed energy in all areas of the skull is approximately the same. Thus, the intensity at an element located above the highly absorbing site of the skull must be correspondingly smaller. Experiments performed by the authors showed that the quality of focusing in the second approach, which the authors called inverse amplitude correction method, was noticeably better, and the amplitude in the focus increased by 30 % compared to that achieved using the first approach.

In the paper of Ebbini et al. (1988) computer simulations of acoustic field produced by an array in the form of the cylinder with rectangular shaped transducers were carried out. Other computer simulations were conducted, and then based on these results several designs of the array that minimised the influence of the rib cage were tested for potential use in cardiology (Kluiwstra et al. 1995). The aim was achieved by switching off those elements located above the ribs. The quality of focusing remained very high even though the intensity level in the focus was reduced and the levels of grating lobes were increased. The problem of focusing of ultrasound and tissue ablation in the presence of rib cages will be discussed in detail in Section 4.4.

Sharifi and Soltanian-Zadeh (2001) described a computer simulation involving several variants of regular two-dimensional arrays intended for hyperthermia of tumours. In particular, it was shown that by using circular elements in regular arrays instead of square ones, the levels of the grating lobes produced by of the array were reduced. Steering the focus (foci) relative to the array axis was not considered in this paper.

Yin et al. (2004, 2006) calculated the acoustic and thermal fields produced by a miniature flat two-dimensional array, intended for noninvasive thermal destruction of heart muscle tissue by sonicating through the esophagus wall. This 1 MHz intracavitary array had dimensions of 10 x 60 mm<sup>2</sup>, with 20 x 114 elements spaced such that the centre to centre distance was 0.525 mm, a little more than 1/3 of the wavelength. The thickness of the esophageal wall was taken to be 4.4 mm. The simulation results proved the possibility of ultrasound focusing through the wall of the esophagus and the ability to steer the foci (up to 39 in number) in heart tissues at the required distance. Evaluation of the thermal dose in the tissue showed that it is sufficient to create thermal necrosis lesions of various sizes.

The conclusion of this Chapter is to some extent contradictory. Whilst the manufacture and testing of practical therapeutic multiple element arrays is a significant scientific and technological achievement, the quality of acoustic fields generated by the arrays described in this chapter, as estimated by the presence and level of unwanted grating lobes and other secondary intensity maxima in the acoustic field, leave something to be desired. Improved performance could be achieved by randomizing the locations of the array elements (Goss et al. 1996; Gavrilov and Hand 2000a,b). The detailed description of this method is given in the next Chapter.

## Two-Dimensional Phased Arrays with a Random Distribution of Elements

This Chapter discusses two-dimensional phased arrays with elements distributed randomly on their surfaces. Numerical simulations of such arrays with spherical section surfaces and comparative analyses of acoustic fields generated by phased arrays with elements distributed randomly and in a regular pattern are presented below. The influence of the dimensions, number, and shape of individual elements, errors in phase settings at the elements, and frequency modulation of the signal on the quality of the intensity distributions produced by random arrays is also analyzed. Designs of practical two-dimensional phased arrays with randomly distributed elements are discussed and evidence is provided that use of random arrays often provides better spatial distributions of intensity compared to those for regular arrays. The results presented lead to designs that offer the opportunity to minimize the influence of grating lobes whilst using a relatively small number of elements and, hence, to increase the safety of the use of such systems in surgery.

### 3.1. The Basis of the Method

As mentioned in the previous Chapters, if the influence of the grating lobes in the acoustic field of an array is to be reduced, then the distance between the centres of its elements must be less than  $\lambda/2$  (Skolnik 1962), where  $\lambda$  is the wavelength, i.e., for example, less than 0.5 mm at 1.5 MHz. In the case of powerful phased arrays compliance with this condition is difficult to achieve in practice since it requires an impractically large number of elements and electronic channels to achieve a large enough aperture and sufficient acoustic power for therapeutic applications.

The level of grating lobes in the field produced by an array depends on the spatial regularity of the array structure. This regularity is destroyed if the array elements are randomly distributed over its surface. For example, several authors have shown that a much higher quality of ultrasonic intensity distribution in the field may be produced by random arrays compared with regular arrays (Goss et al. 1996; Gavrilov and Hand 2000a, b; Gavrilov et al. 2000). A similar approach is known, for example, in radar (Skolnik 1962), but the effect of randomization of the element distribution in that application does not manifest itself as noticeably as in the case of high-power ultrasonic arrays. It is much simpler to manufacture electromagnetic arrays in which the distance between the element centres is smaller than the electromagnetic half-wavelength thereby eliminating the grating lobes associated with the array structure since the velocity of light is much greater than that of sound.

Moreover, in radar, a common practice was to consider regular multi-element arrays of which some active elements were taken out in a random way (Skolnik 1962). The work of Goss et al. (1996) clearly illustrates the effect of this approach to multi-element ultrasound phased arrays with the regular structure. An experimental array was constructed using 108 individual PZT-8 piezoceramic transducers 8 mm in diameter and with an operating frequency of 2.1 MHz. The active face of the transducers defined a sphere with a diameter of approximately 100 mm and a radius of curvature of approximately 102 mm. In experiments, only 64 randomly chosen elements were excited simultaneously. A sketch of the hexagonal array identifying those excited elements is shown in Figure 20.

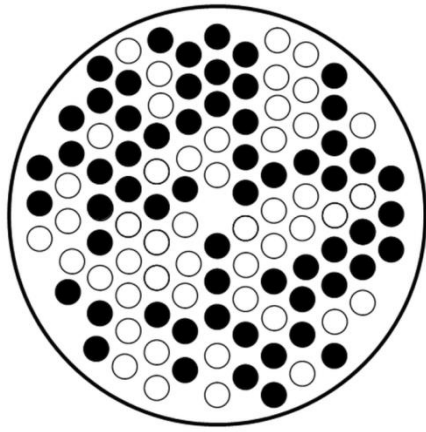


Figure 20. Sketch showing a subset of excited elements (filled circles) at random locations within a set of elements on a regular hexagonal grid (after Goss et al. 1996).

Referring to the original paper by Goss et al. (1996), their figure 3 depicts that in spite of the random selection of the subset of 64 elements from the total set of elements positioned on a regular hexagonal grid, the acoustic field demonstrates six grating lobes corresponding to the initial regularity of the array structure. Thus these data show that this method of randomizing the array based on the extraction of some of the elements from the regular structure of the array is not very effective in reducing grating lobes.

Goss et al. (1996) also demonstrated theoretically that the use of elements randomly distributed at the array surface leads to an improved spatial distribution of intensity in the field.

Subsequently the authors of this book developed this approach based on several conditions, namely (1) randomization of the distribution of the elements over the surface of the array; (2) the elements should not be very directive, i.e. their diameters must not exceed five wavelengths; (3) the sparseness of the array should not be excessive and not less than 40%. Further details can be found in several patents (Hand and Gavrilov 2000, 2002 a-c).

It is worth noting that in the work of Goss et al. (1996) one of these conditions was not satisfied and the diameter of the elements (8 mm for the frequency 2.1 MHz) was equal to  $11.2 \lambda$ . As a result, the level of grating lobes in that study was relatively high.

It will be shown in this section that, with the use of randomization of the element distribution in a high-power two-dimensional array, it is possible in some cases to increase the element size up to five sound wavelengths while retaining an acceptable level of side lobes. In Gavrilov and Hand (2000a, b) and Gavrilov et al. (2000) it was shown that sparse apertures with randomly distributed elements reduce the grating lobes by spreading their energy among the side lobes, whose level increases slightly.

Another important point for practical random arrays is to achieve using maximally tight packing of elements (see Section 3.8). Randomization of the distribution of elements *per se* and need to avoid making them directive is more important than their sparseness.

### 3.2. Methods of Calculations of Ultrasound Fields Generated by the Arrays

Calculations of intensity distributions induced by two-dimensional phased arrays are described in a number of works (Goss et al. 1996, Gavrilov and Hand 2000a,b). There are three main stages: (i) calculation of the distribution of the complex sound pressure generated by a single radiating element in the shape of a disk; (ii) calculation of the distribution of the total complex sound pressure from all single elements positioned on a section of a spherical shell; and (iii) calculation of the distribution of relative intensity in the field produced by the whole array and the analysis of such distributions with the use of criteria for the evaluation of the distribution quality. Figure 21 (Gavrilov and Hand 2000a) is a schematic illustration of the method used.

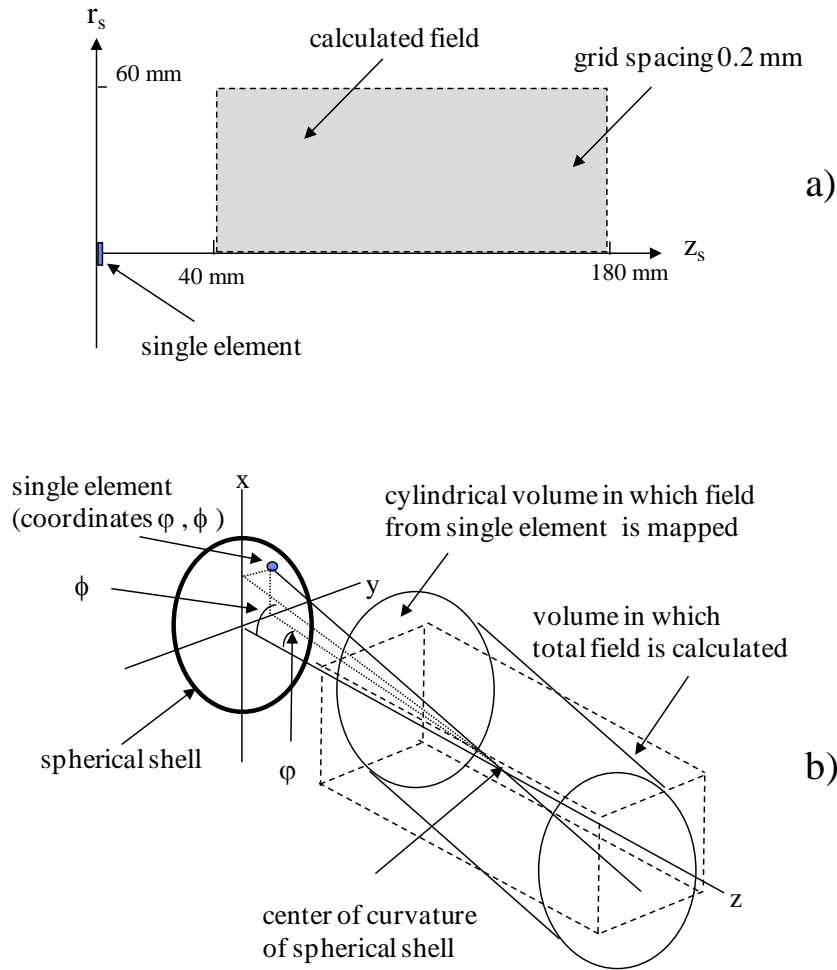


Figure 21. Schematic illustration of the method used for calculations: (a) calculated field of a single element; (b) calculated field of an array (Gavrilov and Hand 2000a).

The complex pressure distribution associated with a single plane circular element is found using the Point Radiator Method (or the Point Source Method) in which the acoustic piston source is represented by many point radiators (Ocheltree and Frizzell 1989). Square elemental radiators of side length 0.25 mm are used to describe the radiating surface of each circular element. Assuming radial symmetry for a circular element, its 3-dimensional acoustic field is found (Goss et al. 1996) by calculating the complex pressure  $p(r_s, z_s)$  as a function of axial distance from the element,  $z_s$ , and distance off its central axis,  $r_s$  according to

$$p(r_s, z_s) = \frac{j\rho c k u_o \Delta A}{2\pi} \sum_{\text{surface}} \frac{e^{-(\alpha + jk)R}}{R} \quad (3)$$

where  $\rho$  is the tissue density ( $= 1000 \text{ kg m}^{-3}$ ),  $c$  is speed of sound in the tissue ( $= 1500 \text{ m s}^{-1}$ ),  $k$  is the propagation constant,  $u_o$  is the velocity amplitude of the surface of the elemental sources,  $\Delta A$  is the area of each elemental source,  $\alpha$  is the attenuation coefficient in the tissue and  $R$  is the distance from the centre of an elemental source to the point  $(r_s, z_s)$  where the field is calculated. In Gavrilov and Hand (2000a,b) calculations were carried out for  $40 \leq z_s \leq 180 \text{ mm}$  and  $0 \leq r_s \leq 60 \text{ mm}$ , both in spatial increments of 0.2 mm (Figure 21a). The attenuation coefficient in the tissue  $\alpha$  was taken to be  $10 \text{ Np m}^{-1} \text{ MHz}^{-1}$ , which, although towards the high end of the range found in the literature (Duck 1990), is a value used by many authors for similar calculations (Fan

and Hynynen 1996a; Ebbini and Cain 1991b; Hutchinson et al. 1996; Hutchinson and Hynynen 1996).

The total complex pressure distributions from various arrays of plane circular elements mounted on a spherical shell are calculated by summing the complex pressure contributions from each element in an array at each point in the 3-dimensional volume of interest (Figure 21b). Knowing the complex pressure as a function of axial and radial distances for the single element whose centre is defined by the angular co-ordinates  $\phi$  and  $\varphi$  (the angles subtended at the centre of curvature in the vertical and horizontal planes, respectively), the values are mapped from the rotated cylindrical volume to points on a 0.2 mm, 3-dimension rectangular array aligned with the Cartesian axes. In Gavrilov and Hand (2000a,b) calculations are carried out over the volume defined by  $50 \leq z \leq 160$  mm axially and  $-30 \leq x$  and  $y \leq 30$  mm (in a few cases to  $\pm 40$  mm to ensure inclusion of grating lobes). The relative phases of the surface velocity at each circular element required to produce a single focus are determined from the paths between the centres of each element and the position of the focus. Finally, the intensity in each cell of the array was calculated and the intensity distribution normalized with respect to the maximum value of intensity in the region of analysis is determined.

To form and move several foci, this method is modified as follows. To produce simultaneous multiple foci, the complex surface velocity  $u_n$  at the  $n^{\text{th}}$  of the  $N$  circular elements is determined using the method first described by Ebbini and Cain (1991b). The  $u_n$  are related to the complex pressures  $p_m$  at each of  $M$  target or control points, by the matrix equation

$$\mathbf{u} = \mathbf{H}^{*t} (\mathbf{H}\mathbf{H}^{*t})^{-1} \mathbf{p} \quad (4)$$

where  $\mathbf{u} = [u_1, u_2, \dots, u_n, \dots, u_N]^t$ ,  $\mathbf{p} = [p_1, p_2, \dots, p_m, \dots, p_M]^t$ , and  $\mathbf{H}$  is the  $M \times N$  matrix with

elements  $h_{mn} = \frac{j\rho ck}{2\pi} \int_S \frac{e^{-ikr_{mn}}}{r_{mn}} dS$  where  $\rho$  is the tissue density,  $c$  is speed of sound in the

tissue,  $k$  is the propagation constant,  $S$  is the area of an element of the array;  $r_{mn}$  is the distance from the  $m^{\text{th}}$  target point to the centre of the  $n^{\text{th}}$  element.  $\mathbf{H}^{*t}$  is the conjugate transpose of  $\mathbf{H}$  and  $[ ]^t$  denotes transpose. The set of  $M$  target points is selected to be within the same focal plane and to lie on a uniformly spaced  $\sqrt{M} \times \sqrt{M}$  grid. To determine the  $u_n$  ( $n = 1, 2, \dots, N$ ) the phases and amplitudes of the  $p_m$  ( $m = 1, 2, \dots, M$ ) must be selected. The amplitudes in the control points can be equal or different; the method of selection of the phases in the control points depends on the specific problem and will be discussed later.

Thus, as the result of calculation, a certain initial distribution of amplitudes and phases over all elements is obtained, at which the indicated  $M$  foci are formed. It is clear that many such combinations are possible with both large and small amplitudes of signals at the elements. Since the aim of calculation is not only to produce a preset number of foci in a given place but also to provide maximum power from the array, it is necessary to determine a phase distribution over the elements such that the desired  $M$  foci are formed at equal amplitudes at the elements. Therefore, in calculating the multiple focus ultrasonic fields, it is necessary to use optimization techniques that provide an opportunity to obtain the preset number of foci at equal amplitudes at all elements and thereby attain the maximum acoustic power of the array. In the calculations described, the optimization technique proposed in Ebbini and Cain (1989) is used. After a series of iterations, the number of which can reach several dozens for a large number of foci, a certain new phase distribution, at which the array efficiency (the ratio of the real power to the maximum possible power) is not less than 99%, is obtained. For a small number of foci (four to five), only one or a few iterations are usually required.

Details of the method for calculating multiple foci ultrasound fields are presented with different degrees of details in a number of papers by Cain and his colleagues (Wang et al. 1990; Ebbini and Cain 1991a,b), as well as by others who have used the pseudo-inverse method for

calculating multi-focal ultrasonic fields produced by arrays and lenses of various configurations (Lalonde et al. 1993; Buchanan and Hynynen 1994; Fan and Hynynen 1996b; Daum and Hynynen 1999; Gavrilov and Hand 2000a,b; Gavrilov et al. 2000; Gavrilov 2003; Filonenko et al. 2004; Lu et al. 2005).

A significant qualitative breakthrough in the development of methods to calculate ultrasound fields created by multi-element phased array was made recently by Sapozhnikov and his co-workers (Ilyin et al. 2012). As mentioned previously, the field of each array element can be calculated using the Rayleigh integral. Usually, the calculation of that integral is performed numerically. However, in view of the fact that the characteristic dimensions of the elements of existing arrays is much smaller than the dimensions of the array ( $a \ll D$ ), the Rayleigh diffraction length of a single element is much smaller than the radius of curvature  $F$  of the surface of the array. In that case, the field of each element can be approximated by the analytic solution in the far field already at small distances from the surface of the array. Although the analytic solution for a single circular piston radiator is well known (O'Neil 1949), it has not been used to calculate the fields of therapeutic multi-element arrays.

In the far field approximation for each of the plane circular elements of the array, the solution has the following form:

$$p_i(\theta, r) = -\frac{ip_0 z_R e^{ikr}}{r} \frac{2J_1(ka \sin \theta)}{ka \sin \theta}, \quad (5)$$

where  $p_0$  is the pressure on element surface,  $k$  is the wavenumber,  $a$  is the radius of the element,  $z_R = ka^2/2$  is the Rayleigh length,  $r$  is the distance from the centre of the element to the point in the field,  $\theta$  is the angle between the element axis and the ray from the centre of the element to the field point, and  $J_1$  is a Bessel function of first order.

Since this solution is applicable only for the far field of the element, the solution was compared with the exact analytical solution along the axis of the transducer. As can be seen from the Figure 22, an approximate analytic solution is very similar to the exact one starting from a distance of 3.5 cm from the element. This enables the far field solution of each element to be used to calculate the entire field of the array which is obtained by summing the solutions for each element:

$$p(\vec{r}) = \sum_i p_i(\theta, r). \quad (6)$$

In case of steering the focus, the initial phase for each of the array elements is set based on the delay of the arrival of waves from the centre of the element to the new focus.

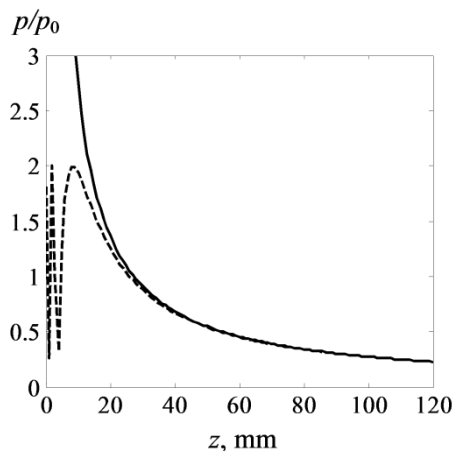


Figure 22. Comparison of pressure distributions along the axis of the element of the array in the case of the exact analytic solution (dash-dotted curve) and analytic solution in the far field of element (solid curve) (Ilyin et al. 2012).

To test the accuracy of the analytic approach, the solution obtained for the entire field of the array was compared with the solution obtained by direct numerical calculation of the Rayleigh integral over the surface of the array (Figure 23). The distributions show that the analytic solution is practically indistinguishable from the numerical one. Moreover, calculations based on the analytic approach were conducted much faster (40 times) than those using a numerical solution.

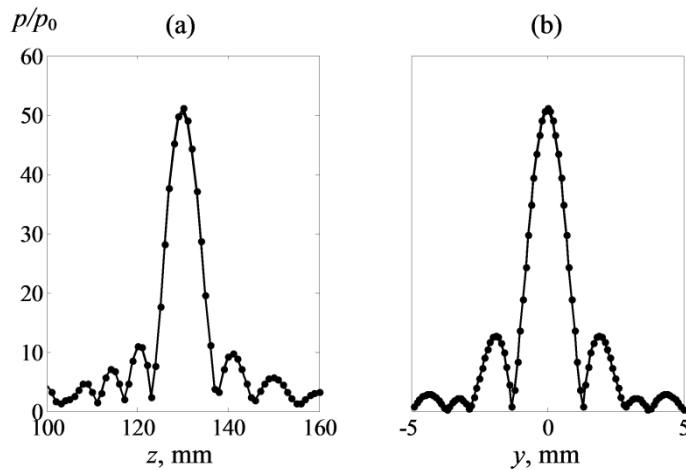


Figure 23. A comparison of pressure distributions along the axis of the array (a) and along the line, which is perpendicular to the array's axis and passing through its centre of curvature (b) in case of an analytic solution (solid line) and direct numerical calculation of the Rayleigh integral (points) (Ilyin et al. 2012).

The proposed method enables the calculation of the field of multi-element phased array to be performed much faster than by direct numerical calculations, while maintaining high accuracy of the results. This method is particularly promising in the analysis of multiple foci acoustic fields generated by an array. It not only allows a very quick assessment of fields of two-dimensional arrays, but also, if necessary, to carry out calculations of three-dimensional fields produced by such arrays within a reasonable computer run time.

### 3.3. Generation and Steering of a Single Focus, Data from Modeling

Gavrilov and Hand (2000a,b) reported calculations of the sound pressure and intensity field distributions. The 2-dimensional intensity distributions represent the main data in the  $y$ - $z$  plane. This plane contained the ultrasound focus when it was not coincident with the centre of curvature and was a “worst case” in terms of the level of grating lobes. In some cases (see below), calculations were also carried out with the focus located in the  $x$ - $z$  plane.

The influence on array performance of several parameters such as the number of elements (64, 128, 255, 256 and 1024), their diameter (2.5, 5, 7, and 10 mm), frequency (1, 1.5 and 2 MHz) and level of sparseness was investigated. Calculations were made for arrays with elements distributed randomly on the shell (see Figure 24) as well as for arrays with elements distributed regularly on the shell in square, annular and hexagonal patterns (Figure 25). The diameters of all the arrays presented in Figure 24 (which shows the locations but not the dimensions of the elements) were equal to 110 mm.

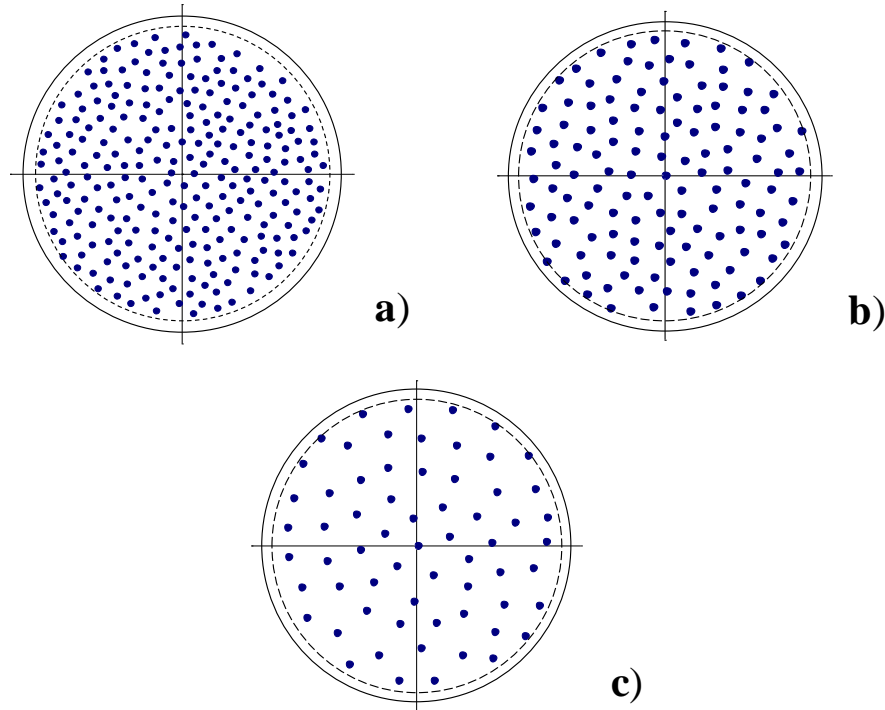


Figure 24. Schematic drawings of arrays with plane circular elements distributed on the spherical shell in a quasi-random manner: (a) 256 elements, each 5 mm in diameter; (b) 128 elements, each 7 mm in diameter; (c) 64 elements, each 10 mm in diameter. The minimum centre to centre distance between elements is 5.5 mm, 7.5 mm and 10.5 mm, respectively. The diameter of all arrays is 110 mm and the maximum centre to centre distance between elements is 100 mm (Gavrilov and Hand 2000).

The first array consisted of 256 elements, each 5 mm in diameter, distributed in a quasi-random manner (a completely random distribution was modified such that the minimum separation between the centres of elements was 5.5 mm) and is shown schematically in Figure 24a. Three driving frequencies were considered, namely 1, 1.5, and 2 MHz. Several similar quasi-random distributions of elements on the shell were investigated but the differences in results were negligible. Calculations were also made for quasi-randomly distributed arrays of 128 elements, each 7 mm in diameter (Figure 24b), and of 64 elements, each 10 mm in diameter (Figure 24c). The frequency in both of these cases was 1.5 MHz and the minimum separation between centres of elements was 7.5 and 10.5 mm, respectively.

Figure 25 illustrates some regular arrays investigated; all were assumed to operate at 1.5 MHz. Figure 25a is a schematic representation of an array of 256 elements, each 5 mm in diameter, placed on the shell in a square configuration. The minimum separation between centres was 5.5 mm. Figure 25b shows a similar array of 1024 elements, each 2.5 mm in diameter; in this case the centre to centre spacing was 2.75 mm. Figure 25c shows an annular array of 255 elements, each 5 mm in diameter, consisting of a central element and 9 concentric rings with radii increasing from 5.5 mm to 49.5 mm in multiples of 5.5 mm. The rings contain 5, 11, 17, 23, 28, 33, 40, 46 and 51 elements, respectively with centre to centre spacing of 6 mm. Figure 25d shows an array consisting of 255 elements, each 5 mm in diameter, placed in a hexagonal configuration with centre to centre spacing of 5.5 mm. The arrays shown in Figure 25 have approximately the same (within 1.5%) active area of 50 cm<sup>2</sup> and so, in theory, should be able to provide approximately the same acoustic power.

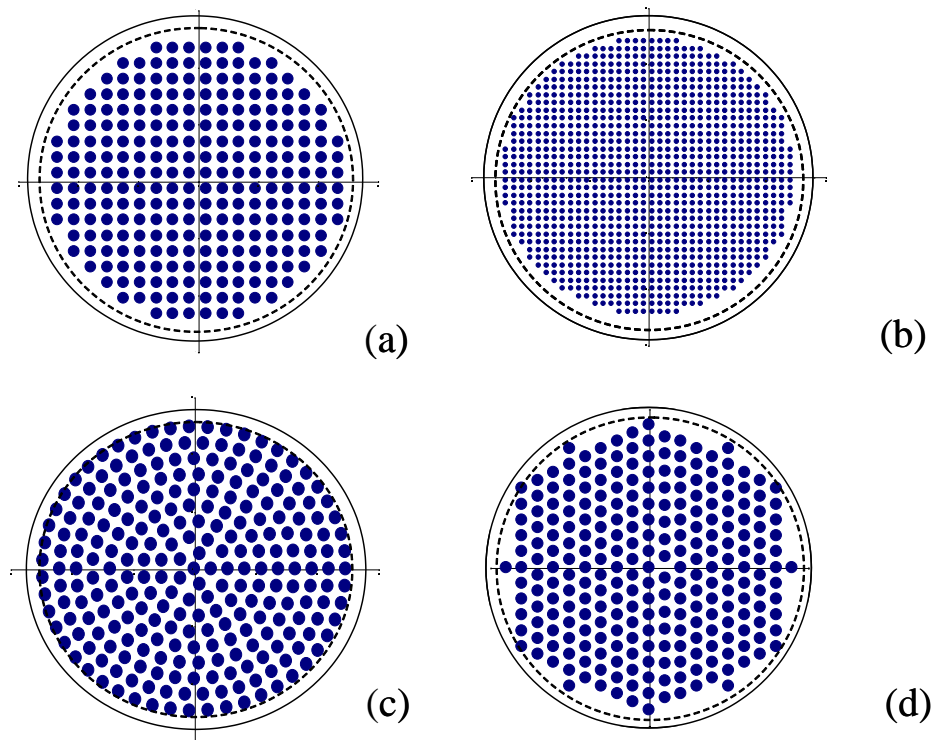


Figure 25. Schematic drawing of arrays with circular elements distributed on the spherical shell in regular patterns: (a) 256 elements, each 5 mm in diameter distributed in a square pattern; (b) 1024 elements, each 2.5 mm in diameter distributed in a square pattern; (c) 255 elements, each 5 mm in diameter, distributed in an annular pattern; (d) 255 elements, each 5 mm in diameter, distributed in a hexagonal pattern. The diameter of all arrays is 110 mm (Gavrilov and Hand 2000a,b)

In Gavrilov and Hand (2000a,b), four criteria were selected to assess the “quality” of the normalized intensity distributions calculated for the above arrays used to produce a single focus (see Figure 26). First, an intensity distribution was deemed to be “grade A” when intensity  $I \geq 0.1 I_{max}$  occurred only within the focal region and was absent in the remainder of the plane investigated. This criterion is in agreement with the commonly expressed opinion that the maximum intensity in grating lobes should be at least 8-10 dB lower than that in the main lobe for safe delivery of treatment (Goss et al. 1996; Ebbini and Cain 1991; Hutchinson et al. 1996). The intensity distribution was described as “grade B” when there were less than 10 localized areas in which the intensity was in the range  $0.1 \leq I \leq 0.15 I_{max}$  outside the focal area in the plane considered. Intensity distributions with more than 10 localized areas outside the focal area in the plane considered in which  $0.1 \leq I < 0.15 I_{max}$  were classified “grade C”. Finally, further discrimination amongst poor intensity distributions was provided by a “grade D” classification for those where there was at least one localized area in which  $I \geq 0.2 I_{max}$ .

Figure 26 show examples of intensity distributions for the random array of 256 x 5 mm elements (see Figure 24a) driven at a frequency of 1.5 MHz in the single focus mode. It illustrates the dependence of quality of the intensity distribution on the location of the focus. Displacement of the focus from 10 mm to 16 mm off the acoustic axis (at a range of 110 mm) changes the quality from grade A to grade D. In Figure 26a nine contours (10-90%  $I_{max}$  in increments of 10%  $I_{max}$ ) are drawn inside the focal region. The intensity distribution in the remainder of the plane outside the focal region was assessed in terms of contours at 10-20%  $I_{max}$  in increments of 5%  $I_{max}$  and, in a few cases, by contours at 10-20%  $I_{max}$  in increments of 2%  $I_{max}$ .

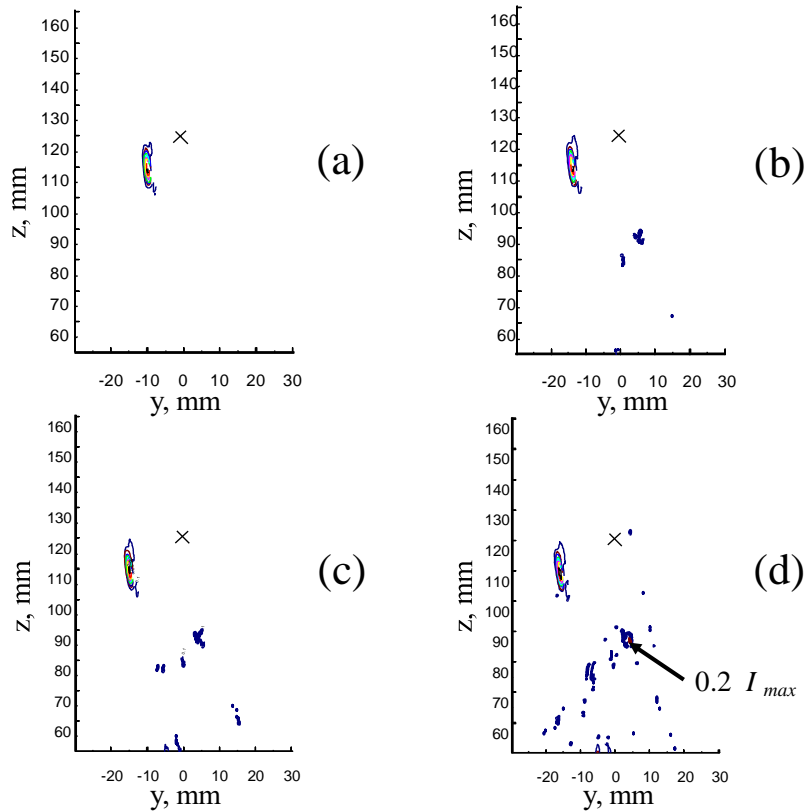


Figure 26. Examples of the intensity field distributions for the single focus mode and criteria used for estimating the quality of the intensity distributions: (a) A grade; (b) B grade; (c) C grade; (d) D grade. The symbol “ $\times$ ” corresponds to the location of the centre of curvature. These examples are for a random array of 256 5 mm diameter circular elements driven at 1.5 MHz. The focus is located at (0, -10, 110 mm) (a); (0, -14, 110 mm) (b); (0, -15, 110 mm) (c); (0, -16, 110 mm) (d) (Gavrilov and Hand 2000a,b).

Characterization of the intensity distributions associated with this array driven at 1, 1.5 and 2 MHz is summarized in Figure 27 (Gavrilov and Hand 2000a,b). Figures 27-29 present data for displacements of the focus in the positive  $y$ -direction. Calculations were also carried out for foci displaced in the negative  $y$ -direction and the results were qualitatively very similar. Quantitative differences in intensity distributions were typically very small.

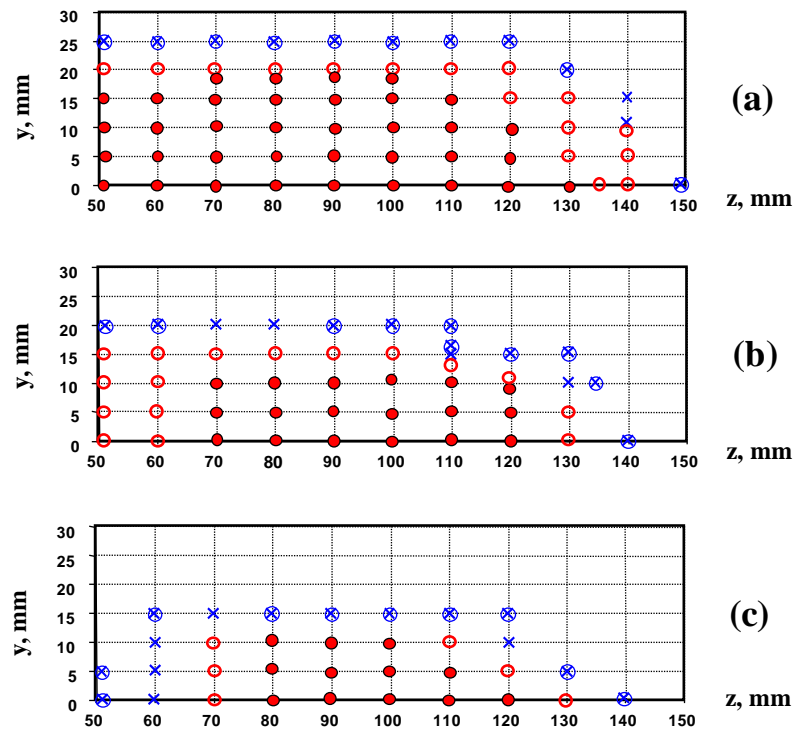


Figure 27. Summary of results of calculations and quality assessment of the intensity distributions for the single focus mode associated with the random array of 256 5 mm diameter elements (Figure 24a). Frequencies: (a) 1 MHz; (b) 1.5 MHz; (c) 2 MHz. The quality levels are: ● A grade; ○ B grade; × C grade; ⊗ D grade (Gavrilo and Hand 2000a,b).

In contrast to the study of Goss et al. (1996), Gavrilo and Hand (2000a,b) analyzed the ratios of the secondary and main intensities not only in the focal plane, but also in a relatively large field of interest anterior to and beyond the focus. It was shown that a random array of 256 5 mm diameter elements excited at 1 MHz could scan the focus over distances up to  $\pm 20$  mm from the acoustic axis, for  $z$  values (axial distances) ranging from 50 to 130 mm, and still maintain the highest quality criterion (A) (Figure 27a). In the single focus mode, the 1 MHz array consisting of 256 plane circular elements, each 5 mm in diameter, distributed in a quasi-random manner could steer the focus up to  $\pm 20$  mm off the central axis for  $z$  ranging from 50 mm to 120 - 140 mm and still achieve a good quality rating (grades A - B) (see Figure 27a). At 1.5 MHz, the distances over which the focus could be steered compatible with A and B ratings were  $\pm 10$  mm for  $z$  ranging from 70 mm to 120 mm and  $\pm 15$  mm for  $z$  ranging from 50 mm to 120 mm, respectively (Figure 27b). At 1 MHz the volume of the targeted region in which intensity distributions had quality A was  $63 \text{ cm}^3$  whilst that for quality B was  $106 \text{ cm}^3$  (Figure 27a); at 1.5 MHz the volumes were  $16 \text{ cm}^3$  and  $49 \text{ cm}^3$ , respectively (Figure 27b). At 2 MHz, the volumes were reduced to  $12.5 \text{ cm}^3$  and  $16 \text{ cm}^3$ , respectively (Figure 27c).

The performance of the array as assessed by the quality of the intensity distribution is dependent upon both the distance of the focus from the centre of curvature of the shell and attenuation. Figure 27 shows that when the focus is steered beyond the centre of curvature, the quality of the intensity distribution is degraded abruptly. It is seen also that the greatest steering of the focus off centre with a grade A quality may be achieved at a range approximately 1- 2 cm proximal to the centre of curvature.

In the array consisting of 256 5 mm diameter elements the ratio of the total area of elements (active area) to the area of the shell was approximately 51%. Assessments of the intensity distributions for the 1.5 MHz random arrays of 128 7 mm diameter elements (see Figure 24b) and 64 10 mm diameter elements (see Figure 24c) are shown in Figures 28b and 28c,

respectively. Data shown in Figures 27 and 28 were based on calculations carried out with the focus located in the  $y$ - $z$  plane. Calculations in the  $x$ - $z$  plane (not shown here) gave qualitatively very similar results.

It is seen that significant deterioration of the array performance occurs when the sparseness of the array is increased (half of the 256 elements were switched off at random) (Figure 28a). In this case, not only did the useful treatment volume become much smaller, but the greatest range at which the focus could be located compatible with an A-graded intensity distribution rating, was reduced to 100 mm. Decreasing the number of randomly distributed elements from 256 through 128 to 64, whilst simultaneously increasing the diameter of the elements (from 5 mm through 7 mm to 10 mm, respectively) to maintain a constant active area also led to progressive deterioration of the array's performance (Figures 28b and 28c). The differences in the qualities of intensity distributions associated with the array of 128 elements, each 5 mm in diameter, and that of 128 elements, each 7 mm in diameter, and therefore of higher directivity at the same frequency, were not great (Figures 28a and 28b).

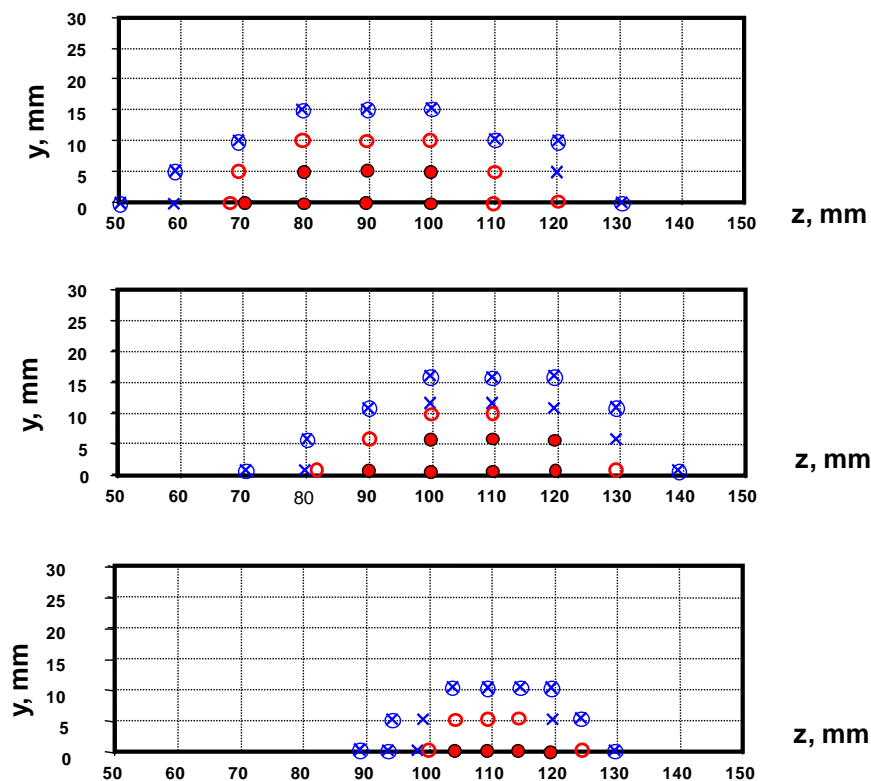


Figure 28. Assessment of the quality of intensity distributions for the single focus mode associated with (a) the random array consisting of 128 elements, randomly selected from the 256 x 5 mm elements array shown in Figure 24a; (b) the array of 128 x 7 mm diameter randomly distributed circular elements (Figure 24b); (c) the array of 64 x 10 mm diameter randomly distributed circular elements (Figure 24c). The frequency is 1.5 MHz. The meaning of the symbols is as in Figure 27 (Gavrilov and Hand 2000a,b).

The results of assessing intensity distributions for 1.5 MHz, regular spaced arrays (see Figures 25a - d) are shown in Figure 29 (Gavrilov and Hand 2000a,b). For the regular arrays with square and annular patterns, calculations were carried out with the focus located in the  $y$ - $z$  plane. Calculations were also made in the  $x$ - $z$  plane (not presented) and gave qualitatively very similar results. The hexagonal regular array had different performance in  $y$ - $z$  and  $x$ - $z$  planes and both are shown in Figure 30 (Gavrilov and Hand 2000a,b).

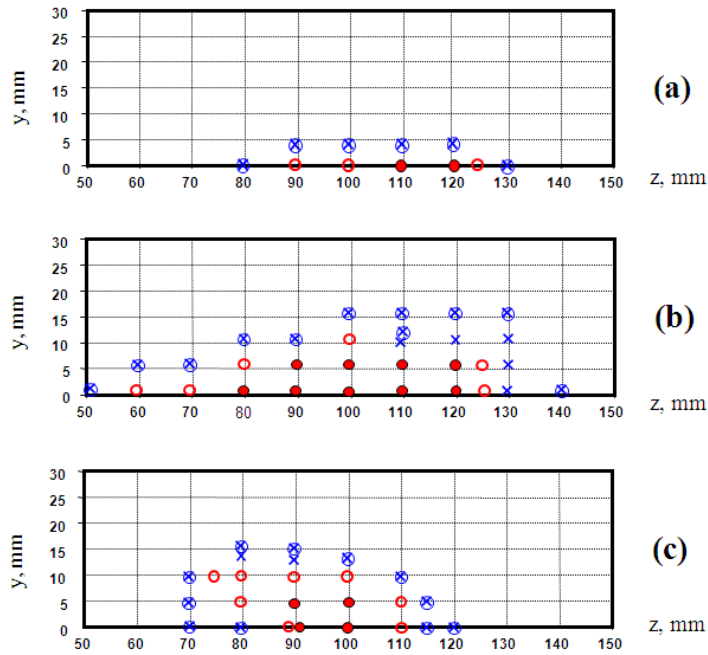


Figure 29. Assessment of the intensity distributions for the single focus mode associated with regular arrays: (a) 256 elements, each 5 mm diameter, distributed on the shell in a square pattern (Figure 25a); (b) 1024 elements, each 2.5 mm diameter, distributed on the shell in a square pattern (Figure 25b); (c) 255 elements, each 5 mm diameter, distributed on the shell in an annular pattern (Figure 25c). The frequency is 1.5 MHz. The meaning of the symbols is as in Figure 27 (Gavrilov and Hand 2000a,b).

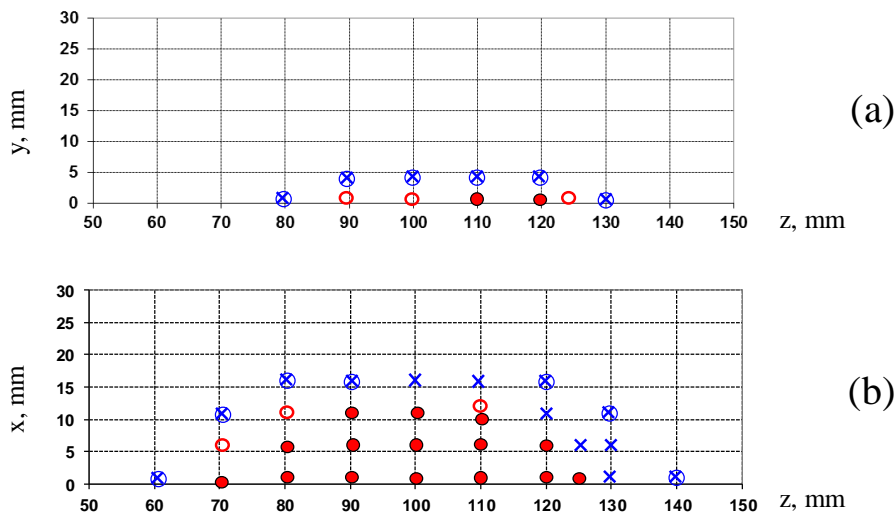


Figure 30. Assessment of the intensity distributions for the single focus mode associated with regular array of 256 elements, each 5 mm diameter, distributed on the shell in a hexagonal pattern (Figure 25d): (a) shift of the focus in y-z plane; (b) shift of the focus in x-z plane. The frequency is 1.5 MHz. The meaning of the symbols is as in Figure 27 (Gavrilov and Hand 2000a,b).

It is seen that in the single focus mode, the performance of arrays consisting of 255 or 256 5 mm elements driven at 1.5 MHz and distributed as square, annular or hexagonal patterns (Figures 29a, 29c and 30a) was considerably inferior to that of the 1.5 MHz 256 5 mm elements random array (Figure 27b). As was mentioned previously, the calculations were carried out with displacements of the focus in both y-z and x-z planes. For arrays with square (Figures 25a, 25b) or annular (Figure 25c) patterns, the intensity distributions in the y-z and x-z planes were the same or essentially the same; therefore, in these cases, only the data for the y-z plane are reported

here. If the projected views of the array structure from location of the focus were different, as in the case of the hexagonal array, the intensity distributions in the  $y$ - $z$  and  $x$ - $z$  planes were also different (Figures 30a, 32b). The best performance amongst the regular arrays of 255 or 256 elements was that associated with the annular pattern (Figure 29c); the poorest was that associated with the square pattern (Figure 29a).

The performance of the 1024 2.5 mm element square array (Figure 29b) was considerably inferior to that of the 1.5 MHz 256 5 mm element random array (Figure 29b) but comparable with the 128 7 mm element random array (Figure 28b). This implies that randomization of the elements in the array leads in this case to a (6-7)-fold decrease in the number of elements (and driving channels) that maintains approximately the same quality of intensity distribution.

There was a marked difference in the character of the intensity distributions associated with arrays with randomly and regularly distributed elements. In the former only secondary intensity maxima outside the focal area were observed and grating lobes in the focal plane occurred only in the intensity distributions of very poor quality (data not presented). In the case of regular arrays, relatively high intensities corresponding to grating lobes were seen in the focal plane only.

The results of single focus studies show that if beneficial effects of randomization are to be achieved, then the sparseness of the random array with disk shaped elements should be within a limited range, approximately from 40% to 70%. Reduction of the area of elements and corresponding decrease of radiated power leads to deterioration of the quality of the intensity distribution.

Other results presented in Gavrilov and Hand (2000b) include:

1. The results testify that the dimensions of individual elements have a decisive effect on the ability of random arrays to scan the focus whilst maintaining an intensity distribution of acceptable quality for practical applications. If the diameter of elements is too large (e.g., 10 mm for the frequencies of, e.g., 1-1.5 MHz) and the directivity pattern of the elements is too narrow, then even an extremely large number of elements in the array will not permit scanning the focus whilst maintaining an acceptable quality of intensity distribution. For example, calculations show that, in the case of using an array of 256 elements with a diameter of 10 mm (note that such an array is physically impossible because the total area of elements exceeds almost twice the physical area of its surface), it is impossible to move the focus off the axis to the distance greater than 10 mm with an acceptable quality. It follows from the obtained data that, in order to scan the focus at a distance of 10-15 mm with acceptable quality, it is necessary to have the diameter of elements not larger five wavelengths. If this condition is satisfied, an increase in the number of elements and, therefore, in the total active area of the array leads to an increase in the maximum intensity in the focus and to an improvement of the quality of intensity distributions.
2. The shape of an individual element (concave, flat, or convex) is essentially irrelevant regarding the quality of intensity distributions produced by an array. For example, the quality of intensity distributions for a 1.5 MHz array, consisting of 64 elements each of 10 mm in diameter but with different shapes (concave elements with the curvature radii 6 and 12 cm and convex elements of the same radii), barely differ from each other and from the characteristic of a similar array consisting of flat elements (Figure 24c). This result is predictable, because, despite a significant difference between the intensity distributions immediately near the surface of the elements of different shape ( $z = 0$ -5 cm), the distributions in the focal region ( $z = 8$ -14 cm) are essentially the same. It follows that there is no need to use more expensive, i.e. non-planar elements in the design of such arrays.
3. The shapes of the apertures of random arrays (square or circular) do not noticeably affect the quality of intensity distributions. For example, the intensity distributions of arrays of 256 x 5

mm elements (1.5 MHz) with the apertures of a circle shape (Figure 24a) and a square one with equal active areas and sparseness of elements almost did not differ from each other.

4. Errors in setting the necessary values of phases at individual elements, for example, because of errors in the element location at the surface, can lead to a deterioration of quality of intensity distributions. The calculation of intensity distributions was conducted for a random array of  $256 \times 5$  mm elements (1.5 MHz) with three different phase distributions at the elements: (a) the calculated phase distribution corresponded to the ideally precise positioning of elements; (b) random numbers selected from the range from -0.4 to 0.4 radian were added to the values of phases from case (a); and (c) random numbers from the interval between -1.0 and 1.0 radian were added to the values of phases from case (a). It was found out that the deterioration of the quality of distributions for case (b) in comparison with case (a) was relatively small. These data agree with the results obtained by Hutchinson et al. (1996) and Wang et al. (1991) who demonstrated that a discrete phase setting in 4 bit ( $22.5^\circ$ ) is sufficient for the satisfactory operation of arrays in practice. A further increase in the phase setting error (case (c)) leads to a significant deterioration in the quality of intensity distributions.
5. The use of such distributions of the amplitudes of particle velocity at the surface of a random array, when the amplitude values decrease from the array centre to the periphery, does not lead to an improvement of the quality of intensity distributions. In particular, calculations were performed for the distributions of the type  $[1 - (r/r_o)^2]^n$  (where  $n = 1, 2$ , and  $r_o$  is the array radius) used by Skolnik (1962) for regular arrays with circular apertures. This approach, which is effective for regular arrays, in the case of random arrays leads only to an increase in the relative intensity values in the grating lobes, because the maximum intensity value in the focus, which is used for the normalization of these values, decreases considerably.
6. The use of the frequency modulation of signals at the elements of a random array provides an opportunity to improve a little the quality of intensity distributions. For example, calculations were performed for the intensity distributions of a random array of  $256 \times 5$  mm elements for different frequencies ( $0.9f$ ;  $0.95f$ ;  $1.0f$ ;  $1.0f$ ; and  $1.1f$ ) where  $f$  is the central frequency (1.5 MHz). The averaged distribution for the five indicated frequencies turned out to be better than all the others individually, including the distribution for the central frequency.

The performance of the arrays described by Gavrilov and Hand (2000a,b) for the single focus mode may be compared with the sparse random arrays studied by Goss et al. (1996) who used an array consisting of 108 elements (only 64 of which were activated at any one time), each 8 mm in diameter, and driven at a frequency of 2.1 MHz. The elements were mounted in a hexagonal pattern on a section of a spherical shell of diameter 100 mm and radius of curvature 102 mm. The sparseness of the array was approximately 45%. It was shown theoretically that when the array was focused at the geometrical centre of the shell, the intensity in the grating lobes in the focal plane was  $0.13 I_{max}$ . When the array was focused 5 mm off its central axis this level was increased to  $0.6 I_{max}$ . In experimental measurements these levels were as high as  $0.38 I_{max}$  and  $0.9 I_{max}$ , respectively. Goss et al. (1996) investigated the effect of random distribution the elements on the shell and showed theoretically that the expected level of the intensity in grating lobes in the focal plane would be in this case  $0.04 I_{max}$  with no steering and  $0.16 I_{max}$  for steering of  $\pm 5$  mm. Such a modest effect of randomization achieved in this work might be explained by the fact that the ratio of the element diameter to the wavelength was 11.2 in that study. Our data show that a significant effect of randomization could be expected only when the elements are not very directional (element diameter/wavelength  $\sim 0.5 - 5$ ). Our estimations show that increasing this ratio leads to a significant deterioration of the intensity distributions with the existence of grating lobes.

Thus, the results of our study suggest that a random distribution of elements on a spherical shell leads to marked improvement of the performance of the array, in terms of the intensity distribution, compared with cases in which regular annular, hexagonal or square packing is used. As an example, for the case of a single focus, a random array of diameter 110 mm and consisting of 256 circular elements 5 mm in diameter, driven at 1-1.5 MHz, and placed on a spherical shell with a radius of curvature 120 mm, was predicted to provide good performance in terms of intensity levels in grating lobes or in pre-focal regions. The results obtained for the single focus mode also suggest that comparable performance with a regular array can be achieved whilst providing a several-fold reduction in the number of elements used. Finally, it was shown that array performance in producing and steering a co-planar square multiple foci pattern, assessed in terms of intensity distributions, is dependent upon the degree of order in the array structure. The random array performed better than an array of elements arranged in concentric rings; both performed considerably better than arrays in which the elements were arranged in square or hexagonal patterns, primarily due to reduced presence of grating lobes in the acoustic field.

### 3.4. Generation and Steering of Multiple Foci, Data from Modeling

Since in practice clinically relevant treatment volumes are usually larger than that of a single focus, multiple lesions are needed and can be achieved by electronically scanning a single focus, or by synthesizing and scanning a pattern of multiple foci (Fan and Hynynen 1996a,b; Wan et al. 1996; Daum and Hynynen 1998). In all of these cases, the pre-focal intensity will be considerably greater than that associated with steering of the single focus. Correspondingly, possible criteria for evaluation of quality of intensity distributions associated with multiple foci will be less rigorous than those for the single focus mode.

Such criteria have been developed by Gavrilov and Hand (2000a,b). First, it was assumed that the values of ultrasonic intensity in the pre-focal region are much less than the values of the cavitation threshold in tissues. It is known that at frequencies 1-1.5 MHz, the cavitation threshold in tissues under the action of focused ultrasound corresponds to an intensity of approximately 1000-1500 W cm<sup>-2</sup> (Gavrilov 1974; Hynynen 1991). In other words, it was assumed that the mechanism of possible destruction in the pre-focal region (if such destruction occurs) is of purely thermal origin. The further logic is based on the paper of Fan and Hynynen (1996a) who reported that elevations of tissue temperature to 53.5 °C for 10 s and 56.8 °C for 1 s each result in the same thermal dose that is a threshold value for tissue necrosis. The maximum temperature  $T_{max}$  achieved during ultrasound surgery is often in the range 80 - 90 °C (Hill and ter Haar 1995; Fan and Hynynen 1996a,b). Thus, in terms of the maximum temperature increase  $\Delta T_{max}$  (with respect to 37 °C), tissue necrosis is likely to be achieved over the approximate range  $0.4\Delta T_{max} - 1.0\Delta T_{max}$ . If the effects of thermal conduction and perfusion are neglected during relatively brief exposures of a few seconds, and  $\Delta T$  and intensity  $I$  are assumed to be linearly related, then to a first order approximation, a basis of classifying pre-focal intensity levels and intensity hot spots in distributions associated with multiple foci might be as follows (Gavrilov and Hand 2000a,b). Grade I:  $I \leq 30\% I_{max}$  outside the multiple foci pattern; Grade II:  $30\% I_{max} < I \leq 40\% I_{max}$  outside the multiple foci pattern; Grade III:  $I > 40\% I_{max}$  outside the multiple foci pattern. The risks of producing thermal necrosis outside of the target area should be low for grade I and significant for grade III. These grades may be conservative since no account of cooling between ultrasound pulses is considered. The examples of all three grades are presented in Figure 31 (Gavrilov and Hand 2000a) for the case of the 256 x 5 mm element random array and the 3x3 coplanar multiple foci pattern at  $x = y = 0, z = 100$  mm (left);  $x = y = 0, z = 110$  mm (centre);  $x = y = 0, z = 120$  mm (right).

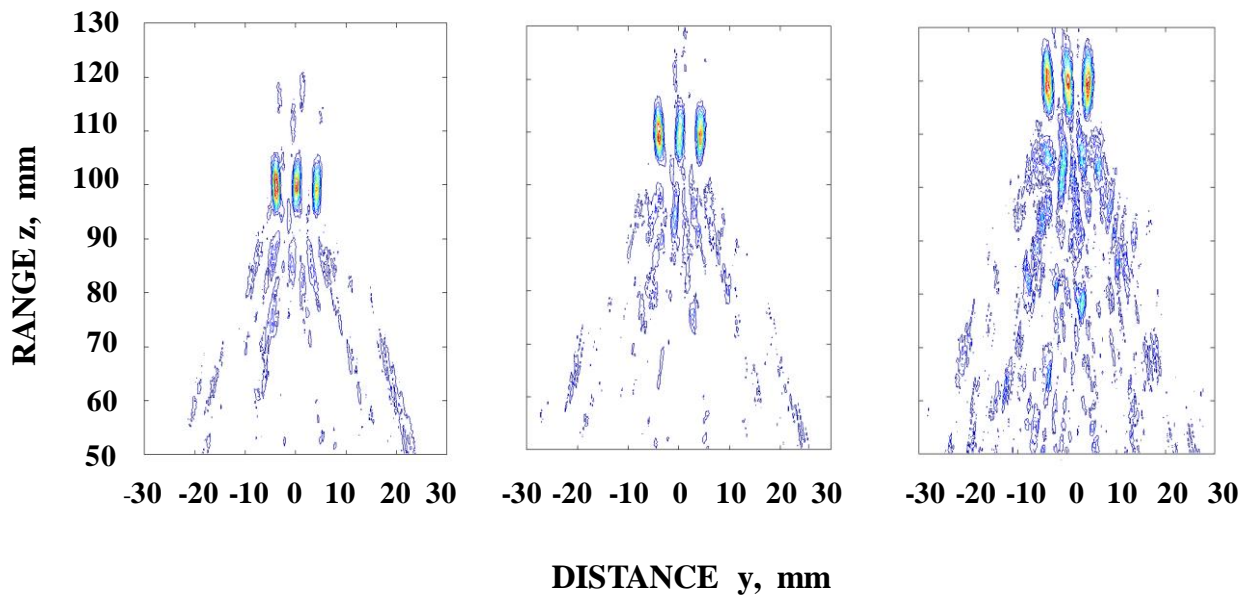


Figure 31. Classification of intensity distributions associated with generation of simultaneous multiple foci. *Left*: Grade 1 ( $I \leq 30\% I_{max}$  outside the focal pattern), *Centre*: Grade 2 ( $30\% I_{max} < I \leq 40\% I_{max}$  outside the focal pattern); *Right*: Grade 3 ( $I > 40\% I_{max}$  outside the focal pattern). The intensity distributions (in the  $y$ - $z$  plane) shown are for the  $256 \times 5$  mm element random array with the central focus of the  $3 \times 3$  coplanar multiple foci pattern at  $x = y = 0$ ,  $z = 100$  mm (left);  $x = y = 0$ ,  $z = 110$  mm (centre);  $x = y = 0$ ,  $z = 120$  mm (right) (Gavrilov and Hand 2000a).

In Gavrilov and Hand (2000a) and Gavrilov et al. (2000) an assessment of the relative performance of two-dimensional arrays when used in a simultaneous multiple foci mode is reported. The intensity distributions in the fields formed by four types of arrays are compared:

- (1) An array of 256 elements distributed on the surface in a quasi-random manner. The minimum and maximum distances between the centres of the elements are 5.5 mm and 100 mm, respectively:
- (2) An array of 256 elements positioned on the surface regularly, in square patterns. The minimum distance between the centres of elements is 5.5 mm.
- (3) An array of 255 elements positioned on the surface regularly, in hexagonal patterns. The minimum distance between the centres of elements is 5.5 mm.
- (4) A regular array of 255 elements consisting of a central element and nine concentric rings with the radii from 5.5 to 49.5 mm (with a step of 5.5 mm). The rings consist of 5, 11, 17, 23, 28, 33, 40, 46, and 51 elements, respectively. The distance between the centres of elements is 6 mm.

Schematic representations of these arrays are shown in Figures 24a, 25a, 25d and 25c, correspondingly.

The phases in the control points were rotated around the pattern of foci, in a manner similar to that used in Fan and Hynynen (1996b), and shown for the case of a  $3 \times 3$  pattern with 4 mm spacing in Table 5 (Gavrilov and Hand 2000a). Here, co-ordinates (upper figures) are referenced to the central focus at the point  $(0, y, z)$  and shifts are in mm. The relative phases of the complex pressure at these 9 locations are shown by the lower figures.

**Table 5. Locations and relative phase values for the 9 co-planar foci (Gavrilov and Hand 2000)**

$x+4, y-4, z$ 0	$x+4, y, z$ $\pi/4$	$x+4, y+4, z$ $\pi/2$
$0, y-4, z$ $7\pi/4$	$0, y, z$ $\pi/2$	$0, y+4, z$ $3\pi/4$
$x-4, y-4, z$ $3\pi/2$	$x-4, y, z$ $5\pi/4$	$x-4, y+4, z$ $\pi$

Figure 32 (Gavrilov and Hand 2000) summarizes the characteristics of intensity distributions associated with four 1.5 MHz arrays when the co-ordinates of the central focus in the 3 x 3 coplanar pattern are varied over the ranges of  $z$  and  $y$  shown. Figures 32 (a-d) show data obtained for 256 5 mm randomly distributed elements, 256 5 mm elements in a square pattern, 255 5 mm elements in a hexagonal pattern, and 255 5 mm elements in the annular configuration.

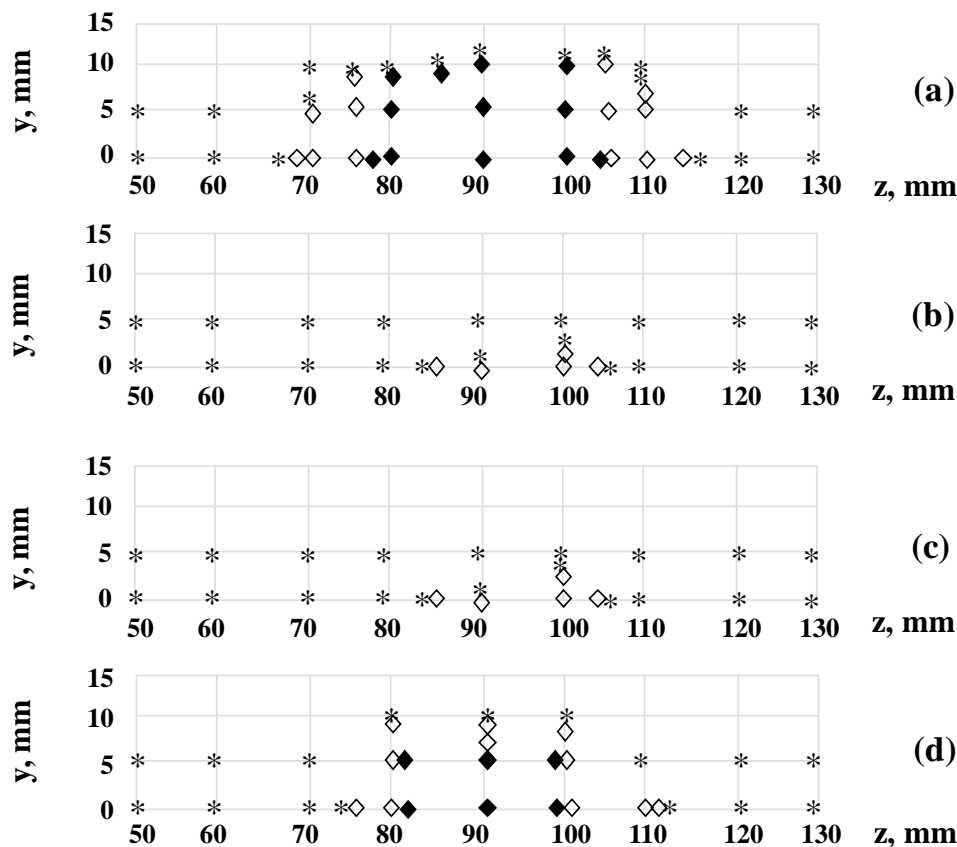


Figure 32. Summary of results of calculations and quality assessment of the intensity distributions associated with production of simultaneous multiple foci. In each case 9 co-planar foci located on a 3 x 3 square grid with 4 mm spacing were produced. The co-ordinates shown refer to those of the central focus in the pattern. (a) 256 5 mm diameter elements randomly distributed (Figure 24a); (b) 256 5 mm elements distributed in a square pattern (Figure 25a); (c) 255 5 mm elements distributed in a hexagonal pattern (Figure 25d), (d) 255 5 mm elements distributed in an annular pattern (Figure 25c). In all cases the frequency was 1.5 MHz. The quality levels are: grade I (solid diamond); grade II ( $\diamond$ ); grade III (\*) (Gavrilov and Hand 2000).

Figure 33 (Gavrilov and Hand 2000) shows intensity distributions in the  $x$ - $y$  plane for the 4 arrays referred to in Figure 32 when the 3x3 pattern is produced at a range of 100 mm. The

patterns relate to a) elements in the random pattern, b) elements in the square pattern, c) elements in the hexagonal pattern, and d) elements in the annular pattern. For all arrays the upper graphs show the central focus in the pattern at (0, 0, 100 mm) whilst the lower ones show the case when it is steered to (0, 10, 100 mm).

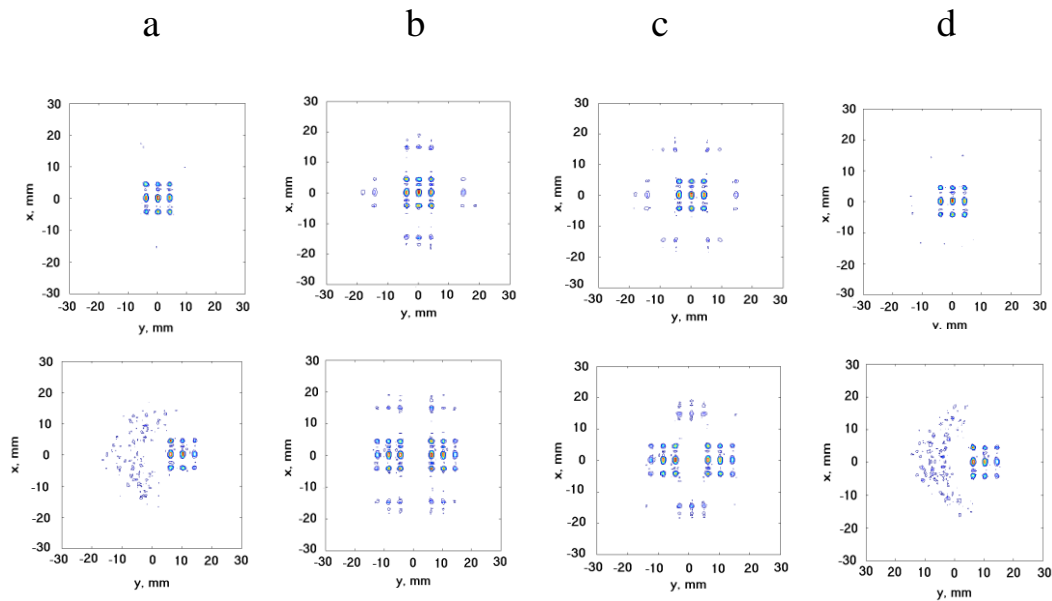


Figure 33. Intensity distributions calculated in the  $x$ - $y$  plane at a range  $z = 100$  mm for a  $3 \times 3$  coplanar pattern of foci separated by 4 mm. The upper graphs are for the central focus in the pattern located at (0, 0, 100 mm) and the lower graphs are for when it is located at (0, 10, 100 mm). a) 256 5 mm elements randomly distributed; b) 256 5 mm elements distributed in a square pattern, c) 255 5 mm elements distributed in a hexagonal pattern, d) 255 5 mm elements distributed in an annular pattern (Gavrilov and Hand 2000).

The results of investigations into the relative performance of four 1.5 MHz arrays: 256 5 mm elements (random pattern), 256 5 mm elements (square pattern), 255 5 mm elements (hexagonal pattern), and 255 5 mm elements (annular pattern) used to produce a pattern of 9 foci, spaced from each other at 4 mm on a square  $3 \times 3$  grid in a focal plane reflected the general findings of the single focus studies. In the case of the random array, the pattern of 9 foci could be steered along the central axis from 76 mm to 104 mm and up to 10 mm off the central axis whilst maintaining a grade I intensity distribution. These distances are with respect to the co-ordinates of the centrally located focus within the  $3 \times 3$  pattern. The performance was considerably degraded when the elements were distributed in either a square or a hexagonal pattern. In these cases the best performance was grade II and this could be achieved only over  $z$  values from 86 mm to 106 mm. With very few exceptions (for example 1 mm off axis at  $z = 100$  mm for the square array and up to 2 mm off axis at  $z = 100$  mm for the hexagonal array), any steering off the central axis produced a grade III intensity distribution, primarily due to the production of secondary, contra-lateral foci in the focal plane. The 255 elements distributed in the annular pattern achieved intermediate performance with grade I distributions produced when the multiple foci pattern was centred from 81 mm to 99 mm along the central axis or up to 5 mm off axis. The nature of the problem encountered with the square and hexagonal arrays is highlighted in Figure 33. The intensity distributions in the focal plane  $z = 100$  mm for the cases when the central focus in the  $3 \times 3$  pattern is either on the central axis or steered off it by 10 mm are both grade III for these arrays (Figures 31b and 31c). In the latter case, the intensity values in the grating lobes can be comparable or even higher than in the main lobes. The corresponding intensity distributions for the random and annular

arrays (Figures 31a and 31d) are grade I. It is necessary to note that for annular array the large secondary maxima on the axis of the array are inherent.

The intensity distributions for multiple foci mode operation were sensitive to the phase values chosen at the foci locations. The phase rotation used here and shown in Table 5 was chosen empirically. Following Cain and Umemura (1986), Fan and Hynynen (1996a,b) proposed uniformly rotating phases in the control points around the central axis, and the equal amplitudes in the control points equidistant from the centre. This achieved a reduction in undesirable secondary intensity maxima on the axis of the array. Typically, the control points were selected on a square grid in the focal plane, the phases of 4 neighbouring points, which form a square, differed in increments of  $90^\circ$ . Other methods of distributing the phase were also investigated. One method that optimizes the gain has been described (Ebbini and Cain 1991b) but it does not minimize acoustic interference in the near-field (Fan and Hynynen 1996b). The separation between multiple foci of 4 mm used in the described modeling was not optimized in any way but was comparable with those found to be practicable in other studies (Fan and Hynynen 1996; Wan et al. 1996; Daum and Hynynen 1998).

Thus, the results obtained in this study demonstrate that arrays with a random distribution of elements on the array surface provide a distinctly better quality of intensity distributions when steering multiple foci as compared to arrays with a regular positioning of elements.

In Gavrilov (2003) calculations of the sound fields created by regular and random arrays were reported for generation and steering of 25 foci.

The calculation of the spatial distributions of acoustic fields was conducted for arrays whose surface was shaped as a part of a spherical shell with a radius of curvature of 120 mm. The array diameters were identical and equal to 130 mm. The arrays consisted of flat circular elements 5 mm in diameter. The intensity distributions in the field produced by arrays of the two following types were compared:

- (1) an array of 256 elements distributed on the surface of the array in a regular manner, as a square pattern; the minimum distance between the element centres was 6 mm;
- (2) an array of 256 elements distributed on the surface quasi-randomly. The minimum distance between the element centres should be no smaller than 5.5 mm.

The arrays are represented schematically in Figure 34 (Gavrilov 2003).

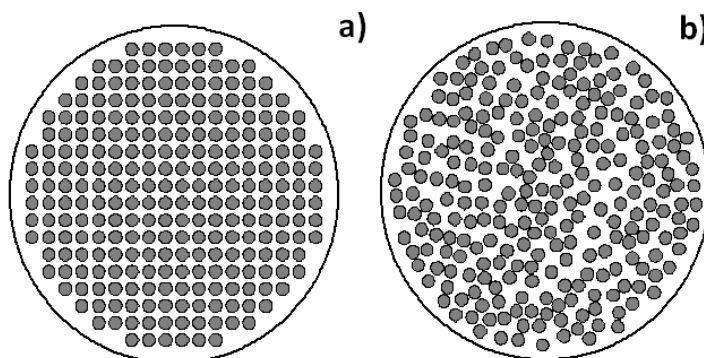


Figure 34. Schematic representation of arrays consisting of 256 elements 5 mm in diameter distributed on the surface of the array (a) in a square pattern and (b) randomly (Gavrilov 2003).

The total area of all elements (the active area) in each array was  $50.2 \text{ cm}^2$  and the frequency was 1.5 MHz in both cases. Ultrasound was assumed to propagate through a biological tissue with a density of  $1000 \text{ kg m}^{-3}$ , a sound velocity of  $1500 \text{ m s}^{-1}$ , and an attenuation coefficient equal to  $0.75 \text{ dB cm}^{-1}$  (at 1.5 MHz). The computational technique used was that described in Gavrilov and Hand (2000a,b), as well as in the previous Sections. It is worth noting that the computer codes developed in Gavrilov (2003) for calculating the spatial distributions of the acoustic fields produced by the arrays additionally provided an opportunity to

calculate the maximum intensity at the foci and the location of the focus with the maximum intensity, to estimate the acoustic power of the array in the focal plane and in the vicinities of the foci, to determine the intensity gain factor, *etc.* The power calculations were carried out on the assumption that the particle velocity was the same at all elements ( $0.365 \text{ m s}^{-1}$ , corresponding to an intensity of  $10 \text{ W cm}^{-2}$  at each element) and was distributed uniformly over their area. Thus, it was assumed that the maximum acoustic power obtained from the array surface was  $502 \text{ W}$ .

A quantitative analysis of the intensity distributions was performed using two-dimensional contour distributions in the focal plane (the  $xy$  plane) and in the plane perpendicular to it and passing through the acoustic axis of the array (the  $xz$  plane). Nine contours corresponding to the intensity values from 10% to 90% of  $I_{\max}$  with a step of 10% of  $I_{\max}$  are presented in the following figures.

Figure 35 (Gavrilov 2003) shows the distributions of ultrasonic intensity, which correspond to the simultaneous generation of 25 foci, for the arrays with a regular (Figure 35a) and random (Figure 35b) distribution of elements. The intensity distributions in the  $xy$  plane are given in the upper part of the plot, and the intensity distributions in the  $xz$  plane, in the lower part. The distance between the centres of foci is  $2.5 \text{ mm}$ . The focal plane is at the distance of  $z = 120 \text{ mm}$  from the co-ordinate origin, which coincides with the deepest point on the array surface.

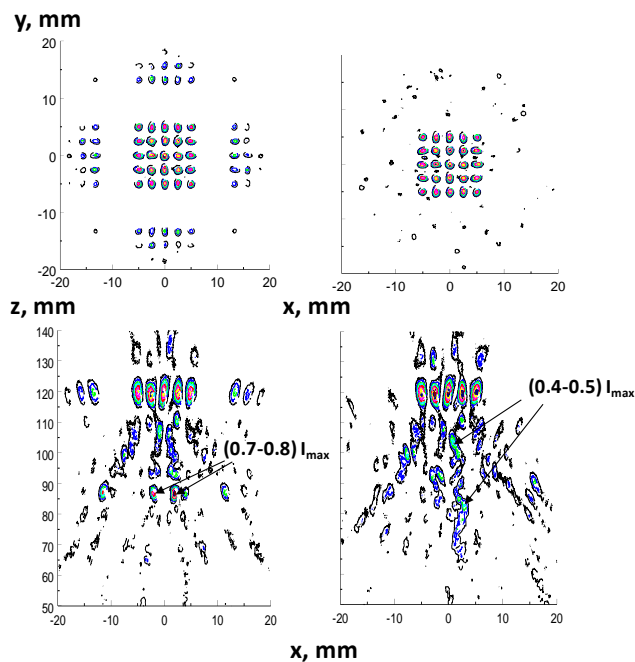


Figure 35. Ultrasonic intensity distributions corresponding to a simultaneous generation of 25 foci in the  $xy$  plane (the upper plots) and in the  $xz$  plane (the lower plots) for arrays with (a) regular and (b) random distributions of elements. The distance between the focus centres is  $2.5 \text{ mm}$  (Gavrilov 2003).

It is seen that, for the regular array, clearly pronounced grating lobes related to the geometrical repetition of the array structure are observed in the focal plane. In contrast, there are no such maxima for the field of the random array: the energy is spread in the focal plane. However, in both cases, the intensity values in the secondary maxima proximal to the focal plane reach  $0.4-0.8$  of the maximum value  $I_{\max}$ , which is unacceptable for using this technique in surgery according to the distribution quality criteria proposed earlier for the multiple foci case (Gavrilov and Hand 2000a). The appearance of the points with elevated intensity is especially dangerous, because sonication affects the tissue during the whole time of ultrasonic action on tissues. However, this method can be used in high-temperature hyperthermia, if the overheating in the hot points along the ultrasound propagation path does not cause necrosis of the tissues.

From the data obtained, it follows that, when using a large number of simultaneously produced foci in surgery (i.e., for the destruction of a predetermined tissue volume), it is necessary to find the ways to reduce the levels of the secondary intensity maxima in the acoustic field proximal to the focal plane. One such method was first proposed by Ebbini and Cain (1991b) and subsequently developed by Daum and Hynynen (1998, 1999) and Fan and Hynynen (1996a,b). The basis of this method, discussed in Section 2.3, is as follows: instead of a static field with a certain set of secondary maxima ("hot points"), one can use the fields of several configurations with a smaller number of foci, which are switched electrically with a frequency of 10-20 Hz. For example, Daum and Hynynen (1998, 1999) and Fan and Hynynen (1996a,b) proposed the use of six such configurations consisting of 1+4+4+4+8+4 foci, respectively, to synthesize 25 foci.

Gavrilov (2003) proposed the selection of configurations consisting of approximately equal numbers of foci, thus ensuring a more uniform distribution of energy amongst different configurations of foci. For example, it is expedient to use a combination of 5+4+4+4+4+4 foci to generate a set of 25 foci. Figure 36 (Gavrilov 2003) shows the intensity distributions in the  $xz$  plane ( $z = 100$  mm) for this configuration of foci for the cases of regular (Figure 36a) and random (Figure 36b) arrays. One can see that, in the case of a regular array (Figure 36a), multiple grating lobes with the intensity up to  $0.3 I_{\max}$  are observed in the focal plane, while in the case of a random array, no such maxima are present. The intensity values vary from  $1100 \text{ W cm}^{-2}$  (a configuration of five foci) to  $1500 \text{ W cm}^{-2}$  (a configuration of four foci) for a regular array and from  $1070 \text{ W cm}^{-2}$  (five foci) to  $1400 \text{ W cm}^{-2}$  (four foci) for a random array. In all cases the power delivered by the array was optimized. The scatter of the intensity values can be minimized in such a way that the time-average intensity at the foci does not exceed  $1100 \text{ W cm}^{-2}$ .

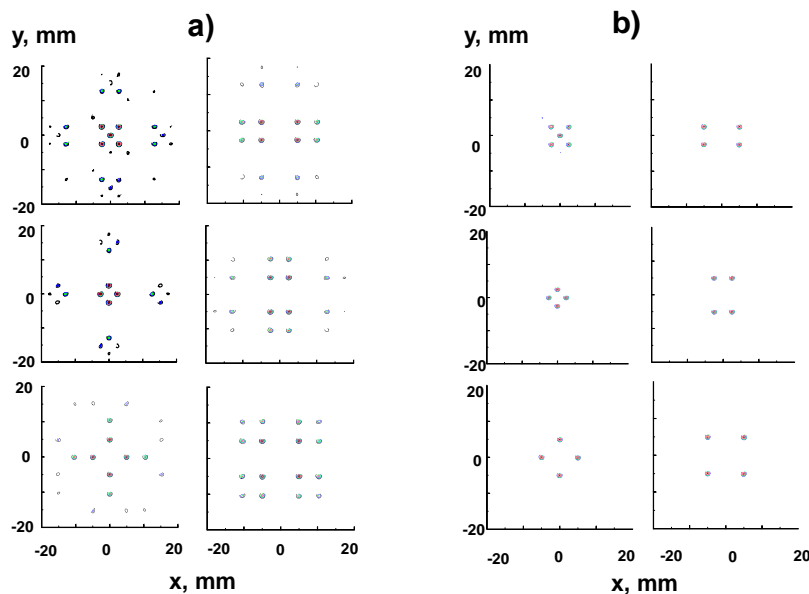


Figure 36. Intensity distributions in the  $xy$  plane for six configurations of foci (5 + 4 + 4 + 4 + 4 + 4 foci), for (a) regular and (b) random arrays (Gavrilov 2003).

Figure 37 (Gavrilov 2003) shows how it is possible to generate a set of 25 foci with their centre to centre distance of 2.5 mm by using the six configurations of foci that are shown in Figure 36. The central focus is located on the array axis, at the distance  $z = 100$  mm. The time-average intensity at all foci is approximately equal to  $180 \text{ W cm}^{-2}$ , and the peak intensity to  $1100 \text{ W cm}^{-2}$ . It is seen from Figure 37 that, in the case of using several configurations of foci, the quality of the time-average intensity distributions along the path of the ultrasonic beam (in the  $xz$  plane) is considerably improved in comparison with the distribution for 25 foci generated

simultaneously (Figure 35). It is also seen that in the field of a regular array there are regions where the intensity of the secondary maxima reaches  $0.5 I_{\max}$ . There are no such potentially dangerous regions in the field of a random array.

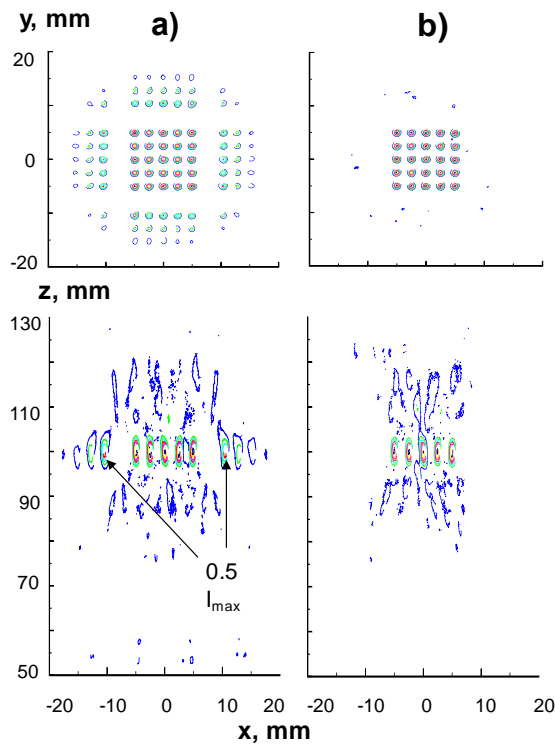


Figure 37. Intensity distributions in the focal plane (the  $xy$  plane,  $z = 100$  mm) and along the path of the ultrasonic beam (the  $xz$  plane) for (a) regular and (b) random arrays in the case of 25 foci generated using six configurations of foci (Figure 36). The distance between the foci centres is 2.5 mm. The central focus is on the array axis (Gavrilov 2003).

When large volumes of tissue require sonication, such as in the treatment of a typical tumour, it is necessary to move the focus (or foci) in increments of 1-2 mm. This can be accomplished either mechanically with the help of positioning systems, or more logically when using phased arrays, electronically. Therefore, it is of practical interest to evaluate the possibility of electronic scanning of a set of 25 foci using regular or random arrays.

Figure 38 (Gavrilov 2003) presents the comparison of intensity distributions in the focal plane (the  $xy$  plane,  $z = 100$  mm) and along the path of the ultrasonic beam (the  $xz$  plane) for regular (Figure 38a) and random (Figure 38b) arrays for the set of foci shifted 7 mm off the axis in the case of 25 foci generated using six configurations of foci (Figure 36). It is seen that, with a regular array, a set consisting of 25 grating lobes is observed together with the main set, and this secondary set has almost the same intensity values (up to  $0.8 I_{\max}$ ) as the main set. This would be undesirable for surgical or any other therapeutic application. In the case of a random array, there are only several points or regions with an intensity of  $0.2 I_{\max}$  in the acoustic field, which is quite acceptable for practical purposes. Thus, the use of random arrays provides an opportunity to scan the required set of foci in the plane through a distance of at least 15 mm. Such scanning is practically impossible using regular arrays.

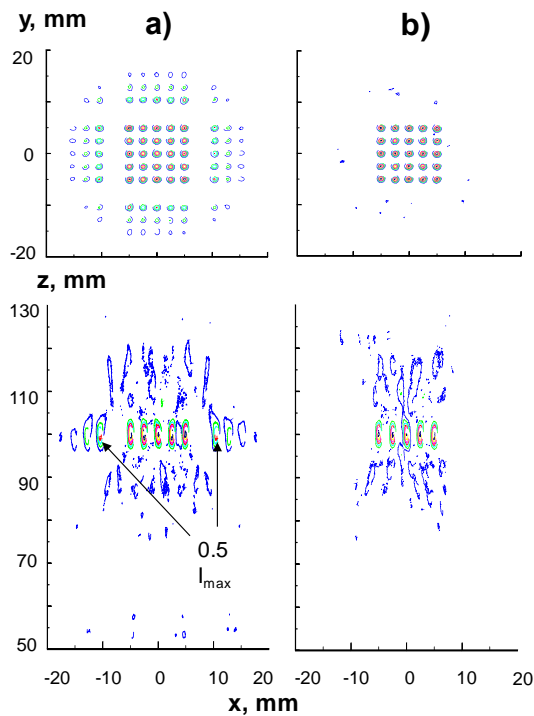


Figure 38. Intensity distributions in the focal plane (the  $xy$  plane,  $z = 100$  mm) and along the path of the ultrasonic beam (the  $xz$  plane) for (a) regular and (b) random arrays in the case of 25 foci generated using six configurations of foci (Figure 36). The set of foci is shifted 7 mm off the array axis in both cases (Gavrilo 2003).

Thus, random two-dimensional phased arrays can generate multiple foci within a predetermined volume and so considerably reduce the duration of the surgical or therapeutic procedure. The capability of such arrays to move the set of foci in the focal plane (at least within the limits of 7 mm) without the formation of potentially dangerous grating lobes and other secondary intensity maxima is also useful from the practical point of view.

It should be noted that the results obtained from this study demonstrate that arrays with a random distribution of elements over the array surface provide a better quality of intensity distributions in the case of the multiple focus generation and scanning (for example, for 25 foci), as compared to the arrays with a regular distribution of elements such as a square pattern.

### 3.5. Generation of Focal Regions of Complex Configurations

In practice there is often a need to generate focal regions of complex configuration. For example, it will be shown in Chapter 4 (Section 4.8) that such a configuration can be used in development of tactile displays. In this area of research, one of the most promising lines of work is the development of tactile displays based on the effect of radiation pressure (Iwamoto et al. 2001; Iwamoto and Shinoda 2005, 2006). Such a task can be solved by using a two-dimensional array with elements randomly distributed on its surface. The capability to generate simultaneously a large number of foci and to spatially steer them is, perhaps, the major advantage of two-dimensional phased arrays.

The possibility of using random two-dimensional phased arrays for generating focal regions of complex configurations in connection with the problems of stimulation of human receptor structures is discussed by Gavrilo (2008). To demonstrate this possibility modeling has been carried out.

The calculation of the spatial distributions of acoustic fields was performed for arrays with surfaces shaped as a part of a spherical shell with a curvature radius of 60 mm and a diameter of

65 mm. The investigation included arrays of two types: (i) an array of 256 elements distributed regularly on the surface in a square manner (as the most popular distribution amongst existing distributions of elements in regular two-dimensional arrays); the minimal distance between the element centres was 3 mm; (ii) an array of 256 elements randomly distributed on the surface; in this case, the distance between the element centres varied and was  $\geq 3$  mm. The ultrasonic frequency was in both cases 3.0 MHz. The diameter of the disk shaped elements was 2.5 mm (i.e.,  $5 \lambda$  at this ultrasonic frequency). The total active area of the array elements in both cases was  $12.5 \text{ cm}^2$ , which provides up to 20–30 W acoustic power at appropriate values of intensity at the element surfaces. Figure 39 (Gavrilov 2008) shows the distribution of elements in the random array.

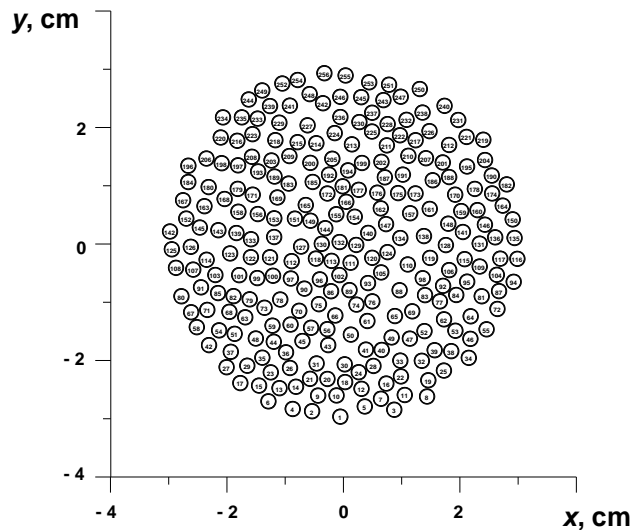


Figure 39. Distribution of elements on the surface of the random array used for simulation (Gavrilov 2008).

Figure 40 (Gavrilov 2008) presents the intensity distributions using of this random array, which correspond to the images of three arbitrarily chosen symbols shown in the left part of the Figure. The ultrasound generated symbols in Figures 40a and 40b were obtained using four configurations of foci with four foci in each of them (16 foci in total, which are positioned at a distance of 1 mm from each other). The symbol in Figure 40c is obtained using three configurations with eight foci in each of them (24 foci in total, which are positioned on a circle at a distance of 0.52 mm from each other; this value just slightly exceeds the wavelength).

In the left and right columns, the intensity distributions in a relatively wide acoustic field ( $4 \times 4$  cm) are given. These distributions allow to monitor the presence or absence of the grating lobes and other secondary intensity maxima within the whole field of interest (an important criterion for evaluating the quality of the acoustic fields generated by an array). The distributions in the left and central columns are obtained for the case where multiple foci were not shifted off the array axis, and the distributions in the right column for the case where the set of foci is shifted to a distance of 5 mm off the axis, which corresponds to the selected dimensions of the tactile display ( $1 \times 1$  cm). The central column gives the same distributions as in the left column, but in a much narrower field with the sizes corresponding to the display dimensions. These distributions provide an opportunity to examine the field structure in more detail within the display area.

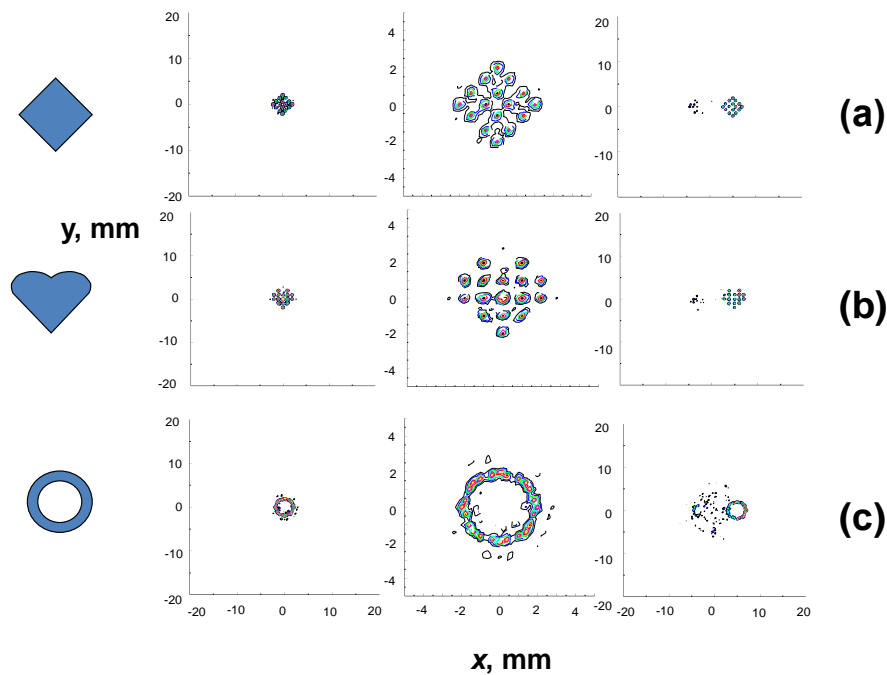


Figure 40. Generation of regions of action by focused ultrasound in the form of different symbols (see at the left of the Figure) using a random array. Foci used: (a, b) 16 foci (four configurations with four foci in each) and (c) 24 foci (three configurations with eight foci in each). The dimensions of the field under investigation are  $4 \times 4$  cm (the left and right columns) and  $1 \times 1$  cm (the central column). At the left: the absence of the shift of the set of foci off the array axis. In the middle: the same but on an increased scale. At the right: the shift of the set of foci by 5 mm (Gavrilov 2008).

From the distributions given in Figure 40, it follows that, using random arrays, it is possible to generate complex-shaped regions of action by focused ultrasound. In this case, the symbols selected for imaging were reproduced with an acceptable quality (according to the criteria of the intensity level in the grating lobes and other secondary intensity maxima). It is seen that the displacement of the set of foci to a distance of 5 mm off the array axis does not noticeably deteriorate the distribution quality (especially in the cases of the symbols in Figures 40a and 40b).

Figure 41 (Gavrilov 2008) shows for comparison the intensity distributions similar to those given in the right column of Figure 40 but obtained using a regular array with the same parameters as in the case of the random array. The shift of the set of foci is 5 mm relative to the array axis in all cases. One can see that, in the case of the regular array, a side set of foci with almost the same values of peak intensity (up to  $0.6-0.7 I_{\max}$ ) as in the main set of foci arises together with the main set of foci. This may lead to erroneous perception of symbols. If the shift of the foci increases, the peak intensity in the secondary set of foci may exceed the corresponding value in the main set of foci. As it is seen in Figure 40 (the right column), this effect is absent in the case of the random arrays.

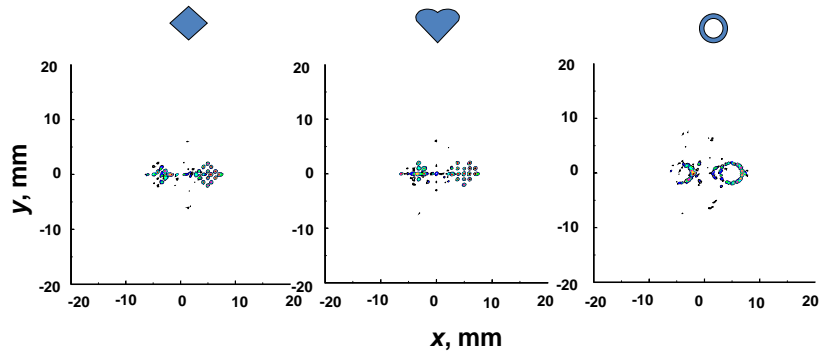


Figure 41. Intensity distributions in the focal plane, which are similar to those shown in the right column of Figure 40 but obtained using a regular array. The shift of all foci is 5 mm off the array axis (Gavrilov 2008).

Finally, Figure 42 (Gavrilov 2008) illustrates the possibility of “drawing” more complex symbols, for example, Latin letters with the use of random arrays. This Figure represents the intensity distributions in the focal plane that correspond to the letters S and W. To synthesize these symbols, 24 and 25 foci, respectively, which consisted of three and five configurations containing a smaller number of foci (eight and five, respectively) were used. The dimensions of the field where the calculation was conducted were 4 x 4 cm (Figure 42a,b) and 1 x 1 cm (Figure 42c,d). The absence of considerable grating lobes within the field under investigation is evidence of an acceptable quality of the intensity distributions obtained.

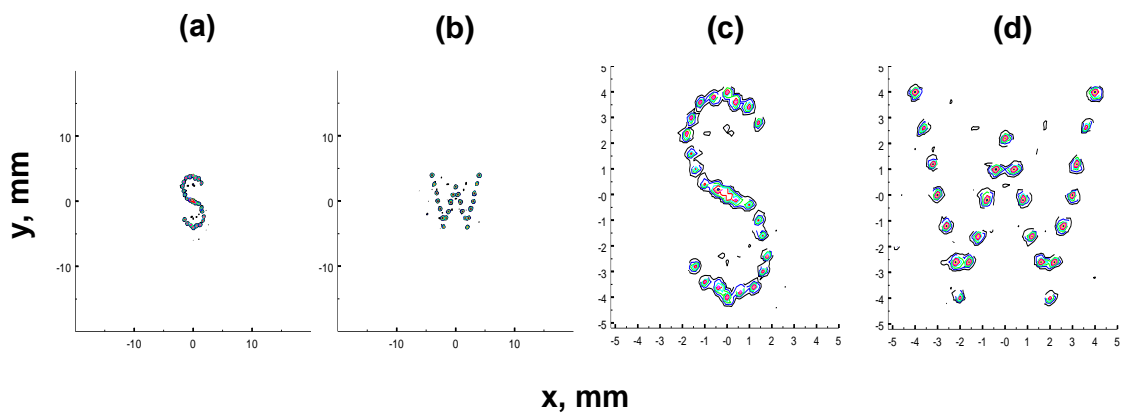


Figure 42. Synthesis of complex symbols, for example, in the form of some Latin letters, by a random array. The dimensions of the field under investigation are (a) and (b) 4 x 4 cm and (c) and (d) 1 x 1 cm (Gavrilov 2008).

The results obtained in this study demonstrate that arrays with a random distribution of elements on the surface can produce regions of action by focused ultrasound with a predetermined and, if necessary, rather complex, configuration. Together with other potential practical applications, this capability may be useful for research in physiology and in the search for new methods to transfer information to a human (see Section 4.8).

### 3.6. Ability to Focus Ultrasound Energy behind Acoustic Obstacles

One of the limitations for widening the applications of high intensity focused ultrasound (HIFU) for noninvasive destruction of deeply located tissues is related to the presence of

strongly reflecting or strongly absorbing acoustic obstacles in the ultrasound propagation path. A possibility to implement local and controlled lesions in the deep structures of the brain by sonication through the intact skull will be discussed in Session 4.1. Another example of such an obstacle is the rib cage that complicates noninvasive HIFU surgical operations on liver or heart.

Due to the extremely high absorption of ultrasound in the ribs and reflection from them, the overheating of rib bones and overlying tissues, including the skin, is the major side effect and limitation of the treatment of organs within the rib cage (Li et al. 2006). Additionally, the screening effect of the ribs leads to lower intensity levels in the focal region, which may compromise ablation of liver tissues.

Several research groups have investigated the problem of HIFU focusing in the presence of the rib cage. Theoretical feasibility studies using a phased array for treating liver tumours shadowed by ribs were reported (Botros et al. 1998); however the methodology developed was not tested experimentally. The clinical application of HIFU using a single-element transducer to treat different solid tumors was described (Wu et al. 2004), and in some cases treatment involved the surgical removal of the ribs located above the liver to provide an acoustic window during the HIFU procedure. A device based on a linearly segmented single focused transducer was developed for treating liver tumors that lie behind the ribs but close to the bottom of the ribcage (Civale et al. 2006). All the active elements were driven in phase but the device was oriented so that one or more segments of the array lying over the ribcage could be switched off to protect the ribs. The effect of ribs on therapeutic ultrasound treatment was investigated both theoretically and experimentally for two kinds of rib configuration, i.e. with the transducer centred either on an intercostal space or on a rib (Li et al. 2007). The first of these approaches appeared to be the most effective for the conditions considered in the paper. Then, the time-reversal method for pulsed beams was proposed to evaluate the aberration caused by the presence of the rib cage (Aubry et al. 2008). It was demonstrated that using the method in combination with random phased arrays minimizes the heating of the ribs by automatically sonicating between the ribs. In discussing their work, the authors considered an alternative approach to address this problem by switching off the elements of a phased array that are located in front of the ribs.

In the work of Bobkova et al. (2010) a method for focusing high intensity continuous ultrasound wave through ribs was proposed and tested theoretically and experimentally. The method aimed at minimizing heating of the ribs whilst maintaining high intensities at the focus (or foci) using a 2D random phased array.

The geometry of focusing and the position of the ribs used in these modeling studies are shown in Figure 43 (Bobkova et al. 2010). The radiator was a spherical shell with a radius of curvature  $F$ , aperture  $a$  and operating frequency  $f$ . The rib plane was located at a distance  $z_0$  from the centre of the radiator and infinitely thin, 100% absorbing parallel strips of width  $d$  and with “intercostal” spaces  $b$  were used to simulate the rib cage. The focus was located at the centre of curvature of the radiator. At the first stage, an idealized radiator, i.e., a transducer for which the magnitude and phase of excitation were both continuously variable over its surface, was considered. Two methods were proposed and tested to determine the “optimal” amplitude-phase distribution of the acoustic field at the surface of the radiator that resulted in the radiated field being minimised on the ribs but focused at the desired location. In the “geometric” approach the velocity amplitude at the source surface shadowed by ribs is set to zero. In the second approach, diffraction effects and the phase conjugation method are included to improve focusing and to provide better protection of the ribs. In both methods a spherical wave radiated from a point source placed at the focus was considered. The wave propagated between the ribs and formed an amplitude-phase distribution of the velocity at the surface of the radiator (Figure 43). After this distribution was calculated, the phase was inverted and field was reradiated back to the focus.

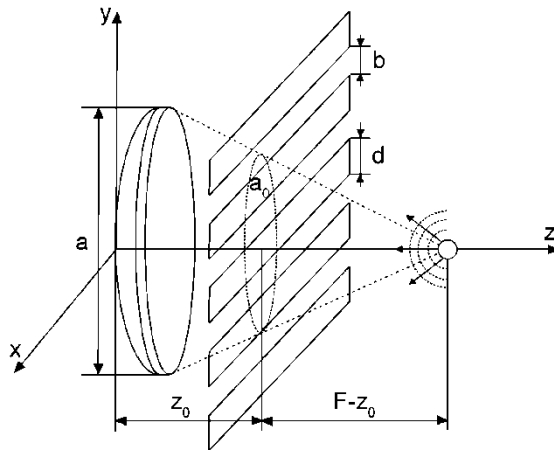


Figure 43. Geometry of modeling the propagation through ribs as infinitely thin strips (idealized ribs). Vibration amplitude and phase can have arbitrary shape over the surface of the radiator (idealized radiator). Reprinted from *Ultrasound Med. Biol.* 36(6) Bobkova, S., Gavrilov, L., Khokhlova, V., Shaw, A., & Hand, J. Focusing of high intensity ultrasound through the rib cage using therapeutic random phased array 888-906. Copyright (2010), with permission from Elsevier.

In the first method the field distribution at the radiator surface was obtained using geometrical acoustics. Spherically diverging rays from the point harmonic source were considered and the distribution of velocity amplitude in space collinear with the radial coordinate was  $V = V_0 F \exp(ikr)/r$ , where  $k = 2\pi f/c$  is the wave number,  $f$  is the sound frequency,  $c$  is the sound velocity in the media,  $r$  is the distance from the point source;  $r = F$  on the radiator surface. If a ray connecting the point source with the point of the radiator surface intersected the intercostal space, the velocity amplitude at the radiator surface was set to  $V = V_0 e^{ikF}$ ; if a ray intersected a rib, the amplitude of the velocity was set equal to zero.

In the second method, diffraction effects were included to set boundary conditions at the radiator. The velocity field of a spherically diverging wave from the point source was calculated in the intercostal spaces in the plane of ribs. This velocity distribution between the ribs was then used as a boundary condition to obtain the distribution of the normal component of the velocity at the surface of the radiator using the Rayleigh integral:

$$V_n(x, y, z) = -\frac{\partial}{\partial n} \left( \frac{1}{2\pi} \int_S V'_n(x', y', z') \frac{\exp(ikR)}{R} dS \right). \quad (7)$$

Here  $V_n(x, y, z)$  is the component of the velocity normal to the surface of the radiator,  $R = \sqrt{(x-x')^2 + (y-y')^2 + (z-z')^2}$ ,  $S$  is the surface where the distribution of normal velocity component  $V'_n(x', y', z')$  is given (between the ribs), and  $dS$  is the spatial element of this surface. Once the velocity distribution  $V_n(x, y, z)$  at the radiator surface was obtained, then the phases were inverted and the acoustic field was radiated backward to the focus.

In both the geometric and diffraction methods the pressure distributions in the focal region were calculated in two steps. First, the spatial distribution of the velocity was calculated in the plane of the ribs using the boundary condition at the source and the Rayleigh integral in the form of the Eq. (7). Then the velocity on the ribs was set to zero and pressure amplitude distribution in the focal region,  $p(x, y, z)$ , was calculated from the velocity distribution between the ribs using another form of the Rayleigh integral:

$$p(x, y, z) = -if\rho \int_S V'_n(x', y', z') \frac{\exp(ikR)}{R} dS, \quad (8)$$

where  $\rho$  is the density of the propagation medium. The intensity distributions in the plane of ribs and in the focal plane were calculated from the distributions of the pressure amplitude in the quasi-plane wave approximation as

$$I(x, y, z) = |p|^2 / 2\rho c, \quad (9)$$

where  $|p|$  is the pressure amplitude.

Calculations of the power losses on the ribs, peak intensities at the focus, and the power in the focal region within the -6 dB contour were compared for the two boundary conditions assuming the same total power transmitted by the radiator.

In reality, it is not possible to provide an arbitrary pressure or velocity distribution at the surface of a single-element radiator, but multiple element arrays can be used to approximate such a distribution. Therefore, the next problem was to calculate the field of a realistic 2D phased array and compare it with the fields radiated by the idealized source to reveal additional distortions of the field distributions on the ribs and in the focal region due to the discrete structure of the array.

The array used in simulations and in experiments consisted of 254 circular elements, each of 7 mm in diameter and 1 MHz operational frequency. The elements were distributed on a spherical surface in a quasi-random manner. The minimum centre to centre spacing between the elements was 7.9 mm and the largest spacing was 9.4 mm. The radius of curvature of the spherical shell and its diameter were 130 mm and 170 mm, respectively. A central hole of 40 mm diameter was provided for insertion of an imaging transducer. The active area of the array was about 100 cm<sup>2</sup>. Further details of the array, its specifications, and results of free field laboratory testing in water are given in Hand et al. (2009).

Generation and control of RF signals applied to the array elements were provided by a commercially available system (Model 500-013, Advanced Surgical Systems, Inc., Tucson, AZ). The 256 channel system had a power capability of up to 60 W per channel, constrained within a total power of 1800 W and frequency was adjustable from 0.8 to 1.25 MHz.

As an experimental model, a rib cage phantom and samples of porcine rib cages were used to simulate HIFU propagation through ribs (Figures 44 and 45).

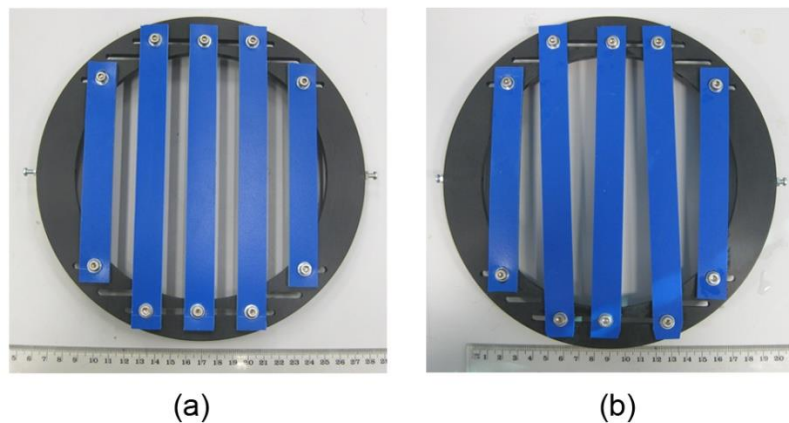


Figure 44. Photo of the phantom (a) with parallel and (b) nonparallel strips Reprinted from *Ultrasound Med. Biol.* 36(6) Bobkova, S., Gavrilov, L., Khokhlova, V., Shaw, A., & Hand, J. Focusing of high intensity ultrasound through the rib cage using therapeutic random phased array 888-906. Copyright (2010), with permission from Elsevier.

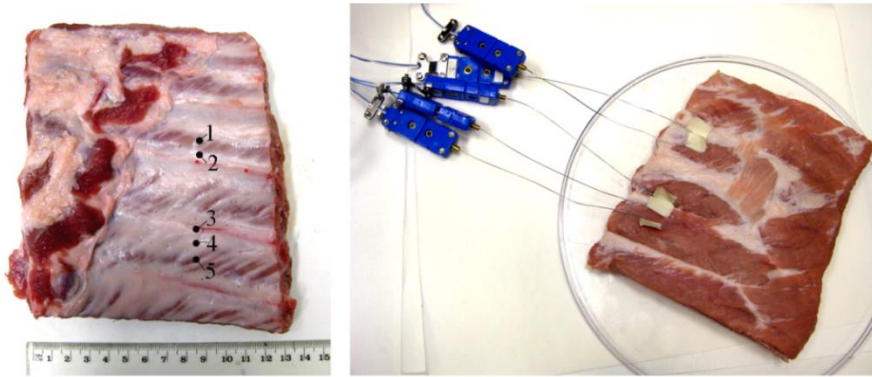


Figure 45. Photo of rib cage with thermocouples located on the ribs (2 to 5) and in the intercostal spaces (1) Reprinted from *Ultrasound Med. Biol.* 36(6) Bobkova, S., Gavrilov, L., Khokhlova, V., Shaw, A., & Hand, J. Focusing of high intensity ultrasound through the rib cage using therapeutic random phased array 888-906. Copyright (2010), with permission from Elsevier.

To investigate possible thermal effects of ultrasound on the ribs and intercostal tissues, temperature measurements were carried out using five copper-constantan thermocouples inserted in the porcine rib cage.

Certain elements of the array were switched off in the following way: if the ray connecting the centre of the element intersected the rib then the element was switched off, otherwise it was on. For this case the number of working elements was 114. Figure 46 (Bobkova et al. 2010) shows the distribution of working elements of the array surface; filled circles denote the elements that are switched on, open circles are the disabled elements. The distribution is calculated in spherical co-ordinates similar to the case of the ideal radiator. For total acoustic power of the array of  $W_0 = 11 \text{ W}$ , the amplitude of the velocity for each working element was  $V=0.06 \text{ m s}^{-1}$ .

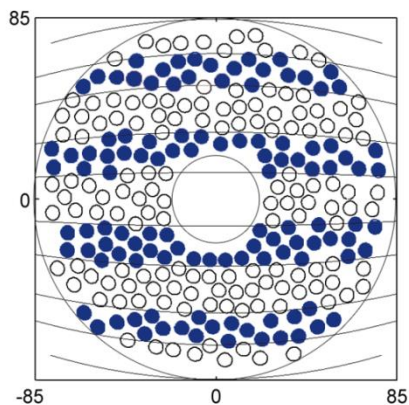


Figure 46. The distribution of working elements at the array surface in spherical co-ordinates. Filled circles denote the elements that are switched on, open circles are the disabled elements Reprinted from *Ultrasound Med. Biol.* 36(6) Bobkova, S., Gavrilov, L., Khokhlova, V., Shaw, A., & Hand, J. Focusing of high intensity ultrasound through the rib cage using therapeutic random phased array 888-906. Copyright (2010), with permission from Elsevier.

It has been observed in previous studies that the presence of acoustic obstacles similar to ribs in the ultrasound propagation path may cause a splitting of the focus (Li et al. 2007; Liu et al. 2007). This phenomenon is of particular importance in the case of a real-size rib cage and large-aperture, multiple-element, phased arrays. The splitting effect when focusing through ribs was present in both modeling and measurements (Tanter et al. 2007; Li et al. 2007; Liu et al.

2007; Aubry et al. 2008), but the physical nature and general properties of this phenomenon were not discussed in detail. The rib cage serves as a periodic spatial pattern and leads to splitting the focus into three foci (Figure 47, Bobkova et al. 2010). This Figure shows (a) simulated and (b) measured intensity distributions in  $x$ - $y$  co-ordinates in the focal plane ( $z = 130$  mm) for the array with some elements switched off; acoustic power of 11 W and time of heating of 0.2 s; here no ribs were present in the beam path. The intensity distributions are presented as contour lines from  $10 \text{ W cm}^{-2}$  to  $110 \text{ W cm}^{-2}$  in increment of  $10 \text{ W cm}^{-2}$ . Figure 47c shows the 1D intensity distribution along the  $y$ -axis at  $x=0$ . The amplitude level in two side foci is 0.54 and 0.47 of the peak intensity in the main lobe for geometrical and diffraction approaches, respectively. The distance between the main and secondary maxima is 4.7 mm in both cases. The parameters of splitting the focus can be obtained using the basic results of wave diffraction on aperiodic spatial structure (Gorelik 1959; Goodman 2004).

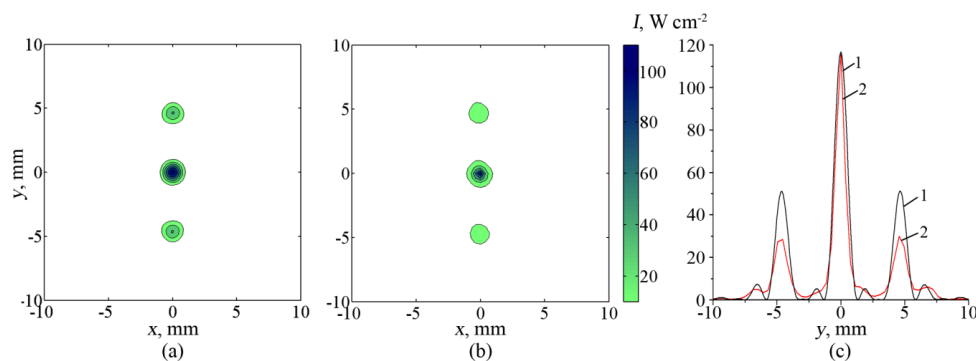


Figure 47. Intensity distributions in the focal plane ( $z=130$  mm) for the partially activated array for a single focus located at  $(0, 0, 130$  mm) without a rib phantom placed in the beam path. (a) Predicted intensity distribution, (b) IR-measured intensity and (c) 1-D distribution of the corresponding quantities over the vertical co-ordinate  $y$  perpendicular to the direction of ribs for theory (curve 1) and experiment (curve 2). The contours in (a,b) are given with increments of  $20 \text{ W cm}^{-2}$ . Measurements and simulations were carried out for the acoustic power of 11 W and time of heating of 0.2 s. Reprinted from *Ultrasound Med. Biol.* 36(6) Bobkova, S., Gavrilov, L., Khokhlova, V., Shaw, A., & Hand, J. Focusing of high intensity ultrasound through the rib cage using therapeutic random phased array. 888-906. Copyright (2010), with permission from Elsevier.

The mechanism of splitting of the focus and the appearance of the side foci, leading to an additional  $\sim 50\%$  reduction of the intensity in the main focus and undesired hot spots in tissue diffraction effects due to the regular structure of ribs has been discussed in several papers (Khokhlova et al. 2010, Bobkova et al. 2010; Yuldashev et al. 2013).

The feasibility of producing thermally ablated lesions in porcine tissues *ex vivo* behind the phantom and the sample of rib cage, as demonstrated by the results reported by Bobkova et al. (2010), will be presented in Section 4.4. The approach used provides an acceptable quality of focus for real bones in the chest and shows the possibility of applying the method in clinical practice for tissue destruction beyond the rib cage without overheating the bone and overlying tissues.

Recently, Kim et al. (2011) proposed a method to eliminate the effects of the splitting of the foci by means of the use of very short, but powerful pulses of focused ultrasound. According to this approach, the intensity in the focus has to exceed the threshold of cavitation damage, but in the secondary foci it should be below this threshold. Furthermore, the use of such a regime should substantially reduce the heating of the bone in comparison with to the use of continuous irradiation. In turn, Khokhlova and co-authors (Ilyin et al. 2011; Yuldashev et al. 2013) proposed a similar effect by pulsed high intensity focused ultrasound in the nonlinear regime with the formation of shock fronts in the focus. This enhances the thermal effect in the main focus,

without affecting significantly the heat generated in the side foci, and increases the local impact of ultrasound on a predetermined volume of tissue whilst reducing the thermal effect on the rib cage.

The design of a prototype of a transcostal HIFU system for the treatment of liver lesions was started recently ter Haar and colleagues (Gelat et al. 2011, 2012) based on modeling of the acoustic field of a random multi-element HIFU array scattered by human ribs and optimization of acoustic fields for ablative therapies of tumours in the upper abdomen.

### 3.7. Real Constructions of 2D- Random Powerful Phased Arrays and Methods of Measuring their Acoustic Parameters

Despite the evident advantages of random arrays, all 2D phased arrays developed and fabricated in different laboratories have been regular until recently. Arrays with elements distributed in a square pattern (according to our investigations, the most disadvantageous method for arranging elements) have been used the most frequently (Ebbini and Cain 1991; Wan et al. 1996; Daum and Hynynen 1998; Fan and Hynynen 1996; McGough et al. 1996). Until recently, the only exception has been the work fulfilled at the Laboratoire Ondes et Acoustique, ESPCI, Université Paris (Pernot et al. 2003), in which a sparse quasi-random array was fabricated for the first time. The array was made of 200 high power piezocomposite transducers (8 mm diameter, 0.5 cm<sup>2</sup> active areas, Imasonic, Besançon, France), which were mounted in a sealed spherically curved holder. Each element worked at 0.9 MHz central frequency. Thus, the diameter of the elements was  $4.8 \lambda$ . The diameter and radius of curvature of the array were, respectively, 180 and 120 mm. Thus, all these parameters were close to those proposed in previous simulations and patents (Gavrilov and Hand 2000a,b; Hand and Gavrilov 2000, 2002a-c). Each transducer element was individually matched to the 50  $\Omega$  output impedance of the generator. The coaxial lines from the matching boxes were connected to a computer controlled 200-channel electronic driving system, each channel of which was fully programmable and had its own transmit and receive electronics board. The maximum intensity at the transducer surface could be as high as 20 W cm<sup>-2</sup>. The photographs of this array are presented in Figure 48 (Pernot et al. 2003).



Figure 48. The 200-element sparse array prototype and the electronic system. The waterproof box contains the 200 electrical matching boxes. On the right: the quasi-random distribution of transducers mounted in a sealed spherically curved holder. From Pernot, M., Aubry, J.-F., Tanter, M., Thomas, J.-L., and Fink, M. (2003). High power transcranial beam steering for ultrasonic brain therapy. *Phys. Med. Biol.*, 48, 16, 2577–2589. © Institute of Physics and Engineering in Medicine. Published on behalf of IPEM by IOP Publishing Ltd. All rights reserved.

A modification of this array (Pernot et al. 2007; Marquet et al. 2011, 2013) contained 300 fully programmable individual electronic channels with 220 emitting channels and 80 emitting and receiving channels. The 8 mm diameter individual transducers with  $0.5 \text{ cm}^2$  active area had a 1 MHz central frequency and supported a maximum output power of more than  $40 \text{ W cm}^{-2}$  during 5 seconds.

The experimental studies conducted confirmed a high quality of the performance of such arrays (Pernot et al. 2003, 2007; Marquet et al. 2011, 2013). The results of research into the propagation of focused ultrasound through the bones of a human skull and ribs obtained using these arrays are presented in Section 4.4.

Recently Marsac et al. (2012) reported a novel modification of a phased-array system consisting of 512 ultrasonic elements positioned inside a whole body 1.5 T clinical Magnetic Resonance (MR) imaging system. The probe was partially spherical (15 cm focus and 23 cm aperture) in order to focus the acoustic energy at the geometrical focus. The circular elements were 6 mm in diameter, the operating frequency was 1 MHz and the maximum acoustic intensity was  $20 \text{ W cm}^{-2}$ . The elements were oriented in a non-periodic geometry in order to lower grating lobes while permitting a tight ellipsoidal focal pattern (half-pressure beam dimension of 1.5 mm laterally and 5 mm axially). Only 384 of the 512 elements were active. The array was composed of non-ferromagnetic materials to avoid imaging artifacts during MR-guided experiments.

In 2007 Imperial College London (London, United Kingdom) was funded by Cancer Research UK (CRUK) to fabricate an array in accordance with patents described by Hand and Gavrilov (2000, 2002a-c). In 2008 the array was manufactured from a composite material by Imasonic (Voray sur l'Ognon, France) (Figure 49), and a 256-channel electronic system for driving and digital control of phases and amplitudes at all the elements was obtained from Advanced Surgical System, Inc. (United States). The array transducer consisted of 254 circular elements, each 7 mm in diameter (somewhat smaller than 5 wavelengths), distributed randomly, but with a minimum inter-element (centre to centre) spacing of 7.9 mm, on a spherical surface with a radius of curvature of 130 mm and a diameter of 170 mm. The largest spacing between centres of neighbouring elements was 9.4 mm. The active area of the array was approximately  $100 \text{ cm}^2$ . A biocompatible epoxy-resin-based matching layer was incorporated at the array surface to improve transmission of acoustic energy and provide electrical insulation. A central aperture 38 mm in diameter was provided for insertion of an imaging transducer. Figures 49(a)–(b) show the front and side views of the array and its holding mechanism that provided adjustment. More details about the design of the device are given in (Hand et al. 2009).

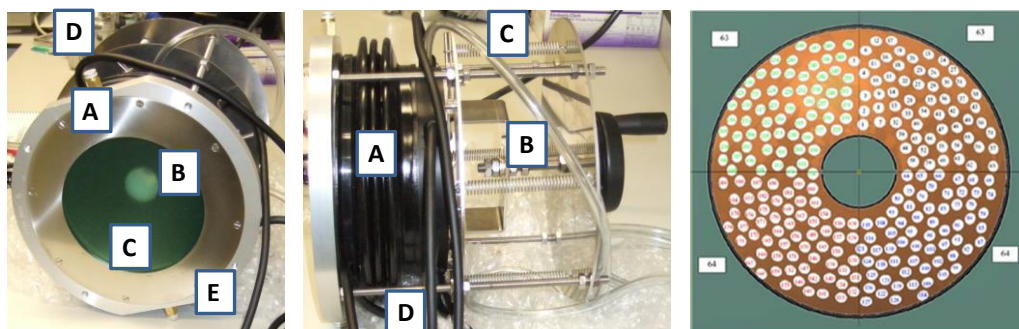


Figure 49. (a) Front view of the array and positioning mechanism: (A) stainless steel ring used to hold and seal the thin membrane, (B) the central hole for locating the imaging transducer (not shown), (C) part of the spherical surface of the array, and (D) and (E) entry and exit ports for the circulating temperature controlled, degassed water bolus. (b) (A) Flexible housing containing the water bolus, (B) screw mechanism for adjusting the position of the array with respect to the front membrane, (C) protective tube containing thermocouples for monitoring the array's temperature and (D) two of the four bundles of cables supplying RF signals to the four quadrants of elements. (c) The distribution of elements and their

grouping into four quadrants containing (clockwise from top right) 63, 64, 64 and 63 elements, respectively. The outer diameter is 170 mm and the diameter of the central aperture is 38 mm. From Hand, J. W., Shaw, A., Sadhoo, N., Rajagopal, S., Dickinson, R. J. & Gavrilov, L. R. (2009). A random phased array device for delivery of high intensity focused ultrasound. *Phys. Med. Biol.*, 54, 5675-5693. © Institute of Physics and Engineering in Medicine. Published on behalf of IPEM by IOP Publishing Ltd. All rights reserved.

The 256-channel system had a power capability of up to 60 W per channel, constrained within a total power of 1800 W and frequency was adjustable from 0.8 to 1.25 MHz. The resolution in control of the power and phases at each channel is 8 bit, the total acoustic power in the experiments was not elevated above 250 W. Phase and power data for each of the 254 channels were generated using the theoretical data obtained in the modeling to produce and steer a single focus or create patterns of multiple simultaneous foci.

The generator was controlled by a laptop computer (Dell Latitude, Intel® Core™ 2 Duo U7600 1.2 GHz processor, 2 GB RAM) via an RS-232 link. Proprietary software (Large Array Interface v1.2.0.0, Advanced Surgical Systems Inc., Tucson, AZ) was used to set the operating frequency and to select active channels and their relative phases (0 to 360° in increments of 2.25°) and relative powers (8 bit control) via a text file. The nominal electrical power level, limits on forward and reflected power per channel, and the duration of sonication were set via the main window of the user interface. The array could also be driven with a stack of files containing differing relative phases and powers. The rate at which this stack was sequenced and the relative power applied to each set of driving parameters within the stack could also be selected, or for refresh rates greater than 9 Hz, could be controlled by an external timing signal. Phase and power data for each of the 254 channels to produce and steer a single focus and patterns of multiple simultaneous foci were generated using a Fortran 90 code based on theory described in full by Gavrilov and Hand (2000a,b).

Ultrasound power was determined using radiation force measurements with a target containing castor oil (Shaw 2008). The array and its holding system, pointed vertically, were fixed to a frame, which also supported a water tank mounted above the array (Figure 50, Bobkova et al. 2010). The oil-filled target was placed in the tank and was suspended from a balance and positioned to intercept the whole of the ultrasound field generated by the array. A series of experiments were performed in which the array was driven on for 6.5 s and off for 6.5 s and when on, the power was stepped from 20% to 100% of the maximum power level set in steps of 20%. The output of the balance was recorded at 100 ms intervals throughout each experiment. The maximum electrical power applied to the array in these experiments was approximately 490 W.

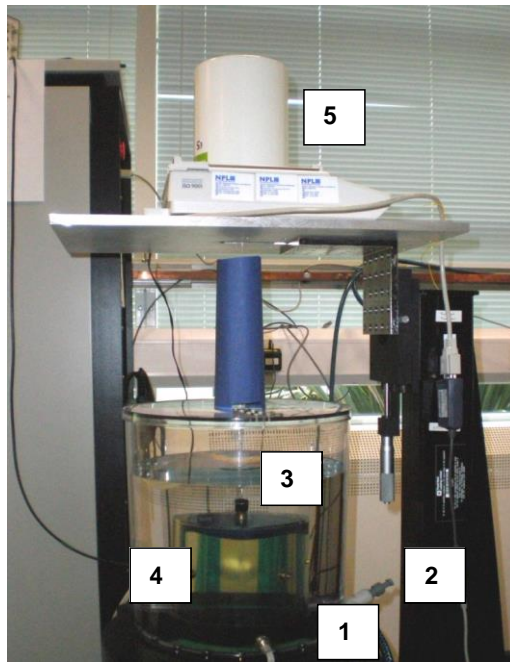


Figure 50. Arrangement for ultrasound power measurement. Reprinted from *Ultrasound Med. Biol.* 36(6) Bobkova, S., Gavrilov, L., Khokhlova, V., Shaw, A., & Hand, J. Focusing of high intensity ultrasound through the rib cage using therapeutic random phased array 888-906 Copyright (2010), with permission from Elsevier.

Since a method based on a scanned hydrophone would be prohibitively slow given the potentially large number of focusing conditions and fields that can be generated by the array, an alternative technique based on measurements made by using an infrared (IR) camera was used to provide a rapid qualitative assessment of field distributions, including identification of the existence and location of grating lobes and other local regions of high intensity. The method is based on imaging the temperature distribution produced in a thin absorbing layer by a short (0.1–0.2 s) burst of relatively low power (a few watts) ultrasound. In this case, it may be assumed that the rate of change of temperature is proportional to intensity in a monofrequency field, and so the temperature distribution after a sufficiently short time should also be proportional to intensity. The development of an IR-method with the aim to turn it in the quantitative method of measuring absolute values of intensity in acoustic fields of different transducers are presented in several papers (Bobkova et al. 2010; Shaw et al. 2011; Khokhlova et al. 2013; Shmeleva et al. 2013).

The experimental setup used for the investigation of the described phased array with the use of IR-method is shown in Figure 51 (Hand et al. 2009). IR measurements were carried out using a modified ThermoScope® pulsed thermography system (ThermalWave Imaging Inc., Ferndale, MI) consisting of an IR camera and a PC running EchoTherm® v6.4 software (ThermalWave Imaging Inc., Ferndale, MI). The camera was a Phoenix MWIR 9705 (FLIR Systems, Boston, MA) operating in the band 1.5 to 5.0  $\mu\text{m}$  with a 14 bit indium antimonide detector providing 320 x 256 pixels at a pitch of 30  $\mu\text{m}$ . Image data were transferred via an RS422 link to the PC. The system and software provided a method of acquiring, viewing and saving IR images synchronized to a pulsed source. The system was configured to capture a sequence of frames at a rate of 50 fps, with the ultrasound burst starting at the tenth frame that was stored as a movie in RAW format to preserve the maximum dynamic range for later analysis. The distributions shown were of temperature change over a period of 0.08 s and were derived from the subtraction of the 10th frame from the 14th. The ultrasound beam was directed vertically upwards onto a 2.5 mm thick sheet of NPL F28 ultrasonic absorber (Precision

Acoustics, Dorchester, UK) with a single-pass insertion loss of 7.5 dB at 1 MHz. The distance between the absorber and the transducer was adjustable using a micrometer positioning stage with  $\pm 25$  mm of travel. The other side of the sheet was air-backed and viewed from above by the IR camera, which was focused on the upper surface of the sheet. The distance between the lens and the sheet was approximately 24 cm, giving a spatial resolution of 0.28 mm using a 25 mm lens. The thermal resolution was approximately 5.6 mK. The plane of the geometric focus of the array was determined by driving all elements with the same phase, and identifying the position of the micrometer where the maximum temperature rise was observed. This was determined at the start of each set of experiments and used as a datum. For the majority of measurements made, the nominal RF power supplied to the array was less than 20 W.

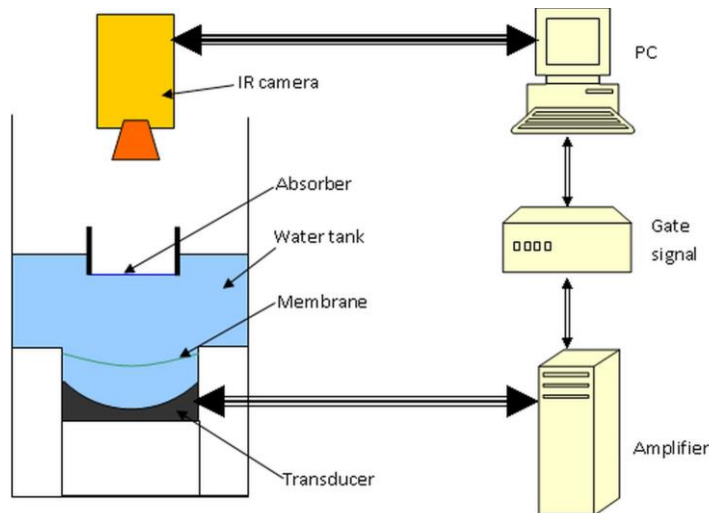


Figure 51. IR camera and absorber setup for assessment of intensity distributions produced by the array From Hand, J. W., Shaw, A., Sathoo, N., Rajagopal, S., Dickinson, R. J. & Gavrilov, L. R. (2009). A random phased array device for delivery of high intensity focused ultrasound. *Phys. Med. Biol.*, 54, 5675-5693. © Institute of Physics and Engineering in Medicine. Published on behalf of IPEM by IOP Publishing Ltd. All rights reserved.

As an example, Figure 52 (Hand et al. 2009) presents measured temperature change and predicted intensity distributions in  $x$ - $y$  planes at  $z = 120, 125, 130, 135$  and  $140$  mm for a single focus located at  $(x, y, z) = (0, -10, 130$  mm). Each case is normalized to its maximum value.

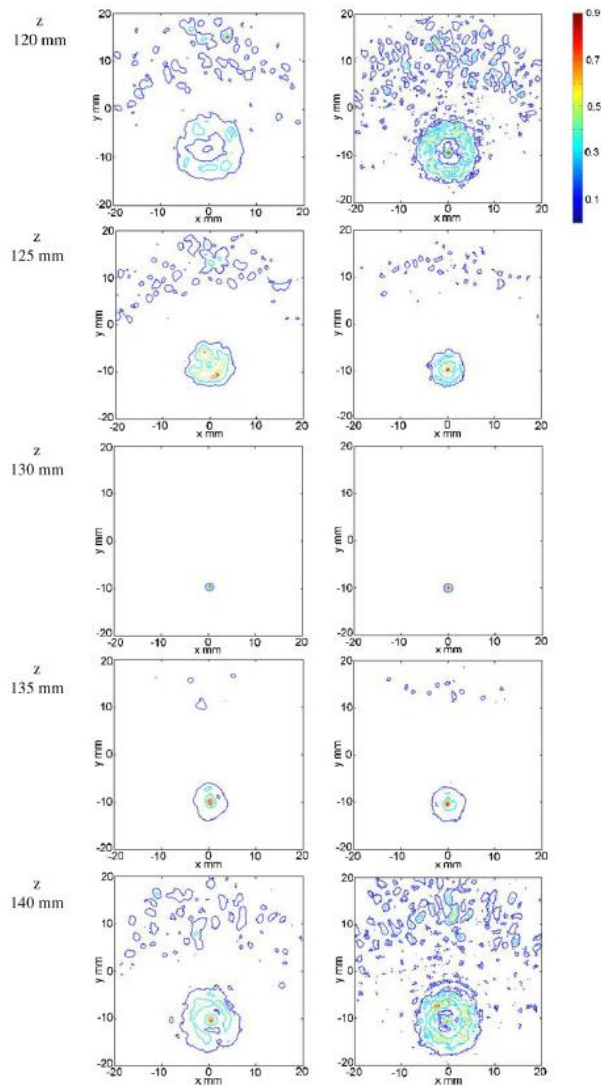


Figure 52. Measured temperature change (left column) and predicted intensity (right column) distributions in  $x$ - $y$  planes at  $z = 120, 125, 130, 135$  and  $140$  mm for a single focus located at  $(x, y, z) = (0, -10, 130)$  mm). Each case is normalized to its maximum value From Hand, J. W., Shaw, A., Sadhoo, N., Rajagopal, S., Dickinson, R. J. & Gavrilov, L. R. (2009). A random phased array device for delivery of high intensity focused ultrasound. *Phys. Med. Biol.*, 54, 5675-5693. © Institute of Physics and Engineering in Medicine. Published on behalf of IPEM by IOP Publishing Ltd. All rights reserved.

The possibility to generate and steer simultaneous multiple foci was also demonstrated, an example of which is shown in Figure 53 (Hand et al. 2009)

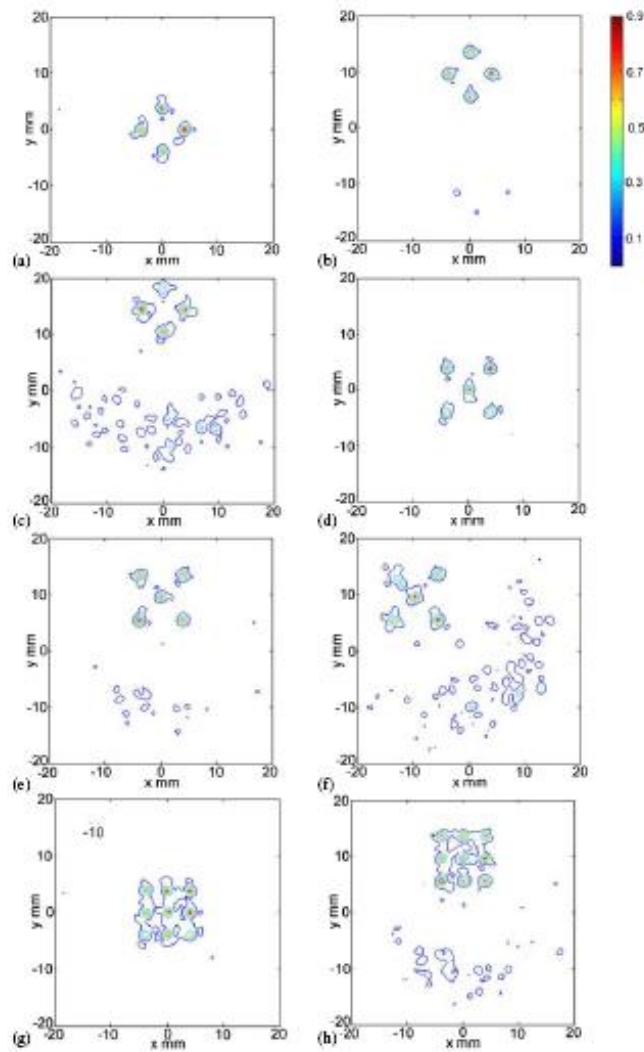


Figure 53. Measured temperature changes for multiple simultaneous foci in the plane  $z = 130$  mm on and steered off the central axis. Four foci at (a)  $(x, y, z) = (0, 0, 130$  mm); (b)  $(x, y, z) = (0, 10, 130$  mm); (c)  $(x, y, z) = (0, 15, 130$  mm). Five foci at (d)  $(x, y, z) = (0, 0, 130$  mm); (e)  $(x, y, z) = (0, 10, 130$  mm); (f)  $(x, y, z) = (-10, 10, 130$  mm). Results of switching between patterns of four and five foci at (g)  $(x, y, z) = (0, 0, 130$  mm) and (h)  $(x, y, z) = (0, 10, 130$  mm). In all distributions, contours are at 10, 30, 50, 70 and 90% of the maximum value in each case From Hand, J. W., Shaw, A., Sadhoo, N., Rajagopal, S., Dickinson, R. J. & Gavrilov, L. R. (2009). A random phased array device for delivery of high intensity focused ultrasound. *Phys. Med. Biol.*, 54, 5675-5693. © Institute of Physics and Engineering in Medicine. Published on behalf of IPEM by IOP Publishing Ltd. All rights reserved.

Several experiments were carried out to produce thermal ablation in various pieces of pork (pork chops, leg of pork). Typical examples of ablation in porcine soft tissue samples will be presented in Section 4.4.

A multi-element ultrasound phased array for the ablation of deep-seated tissues has also been developed by Chinese scientists (Ji et al. 2011). A 90-element HIFU spherical phased array applicator with annular element distribution and unequal element spacing was operated at 1MHz. The array was constructed from piezoelectric lead zirconate titanate (PZT-8) circular elements of 1.4 cm in diameter (i.e.  $9.3 \lambda$ ) and had a focal length of 11 cm. The simulations carried out by the authors demonstrated that the array can steer the focus with intensity distributions of good quality up to 6 mm off the axis over distances ranging from 17 to 21 cm along the axis. The beam focusing capability was demonstrated in deep tissue through a series of *ex vivo*

experiments. The authors suggested that these results indicated that the array was appropriate for the ablation of deep-seated tissue.

Randomization of the distribution of elements has been used by applied by Philips Healthcare in the development of a multi-element clinical HIFU system (Yuldashev and Khokhlova 2011; Kreider et al. 2013). The transducer array was part of a Sonalleve V1 3.0T MR-HIFU system (Philips Healthcare, Vantaa, Finland) installed at the Bio-Molecular Imaging Centre at the University of Washington (Seattle, WA). The array consists of 256 circular elements each 6.6 mm in diameter, arranged on a surface with a 120 mm radius of curvature and an aperture of 127.8 mm and is operated at a frequency of 1.2 MHz; the other parameters of the array resemble those presented in Hand et al. (2009).

Another patented design of an array with random or irregularly distributed elements was that of Clark et al. (2013) in which the locations of 1/8 of randomized elements were copied and then rotated to fill the other 7/8 of the array surface.

### 3.8. Studies of Randomized Arrays

A number of papers demonstrating the role of randomization and usefulness its application in the design of two-dimensional phased arrays have been published in recent years.

ter Haar with co-authors (Gélat et al. 2012) investigated theoretically the optimization of acoustic fields for ablative therapies of tumours in the upper abdomen. The HIFU transducer modeled as part of the underlying work was a spherically shaped bowl of radius of curvature 18 cm populated with 256 plane circular elements each of 3 mm radius mounted on its surface. The outer diameter of the HIFU transducer was 16 cm. The elements were pseudo-randomly spatially distributed on the surface of the array. The excitation frequency was 1 MHz. A sketch of a frontal view of the array is shown in Figure 54 (Gélat et al. 2012).

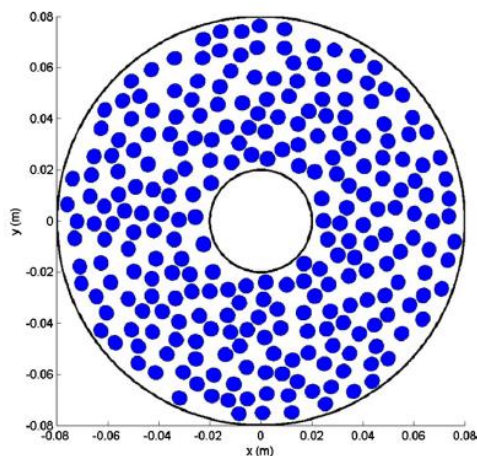


Figure 54. Frontal view of HIFU random phased array configuration. 3 mm element diameter, 16 cm array diameter, 18 cm focal length, 1 MHz frequency of operation (Gélat et al. 2012). From Gélat, P., ter Haar, G. & Saffari, N. (2012). The optimization of acoustic fields for ablative therapies of tumours in the upper abdomen. *Phys. Med. Biol.* 57, 8471–8497. © Institute of Physics and Engineering in Medicine. Published on behalf of IPEM by IOP Publishing Ltd. All rights reserved. Courtesy of the National Physical Laboratory, UK.

Another example of the use of a quasi-random two-dimensional array was given in the paper of Lee et al. (2010). An ultrasound applicator for trans-esophageal cardiac ablation without surgical incisions or blood contact was designed, developed and evaluated in this study. The transducer design was a two-dimensional sparse phased array with flat tapered elements operating at 1.6 MHz. This array used 64 active elements spatially sampled from 195 rectangular

elements. The diameter of the hole for the imaging probe was 19 mm. A prototype applicator was successfully tested *in vitro* using fresh porcine myocardial tissue. The experimental results indicated that the prototype array achieved the requirement for thermal ablation.

Scientists from France and Switzerland (Auboiroux et al. 2011) recently proposed and investigated a novel architecture for a HIFU phased-array designed to increase the capabilities of electronic steering without reducing the size of the elementary emitters. The principal medical benefit expected from the application of such devices is the time-effective sonication of large tumours in moving organs. They proposed to divide a focused phased array into two mechanically interleaved sub-arrays of different resonance frequencies, and further, to modify the orientation of each individual radiator such that all elements of a given sub-array were pointed at a distinct natural focus. The focal region of each sub-array was defined as the region of intersection of the normal directions of the elements that belong to that sub-array. As a result, each sub-array provides the generation of a focal region (using electronic steering) within a centimeter-range area surrounding its associated natural focus. The resulting compound steering range (defined as the integration of the two sub-array steering areas) was therefore larger than the steering range achievable using the usual focused phased array, for the same total number of elements. An appropriate set of phases was calculated for each sub-array, based on the spatial locations of the individual radiators and on the co-ordinates of the prescribed focus.

To half the number of output channels from the RF generator a passive spectral multiplexing technique consisting of parallel wiring of frequency-shifted paired piezoceramic radiators with intrinsic narrow-band response was used. Two sets of 64 emitters (circular, 5 mm diameter) were mounted, with operating frequencies of 0.96 and 1.03 MHz, respectively. Two different prototypes of the arrays device were built and tested, each incorporating the same two sets of emitters, but differing in the sizes of spherical caps supporting the transducers (radius of curvature/aperture of 130 mm/150 mm and, respectively, 80 mm/110 mm).

Acoustic measurements, MR-acoustic radiation force imaging (ARFI) *ex vivo* and MR-thermometry *ex vivo* and *in vivo* were used for the characterization of the prototypes. Experimental results demonstrated an enlargement of the steering range by 80% along one preferentially chosen axis, compared to that produced by a classic spherical array with the same total number of elements. The electric power density provided to the piezoceramic transducers exceeded  $50 \text{ W cm}^{-2} \text{ CW}$ , without need of active circulation of cooling water. Another important advantage of this approach is the versatility of reshaping the array at low cost. The experimental limitations of the fabricated devices are expected to be overcome by increasing the total number of individual elements.

Lu et al. (2008) suggested three methods to improve the quality of acoustic fields created by arrays with regular distributions of elements and to decrease the level of grating lobes and side lobes. These authors considered that adding random-amplitude signals greater than 10% of the maximum value to the original driving signals will suppress unwanted grating lobes and side lobes. The addition of random-phase signals to the original phase driving signals and a random arrangement of the multiple foci locations within a certain range were suggested.

All two-dimensional phased arrays systems intended for therapeutic applications in medicine require a large aperture to provide sufficient acoustical power and should have the ability to steer a focus or foci whilst keeping grating lobe levels to a minimum. At the same time it is desirable to minimize the total number of elements and electronic driving channels. Therefore investigation of an optimal distribution of elements on the surface of the array is a task of utmost importance. In this regard, Raju, Hall and Seip from the Philips Research North America, Briarcliff Manor, NY designed two 2-D space-filling therapeutic arrays with 128 elements arranged on a spherical shell (Raju et al. 2011). One was based on the two-shape Penrose rhombus tiling (Figure 55a) and the other was based on a single rectangular shape arranged non-periodically (Figure 55b). The steerability performance of these arrays was studied using acoustic field simulations. For comparison, the authors also studied two other arrays, one

with circular elements distributed randomly, and the other a periodic array with square elements. All arrays had an aperture of 100 mm, were on a spherical shell with a 100-mm radius of curvature, and had a 31-mm-diameter central opening for the potential installation of an imaging transducer.

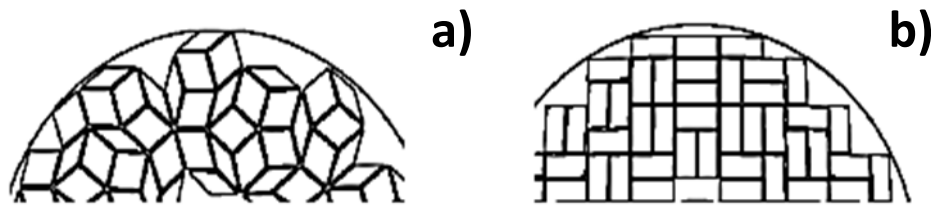


Figure 55. Sketch illustrating methods of tight packing of elements: a) Penrose rhombus tiling; b) rectangular shape elements arranged non-periodically.

Referring to the original paper by Raju et al. (2011), their figure 4 shows simulated beam plots, in a plane 100 mm from the aperture, when the beam was steered to a point 8 mm off the axis along the  $x$ -direction. As expected, the space-filling non-periodic arrays (Penrose array and rectangular array) and the random circles array produced beams in which the energy was mostly concentrated at the intended focal spot. Energy in the regions outside the intended focal spot was generally diffuse with one or few noticeable grating lobes. The random circles array showed a pattern in which the off-focus energy was more widely distributed than the other arrays, because of the random nature of the element placement, whilst the Penrose array showed some evidence of concentration of off-focus energy because of rotational symmetry in the tiling pattern. The rectangular array showed more evidence of concentration of off-focus energy, but the relative grating lobe level was still less than -10 dB. The periodic array, however, showed a strong relative grating lobe of -4.9 dB located at (-15.5, 0 mm).

The results showed that the two space-filling aperiodic arrays were able to treat a volume of 16 x 16 x 20 mm while ensuring that the grating lobes were under -10 dB compared with the main lobe. The rectangular aperiodic array (Figure 55b) was able to generate two and half times higher power compared with the random circles array. The rectangular array was then fabricated by patterning the array using laser scribing methods and its steerability was validated using hydrophone measurements.

This work demonstrates that the concept of space-filling non-periodic tiling can be used to generate therapy arrays that are able to provide higher power for the same total transducer area compared with fully random arrays while maintaining acceptable grating lobe levels and a low element count. The Penrose and rectangular arrays were able to handle the steering requirements to cover the intended treatment volume. The rectangular array was particularly advantageous because the elements were all uniform in shape and size and required simpler electrical matching networks. The concept can be extended to handle larger treatment volumes by increasing the number of elements, which still requires fewer elements than traditional array design methods.

Ellens et al. (2011) carried out simulation studies of sparse 2D fully electronically steerable focused ultrasound phased arrays for thermal surgery. Their study affirms the established observation that random sparse phased arrays can provide a comparable level of energy focus and grating lobe suppression as a fully-populated array with considerably less technical complexity. However the authors consider that for deep, non-invasive therapeutic ultrasound, the use of a flat phased array instead of a spherically-curved phased array presents a clear benefit: a large volume of tissue can be ablated without any mechanical motion suggesting that entire treatments can be performed by a fixed transducer. The design of such a transducer, however, presents a challenge. As others have shown and this study affirms, a solution to this problem is the use of random sparse arrays. However, this study also presents two primary, related

drawbacks to sparse arrays: significantly more power is required to perform equivalent ablation and, as a result additional energy is deposited elsewhere in the medium.

In addition to these conclusions, a further comment is that whilst “sparse” and “random” are essential for improvement of the quality of acoustical fields produced by the arrays, the key word is “random” because only randomness defines the elimination of grating lobes in the acoustical fields, even if the sparseness is very low.

It is noteworthy that in recent works arrays with a spiral arrangement of elements were studied. This simple and ingenious solution on the one hand avoids the regularity in the arrangement of the elements, and on the other hand places them with maximum density on the surface of the array, and achieves the maximum possible acoustic power from the given array aperture. Many simulations of fields of phased arrays with a spiral distribution of elements, demonstrating marked advantages of this approach, were made by Sapozhnikov (2010, unpublished data). Some configurations of spiral distributions of elements over the surface of the random array suggested and investigated by Sapozhnikov are presented in Figure 56. This idea was used also in other works (Stephens et al. 2011; Pinton et al. 2012).

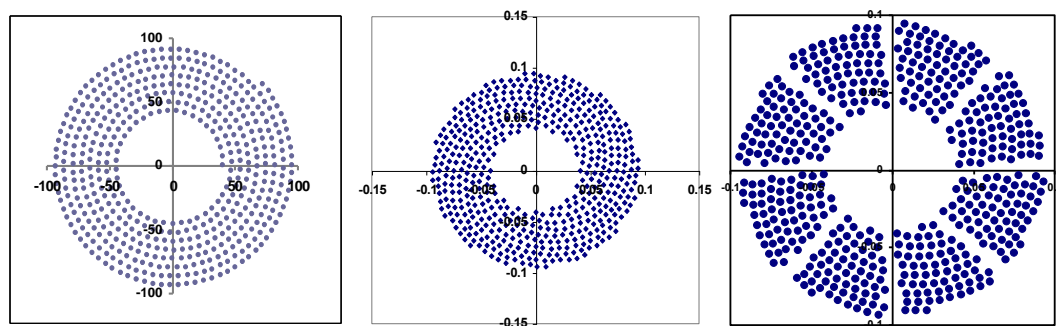


Figure 56. Some configurations of the spiral distribution of elements over the surface of the random array offered and investigated by Dr. O. Sapozhnikov (published from the permission of Dr. Sapozhnikov).

It was of interest to estimate the influence of a tight packing of elements on the value of maximum intensity in the focus and compare qualities of the intensity distributions of “usual” random phased arrays and tightly packed array with spiral distributions of elements over the surface of a random array.

Two random phased arrays consisting of 512 elements with operating frequency of 1 MHz were compared. There were two differences between them. The first array consisted of elements in the form of disks of diameter 6 mm; the second one included elements in the form of squares 6 mm x 6 mm. In the first case the elements were randomly distributed over the array surface. This array and location of elements are presented in Figure 57a. The remaining parameters of the first array were:

Diameter of the array	200.6 mm
Radius of curvature	150 mm
Diameter of the central hole for diagnostic probe	75 mm
Intensity at the surface of the elements	$5 \text{ W cm}^{-2}$ .

The minimal spacing between the elements was 0.44 mm and the maximal spacing was 1.35 mm.

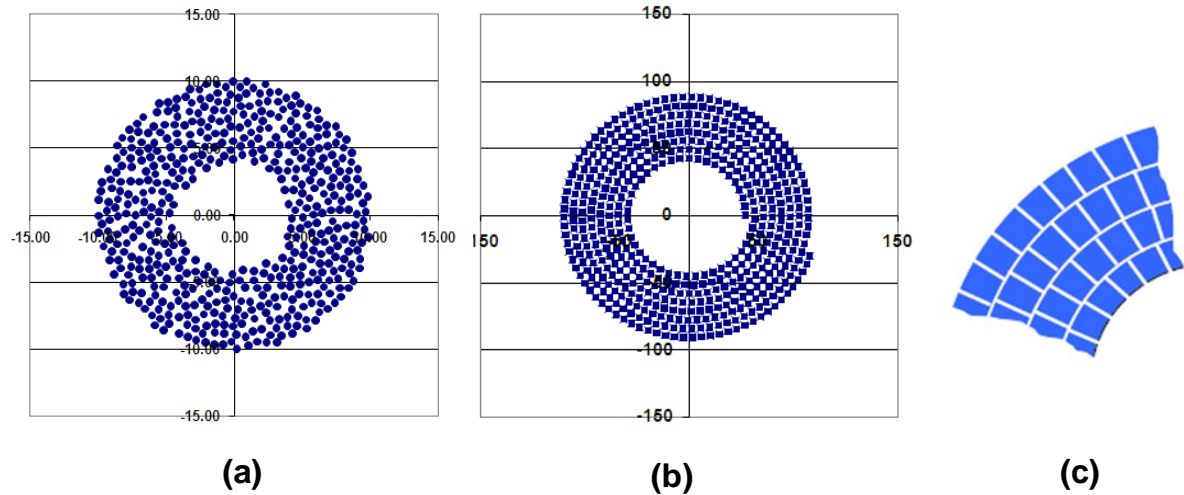


Figure 57. Two random phased arrays consisting of 512 elements with operating frequency of 1 MHz. (a) array with elements in the shape of disks 6 mm diameter randomly distributed over the array surface; (b) array with elements in the shape of squares (6 x 6 mm) located in the shape of an Archimedean spiral; (c) the way of location of elements in the array (b).

The elements in the second array were located in the shape of an Archimedean spiral (see Figure 57b). The spacing between all elements was 0.5 mm. The method of locating the elements is shown schematically in Figure 57c. The remaining parameters of the second array were:

Diameter of the array	191.3mm
Radius of curvature	150 mm
Diameter of the central hole	75 mm
Intensity at the surface of the elements	$5 \text{ W cm}^{-2}$ .

Calculations and estimations of qualities of the intensity distributions of random phased arrays and array with spiral distributions of elements were made with the use methods described in details in Sections 3.2 and 3.3. The summary of results of calculations and quality assessment of the intensity distributions for the single focus mode is presented in Figure 58.

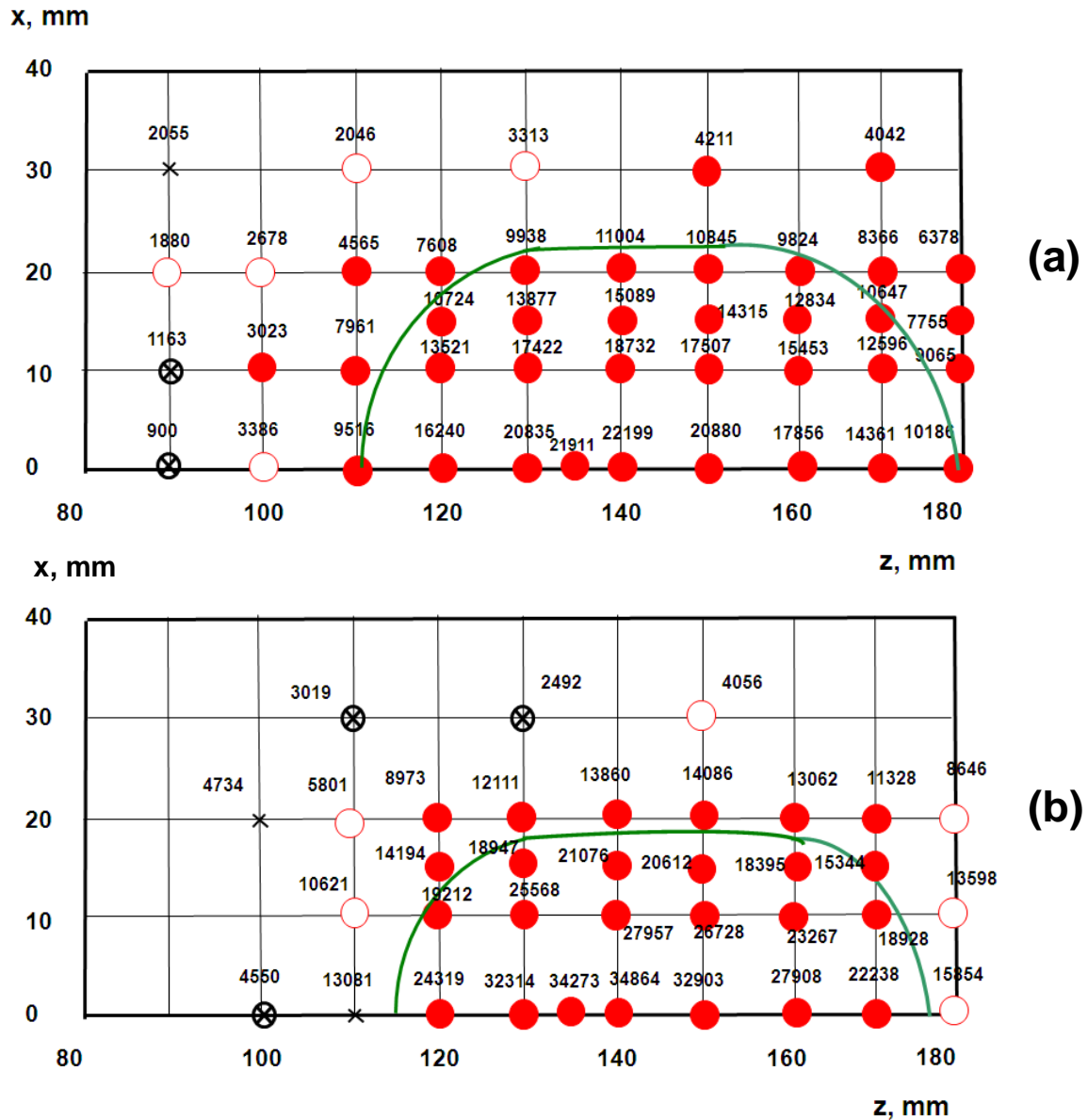


Figure 58. Summary of results of calculations and quality assessment of the intensity distributions for the single focus mode associated with the random array with elements in the shape of disks randomly distributed over the array surface (a); array with elements in the shape of squares (6 x 6 mm) located in the shape of an Archimedean spiral (b). The quality levels are: ● A grade; ○ B grade; × C grade; ⊗ D grade in accordance with Gavrilov and Hand (2000).

The filled circles correspond to the A grade quality which means that there are no secondary maxima excluding the focus itself with intensity  $\geq 0.1 I_{max}$  anywhere in the field. The curve inside the figure corresponds to the region limited by the value of the intensity of  $0.5 I_{max}$ . In practical application of arrays and with increased requirements to the intensity of focus, it is impractical to move the focus outside this area. The numbers adjacent to the points are the intensity values when focusing in the given point.

It is seen that in both the cases the maximum values of the intensity in the focus correspond to the point (0, 0, 140 mm) which is 10 mm nearer to the array than the geometric focus. For the “usual” random phased array (Figure 58a) that value is equal to  $22199 \text{ W cm}^{-2}$ , and for the second array it is  $34864 \text{ W cm}^{-2}$ , which is 1.57 times more. This result could be predicted because the active area of the tightly packed array becomes about 25% larger, and hence the intensity was increased in 1.25 squared.

Interestingly, the size of the area corresponding to the “effective” use of the array (limited by the curve shown in Figure 58) at the Archimedean array was markedly lower (approximately 4-5 mm in the range  $z = 130-160$  mm). The volume corresponding to such an “effective” region was reduced from about  $80 \text{ cm}^3$  to about  $50 \text{ cm}^3$ . This rather large reduction is the cost for achieving the increased maximum intensity in the main focus. The probable causes of this effect are a decrease in the angle convergence (an aperture became 190 mm instead of 200 mm) and the fact that the effective size of square elements is larger than those for the disk element and therefore the directivity of square elements is a somewhat narrower than that of the disk elements.

A possibility to increase the value of the maximal intensity in the focus of tightly packed array by about 60% in comparison with usual random arrays is of special interest in relation to recent attempts to use high intensity focused ultrasound in the nonlinear regime with the formation of shock fronts in the focus (see section 3.6 and works of Khokhlova and co-authors: Ilyin et al. 2011; Yuldashev et al. 2013).

The purpose of this Chapter was to show that the use of random instead of regular arrays can, in some cases, significantly improve the spatial intensity distribution in the field generated by the array. Recently Reverdy et al. (2012) gave a very visual illustration of the quality of acoustic fields, which can be created by array of different configurations (regular in the shape of squares, annular, hexagonal, with spiral distribution of elements, and random) - see Figure 59. The aperture and the element size were identical for all designs. The unquestionable advantage of two last types of the arrays can be clearly seen.

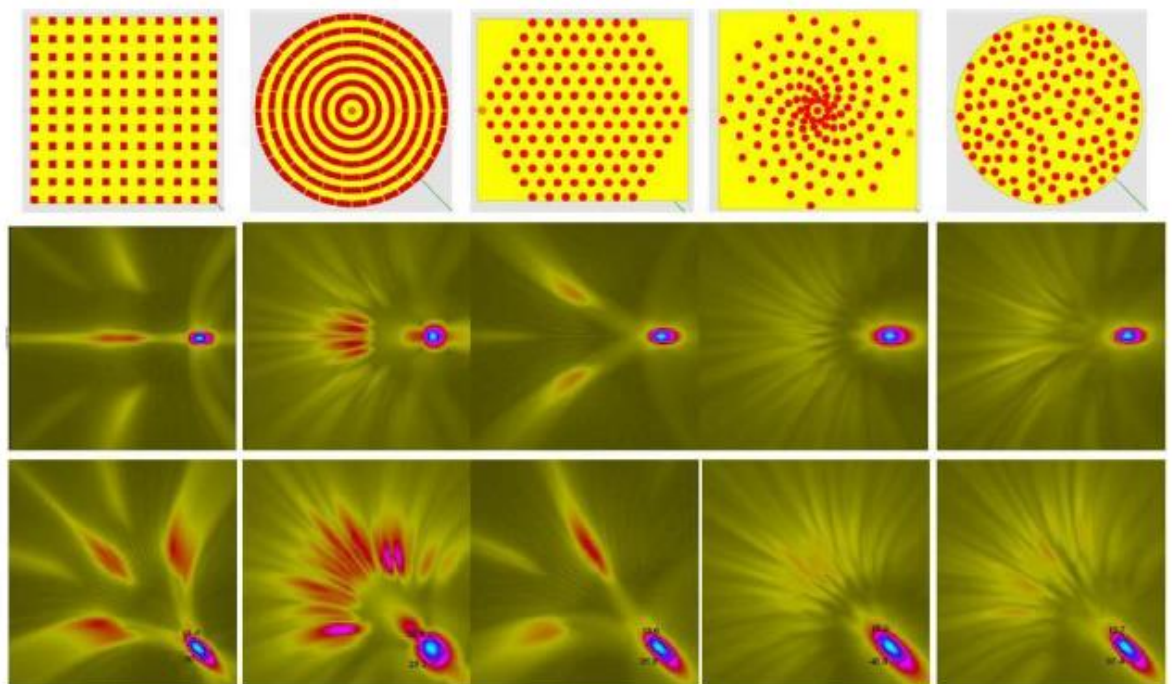


Figure 59: 2D array designs (above) and beam field calculations along the axis (middle row) and at  $45^\circ$  to the axis (bottom) (Reverdy et al. 2012).

More quantitative estimations are presented in Table 6; the reference value is the amplitude of the main lobe.

**Table 6. Main lobe and grating lobes for various 2D arrays (Reverdy et al. 2012)**

	Square	Annular	Hexagonal	Spiral	Random
Grating lobes (dB)- along the axis	-9	-8	-12	-19	-17
Grating lobes (dB)- at 45° to the axis	-8	-4	-7	-14	-13

In recent years, interest in random arrays has become obvious, and this approach has been used or discussed in a number of studies related to the use of focused ultrasound in medicine (Yin and Hynynen 2005, 2006; Pernot et al. 2007; Aitkenhead et al. 2008; Ji et al. 2009; Werner et al. 2010; Stephens et al. 2011; Raju et al. 2011; Ellens et al. 2011; Gélat et al. 2011, 2012; *etc.*).

In conclusion to this Chapter it is worth noting that the terms “random” and “randomization” are used here for convenience but in reality imply not only a method of placement elements on the array surface, but also the above mentioned limitations on the characteristic dimensions of the elements. The data given in Section 3.8 lead to an important conclusion for practice: a good quality of acoustic fields produced by a random array is possible to achieve using maximally tight packing of elements. So, of the requirements for the design of randomized array, the degree of sparseness is less important than the need for a randomized distribution of elements *per se* and need for the elements not to be highly directive.

## Potential Medical Applications of Powerful Phased Arrays

Potential medical applications of focused ultrasound and HIFU are very wide and diverse (see e.g. Jolesz and Mc Dannold, 2014) and have been discussed and analysed in many scientific papers and books. In some applications there is no need to employ such relatively expensive and complicated devices as multi-element phased arrays since simpler devices based on single element focused transducers are adequate. However, as has been mentioned earlier, the disadvantage of single element transducers is that they are able to focus ultrasound energy only at a fixed focal distance. Therefore if the dimensions of the targeted site for ultrasonic treatment are sufficiently large, the use of focused transducers with a fixed focal length is not always possible, even when mechanical scanning is used. In contrast, the greatest advantage of phased arrays is their ability to create multiple foci and resulting fields complex geometry. In this Chapter we shall only discuss those applications, which have been implemented entirely with the use of multiple elements phase arrays.

### 4.1. Surgery of Deep Brain Structures by Sonication through the Intact Skull

One example of an application which can only be solved by using multi-element phased arrays to compensate for the distortion caused by the skull is local and controlled lesioning in deep structures of brain by sonication through the intact skull.

In the 1990s two approaches were introduced almost simultaneously to correct the aberrations induced by the skull bone: time-reversal-based techniques (Fink 1992; Thomas and Fink 1996; Tanter et al. 1998, 2000) and the phase conjugation method (Hynynen and Jolesz 1998).

The first method implements the remarkable properties of the piezoelectric transducers, such as the reversibility of their properties (i.e., the ability to work both in transmit and receive modes), the linearity, and the ability to almost instantaneously measure the characteristics of a sound wave. The basis of this method is that the pressure field  $p(r_i, t)$  registered by a set of receivers with the location  $r_i$ , is digitized and stored during the time  $T$ . Then, the pressure field is re-emitted by the same transducers in the reverse temporal order (i.e., starting from the last and ending with the first signal). This is equivalent to the radiation of the field  $p(r_i, T - t)$ .

This procedure enables the conversion of the divergent field of a source to a converging wave, focused on this source. The method is implemented by using one-dimensional or two-dimensional array transducers. Each transducer is connected to its own electronic circuit, which consists of an amplifier of received signals, an analog-to-digital converter, the storage unit and the programmable radiator, able to synthesize the time-reversed version of the stored signal (Fink 1992).

The method was originally developed to control the location of stones accurately for lithotripsy (Fink 1992). The focusing of destructive ultrasonic waves under such conditions is a challenging task due to the non-uniformity of the sound velocity in the tissue and the distortion of ultrasonic beam. Furthermore, due to the respiration, the displacement of a stone can be up to 2 cm. Thus the aims of the procedure were to ensure the focusing of the ultrasonic beam and that it was aimed precisely at the stone.

Subsequently this method was used to study the propagation of focused ultrasound through an intact human skull (Thomas and Fink 1996; Tanter et al. 1998; Aubry et al. 2003; Pernot et al. 2003). In the first of these papers a single element of dimensions 1 x 10 mm was used as a source. A linear array consisting of 128 elements, each 1 x 25 mm and with a central frequency of 1.5 MHz, located on a concave surface with a radius of curvature of 100 mm. The

pressure field generated by the single element was recorded by the array and the recorded signals were time reversed, and then simultaneously emitted by the 128 elements.

A serious problem arose that was related to the need to steer the focus when using regular phased arrays. Successful attempts to overcome this problem were realized by Pernot et al. (2003) who used an array with elements randomly distributed on its surface (see Section 3.7). The array consisted of 200 elements, each 8 mm in diameter and driven at 0.9 MHz, and the diameter and radius of curvature of the array were 180 mm and 120 mm. By correcting signals at the array elements, the sound pressure in the focus after passing of focused ultrasound through the skull was increased by a factor of 4.5 compared with the case when no correction was applied. This is equivalent to increasing the temperature at the focus 20-fold using the same radiated power. Similar experiments were carried out at several positions of the skull bones, and in all cases the quality of the focus remained very good.

The ability to create tissue lesions in samples of bovine liver and sheep brain placed behind the human skull was demonstrated in this study (Pernot et al. 2003). Typically the diameter of the lesion was approximately 2 mm at a frequency of 0.9 MHz. The characteristics of the ablated tissues did not differ from those obtained without the skull bone in the path of the ultrasound propagation. The ability to move the focus electronically off the array axis and along the axis, in principle, enabled a volume of tissue  $3 \times 3 \times 4 \text{ cm}^3$  to be coagulated.

In the other reports (Pernot et al. 2004a, 2005a) an array consisting of 300 randomly arranged 1 MHz elements was used in experiments *in vivo*, performed on 22 sheep. Of these, 10 animals were sacrificed immediately after sonication. In half of them a craniotomy was performed for later comparison. In the other half a hydrophone was positioned in the targeted area of the brain, and then focused ultrasound was applied. The remaining 12 animals were divided into 3 groups which were sacrificed, after one, two and three weeks following exposure. In total, histological analyses were carried out in 12 animals, in 10 of which thermal destructions of the brain were detected. In other publications Pernot et al. (2004b, 2005b) investigated the possible overheating of the human skull during this procedure and theoretical and experimental methods to assess it.

The second approach for inducing local lesions in deep structures of brain by means of sonication through the intact skull was suggested and developed by Hynynen and his colleagues.

In an early publication (Hynynen and Jolesz 1998) the possibility of destroying deep brain structures by sonication through the intact skull by means of cavitation, rather than thermal coagulation necrosis was shown. Since cavitation thresholds in tissues are relatively weakly dependent on the duration of exposure, ablations may be obtained by using several short pulses of high intensity ultrasound, thereby avoiding the thermal damage of the bone. Studies were carried out using single element focused radiators with a diameter of 10 cm and different frequencies (0.246, 0.559, 1.0 and 1.68 MHz), as well as two-dimensional arrays (frequencies of 0.6 and 1.58 MHz) of the same diameter, consisting of 60 square elements with dimensions  $1 \times 1 \text{ cm}^2$ . A miniature hydrophone was used to measure the acoustic fields. It enabled the phase shift on each element of the array to be determined; these data were required, to compensate distortions caused by the human skull bone. A burr hole was made in the skull of a rabbit and lesions in the rabbit brain *in vivo* were created after passage of ultrasound through the human skull. Phase measurements using the two-dimensional 60 element arrays showed that at 0.6 MHz (wavelength of 2.5 mm) 80% of the phase errors caused by the presence of the human skull were less than  $90^\circ$  and, thus, the field from each element was adding to the pressure wave at the focus. However, when the frequency was increased to 1.58 MHz (i.e., the wavelength became less than 1 mm), the number of elements adding to the pressure wave at the focus was only 50%, and the quality of focusing sharply deteriorated. By using phased arrays the phase of signals at each of the elements can be corrected and a satisfactory quality of focusing can be achieved even at a frequency of 1.58 MHz. Lesions in the rabbit brain were achieved without heat damage to the

human skull above them. The results showed that transcranial delivery of therapeutic ultrasound into the brain may be feasible.

A numerical model, in which a human skull was represented as a three-layer structure (water, bone, brain) and geometrical characteristics of the skull were presented in a digital form on the basis of analysis of MR images of the skull, was described by Sun and Hynynen (1998). The model allowed the propagation of focused ultrasound through the skull to be calculated, taking into account absorption, diffraction, reflection and refraction of waves. It was assumed that focusing was performed using a two-dimensional phased array with diameter of 10 cm and radius of curvature of 10 cm, the surface of which was divided into different numbers of square elements (from 4 x 4 to 16 x 16), and the frequency was varied from 0.5 to 1.5 MHz. Without phase correction at the elements, the quality of focusing was very poor. However, despite the high attenuation in the bone, the complex shape and structure of the skull and its varying thickness in different areas, phase correction at the array elements minimized the shift of the focus from the calculated position, reduced the level of side lobes, and increased the intensity in the focus. The authors suggested that the optimum size of elements was 5-6 wavelengths. In other words, at 1 MHz, the optimal array should consist of  $10 \times 10$  elements of size 1 x 1 cm. It is desirable that the frequency for ultrasound surgery through the intact skull does not exceed 1 MHz to avoid possible overheating of the skull.

In a subsequent theoretical paper Sun and Hynynen (1999) considered a two-layer model consisting of bone and brain. It was assumed that the elements of a phased array were in direct contact with the skull. To enhance the sound pressure at a predetermined point in the brain, the surface of the array (and thus the sonicated surface of the skull) was chosen to be as large as possible - in reality six times greater than the case when a single focusing transducer was used. The amplitudes of the signals at the elements and hence on the outer surface of the skull were equalized, which achieved not only a threefold increase of pressure in the brain, but also reduced the possibility of local overheating of the skull. The optimal frequency for obtaining the greatest gain in sound pressure and acceptable heating of tissues in the focus was 0.6-0.65 MHz.

During the simulation it was assumed that there are no multiple reflections, standing waves or shear waves in the skull bones. It was assumed that the bone was homogeneous, and variations in the shape and thickness of the skull in different people were not considered. It was estimated that the number of elements in the array, covering the greatest surface of the skull, should be 800 and 3000 at the frequencies of 0.5 and 1.0 MHz, respectively. It is clear that for the practical implementation of such systems, the number of elements should be reduced.

Experimental verification of the above data from modeling was also reported (Hynynen and Sun 1999). A section of skull with dimensions 18 x 12 cm was selected. The array consisted of 76 elements fabricated from a single element transducer (10 cm in diameter, with a curvature radius of 8 cm, and driven at 1.1 MHz). Elements were driven from a multi-channel power amplifier with digital adjustment of the amplitude and phase of each channel. The array and the skull bone were installed in a tank containing degassed water and a hydrophone was used to control the acoustic field.

Two methods were used for the correction of the phases on the elements of an array: the first was based on calculations of the geometric characteristics of the skull based on MRI scans, and the second - on measurements of the phase shifts on the elements when the hydrophone was located in a given point behind the bone and used as a point source. The experiment showed that the first method of correcting the phases increased the sound pressure at the focus by 95% compared with the case when all phases on the elements were the same (i.e., without a phase correction). With such a correction the pressure in the focus was 9% of the pressure measured in water without the skull. Phase correction, made with the hydrophone, resulted in sound pressure at the focus which was only 3% higher than the pressure obtained with the first correction method. The authors concluded that calculating phases at the elements based on MRI data

providing the shape and thickness of the skull, is suitable for ultrasonic therapy with sonication of the brain through the unopened skull.

Furthermore the possibility to determine the acoustical properties of the skull from MRI (Sun and Hynynen 1998) or computed tomography (CT) (Aubry et al. 2003) raised new hopes for non-invasive brain therapy.

Hynynen et al. (2004) and Clement et al. (2005) tested a prototype MR-compatible focused ultrasound phased array system for trans-skull brain tissue ablation. Rabbit thigh muscle and brain were sonicated with a prototype, hemispherical 500-element array operating at frequencies of 700–800 kHz. An *ex vivo* human skull sample was placed between the array and the animal tissue. The temperature elevation during 20–30s sonications was monitored using MRI thermometry. High-power sonications (600–1080 W) produced peak temperatures up to 55 °C and focal lesions that were consistent with thermal tissue damage. The lesion size was found to increase with increasing peak temperature. The device was then modified for clinical conditions and successfully tested in phantom experiments. These studies demonstrated that it is possible to create ultrasound-induced lesions *in vivo* through a human skull under MRI guidance with this large-scale phased array.

White et al. (2005) investigated techniques to achieve optimal amplitude corrections on the elements of the array, leading to the best quality of the focus whilst sonicating through the skull. In principle, two approaches are possible. The basis of the first is that if the attenuation in some site of the skull is large (or small), the amplitude of the signal on the element located above it should be increased (or decreased). In the second method the amplitudes on the elements are chosen in such way that the absorbed energy in all areas of the skull is approximately the same. Thus, the intensity of an element located above a highly absorbing part of the skull, is reduced. Experiments were carried using a 448-element, 1-3 composite spherically focused array with a diameter of 120 mm and a radius-of-curvature of 120 mm operated at 1.1 MHz and described in Section 2.2. The array consisted of elements distributed in a regular manner as 12 rings. In their experiments, four *ex vivo* human calvaria were submerged in degassed, deionized water. Each calvarium was positioned between the sonicating transducer and the receiving hydrophone. The skull mount allowed for variable positioning normal to the sonicating transducer's axis of propagation at a resolution of 0.5 mm so that multiple points on the skull could be sonicated. Experiments performed by the authors showed that the second approach, which they called an inverse amplitude correction, maintained the acoustic intensity at the focus and did not significantly alter the side lobes or the beam profile. Using the first method of correction resulted in a significant reduction (17%) in the focal acoustical intensity. Thus, the inverse amplitude correction is the more likely candidate for investigations of amplitude correction effects in transcranial ultrasound applications.

Hynynen et al. (2006) described MRI-guided and monitored focused ultrasound thermal surgery of brain through the intact skull in three rhesus monkeys. The aim of this study was to determine the amount of skull heating in an animal model with a head shape similar to that of a human. The ultrasound beam was generated by a hemispherical ultrasound array with 512 equal area elements, a 30 cm diameter, a radius of curvature of 15 cm and driven at 670 kHz (Exablate® 3000, see Section 2.2). Due to the small size of the monkey brain, the focal spot distance from the skull was approximately 20 mm. Thus, it was not possible to induce brain tissue coagulation at the focus without overheating the brain surface. Therefore the skin was pre-cooled by degassed temperature controlled water circulating between the array surface and the skin. The skull surface temperature was measured by means of invasive thermocouple probes. The results showed that by applying surface cooling, the skin and skull surface could be protected, and that the brain surface temperature became the limiting factor. MRI thermometry was shown to be useful in detecting the tissue temperature distribution next to the bone, and it should be used to monitor the brain surface temperature. Based on the temperature elevation measured, it was predicted that an acoustic power of approximately 600 W would be required to

elevate the focal temperature above the tissue coagulation threshold. Intensity on the elements of  $2 \text{ W cm}^{-2}$  for 20 s would provide a total acoustic power of approximately 1000 W if the surface area covered was  $500 \text{ cm}^2$  (Sun and Hynynen 1998). One should note that the brain surface cools relatively slowly after ultrasound exposures and thus, careful selection of adequate sonication intervals is mandatory when multiple sonications are used. Experiments showed that the acoustic intensity values during the 20 s sonications were adequate for thermal ablation in the human brain provided that surface cooling is used.

On the other hand, Fink and co-workers developed a high power phased array prototype for clinical use of High Intensity Focused Ultrasound (Pernot et al. 2007). The system was driven by 300 fully programmable individual electronic channels with 220 emitting channels and 80 emitting and receiving channels (see Section 3.7). In order to perform noninvasive transcranial brain therapy, this system was used as follows: from CT scans, acoustical properties of the skull are first extracted; then the propagation of a wave front originating from the targeted location is simulated through the skull with a 3D finite differences code developed by the authors. Once the simulation has been performed, the global amplitude of the emitted signals is adjusted and the same energy is also delivered on the contra lateral hemisphere but without any correction (the simulation process was performed in the same way except that the targeted location was symmetric and the simulation medium was water, without any skull bone).

This protocol was tested *in vivo* on a monkey. Therapeutic sequences were optimized to avoid skin burns. A series of ten shots of 10 seconds duration and with a delay time of 20 seconds between consecutive shots was used without occurrence of skin burns. The lesion induced in the brain was observed by MRI image and the histological confirmation.

Pulkkinen et al. (2011) paid special attention to skull-base heating as well as to methods to minimise such heating in transcranial focused ultrasound therapy when sonicating near the base of the skull.

Marsac et al. (2012) demonstrated the feasibility of a novel method of optimal focusing of ultrasound waves, which they referred to as “energy-based adaptive focusing”. The general principle of the method relies on the indirect estimation of wave intensity at the target for different coded excitations in order to determine the phase shifts, which provide the best correction for aberrations. By transmitting coded signals with an array of transducers and estimating the beam intensity at the target, this approach was shown to achieve direct and accurate phase aberration correction without any phase measurement. In medical ultrasound there is a direct link between the wave intensity and the acoustic radiation force or tissue heating due to the absorption of ultrasound. Thus, the quantitative measurement of tissue displacement or temperature elevation at the target can be used for the indirect estimation of local beam intensity.

For transcranial application, MRI is most appropriate for guiding the energy-based adaptive focusing technique. Motion sensitive MR sequences have been previously developed to map microscopic displacements induced by the acoustic radiation force in biological tissue and called MR-ARFI (Sinkus et al. 2008; McDannold and Maier 2008; Hertzberg et al. 2010b). In these sequences the displacement is encoded in the phase of the reconstructed MR images. Such MR displacement measurement was later used for adaptive focusing.

Evaluation of the method was implemented using human cadavers (48 hours post mortem) and the MR-ARFI sequences in the framework of non-invasive transcranial high intensity focused ultrasound (HIFU) therapy. A 1 MHz, 512 element HIFU array (Imasonic, France) with random distribution of elements (see also Section 3.7) was employed in experiments. Only 384 elements were active. The aperture was 23 cm and the focal distance was 15 cm. The HIFU system was positioned inside a 1.5 T clinical MRI system.

Cadaver heads were mounted onto a stereotactic frame. The ultrasonic wave intensity at the chosen location was indirectly estimated by the MR system measuring the local tissue displacement induced by the acoustic radiation force of the ultrasound beams. For aberration correction, a set of spatially encoded ultrasonic waves was transmitted from the ultrasonic array

and the resulting local displacements were estimated with the MR-ARFI sequence for each emitted beam. A non-iterative inversion process was then performed in order to estimate the spatial phase aberrations induced by the cadaver skull. As a result, the corrected beam resulting from the direct inversion process was found to focus at the targeted location with an acoustic intensity 218% higher than the conventional non corrected beam. In addition, this corrected beam was found to give an acoustic intensity 1.5 times higher than the focusing pattern obtained with an aberration correction using transcranial acoustic simulation based on CT scans. Thus, the authors demonstrated that energy-based adaptive focusing can successfully achieve optimal focusing and restore sharp focus in the human brain. They suggested that by implementing further acceleration and measurement optimization, this approach could lead to more accurate HIFU treatments of central regions of the brain such as thalamus or hypothalamus for neuropathic pain, essential tremors or others pathologies.

A current practice in preparing a patient for a trans-cranial MR-guided focused ultrasound procedure, is to shave the patient's head on treatment day. Eames et al. (2013) investigated the feasibility of trans-cranial focused ultrasound in an unshaved, *ex vivo* human head model. A human skull filled with tissue-mimicking phantom and covered with a wig made of human hair was sonicated using 220- and 710-kHz head transducers to evaluate the feasibility of acoustic energy transfer. The ultrasound transducer used was the ExAblate Neuro array (InSightec, Israel). Heating at the focal point was measured by MR proton resonance shift thermometry. The results showed that the hair introduces minimal additional loss compared to the skull itself. The effect of the hair alone corresponds to a 17% decrease in temperature elevation at the focus at 710 kHz and no noticeable change at 220 kHz. Temperature elevation at the focus, being proportional to the square of the focal pressure, corresponds to a 4% decrease in the pressure at 710 kHz and no significant decrease at 220 kHz.

The aim of the study of Marquet et al. (2013) was to induce lesions in a non-human primate brain non-invasively and investigate the potential side effects. Stereotactic targeting was performed on five *Macaca fascicularis*. The HIFU system used was a 300 element high-power piezocomposite phased array (8mm diameter, 0.5 cm<sup>2</sup> active area, 1 MHz central frequency, Imasonic, Besançon, France). The elements were mounted quasi-randomly onto a spherical surface with a 14-cm radius of curvature and an aperture size of 20 cm. The transducers were connected to a 300-channel electronic driving system. Each electronic channel was individually programmable (phase and amplitude) and possessed its own transmit/receive electronic board. Either continuous waves or pulsed programmable signals could be transmitted. Chilled (14 °C) degassed water was circulated between a latex membrane and the front of the transducers to cool them. A thin layer of acoustic gel was applied to the skin and to the latex membrane before placing them in contact, to facilitate acoustical coupling.

Seven days before treatment, the animal was anesthetized and a CT scan performed. Using 3D CT scan data, the whole volume of the monkey skull was reconstructed so that the neurosurgeon could choose the target point. By applying the electronic steering capabilities of the ultrasonic array, the target could be chosen at any location inside a 1.5-cm radius sphere centred on the geometrical focus. Targets were chosen at the centre of the hemispheres, 2 cm from the outer surface of the brain, 2 cm away from the skull base, and 1 cm from the brain midline. The propagation of the ultrasonic wave from the target point to the array was then simulated by a 3D finite difference simulation code. The simulated wavefront was then time reversed (Tanter et al. 2007), to compensate for diffraction and refraction effects induced by the skull bone, and finally convolved by a 10-s therapeutic wave (1 MHz) to generate a set of transmitted signals to be used for treatment. In practice, each transducer was driven by an independent electronic channel capable of generating a temporally inverted signal stored in memory.

The ultrasonic dose delivered at the focus was increased from one treatment location to the next to estimate the thermal dose for tissue alteration. For each targeted area, a 10-s

sonication at a fixed power was repeated 10 times at the same location with a 20-s cooling delay between sonications to allow the skin temperature to return to baseline. A mean temperature of 20 °C was measured in real time on the skin with a thermocouple. The acoustic power was varied from one treatment location to another to explore various thermal depositions at the focus. The output power of the prototype ranged from 430 to 780 acoustical watts for the different experiments; corresponding pressure levels in water ranged from 7.5 to 15 MPa.

Each hemisphere was treated separately with a 15-day interval and animals were sacrificed two days after the last treatment. Treatment efficiency and safety were evaluated histologically. Thermal doses in the brain (Sapareto and Dewey 1984) were determined by numerical computations. The threshold for tissue damage in the brain was measured to be between 90 and 280 cumulative equivalent minutes at 43 °C. According to the authors, this method could be used for the treatment of neurological disorders such as essential tremors and recurrent deep-seated metastases (Marquet et al. 2013). Moreover, the treatment of other tumours with well-defined borders might also be feasible (meningiomas, schwannomas) and the possibility to selectively open the blood brain barrier with ultrasound to enhance local drug delivery could create new avenues of treating various brain disorders.

## 4.2. Neurological Disorders

Some authors consider that MRgFUS is potentially the ideal approach for the treatment of neurological diseases (Medel et al. 2012). It offers almost real time monitoring of treatment location and energy deposition. Furthermore it is noninvasive, thereby limiting or eliminating disruption of normal tissue and provides focal delivery of therapeutic agents, enhances ultrasound radiation delivery, and permits modulation of neural function. Some possible applications of ultrasound phased arrays for the treatment of neurological disorders are discussed below.

### *Essential Tremor*

Tremor is a common neurological disorder that affects 10 million people in the United States (<http://www.fusfoundation.org/focused-ultrasound-technology/clinical-applications/essential-tremor>). It typically involves a tremor of the arms, hands or fingers but sometimes involves the head or other body parts during voluntary movements such as eating and writing. Treatment options include medication, lesioning procedures, and implantation of a deep brain stimulator (DBS).

Medication is usually the first-line therapy, and most patients maintain a good quality of life with this treatment alone. However, up to 30% of essential tremor patients do not respond to first-line medical therapy and may therefore consider surgical treatment options. Lesioning for essential tremor is a surgical procedure whereby the surgeon destroys a small volume of tissue in the brain by using either stereotactic radiosurgery or radiofrequency ablation. The neurosurgeon targets a small cluster of cells (a few mm in diameter) in the thalamus called the ventralis intermedius, which are causing the tremor. The procedure uses an anatomical atlas and some level of real-time imaging.

In October 2011 in a presentation at the Congress of Neurological Surgeons, neurosurgeon W. Jeffrey Elias (University of Virginia), reported preliminary results of a pilot clinical trial that indicated that MR-guided focused ultrasound has the potential to safely and effectively control essential tremor (Monteith et al. 2013 b). Potential advantages of this approach are: it is a noninvasive method when a patient can quickly return to normal life; the risk of infection is reduced; ultrasound therapy avoids the use of ionising radiation. Results from the first 10 patients in this study showed a 78 percent improvement in contralateral tremor scores in the hand, as assessed with the Clinical Rating Scale for Tremor (Newsletter of the Focused Ultrasound Surgery Foundation V. 38, Dec. 2011). Patients' functional activities scores

improved by 92 percent, as measured in the “Disability” subsection of the Clinical Rating Scale for Tremor. Outcomes and complications were comparable to other procedures for tremor, including stereotactic thalamotomy and deep brain stimulation. The patients were able to leave the hospital the next day.

The method is based on the destruction by MR-guided focused ultrasound of nerve cells in the thalamus responsible for tremor. The ExAblate Neuro (InSightec Ltd.) system was used, which combined the effects of high intensity focused ultrasound on deep structures of the human brain with MRI control for visualizing of brain tissue, as well as for planning and monitoring of the ultrasonic treatment and its results. During treatment the patient, who is awake the entire time and interacts with the treatment team, lies in the MRI scanner wearing a helmet-like, multi-channel high power phased array transducer which is used to destroy targeted tissue. After the ultrasound procedure, patients could legibly write, eat, drink without spilling liquid, buttoning, *etc.* The results obtained were the basis for larger studies to test the efficacy and safety of the method.

Recently several scientific publications on the subject have appeared. One of these studies was carried out in Toronto, Canada between May, 2012, and January, 2013 (Lipsman et al. 2013). Four patients with chronic and medication-resistant essential tremor were treated with MR-guided focused ultrasound. Patients underwent tremor evaluation and neuroimaging at baseline and 1 month and 3 months after surgery. Patients showed immediate and sustained improvements in tremor in the dominant hand. Mean reduction in tremor score of the treated hand was 89.4% at 1 month and 81.3% at 3 months. This reduction was accompanied by functional benefits and improvements in writing and motor tasks. The authors present impressive drawings by a patient before and immediately after ultrasound thalamotomy, showing the change from having difficulty in putting pen to paper to improved drawing ability. The authors concluded that additional trials in more patients are needed. Should such trials validate the obtained encouraging preliminary results that could be a stimulus to move away from existing neurosurgical procedures for medication-resistant essential tremor, with MR-guided focused ultrasound emerging as a new and potentially preferred choice for patients.

In the work of a large group of scientists from the University of Virginia (Wintermark et al. 2013) fifteen patients with medication-refractory essential tremor were enrolled in a single-site, FDA-approved pilot clinical trial, and were treated with transcranial MR imaging-guided focused ultrasound treatment. MR imaging studies were obtained on a 3T scanner before the procedure and 24 hours, 1 week, 1 month, and 3 months following the procedure. The paper presents a detailed description of the imaging findings obtained in these studies. In the authors’ opinion, MR imaging-guided focused ultrasound treatment can accurately ablate a precisely delineated target, with typical imaging findings seen in the days, weeks, and months following the treatment. Tremor control was optimal early when the lesion size and perilesional edema were maximal and was less later when the perilesional edema had resolved. The details of this study were discussed in another paper from the same group (Elias et al. 2013). The work was carried out using a MR guided focused ultrasound system, consisting of a 3 Tesla MRI (GE) and the ExAblate Neuro (InSightec), which includes a hemispherical, 650-kHz, 1024-element, phased-array transducer. It was shown that unilateral thalamotomy improved tremor in the contralateral, dominant hand and overall tremor, as measured on a validated tremor-rating scale. Patients reported improvements in tremor-related quality of life after the procedure. However the authors drew attention to the limitations of their study including the lack of comprehensive cognitive assessments, the lack of a control group, potential biases, and comparison of efficacy relative to that of other treatments and pointed to the need for future blinded randomized trials with samples sizes appropriate for assessing infrequent but serious adverse events.

Information (not always published) on the activity of a multi-centre pivotal randomized study to evaluate the safety and efficacy of focused ultrasound for the treatment of medication-

refractory essential tremor patients is presented (<http://www.fusfoundation.org/focused-ultrasound-technology/clinical-applications/essential-tremor>).

According to FUSF Bulletin, Jan. 7, 2014 the first treatment was successfully performed in a 20-patient pilot study assessing the feasibility, safety and preliminary efficacy of MR-guided focused ultrasound for dyskinesia in Parkinson's disease. This trial was the first to use focused ultrasound on a new target within the brain, the globus pallidus. In this study, focused ultrasound was only assessed to treat one side of the brain, thus affecting dyskinesia unilaterally. If successful, the study could offer an alternative approach for certain patients with Parkinson's disease who become disabled by dyskinesia, have failed medical therapy and choose not to have a traditional invasive surgical treatment. This first treatment was conducted by Dr. Jin Woo Chang, Brain Research Institute, Yonsei University Severance Hospital in Seoul, Korea. There was also a similar report that this neurosurgeon used transcranial focused ultrasound to treat a patient with Obsessive Compulsive Disorder (OCD), an anxiety disorder that afflicts between one and three percent of the teen-through-adult population.

### ***Neuropathic pain***

In 2009 investigators from two Hospitals in Zurich were the first to use transcranial MR-guided high-intensity focused ultrasound (tcMRg-HIFU) to treat patients with chronic neuropathic pain (Martin et al. 2009). Nine patients were treated with selective medial thalamotomies. Ultrasound neurosurgery operations were performed in a clinical 3T MR-system (Signa HDx; GE, Milwaukee, WI) with the use of a clinical system for HIFU surgery (ExAblate 4000; InSightec, Israel), which was a hemispheric 1024-element phased array operating at 650 kHz. Impacts on certain areas of the brain (thalamotomy) were made through the intact skull under MRI control, whilst the patient's head was fixed in a stereotaxic apparatus. Before the high-power treatment it was confirmed that the thermal hot spot was centred in the target location. For this, several low-power sonications of 10 to 20 seconds duration were applied to induce peak temperatures of 39 °C to 42 °C. These temperatures are known to be below the ablation threshold but are easily visualized on MR thermometry images to assess exact position and size of the hot spot and the overall safety profile of the applied sonication parameters. During treatment several high-power sonications were applied under continuous visual MR guidance and MR thermometry. In order to induce local tissue ablation the acoustic power was increased stepwise to finally achieve a peak temperature at the target of between 51 °C and 60 °C. Typically, continuous wave sonications of 10 seconds to 20 seconds duration, up to a maximum acoustic power of 1200 W and 800 W, respectively, were applied. Patients were awake during the entire procedure. The resulting lesions were clearly visible on follow-up MR imaging. All treatments were well tolerated, without side effects or neurological deficits. This was the first report on successful clinical application of tcMRgHIFU in functional brain disorders, portraying it as safe and reliable for noninvasive neurosurgical interventions.

In a subsequent study by the same group of scientists involving 12 patients suffering from chronic therapy-resistant neuropathic pain, the same technology of central lateral thalamotomies (i.e., tcMRgFUS CLT) was applied. The MR imaging and HIFU systems were the same as in the previous work. In 11 patients, precisely localized thermal ablations of 3–4 mm in diameter were produced in the posterior part of the central lateral thalamic nucleus at peak temperatures between 51 °C and 64 °C with the aid of real-time patient monitoring and MR imaging and MR thermometry guidance. The treated neuropathic pain syndromes had peripheral (5 patients) or central (6 patients) origins and covered all body parts (face, arm, leg, trunk, and hemibody). After the treatment the patients experienced mean pain relief of 49% at the 3-month follow-up (9 patients) and 57% at the 1-year follow-up (8 patients). Notable improvements have been found in other analysis techniques (visual analog scale, somatosensory and vestibular clinical manifestations, quantitative electroencephalography, *etc.*). The targeting precision was within a

millimeter for all 3 co-ordinates. This is comparable with the classic stereotactic techniques involving penetration of an electrode into the brain because of the unforeseeable mechanical shift of brain tissue by the electrode. There was a single complication, a bleeding in the target with ischemia in the motor thalamus, probably induced by cavitation. Thus, the authors suggest that TcMRgFUS offers a noninvasive, precise, and radiation-free neurosurgical technique for the treatment of neuropathic pain. The procedure avoids mechanical brain tissue shift and eliminates the risk of infection. The real-time continuous MR imaging and MR thermometry monitoring of targeting accuracy and thermal effects are major factors in optimizing precision, safety, and efficacy in an outpatient context.

### ***Glioblastoma***

McDannold et al. (2010) evaluated the clinical feasibility of transcranial MR-guided focused ultrasound surgery (MRgFUS) for the treatment of brain tumors. Transcranial MRgFUS for brain tumors offers a potential noninvasive alternative to a surgical procedure (Medel et al. 2012). The method combines a hemispherical phased-array transducer and patient-specific treatment planning based on acoustic models with feedback control based on MR temperature imaging to overcome the effects of the cranium and allow for controlled and precise thermal ablation in the brain. Treatments of 3 glioblastoma patients were performed using the ExAblate 3000 TcMRgFUS system (InSightec, Haifa, Israel), which consists of a 30-cm diameter hemispherical 512-element phased-array transducer operating at 670 kHz coupled with a 512-channel driving system (see Section 2.2). The maximum total acoustic power applied was 650 W for patient 1 and was increased to 800 W for patients 2 and 3. The width and length of the half-intensity of the focal region created by the transducer in water were 2 and 4 mm, respectively. The acoustic power was slowly increased over several 20-second sonications until focal heating was observed in MR temperature imaging to verify the target location within the tumor. Following verification, the acoustic power was increased further over additional 20-second sonications to achieve a sufficient thermal dose (approximately 55 °C peak temperature or 240 equivalent minutes at 43 °C (Sapareto and Dewey 1984)) to cause thermal coagulation. However, limiting factors were the device's maximum acoustic power level and possible pain. Measurements at the focus suggested that a peak focal temperature of 55 °C, which would be sufficient to produce thermal necrosis, would require approximately 1200 W of acoustic power for a 20 s sonication.

The system was integrated with a clinical 1.5-T MRI unit (General Electric Medical Systems, Milwaukee, WI). Temperature changes at the focus and brain surface were evaluated by offline analysis of the MR temperature images. The feasibility of focusing an ultrasound beam transcranially into the brain and to visualize the heating with MR temperature imaging was demonstrated. Although the limitations by the device power available at the time, extrapolation of the temperature measurements at the focus and on the brain surface suggested that thermal ablation would be possible with this device without overheating the brain surface, albeit with some possible limitation on the treatment envelope.

These treatments were of patients with inoperable glioblastoma, which may not ultimately be the best clinical target for TcMRgFUS because of the infiltrative nature of the disease. This treatment is a noninvasive alternative to surgical resection which although it offers a major reduction in side effects, offers only limited improvement in survival for these patients. The authors suggested that better targets for TcMRgFUS will be those for which surgical resection currently offers greater benefit, such as metastases or other tumors with well-defined margins and benign tumors.

This work showed for the first time that ultrasound can be focused through the intact cranium in patients and that the heating can be visualized using MR temperature imaging. Although device power limited the ability to achieve thermal coagulation, extrapolation of the results suggests that ablation will be possible without overheating the cranium. Analysis of the

brain surface heating and the occurrence of sonication-related pain in one patient suggest, however, that the targetable regions of the brain may be limited to deep, central locations in the brain with the device.

### ***Epilepsy***

Although there are currently no active clinical trials evaluating the safety and efficacy of focused ultrasound for the treatment of epilepsy, it is thought (<http://www.fusfoundation.org/Epilepsy/>) that in the future focused ultrasound may be used in the treatment of temporal lobe epilepsy thereby providing a low morbidity means to target and destroy a specific area in the brain while sparing healthy tissue adjacent to the target or along the beam path. In addition, research on focused ultrasound has demonstrated that with the right set of parameters focused ultrasound can be used for neuromodulation to stimulate or block brain activity in a transient and focalized manner (Gavrilov et al. 1996; Gavrilov 2014). Using the blocking effect, it is possible, in principle, to use focused ultrasound as a means to block an ongoing seizure. Some new ideas related with this approach are presented in <http://www.fusfoundation.org/newsletter-articles/can-epilepsy-and-psychological-disorders-be-treated-with-focused-ultrasound.>

### ***Trigeminal neuralgia***

Trigeminal neuralgia is a neuropathic disorder characterized by episodes of intense pain in the face, originating from the trigeminal nerve and lasting from a few seconds to several minutes or hours. The intensity of pain can be physically and mentally incapacitating. The work of Monteith et al. (2013d) is the first to investigate the feasibility of using transcranial MR-guided focused ultrasound surgery (MRgFUS) for the treatment of trigeminal neuralgia. Targeting of the trigeminal nerve was carried out in a cadaveric model with temperature assessments made using computer simulations and an *in vitro* skull phantom model. Preprocedural CT scanning of the head in 4 cadavers was performed to create skull correction algorithm. A focused ultrasound transducer a 650-kHz phased array, ExAblate Neuro, InSightec was used with powers of 25-1500 W and exposures of 10-30 seconds. The cadaver was positioned in a transducer and the focus of the transducer was centred at the proximal trigeminal nerve, allowing for targeting of the root entry zone and the cisternal segment. Thermocouples were used as well as MR thermometry for measurements of temperature rise. A focal heating of up to 18 °C in a cadaveric trigeminal nerve at the root entry zone and along the cisternal segment was demonstrated. Significant heating of the skull base and surrounding neural structures did not occur. The authors considered that *in vivo* studies were necessary to confirm the safety and efficacy of this potentially new, noninvasive treatment.

### ***Sonothrombolysis and intracerebral hemorrhage***

Intracerebral hemorrhage, i.e. a bleeding within the skull, accounts for 10% - 15% of the approximately 15 million strokes that occur worldwide every year (Monteith et al. 2000 a,c). It occurs when a blood vessel within the skull is ruptured or leaks as a result of physical trauma (as occurs in head injury) or nontraumatic causes (as occurs in hemorrhagic stroke). The annual incidence is 10-30 per 100,000 population, and is the cause of significant morbidity and mortality.

Monteith et al. (2000 a,c) investigated the use of transcranial MR-guided focused ultrasound sonothrombolysis to treat intracerebral hemorrhage. Contrary to all previous work related with the transcranial use of MRgFUS when the main effective factor was thermal ablation of brain tissue, these authors considered that the role of temperature rise in ultrasound sonothrombolysis for the treatment of intracerebral hemorrhage is not significant and the

expected mechanism is largely mechanical rather than thermal. Samples of clots were prepared from fresh blood from a healthy human volunteer. The blood samples were left to clot for 18 hours at room temperature to allow for clot retraction and to ensure that the clot was stable across comparison groups. An explanted human calvaria was degassed and placed in the ultrasound transducer (230 kHz; ExAblate Neuro, InSightec) submerged in circulated degassed water. Initial *in vivo* safety studies were carried out in a swine model (n=20) of intracerebral hemorrhage. The following optimum transcranial sonothrombolysis parameters were determined: transducer centre frequency 230 kHz, power 3950 W, pulse repetition rate 1 kHz, duty cycle 10%, and sonication duration 30 seconds. In this model, sonothrombolysis of 4 ml intracerebral hemorrhage was performed. Then a cadaveric model of intracerebral hemorrhage was developed with 40 ml clots implanted into fresh cadaveric brains (n = 10). As a result, intracerebral hemorrhages were successfully liquefied (> 95%) and evacuated in a minimally invasive fashion under MR guidance. The safety and efficacy of such an approach to intracerebral hemorrhage needs to be evaluated in a clinical trial. Thus, the feasibility of transcranial MRgFUS sonothrombolysis was demonstrated in *in vitro* and cadaveric models of intracerebral hemorrhage.

The goal of the recent work of Hölscher et al. (2013) was to test the effects of various combinations of pulse widths and duty cycles on high-intensity focused ultrasound (HIFU)-induced sonothrombolysis efficacy using an *in vitro* flow model. An ExAblate™ 4000 HIFU head system (InSightec Inc., Israel) was used. The main component of this system is a hemispheric phased array transducer with 1000 single piezo elements that can be operated independently. A sharp focus located in the centre of the transducer can be generated. The operating frequency of the system is 220 kHz. To test the impact of various duty cycles and pulse widths on thrombolysis, insonation duration was of 30 s and an acoustic output power of 235 W for all studies. Artificial blood clots were placed into test tubes inside a human calvarium and exposed to pulsatile flow. The thrombi had an average weight of about 0.25 g and the average length of each thrombus was about 2.5 cm. Four different duty cycles (5; 10; 20; 50%) were tested against four different pulse widths (0.1; 1; 10; 100 ms). Using transcranial HIFU, significant thrombolysis can be achieved within seconds and without the use of lytic drugs *in vitro*. Longer duty cycles in combination with longer pulse widths seem to have the highest potential to optimize clot lysis efficacy. A duty cycle of 50% seems to represent an upper limit above which a change of the pulse width does not affect the thrombolysis efficacy. These results might be taken into consideration for future research on HIFU-induced thrombolysis. The authors argued that the development of a noninvasive, transcranial ultrasound technology, which provides the possibility to treat stroke victims who are not eligible for tissue plasminogen activator, would be a significant achievement in today's stroke care.

### 4.3. Prostate

Prostate is a gland in the form of chestnut surrounding the urethra in men and is located under the bladder and in front of the rectum. Chronic prostatitis, i.e., inflammation of the prostate is one of the most common diseases in men, particularly in the elderly. According to statistics, every year in the USA 800000 men undergo surgery associated with benign prostate diseases and 200000 men have malignant prostate tumour (Hutchinson and Hynynen 1996; Hutchinson et al. 1996). Mortality caused by prostate cancer (38000 men annually) makes this type of cancer the second deadliest type of men's cancer in the USA. According to other information obtained from the Internet and several works (Lafon et al. 2005; Penna et al. 2007), prostate cancer is a leader among men in the U.S. and second in the world after lung cancer. It is estimated that 41.5 million men in North America, Europe and Japan have cancer of the prostate. So there is an interest in minimum-damaging prostate surgery methods, which in future could

compete with routine surgery. One of the most promising physical methods is the application of high-intensity focused ultrasound.

As mentioned in Section 1.1, two well-known ultrasound devices for surgery of the prostate were developed and are commercially available, namely the Sonablate® (Focus Surgery, Indianapolis, IN, USA) (Foster et al. 1993; Bihrlé et al. 1994; Sanghvi et al. 1999; Illing and Emberton 2006) and Ablatherm® (EDAP-TMS SA, Vaulx-en-Velin, France) (Gelet et al. 1993, 1999) devices. Both are based on the use of small size single element focusing transducers moved mechanically in the rectum along the prostate. The Sonablate®-500 uses two focusing radiators with different focusing distances (usually 30 and 40 mm). During the past 15 years, over 30000 prostate HIFU treatments have been performed, mainly in Europe, but also throughout the world, including the USA.

The disadvantage of both mentioned focusing devices is that they both have fixed focal distances. Thus, if it is necessary to change the depth of ultrasound irradiation of the prostate tissue, it is required to replace one transducer to another having a different focal length, and to retune the focusing system. There were several attempts to develop intracavitary phased arrays system for hyperthermia and surgery of prostate (see Section 1.1) but only a few of them were accompanied by experiments *in vivo*.

Early work in this area was that of Hutchinson and Hynynen (1998) who carried out *in vivo* experiments on rabbit thigh muscles using an aperiodic 62 element MRI-compatible linear phased array. The array produced therapeutic temperature rises *in vivo* at depths of 3–6 cm and axial locations up to 3 cm off the central axis. The study showed that linear ultrasound applicators can create small (4 mm × 4 mm × 7 mm) lesions *in vivo*. The size of the heated volume could be enlarged with electronic scanning of a single focus. These studies were continued in the work of Sokka and Hynynen (2000). They fabricated and tested an array capable of increasing the treatable tissue volume by using an ultrasonic motor to provide a mechanical rotation angle of up to 100°. In experiments *ex vivo* on bovine tissue samples, it was shown that the potential limits of the focus steering were from 2 to 5 cm in depth, 5.5 cm along the long axis of the array and ± 3 cm in the perpendicular direction at a depth of 4 cm. Experiments evaluating the ability of an array to ablate in tissues with blood flow, were carried out on the rabbit femur *in vivo*. For example, the destruction of 3 x 2.5 x 2 cm<sup>3</sup> could be created with the use of 12 exposures with the power of 150 W and duration of 30 s. After each exposure the tissue was cooled for 1 min, and a side effect of edema surrounding the site of irradiation, was acceptable. Thus, the total procedure time was about 20 minutes. If 8 irradiations with the duration of 30 s and a power of 130 W at intervals of 5 minutes were used, no side effects were observed. Size destruction was thus 1.5 x 2 x 2 cm<sup>3</sup>. Thus, these studies suggest the possibility of ablation the whole volume of the prostate within a practical time. For clinical use of the developed device, it is necessary to develop optimal irradiation protocols to minimize potential side effects (edema, skin burns, *etc.*).

Seip et al. (2005) developed two designs of phased arrays for intracavitary prostate surgery as mentioned briefly in Section 1.3: an annular array and a cylindrical array. Both were successfully tested in experiments *in vitro* and *in vivo* (dog prostate). The annular array was capable of creating defined lesions at the desired depth. Elementary lesions as well as compound lesions were easily created by adjusting HIFU exposure parameters. A simple design makes it an ideal candidate for incorporation into the Sonablate® clinical system. The cylindrical array was capable of creating both elementary and compound lesions at depth and laterally. Its ability to create lesions over a large extent with respect to its aperture (±15 mm lateral, 25-50 mm depth; aperture: 40 mm) within a few seconds demonstrate the effective focusing gain and the range of the focal zone placement for the cylindrical geometry as a HIFU array.

There is information about clinical applications of intracavitary phased array systems for the treatment of localized prostate cancer (Napoli et al. 2013a). In their research, five patients with unifocal, biopsy-proven prostate cancer evident on multiparametric MR imaging were

treated with MR-guided focused ultrasound (MRgFUS) ablation before radical prostatectomy. All treatments were performed using an endorectal focused ultrasound ablation system (ExAblate 2100, InSightec, Haifa, Israel) integrated within a 3T MR scanner (Discovery MR750, GE Medical Systems, Milwaukee, Wisconsin, USA). Patients were positioned supine on the scanner table under spinal anesthesia. The endorectal probe, which contained a 990-element phased-array focused ultrasound transducer, was inserted into the rectum and filled with degassed water to eliminate residual air within the interface between the prostate and the rectal wall. The histopathology report showed extensive coagulative necrosis, with no residual tumor in the ablated area. Significant bilateral residual tumor, not evident on pretreatment MRI, was observed outside the treated area in two patients. The authors consider their preliminary experience, which should be confirmed in a large prospective study, demonstrated the feasibility of MRgFUS ablation of prostate lesions without significant side-effects or short-term treatment-related complications. Furthermore, MRgFUS treatment does not affect the morbidity and oncologic outcome of subsequent radical prostatectomy, which was safely performed in all patients. Further studies on larger populations are required to better define the safety profile and particularly the long-term efficacy of this technique before its introduction in clinical practice.

#### 4.4. Tissue Ablation in the Presence of Ribs

Pernot et al. (2007) carried out early experimental research demonstrating in principle the possibility of heating liver tissue located behind of the rib cage up to hyperthermia temperatures. They used a phased array system, mentioned briefly in Section 3.6, consisting of 300 individual electronic channels with 220 emitting channels and 80 emitting and receiving channels. The frequency was 1 MHz and the diameter of each element was 8 mm ( $5.3\lambda$ ). A freshly excised sheep rib cage was placed in front of the array, partially shadowing the beam; all the samples were immersed in degassed and deionized water. Three different focusing techniques were tested experimentally: time reversal, time reversal coupled with amplitude compensation and no correction (spherical laws). Without any correction, the pressure fields in the focal plane were affected by both inhomogeneous attenuation and phase distortion and three main effects were observed: a mean 2 mm shift of the main lobe, a mean 1.25 mm spreading in the half width of the main lobe and up to 20 dB increase in the secondary lobe level.

Then a time reversal experiment was conducted though the ribs: signals were emitted successively by all the transducers of the array and recorded by a hydrophone placed at focus. The 300 individual signals were stored in memory. Then they were time reversed and reemitted by the array. The signal in the focus was recorded. Unlike the results presented by Bobkova et al. (2010) no splitting of the main focus was observed in this work.

The temperature elevation was measured using implanted thermocouples (Iron-constantan, 40 mm diameter, PhysiTemp Corp.). This was done at several locations over the outer rib surface at the bone for 5 s sonications performed with each focusing technique ( $1600 \text{ W cm}^{-2}$  at the focus). A summary of the mean temperature elevation is given in Table 7.

**Table 7. Temperature elevation on the ribs (Pernot et al. 2007)**

Focusing technique	Mean elevation	Standard deviation	Maximum temperature elevation
No correction	5.9 °C	2.2 °C	9.1 °C
Time reversal (TR)	0.3 °C	0.1 °C	0.4 °C
TR + ampl. compensation	5.2 °C	2.1 °C	8.0 °C

It is seen, in particular, that time reversal maximizes the temperature elevation on the rib surface (a mean 0.3 °C compared to more than 5 °C for the other techniques presented). Nevertheless, such a technique is invasive as it requires an acoustic source (or receiver) at focus. However the authors believed that it is possible to overcome this complication. Their idea is to use the HIFU array first as an echographic device to image the ribs with a conventional grayscale B-mode imaging technique. Thus, a therapeutic transducer can be used to perform ultrasonic imaging of ribs, which can be useful for the procedures of the appropriate targeting.

In Section 3.6 another method for focusing high intensity continuous wave ultrasound through ribs has been proposed and tested theoretically and experimentally (Bobkova et al. 2010). The method aims at minimizing heating of the ribs whilst maintaining high intensities at the focus (or foci) using a 2D random phased array. Experiments carried out with the use of porcine tissues and rib samples *ex vivo* (Bobkova et al. 2010) are discussed below

To demonstrate the feasibility of producing thermally ablated lesions in tissue in the presence of ribs, porcine tissue positioned in the focal region was irradiated through a rib phantom and through a rib sample. The plastic ring (inner diameter 10 cm) was placed in water at 1 cm proximally to the focus and the threads were stretched between several points of the ring to position the porcine tissues each 1 cm thick. Lesions in the tissue samples were subsequently observed macroscopically, without special histological analysis. The soft tissues and rib cages were degassed under vacuum for approximately one hour prior to sonication.

Firstly, the ability to ablate *ex vivo* porcine tissue behind the phantom of rib cage was tested. The ablations presented in Figure 60 correspond to two set of experiments. In the first set with constant exposure (20 s) the acoustic power was 140, 120 and 90 W (lesions 1-3, respectively). In the second set of experiments with constant power (120 W) the exposures were 15, 10 and 5 s (lesions 4-6, respectively). For the shortest exposure (5 s) used in the experiments, macroscopic tissue discolouration (lesion 6) was observable at an acoustic power of 120 W, but may not be obvious in the photograph. The splitting of the focus is observed in all these cases (see Figure 60).

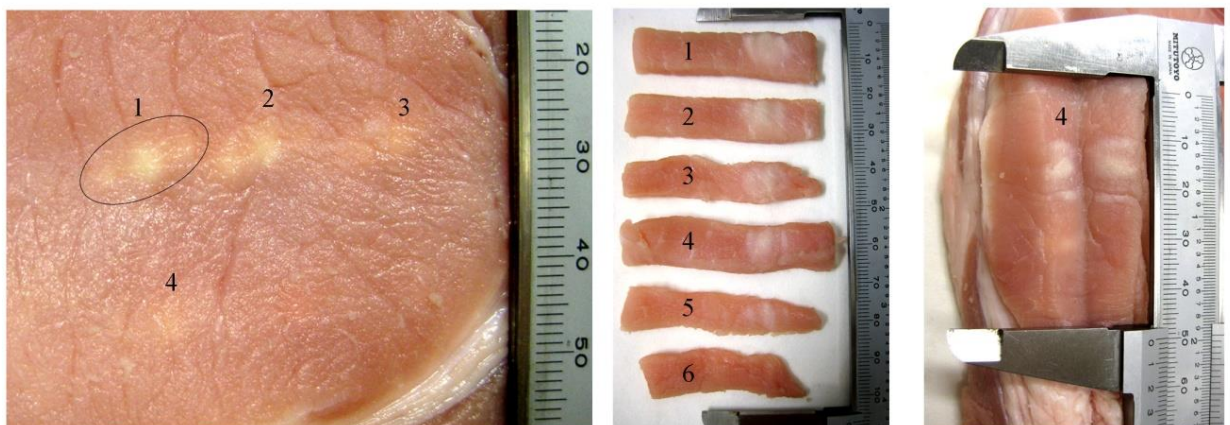


Figure 60. Demonstration of the ability of tissue ablation behind the rib cage phantom. Lesions 1, 2 and 3 correspond to the acoustic power of array 140, 120 and 90 W and exposure 20 s. Lesions 4, 5 and 6 correspond to exposure 15, 10 and 5 s and the acoustic power of array 120 W Reprinted from *Ultrasound Med. Biol.* 36(6) Bobkova, S., Gavrilov, L., Khokhlova, V., Shaw, A., & Hand, J. Focusing of high intensity ultrasound through the rib cage using therapeutic random phased array 888-906. Copyright (2010), with permission from Elsevier.

Intensity distributions obtained experimentally when irradiations were performed through the rib cage in water are presented in Figure 61 (Bobkova et al. 2010) for various locations of the focus. The co-ordinates of the focus were (0, 0, 130 mm; 0, 10, 130 mm; 10, 0, 130 mm), i.e. steering of the focus parallel and transversely to the ribs was used. The acoustic power was 28 W and exposure 0.26 s, the number of working elements in the 254-element array was 138 (see Section 3.6). Triad splitting of the focus was observed, but no significant grating lobes were presented in the field of interest. These results indicate the ability to steer electronically the focus behind the rib cage at the distance equal to at least  $\pm 10$  mm off the array axis.

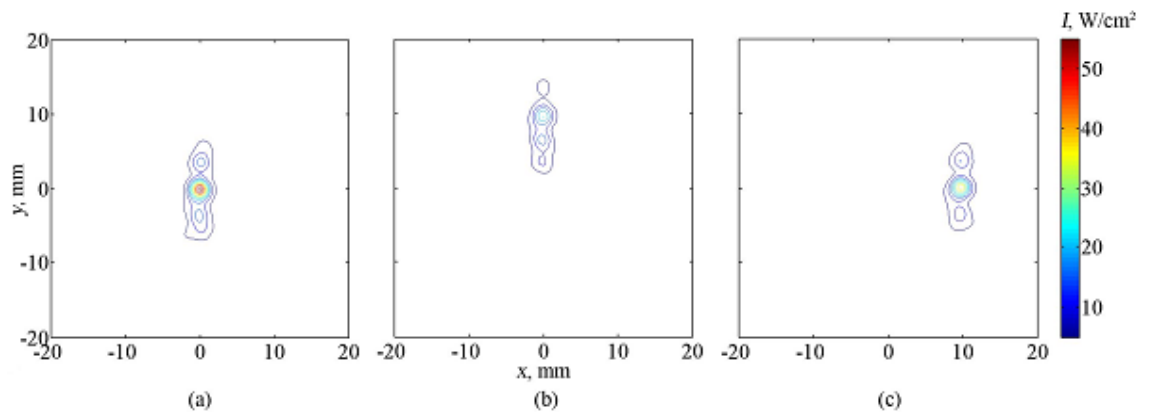


Figure 61. Intensity distributions obtained experimentally for different locations of the focus (0, 0, 130; 10, 0, 130; 0, 10, 130 mm) behind the *ex vivo* rib cage. The contours are given from  $5 \text{ W cm}^{-2}$  with increments of  $5 \text{ W cm}^{-2}$ . Reprinted from *Ultrasound Med. Biol.* 36(6) Bobkova, S., Gavrilov, L., Khokhlova, V., Shaw, A., & Hand, J. Focusing of high intensity ultrasound through the rib cage using therapeutic random phased array 888-906. Copyright (2010), with permission from Elsevier.

To obtain additional information on the safety of possible future applications of the proposed method, experiments in which temperatures were monitored using thermocouples were carried out. In particular, temperature rises were measured on the ribs and in the intercostal spaces. The acoustic power used in these experiments was 60 W and the exposure duration 10 s. The ribs were moved mechanically parallel to themselves to obtain a maximum value at the thermocouple showing the greatest temperature rise. A significant time interval (several minutes) was introduced between each subsequent irradiation of the ribs. The largest temperature rise recorded locally near to a rib was approximately  $5^\circ\text{C}$ . For an acoustic power of 30 W, duration of heating 20 s, and parallel movement of the ribs, the maximum value of the temperature rise was  $2.5^\circ\text{C}$ . These results suggest that overheating of ribs and tissues proximal to the ribs during future applications of the method could be avoided.

The results of experiments showed that it was possible to provide an appropriate quality of focusing in the tissues behind the ribs, in the case of generating a single focus and several (3-4) foci and their steering at  $\pm 10$ -15 mm off the array axis and at least  $\pm 20$  mm along the axis (Bobkova et al. 2010). The level of secondary maxima in the acoustic fields with the steering of a single focus did not exceed 10% of the maximum values excluding, naturally, the triad focus (foci) splitting. The ablations in tissues were observed in samples of *ex vivo* porcine tissue, located beyond the rib phantom, for acoustic power of 90-140 W and durations  $> 5$  s.

Temperature rises in tissues near the bones and in the intercostal spaces were measured using thermocouples. Temperature rise measurements on a rib surface confirmed the absence of dangerous overheating of the tissues. Thus, theoretical and experimental investigations demonstrated the feasibility of the proposed approach to minimise the field on ribs while maintaining high focal intensities sufficient to produce tissue ablations in tissues behind the ribs.

For future clinical application of transcostal HIFU, it may be prudent to additionally protect the ribs by fixing strips made from absorbing (or reflecting in some cases) material to the skin above the ribs.

The ability to ablate tissues through the phantom and maintain an appropriate quality of the field distribution beyond the ribs *ex vivo* provides strong evidence that the technique has the potential for addressing a major problem in clinical HIFU, i.e. ablating tissue behind the ribs without overheating the ribs and overlying tissue. Practical application of the method will require integration of a means of imaging the ribs (CT, MRI, or ultrasound), operating the array in therapy and imaging modes, or using the recently proposed DORT method (Cochard et al. 2009) to optimize the number and location of activated array elements and the phases of driving signals applied to them.

Quesson et al. (2010) studied the possibilities of MR thermometry to precisely guide high-intensity focused ultrasound (HIFU) for the noninvasive treatment of kidney and liver tumors *in vivo* on pigs (five animals, weighing 40–50 kg). A 256-element (1.2 MHz operating frequency) HIFU phased array (Imasonic, Besançon, France) mechanically positioned inside a tank with degassed water was used. The transducer radius and aperture were 120 mm and 126 mm, respectively, creating a focal region with the dimensions at the level of half-maximum of sound pressure of  $1 \times 1 \times 7 \text{ mm}^3$ . The position of the focal region was changed electronically by adjusting the phases of the 256 elements. Sonications in the liver were performed using an acoustic window inferior to the sternum, into the right and left inferior lobes of the liver. The threshold lesions in the liver were obtained with the intensities and time durations of 200 W and 15 s (12 x 7 mm).

A thorough investigation was carried out by Marquet et al. (2011). It is known that an important limitation for abdominal HIFU treatment is the patient movement and in particular respiratory movement. These impeding movements directly affect the precision and the efficiency of the treatment. When significant movements occurred, the acoustic beam could be aiming at surrounding healthy tissues and damaging them. Moreover, the overall dose delivered to tumorous tissues could be insufficient.

The aim of the authors was to optimize the emitted acoustic energy in order to limit unwanted HIFU-induced damage outside the targeted area, due to the presence of the ribs or due to breathing motion. A large spherical phased array designed for transcranial applications was used (see Section 3.7). It consisted of 300 equally sized elements (8 mm diameter,  $0.5 \text{ cm}^2$  active surface, centre frequency of 1 MHz, Imasonic, Besançon, France) mounted semi-randomly (in order to minimize grating lobes) in a sealed, spherically curved holder with a 14 cm radius. The transducers were connected to a 300-channel electronic driving system.

The basis of the approach proposed by Marquet et al. (2011) was as follows. Since the transmitted energy of the wave front is essentially negligible when reflected by the bone the authors applied binarization of the energy of transmitted wave front. Thus, the normalized amplitudes of the transmitted wave front became either zero, due to the shadowing effect of the rib, or unity for propagation through the intercostal space. Therefore a binarized apodization law (adaptive beamforming) was introduced to optimize the shape of the emitted wavefront to avoid sonicating the rib cage. Using the imaging capabilities of the therapeutic system, it was possible to switch off the transducers located directly in front of the ribs to create a binarized wavefront. This idea is very close to that used in Bobkova et al. (2010) (see Section 3.6) when the velocity amplitude at the source surface shadowed by ribs was set to zero.

Thus, the authors proposed a noninvasive transcostal treatment planning combining adaptive focusing and 3D real-time motion correction. The HIFU beam follows the target during respiratory cycles thanks to the electronic steering capabilities of the HIFU phased array. *In vivo* 3D-movement detection was performed on pigs using the ultrasound-based technique. The corresponding movements were reproduced by stepping motors in order to obtain known realistic movements so that the error of the motion detection technique could be evaluated. *Ex*

*vivo* heating experiments were then conducted on liver samples using the same *in vivo* liver motion previously measured on pigs. Finally, a spiral treatment mode designed for large lesions, as proposed by Salomir et al. (2000), was implemented and used *ex vivo* through the ribs in conjunction with motion correction and binarized apodization of irradiation to induce necrosis in a moving liver sample.

The histological findings and other data presented in the work of Marquet et al. (2011) demonstrated *ex vivo* and *in vivo* experiments the feasibility of intercostal focusing, avoiding rib cage sonication and using motion correction. The procedure was based on combination of several ultrasonic procedures: binarized apodization law, motion detection, steering capabilities for both motion correction and spiral heating. Necroses were induced and the procedure used has been shown to optimize energy deposit at the focus lowering rib overheating during treatment (0.3 °C mean elevation compared to 5.9 °C mean elevation using classic approach). It was shown also that the spiral heating mode is prospective for the treatment of large volumes of solid liver tumors and could be used in future HIFU treatments.

Research into focusing through the rib cage for MR-guided transcostal HIFU was carried out in the University of Dundee, UK (Gao et al. 2012a,b). In these studies a tissue mimicking phantom with a rib phantom was sonicated using a 208-element 1.15 MHz bowl transducer and a 1024-element 550 kHz planar matrix transducer (both ExAblate, InSightec, Israel). Those elements shadowed by ribs were switched off. The temperature rise near the ribs was reduced to 16 °C and 4 °C for the 1.15 MHz and 550 kHz transducers respectively. The results of the model analysis demonstrated that ultrasound at frequencies around 0.8 MHz was optimal for maximizing power density gains in these sonications. The temperature rise in the focus was unexpectedly low but investigations are continuing.

In an earlier paper by the same group (Gao et al. 2011) the authors studied the effect of focus splitting on ultrasound propagation through the rib cage during focused ultrasound surgery. The results obtained confirmed in general those published by others (e.g. Bobkova et al. 2010; Khokhlova et al. 2010). Referring to the latter works, the authors note that the parameters of the split-focus (e.g. the distance between adjacent foci, the diameter of foci, and the ratio of the peak intensity in the side foci to the central value) were obtained based on the analytical solution of parabolic approximation of diffraction theory and state "... however, no direct experimental study has been conducted to demonstrate the effect of focus splitting through the rib cage." This statement is not correct since Figure 60 and 61 (see above) taken from Bobkova et al. (2010) demonstrates an experimental confirmation of the possibility of ablating tissues after propagation of HIFU through the phantom and specimen of a rib cage.

Chinese scientists (Qiao et al. 2013) have proposed the modified geometric correction method by adjusting the output of each element according to the area of the element blocked by the projected shadow of the rib cage. The ultrasound propagation through the ribs was computed by a hybrid method including the Rayleigh-Sommerfeld integral, k-space method, and angular spectrum method. The method allowed adjusting the output of elements based on their relative area in the projected "shadow" of the ribs. The simulation results showed that an increase in the specific absorption rate gain up to 300% was obtained by varying the focal length although the optimal value varied in each situation. Therefore, acoustic simulation is required for each clinical case to determine a satisfactory treatment plan. Experiments were carried out with the use of a 112-element phased array (1.36 MHz) and a model of rib cage fabricated from an acoustic absorber cut into strips with a width of 10 mm and a thickness of 5 mm; these strips were installed in parallel and distributed evenly at a spacing of 15 mm to simulate a rib cage. Good agreement of experimental and simulation results was observed. The effect of focus splitting was observed in the simulations and measurements were similar to those obtained in several previous works.

## 4.5. Surgery

There are many papers describing the use of single-element focused transducers and phased arrays for applications in surgery, and primarily for oncology. Here we shall confine discussion to the use of random phased arrays since they ensure the minimal level of grating lobes and side lobes, which are potentially dangerous in practice.

Hand et al. (2009) described a random phased array (see Section 3.7) consisting of 254 elements on a spherical shell of radius of curvature 130 mm and diameter 170 mm has been used. The use of phased arrays offers not only electronically controlled dynamic focusing and the ability to vary and control precisely the range, location and size of a focus during treatment without moving the array, but also a means of synthesizing fields with multiple simultaneous foci. The feasibility of using the system to generate focal regions of complex configurations with preset parameters and geometric characteristics was demonstrated; typical examples of ablations in porcine soft tissue samples are shown in Figures 62 and 63. The goal of these experiments was to ablate a tissue region of a selected size (as a square with a side about 10 mm in projection). Ablations were performed using two consecutive patterns of foci: the first one consisting of four foci (acoustic power 142 W, duration 20 s) and the second one consisting of five foci arranged as a rhomb (188 W, 20 s), which together form a square of three by three foci. The sections made at different depths in tissue demonstrate square-shaped ablations (square side 11 mm). The depth of the ablation was at least 16 mm. Thus, the volume of the ablation obtained under such an exposure was about 2 cm<sup>3</sup>.

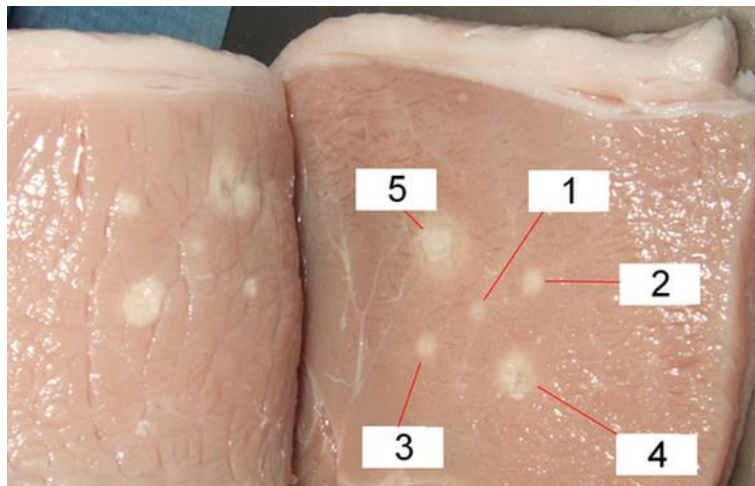


Figure 62. Five lesions produced in pork From Hand, J. W., Shaw, A., Sathoo, N., Rajagopal, S., Dickinson, R. J. & Gavrilov, L. R. (2009). A random phased array device for delivery of high intensity focused ultrasound. *Phys. Med. Biol.*, 54, 5675-5693. © Institute of Physics and Engineering in Medicine. Published on behalf of IPEM by IOP Publishing Ltd. All rights reserved.

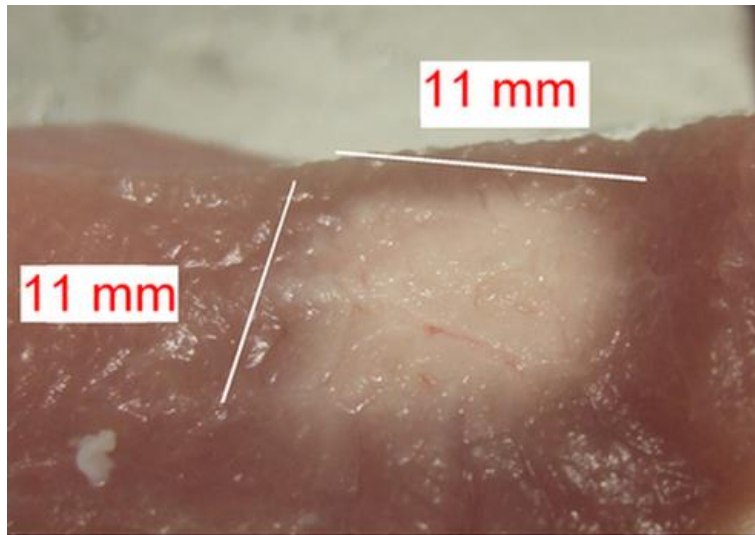


Figure 63. Lesion produced by a sequence of four foci (142 W acoustic power, 20 s) followed by five foci (188 W acoustic power, 20 s). (a)–(e) Sequential sections through lesion showing essentially square cross sections. The sections covered approximately 16 mm of tissue; (f) lesion (11 mm side length) From Hand, J. W., Shaw, A., Sadhoo, N., Rajagopal, S., Dickinson, R. J. & Gavrilov, L. R. (2009). A random phased array device for delivery of high intensity focused ultrasound. *Phys. Med. Biol.*, 54, 5675-5693. © Institute of Physics and Engineering in Medicine. Published on behalf of IPEM by IOP Publishing Ltd. All rights reserved.

Similar examples of lesions obtained with the use of random arrays are presented in several other papers (Pernot et al. 2003; Lu et al. 2008; Ji et al. 2011).

In Section 3.7 a MR-compliant phased-array HIFU transducer with increased electronic steering range, dedicated to abdominal thermotherapy (Auboiroux et al. 2011), has been considered in detail. This novel concept based on the splitting the phased array into two sub-arrays with different foci was tested and validated *ex vivo* (in turkey muscle) and *in vivo* (in sheep muscle).

Borasi et al. (2013) argue that the integration of newest HIFU systems, e.g. Exablate 2100 (InSightec) or other multiple element phased array systems, with external beam radiotherapy could become a potent new weapon against cancer (and, thanks to drug delivery, also against many degenerative diseases). Such a device could integrate, in real time, target and temperature imaging, radiation sterilization, hyperthermia, ablation and drug delivery. It is likely that this type of device would be a lower cost option and, for many cancerous sites in the body, a great deal more effective than expensive and less accessible proton or heavy ion radiotherapy machines.

## 4.6. Hyperthermia

French researchers (Salomir et al. 2000) investigated local hyperthermia with MR-guided focused ultrasound implemented by an MR-compatible 14-ring spherical ultrasound transducer (Laboratoire Electronique de Philips, Paris, France) with operating frequency 1.5 MHz, aperture diameter 96 mm, radius of curvature 130 mm, and maximum acoustic power 44 W averaged over the electrical duty cycle. It was integrated within a Philips 1.5-T ACS-NT clinical scanner (Philips Medical Systems, Best, the Netherlands). The ultrasound probe can be hydraulically moved in the horizontal plane ( $oxz$ ) with a spatial resolution of 0.25 mm in each direction, covering an 80 x 80 mm square. Maximum velocity of the probe is approximately  $2 \text{ mm s}^{-1}$ . The focal length can be electronically adjusted, ranging from 80 to 150 mm. In *in vivo* experiments

four New Zealand rabbits were used to investigate the feasibility of the method. The heating procedure consisted of two successive spiral trajectories covering a circular region of interest inside the rabbit thigh. The outer diameter of the spirals was 16 mm for the first trajectory and 10 mm for the second. The focal point plane was located in the rabbit thigh at approximately 20 mm depth. One hour after completion of the second trajectory, T2-weighted scans (identical to those acquired before the heating procedure) were performed to evaluate tissue edema resulting from hyperthermia. In these experiments it has been shown that spatial control of the FUS heating procedure can be accomplished using a double spiral trajectory of the ultrasound. The approach reduces MR-guided FUS treatment times of large target volumes and might help bringing MR-guided FUS therapy into the clinic. It should be noted that local hyperthermia by focused ultrasound is limited to regions where a relatively large acoustic window exists. For example, the described technology is inappropriate for hyperthermia of liver tumour because of the narrow space between the ribs. The authors believe that phased-array technology will probably improve the potential of focused ultrasound in such cases.

Scientists from National Taiwan University studied the feasibility of external ultrasound hyperthermia using a simple linear phased array with mechanical motion (Ju et al. 2003). The array was mounted on the shaft and moved along it mechanically, while dynamically focusing on the target volume with numerous focal spots. Thus, ultrasound energy was deposited in a 3D volume. Different tumour shapes were evaluated and the results of simulation demonstrated that more than 95% of the target volume reached temperatures higher than 43 °C.

Investigators from the United Kingdom (Aitkenhead et al. 2008) developed a design and simulated a planar phased-array ultrasound transducer suitable for producing localized hyperthermia in solid tumours deep within the body. The simulations helped determine the relationship between the size and position of the focus and parameters of the array. These parameters include the overall size of the array and the size, shape and distribution of the individual elements. A 15-element prototype array has been constructed using the results of the simulation. The array radius was 22 mm, each PZT element was 2 mm in radius. A randomized distribution of elements was chosen to maximize the focal intensity and minimize the power dissipated in the grating lobes. The randomized design of the transducer yielded significant advantages in comparison with regular arrays.

In the work of Salgaonkar et al. (2013) feasibility of hyperthermia delivery to the prostate with a commercially available MR-guided endorectal ultrasound phased array ablation system (ExAblate 2100, Insightec Ltd, 2.3 MHz, 2.3 x 4 cm<sup>2</sup>) was assessed through computer simulations and *ex vivo* experiments.

Exhaustive review regarding ultrasound hyperthermia and the prediction of heating is given in the paper of Hand (1998).

## 4.7. Cardiac Ablation

It is known that cardiac arrhythmias affect millions of people around the world. Therefore minimally invasive or noninvasive methods for treatment of cardiac arrhythmias and other cardiac disorders are needed.

Active work in this area began in the mid-1990s. Such studies were carried out in the University of Michigan, Laboratory of Prof. C. Cain. Kluiwstra et al. (1995) developed phase aberration correction algorithms, and carried out experiments with pork and human rib phantoms to confirm the ability of phased array to precisely form the necessary beams. The developed program allows projection from any point in the myocardium of a "shadow" onto the array aperture surface, thus indicating which elements of the array should be driven or switched off. The active elements or "sub-aperture" was then used to numerically compute the expected beam profile. A pork-rib phantom was used to investigate the feasibility of forming beams around ribs using the developed phase aberration correction techniques. The purpose of these experiments

was to determine the ability of an ultrasound phased array transducer to focus energy through a rib cage. A 64-element linear array, a 96 two-dimensional flat phased array and a 192-element 2-D phased array were used in experiments. The results of experiments showed that precise beam forming in target areas shadowed by obstacles such as the rib cage was possible with the use of aberration correction. Compared with acoustic field measurements in the absence of the ribs, a decrease in intensity level and an increase in relative side lobe levels was seen (the nature of these side lobes is discussed in Section 3.6). Essentially the residual problem is related to the movement of the sonicated region. The authors considered that with a hydrophone probe located inside the heart, real time phase and amplitude aberration correction is possible to locate precisely the foci at the moving target. Thus, in real conditions it is necessary to use very fast aberration correction techniques.

In subsequent work, Kluiwstra et al. (1997) used a single-element focusing therapy transducer with a built-in imaging probe to demonstrate the possibility of precisely forming lesions in the beating heart. Real time image feedback allowed precise identification of the target region and observation of lesion formation. Changes in the electrical activity of the heart were accomplished by precisely positioning lesions in the conduction pathways.

Studies using single-element focused transducers were successfully continued in this laboratory (Strickberger et al. 1999; Xu et al. 2004). These authors plan to use phased arrays to track the septal movement by electronically manipulating the focus.

Active works related with the application of HIFU in cardiology were carried out by Hynynen and his colleagues. The majority of them used single element focused transducers (Hynynen et al. 1997; Smith and Hynynen 1998) or catheters (Zimmer et al. 1995), but a few were related to phased array systems. For example, the acoustic and thermal fields produced by a miniature flat two-dimensional array, intended for noninvasive thermal destruction of the tissues of the heart muscle through the esophagus wall, were calculated (Yin et al. 2004, 2006). Esophagus offers a convenient ultrasound window to the heart, particularly, to the posterior structures, such as the atria. Such a close proximity to the heart makes the proposed transesophageal ultrasound ablation technique very promising, so that minimal distortion of the wave is induced by the esophagus tissue layer. The parameters of this intracavitary array mentioned in Section 2.4 were as follows: frequency of 1 MHz, the dimensions of  $1 \times 6 \text{ cm}^2$ , the distance between the centres of the elements of 0.525 mm (a little more than  $1/3$  of the wavelength), the number of elements of 2280. The simulation results show the possibility of focusing ultrasound through the wall of the esophagus and of steering the multiple foci in heart tissues at the required distance. Evaluation of the thermal dose in the tissue showed that by varying sonication duration and power, the array can produce thermal dose that is high enough to cause tissue necrosis of different sizes. Therefore from the beam propagation point of view, it is feasible to use a planar ultrasound phased array for trans-esophageal cardiac thermal ablation.

Wong et al. (2006) at Stanford University simulated and designed a noncontact, intra-cardiac transducer that can ablate tissue and provide imaging to guide therapy. The device consists of a high-power, 20 mm x 2 mm, 128-element phased array placed on the side of 7-French catheter. The transducer can be used in imaging mode to locate the atrial wall; then, by focusing at that location, a lesion can be formed. As a result, the authors confirmed the feasibility of an intra-cardiac-sized transducer for treatment of atrial fibrillation which affects 1% of the population. In simulations and proof-of-concept experiments the authors showed a  $37^\circ \text{C}$  temperature rise in the lesion location and demonstrated the possibility of lesion imaging. According to simulations, the ultrasound transducer can produce intensities of  $450\text{-}900 \text{ W cm}^{-2}$  at the focal point in cardiac tissues. Using these intensities, it is estimated that tissue necrosis would occur in less than 10 s, taking into account convection from the blood.

Over 2.2 million Americans suffer from atrial fibrillation making it one of the most common arrhythmias (Werner et al. 2010). Cardiac ablation has shown a high rate of success in treating paroxysmal atrial fibrillation. Prevailing modalities for this treatment are catheter based

radio-frequency ablation or surgery. However, there is measurable morbidity and significant costs and time associated with these invasive procedures. Due to these issues, developing a method that is less invasive to treat atrial fibrillation is needed. Werner et al. (2010) studied the feasibility of *in vivo* transesophageal cardiac ablation using a phased ultrasound array. A quasi-periodic two-dimensional sparse phased array with the aperture size of 20.7 mm x 10.2 mm with flat tapered elements was fabricated and evaluated with *in vivo* experiments. Active elements (PZT-8, frequency of 1.6 MHz) were periodically distributed within the 15 x 13 array. The layout involved tapered elements, ranging from 1.04 to 1.55 mm wide and from 0.57 to 0.84 mm high. Thus, there were 64 active elements from 195 in the full matrix. The advantages of such a design were that sparse array had a reduced number of elements and the use of tapered elements suppressed grating lobes. Five pigs were anesthetized; the array was passed through the esophagus and positioned over the heart. The probe was guided through the esophagus with the aid of ultrasound imaging. The array was operated for 8-15 min with an acoustic intensity of 150-300 W cm<sup>-2</sup> resulting in both single and multiple lesions on atrial and ventricular myocardium. The average size of lesions was 5.1 ± 2.1 mm in diameter and 7.8 ± 2.5 mm in length. Based on the experimental results, the array delivered sufficient power to the focal point to produce ablation while not grossly damaging nearby tissue outside the target area. These results demonstrate a potential applicability of the ultrasound applicator to trans-esophageal cardiac surgery in atrial fibrillation treatment.

Lee et al. (2010) investigated the optimal method for distributing elements on the surface of an array intended for application for non-invasive trans-esophageal cardiac ablation. They compared the acoustical fields irradiated by three kinds of array: linear phased array, quasi-periodic sparse phased array and random sparse phased array. The computational simulations and *in vitro* experiments with excised porcine heart tissues showed that the random sparse array showed excellence in both the focusing at the targeted area and controlling grating lobes in the calculated ultrasound fields. These authors reached the same conclusion as was reported in a much earlier study by Gavrilov and Hand (2000)

## 4.8. Stimulation of Neural Structures

### *Development of Tactile Displays*

Two-dimensional phased arrays may find applications in development of promising robotic techniques and systems, sensors, automated control systems, and also “human-machine” interfaces based on the use of tactile sensations.

Japanese scientists suggested and developed an idea to use phased array systems to develop tactile displays (Iwamoto et al. 2001, Iwamoto and Shinoda 2005, 2006). Such displays must create rapidly changing images, especially with a complex configuration (geometric figures, symbols, letters, *etc.*). The principle of action of such displays is based on the stimulation effect of ultrasound on tactile receptors of humans by means of the radiation pressure of ultrasound.

Iwamoto and Shinoda (2006) proposed a design for a tactile display based on the use of a two-dimensional phased array. The focusing system was a combination of eight linear phased arrays, the angle of convergence with respect to the system axis of each array was 70 degrees. The maximum dimension of the housing, in which all arrays were located, was 8 cm, and the focal distance was 3 cm; the operating frequency was 3 MHz. Each array had a trapezoidal shape and consisted of 40 piezoceramic elements with different lengths. Thus, the total number of individually controlled electronic channels was 320. The distance between the element centres was fixed at 0.5 mm. The required size of the tactile display was 1 x 1 cm. Acoustic field measurements performed with a hydrophone demonstrated (Iwamoto and Shinoda 2006) that the focal diameter at the intensity level of 25% of the maximum value at the centre of focus was  $9\lambda$ ,

where  $\lambda=0.5$  mm is the wavelength of ultrasound, and, at the level of 50%, it was about  $5\lambda$ , which is evidence of the very low spatial resolution of the system. The results of computer simulation of the acoustic field generated by this system demonstrated that the intensity in the grating lobes was 13%, even for the case where the focus was located at the acoustic axis of the system. For the case of steering the focus off the system axis, the intensity in the grating lobe would be much greater. Thus, the quality of the acoustic field generated by the system needs considerable improvement. Another important drawback of the system is that it is intended for moving only a single focus along the display area at a given time moment.

The main goals of Gavrilov (2008) were to propose and study in numerical models an alternative method of developing of tactile displays based on the application of a two-dimensional array with elements randomly distributed on its surface. The details of this work and the results obtained were presented in Section 3.5. It was shown that with the use of such array it was possible to synthesize focal regions with complex configurations, in particular, in the form of the letters of the alphabet (see Figure 42).

In connection with the images presented in Figure 42, it is worthwhile to discuss one of the possible designs of an ultrasound tactile display. There are mechanical tactile displays allowing blind and even deaf-and-blind persons to perceive textual information displayed by a relief-dot font due to the effect of the radiation pressure. Small pins, which rise and fall in order to form a symbol, are commonly used in these devices. Letters are depicted in Braille system, which creates the equivalent of a printed symbol using from six to eight dots. To depict Braille's symbols at a display is much easier than the letters of the Latin or Cyrillic alphabet. However, such displays have drawbacks and limitations. The devices in which the pins are moved mechanically are noisy and require a direct contact between the skin of the subject and the pins, and the speed of the change of "images" at the display is very limited. Ultrasonic tactile displays have potential advantages: they are noiseless, contactless, and provide a high update rate on the display. Symbols with a complex configuration (letters, digits, punctuation marks, *etc.*) may be created on the display. Although the feasibility of implementing ultrasonic displays to image printed symbols on the display instead of their Braille equivalents is the subject of a separate study, the technical possibility of creating such devices has been proven (Gavrilov 2008).

During recent years, scientists from Japan tried to develop tactile displays able to produce tactile sensations and to work in air (Iwamoto et al. 2008; Hoshi et al. 2009, 2010; Shinoda 2010; Hoshi 2012). This task is much more complicated rather than the work in water because attenuation in air is extremely high. Meanwhile, Iwamoto et al. (2008) developed a tactile device, which produces stress fields in 3D space. Combined with 3D stereoscopic displays, this device is expected to provide high-fidelity tactile feedback for the interaction with 3D visual objects. The principle is based again on the use of the acoustic radiation pressure. The authors fabricated a prototype device consisting of a 12 channel annular array, a 12 channel driving circuit, and a PC. The measured output radiation force within the focal region was 0.8 gf, and the spatial resolution was 20 mm. Though the radiation force produced was weak for users to feel constant pressure, it was sufficient to induce vibratory sensation up to 1 kHz.

The next version of the device consisted of 324 airborne ultrasound transducers with individual control of phases and amplitudes at each element. The measured output radiation force within the focal region was equal to 1.6 gf (16 mN), which provides suitable touch feeling. The spatial resolution (the diameter of the focal spot) was 20 mm (Hoshi et al. 2009, 2010). The developed interaction system enables users to see and touch virtual objects and therefore realize literally touchable 3D images (Hoshi et al. 2010, Shinoda 2010).

Recently Hoshi (2012) presented a system, which transmits handwriting motion in a tactual manner. It records the writer's handwriting motion and reproduces it on the reader's palm. It enables them to share the handwriting motion and exchange non-verbal information in addition to the appearance of characters and graphics. An ultrasound two-dimensional phased array consisting of 384 ultrasound transducers arranged in a square of side length 20 cm was used for

tactile stimulation. The resonant frequency of the transducers was 40 kHz (i.e.  $\lambda = 8.5$  mm). The width of the focal spot (i.e. the spatial resolution) was 13 mm and the focal length was set at 15 cm. A force of 18 mN was produced with all transducers driven at the maximum power. The ultrasound stimulation was combined with a graphic tablet, and the handwritten characters and graphics were displayed by moving the pressure spot according to the pen strokes. The spot moved at a 1 mm resolution. The experiments showed that users can identify the 26 capital alphabet letters at a 44-percent accuracy rate. Future work will include (1) increasing the output force of the ultrasound tactile display to make sensation clearer, and (2) employing a hand-tracking technology to enable users to feel the sensation at an arbitrary position in midair.

### ***Artificial Prosthesis of a Degenerating Retina***

A separate direction of research is related to attempts to develop methods and devices for artificial prosthesis of a degenerating retina. Hertzberg et al. (2010a) suggest that the use of multi-element phased arrays is very promising for generating multiple foci affecting regions with complex configurations in order to activate and change the functional state of cortical and sub-cortical neural structures. To create appropriate devices and systems, the authors developed effective and fast algorithms for calculating the phase of the array elements necessary for the generation of multiple foci ultrasonic fields with given parameters of the foci. By combining the phased array and MR thermometry it was experimentally demonstrated the simultaneous generation of tightly focused multifocal distributions in a tissue phantom. That is a first step towards the development of patterned ultrasound neuromodulation systems and devices. The authors believe that focused ultrasound directed onto neural structures is able to dynamically modulate their neural activity and excitability, opening up a range of possible systems and applications where the non-invasiveness, safety, mm-range resolution and other favorable characteristics of focused ultrasound are advantageous.

Naor et al. (2012) examined the general feasibility and properties of an acoustic retinal prosthesis, a new vision restoration strategy that will combine ultrasonic neurostimulation and ultrasonic field sculpting technology towards non-invasive artificial stimulation of surviving neurons in a degenerating retina. These authors applied the approach developed by Herzberg et al. and used a miniature two-dimensional phased array to create an artificial prosthesis of a degenerating retina. The main unit of the device was a flat phased array (InSightec Ltd, Israel) with dimensions  $2 \times 4$  cm<sup>2</sup>, consisting of 987 elements. The array was positioned above a cornea, and ultrasound at 0.5 and 1 MHz effected on a retina. The experiments carried out on rats showed occurrence of visually evoked potentials in response to the pulsed ultrasonic stimulation. The range of parameters of the ultrasound stimulation used in animal experiments at 1 MHz was as follows: the burst train duration was 10-20 ms, single burst duration was 100  $\mu$ s, repetition frequency was 1667 Hz, the peak instantaneous intensity was 10-17 W cm<sup>-2</sup> and  $I_{SPPA}$  was 5.15-8.5 W cm<sup>-2</sup>. A device that is aimed at non-invasive patterned excitation of populations of retinal neurons using acoustic interference patterns projected from a multi-element phased ultrasonic array has been conceptually validated and analyzed. The authors believe, that by means of the developed software and device, and also having in mind that the duration of a series of impulses for the effective stimulation of a retina is approximately 10 ms, it is possible to update the information on the retina at a rate of the order of tens images per second. Although many questions about this technological framework remain open, the *in vivo* experiments and subsequent analysis suggest that a low-acuity the acoustic retinal prosthesis with sub-mm resolution and intensities that comply with international ophthalmic safety guidelines appears to be feasible using frequencies in the low MHz range. Moreover, a preliminary assessment showed no short-term damage to the retina, which appeared to remain functionally and morphologically intact. A prosthesis operating in the 2-10 MHz range could potentially become an external, implant-less, alternative to existing implantable systems with a similar spatial resolution. Further

research is clearly required to expand understanding of the mechanisms of ultrasound neuroactivation.

Menz et al. (2013) used the isolated salamander retina to characterize the effect of ultrasound on an intact neural circuit and compared these effects with those of visual stimulation of the same retinal ganglion cells. Ultrasound stimuli at an acoustic frequency of 43 MHz and a focal spot diameter of 90  $\mu\text{m}$  delivered from a piezoelectric transducer evoked stable responses with a temporal precision equal to strong visual responses but with shorter latency. The calculated time-averaged acoustic intensity was 10-30  $\text{W}/\text{cm}^2$  for 50% duty cycle stimulus (1 s on, 1 s off) for most experiments. The 43 MHz carrier frequency was modulated at low frequencies (0.5-15 Hz) to match the temporal pattern used for visual stimulation. For most experiments, this consisted of 1 s of stimulus on and 1 s of stimulus off, repeated for many cycles, for a total duration of 1–5 min. By presenting ultrasound and visual stimulation together, the authors found that ultrasonic stimulation rapidly modulated visual sensitivity but did not change visual temporal filtering. By combining pharmacology with ultrasound stimulation, it was found that ultrasound did not directly activate retinal ganglion cells but did in part activate interneurons beyond photoreceptors. These results suggest that, under conditions of strong localized stimulation, timing variability is largely influenced by cells beyond photoreceptors. It was concluded that ultrasonic stimulation is an effective and spatiotemporally precise method to activate the retina. Because the retina is the most accessible part of the central nervous system *in vivo*, ultrasonic stimulation may have diagnostic potential to probe remaining retinal function in cases of photoreceptor degeneration, and therapeutic potential for use in a retinal prosthesis. The authors consider that ultrasound neurostimulation, because of its noninvasive properties and spatiotemporal resolution, promises to be a useful tool to understand dynamic activity of neural pathways in the retina.

#### 4.9. Uterine Fibroids

An application use of high-intensity focused ultrasound in medicine that appeared relatively recently, but has already achieved wide clinical use is the treatment of diseases of the female reproductive organs and, primarily, surgery of uterine fibroids, the most common benign tumours in females. This disease is also known as uterine leiomyoma, fibromioma, *etc.* The incidence of leiomyomas occurs in 70-80 % of American women (Tan and Raman 2013). Fibroids often cause pain and heavy menstrual bleeding; moreover, they can grow to a considerable size (more than 20 cm). These tumors do not pose a threat to a woman's life, but it is unlikely that in this case the woman can carry and give birth to a child. The disease usually occurs in women older than 30 years and is detected in 20-40 % of women over 35 years. Some fibroids can be removed surgically, and sometimes there is need to remove the entire uterus. If a woman does not feel any discomfort or other harassing symptoms (which often occurs), surgery is not required. However, many women have symptoms that dramatically degrade their quality of life, and then have to resort to various methods of treatment, ranging from drugs to removal of the uterus (hysterectomy).

Held et al. (2006) developed and investigated the use of a 3 MHz, 11 element annular array (Imasonic, Besançon, France), designed for intracavitary surgery of uterine fibroids. The geometric focus of the array was at 50 mm. The experimental verification was carried out on gels and porcine liver tissues. Lesion formation was noted at the entire depth range from 30 to 60 mm in pig liver, which shares similar acoustic properties with uterine tissue. The lesions were obtained at acoustic intensities of 4100 and 6100  $\text{W}/\text{cm}^2$  for 15 s each, with the latter producing average lesion volumes at least 63% larger than the former. The authors believe that the success of their device in producing and monitoring tissue coagulation at the desired focal depths indicates its potential use in a surgical session.

InSightec (<http://www.insightec.com/>) has developed and manufactures a standard ultrasound device for surgery of uterine fibroids ExAblate® 2000, which in 2004 was approved by FDA. The principle of the device is based on the destruction of tumor tissue by powerful focused ultrasound under MRI control. At the end of 2007 more than 3000 women had received surgical treatment with this device.

During the procedure, the patient is positioned within the MRI scanner, and three-dimensional images of the target and surrounding tissues are acquired. Then, the temperature in the focal region of the focusing radiator is raised up to 65-85 °C, which is more than enough to destroy the tumor tissue. The duration of each exposure does not exceed 20 s. The procedure is repeated until the main body of the tumor reaches a temperature sufficient to necrosis. The scanner provides feedback in real time and allows the physician to monitor the progress of the operation, continuing up to 3 hours. The method has proven to be an effective means of fibroids surgery. Compared with hysterectomy, which is currently the main surgical approach, the proposed method has a number of clinical and economic benefits. The method is non-invasive, and therefore the patient avoids the risks associated with surgery. The ExAblate device allows to remove the tumor non-invasively, while preserving the uterus as an organ. Limited sedation is required and the patient can return to normal life within a day, whereas after removal of the uterus a long postoperative recovery period is needed. All of these lead to a substantial positive economic effect. Side effects, according to manufacturers, are rare and include skin burns and reversible damages of nerves. However, FDA has not yet recommended to use this treatment for women who plan to have children in the future, because it may change the composition and strength of uterine tissues.

A summary of the clinical results obtained by using the above method and ExAblate device is contained in a number of papers (Hindley et al. 2004; Funaki et al. 2006; Fennessy and Tempny 2006; Fennessy et al. 2007; Stewart et al. 2007; Rabinovichi et al. 2007; Chapman and Ter Haar 2007; Trumm et al. 2013). One of the articles is devoted to the peculiarities of temperature measurement using the method described above (McDannold et al. 2006).

## 4.10. Other Applications

### *Treatment of osteoarthritis knee pain*

Severe knee pain associated with osteoarthritis is one of the most common and troublesome symptoms in the elderly (see the details in Izumi et al. 2013). Such chronic knee pain has a significant effect on patients' quality of life. Although total knee arthroplasty is a validated and reliable intervention for alleviating severe knee pain, there are some patients who are at high risk during surgery and other patients who are not willing to undergo surgery. The number of these patients is expected to increase because of the aging population; therefore, it is necessary to explore additional nonsurgical treatments for knee osteoarthritis to achieve better pain relief.

Japanese scientists have developed a novel method of treatment for osteoarthritis based on the application of MR-guided focused ultrasound (Izumi et al. 2013). Eight patients with medial knee pain and eligible for total knee arthroplasty were included. The treatment was conducted as an outpatient setting, using the MRgFUS system (ExAblate® 2100, InSightec Ltd, Haifa, Israel) integrated with an MR scanner (GE Signa EXCITE 3.0 T, Milwaukee, WI, USA). Ultrasound treatments were applied to bone surface just below the rim osteophyte of medial tibia plateau with real-time monitoring of the temperature in the target sites. Six patients (75%) showed immediate pain alleviation after treatment, and four of them demonstrated long-lasting effect at 6-month follow up. These initial results illustrate the safety and efficacy of the newly developing MRgFUS treatment. The authors concluded that MRgFUS treatment had the potential of rapid and long-lasting pain alleviation without adverse side effects. Significant

increase of pressure pain thresholds on the treated area showed successful denervation effect on the nociceptive nerve terminals. Thus, MRgFUS is a promising and innovative procedure for noninvasive pain management of knee osteoarthritis.

### ***Pain palliation in patients with bone metastases***

Pain due to bone metastases is a one of causes of cancer-related morbidity, with few options available for patients refractory to medical therapies and who do not respond to radiation therapy (Hurwitz et al. 2014). Bone metastases are common in patients with advanced cancer and are the greatest contributor to cancer-related pain, often severely affecting quality of life. Many patients with advanced cancer are undertreated for pain (Hurwitz et al. 2014). Radiation therapy (RT), together with systemic therapies and analgesics, is the standard of care for localized metastatic bone pain, although up to two-thirds of patients have residual pain after RT. There are reasons to believe that the combination of focused ultrasound with MR could perform precise localized tumor tissue ablation, while using MR thermometry for real-time temperature monitoring (Hurwitz et al. 2014).

Napoli et al. (2013b) studied the ability of high intensity focused ultrasound, under MR guidance (MRgFUS), to be delivered to bone metastases. The objectives of their study were to evaluate the efficacy in pain management of MRgFUS for the primary treatment of painful bone metastases and to assess its potential for local control of bone metastases. The treatment sessions were performed with a focused ultrasound phased-array treatment system ExAblate 2100; InSightec, Israel) integrated with the 3 T MR imager. The authors concluded that MR-guided focused ultrasound can be safely and effectively used as the primary treatment of pain palliation in patients with bone metastases and has a potential role in local tumor control.

In the work of Hurwitz et al. (2014) results of a randomized controlled trial to evaluate safety and efficacy of MRgFUS for treating bone metastases in patients with persistent or recurrent pain after RT, or who were otherwise not candidates for RT, or who declined RT. The primary objective was to evaluate pain reduction after MRgFUS. The secondary objectives of the study included assessment of the treatment's impact on pain-related interference with patient functioning and treatment-related toxicity. Patients were enrolled between July 2008 and May 2012 at 17 centres across the United States, Canada, Israel, Italy, and Russia. Patients were aged at least 18 years with life expectancy equal to or greater than 3 months and had bone metastases 1) that were painful despite previous RT; 2) were otherwise unsuitable for RT (e.g., because of prior definitive high-dose treatment to the area of pain); or 3) who declined RT. One hundred forty-seven subjects were enrolled, with 112 and 35 randomly assigned to MRgFUS and randomized placebo treatments, respectively. Treatment was performed using the ExAblate MRgFUS system (InSightec, Tirat Carmel, Israel). Patients were positioned on the MRgFUS table with the targeted tumour centred above the ultrasound transducer, with positioning and clear ultrasound pathway verified by MR imaging. The response rate for the primary endpoint was 64.3% in the MRgFUS arm and 20.0% in the placebo arm. The multi-centre results showed that MRgFUS provided durable pain relief and improved function in patients who failed radiation or those who were not candidates for or declined radiation. Given the impact of these clinically significant results, coupled with a favorable side effect profile, MRgFUS should be considered a viable treatment option for painful bone metastases. Further studies are required to assess the role of MRgFUS in patients with bone metastases as first-line therapy (Hurwitz et al. 2014).

### ***Liposuction***

The majority of ultrasound procedures of liposuction (removal of extra fat) is carried out with the use of a device UltraShape Contour I, Israel (Brown et al. 2009). Destruction of fat tissue by focused ultrasound at 200 kHz was reported by Goland and Kushkuley (2009). The

design of this device is such that an operator manually moves the transducer over the surface of the patient's body. The diameter of the focal region is 5-6 mm and therefore the duration of a procedure to treat large surfaces is too long and causes inconvenience to both patient and operator. Golland and Kushkuley (2009) proposed the use of a powerful multi-element phased array with a large aperture angle for this purpose. A nonlinear model was developed to describe the acoustic fields emitted by such transducers; the model has a larger area of applicability with respect to the aperture angle, as compared to other approaches. The phased array was manufactured using a single spherical piezoelement produced from a non-composite piezoceramics (diameter of 84 mm, radius of curvature of 54 mm, frequency of 1 MHz) developed at UltraShape Ltd. The method of manufacturing is based on the segmentation of one of the electrodes of the piezoelement into 160 randomly distributed circular elements, each of diameter 5.2 mm.

### *Lithotripsy*

A piezoelectric lithotripter is usually a multi-element transducer with hundreds or even thousands of small elements arranged on a spherical segment. All elements are excited simultaneously due to the discharge of the capacitor. This design (as an array), in principle, allows to control pulsed acoustic beam, and to obtain ultrasound images of stone. The lack of an electric discharger increases the reliability of this device; defective elements can be replaced if necessary.

In the work of Tavakkoli et al. (1997) a two-dimensional array consisting of 274 independent piezocomposite transducers mounted on a spherical shell of 280 mm in diameter and with the radius of curvature of 19 cm was described. The frequency was 360 kHz and the voltage at each of the elements was 6.6 kV. For the purpose of performing electronic steering of shock waves, the delay time of each channel could be adjusted from 100 ns to 100ms in steps of 100 ns. In order to increase the effect of cavitation, the pressure-time waveform started from a half cycle of negative pressure with peak amplitude of  $150 \times 10^5$  Pa, followed by a very steep shock front with a positive peak pressure higher than  $1000 \times 10^5$  Pa and a rise time of about 10 ms. The presence of the negative pressure leads to the formation in the medium of well-developed cavitation, the destructive effect of which is enhanced by the further strong pulse of positive pressure. Using this system, cavitation-induced lesions in rabbit liver were studied.

In comparison with electrohydraulic lithotripters, piezoelectric ones work quieter and cause less pain. The disadvantage of these systems is relatively small energy implemented in focus, so their efficiency is relatively low. Therefore, the natural tendency is the development and application in lithotripter of new high piezoelectric materials.

## Concluding Comments

This book has addressed several aspects of high power ultrasound phased arrays and their potential medical applications. Since the centre to centre spacing between elements in practicable arrays is greater than half the ultrasound wavelength, it follows that grating lobes will be produced in the acoustic field produced by the array. These grating lobes are a potential hazard in medical applications, and so there is a need to reduce them. A means of achieving this, through randomization of the spatial distribution of elements, is central to the text of the book.

Another important design feature for high power ultrasound arrays is that the elements should not be very directive, i.e. their diameters must not exceed a few ultrasound wavelengths ( $\lambda$ ). Arguments have been presented that suggest that the maximum value should not exceed  $5\lambda$ .

An additional but important condition concerns the sparseness of the array. Arguments have been presented that suggest that the total surface area of active elements should not be less than 40% of the total surface area of the array in order to achieve a reasonably high level of intensity in the focus or foci. It is important to realize that the sparseness of an array should not be achieved by simply randomly removing elements from an ordered structure since this does not ensure a high quality of acoustic field as characterized by the level of grating lobes.

It is possible to achieve a high-grade quality of the field as well as a high level of intensity in the main focus or foci using a very tight, and sometimes maximally feasible, density of packing of not highly directional elements distributed randomly on the surface of the array. One example of such an array might comprise a spiral distribution of square elements.

Having introduced the topic through a discussion of linear phased arrays, the advantages of these compared with commonly used devices using fixed focused transducers in such applications as transrectal heating or ablation of the prostate were highlighted. As with most therapeutic applications of phased arrays, the wide clinical use of linear arrays will require the development of systems that not only provide steering of the focus within a target such as the prostate but which also provide means of verification of the location of the focus prior to treatment involving high power sonication, and verification of tissue damage following this treatment.

Next, commonly used 2-dimensional phased arrays in which elements are distributed in a regular manner were discussed. The significant increase in versatility of 2 dimensional arrays compared with linear ones is bought at the extra cost of complexity of the construction and the driving and control electronics. However, the regular distribution of elements leads to high levels of grating lobes, a major disadvantage of this approach. Nevertheless, the wide experience gained in designing, testing, and experimenting with such devices has provided considerable conceptual insight into the potential benefits of 2-dimensional arrays.

An important step in the design of 2 dimensional arrays is to randomly distribute the elements over the surface of the array, an approach which minimizes grating lobe levels and consequently leads to improved safety implications in medical applications. The influence of the dimensions, number, and shape of individual elements, errors in phase setting at the elements, and the frequency modulation of the signal on the quality of the intensity distributions produced by random arrays has been considered. Also highlighted were not only the improved ability of randomized 2 dimensional arrays to steer the focus or a set of simultaneously generated foci, but also the ability to generate focal regions with complex shapes. Furthermore the ability of these arrays to modify the acoustic field in the presence of absorbing obstacles yet still form a focus beyond them has important implications for clinical applications in which the target volume is within the rib cage.

Whilst much clinical experience of high intensity focused ultrasound has been gained in the treatment of prostate diseases, including prostate cancer, recent research has indicated a much wider range of potential clinical applications. Phased arrays will have a fundamental role in these exciting developments.

The ability of phased arrays to sonicate through the skull and create a focal volume within the brain without excessive heating of the skull opens up the possibilities of non-invasive treatments of not only brain tumours but also neurological disorders, intracerebral haemorrhage, and drug delivery across the blood-brain barrier. As mentioned above, the ability to focus acoustic energy at targets distal to the ribs provides an opportunity for HIFU ablation of cardiac tissue.

Whilst tissue ablation by means of high intensity focused ultrasound is often a stand alone treatment, for example in the treatment of uterine fibroids, ultrasound induced hyperthermia can be used as an adjuvant to radiotherapy or chemotherapy in the treatment of a number of tumours. Other novel applications that are emerging include tactile displays, retinal prostheses and pain management.

In summary, the development of ultrasound phased arrays and their potential clinical applications is leading to exciting topics of research. Future implementation, aided by guidance and verification using diagnostic techniques such as MRI, is expected to increase our ability to treat a range of diseases and disorders non-invasively, with important implications for improved patient morbidity and lowering of financial pressures. We believe that in this book we have provided evidence that this is a rapidly changing field of medical acoustics and engineering in as assessed by the rapidly growing number of publications and that our effort is an early attempt to summarise the topic of applications of high-intensity phased arrays in medicine.

## References

- Aitkenhead, A. H., Mills, J. A. & Wilson, A. J. (2008). The design and characterization of an ultrasound phased array suitable for deep tissue hyperthermia. *Ultrasound in Med. and Biol.* 34, 1793–1807.
- Auboiroux, V., Dumont, E., Petrusca, L., Viallon M. & Salomir R. (2011). An MR-compliant phased-array HIFU transducer with augmented steering range, dedicated to abdominal thermotherapy. *Phys. Med. Biol.* 56, 3563–3582.
- Aubry, J. F., Pernot, M., Marquet, F., Tanter, M. & Fink, M. (2008). Transcostal high-intensity-focused ultrasound: *ex vivo* adaptive focusing feasibility study. *Phys. Med. Biol.* 53, 2937–51.
- Aubry, J.-F., Tanter, M., Pernot, M., Thomas, J. -L. & Fink, M. (2003). Experimental demonstration of non invasive transskull adaptive focusing based on prior CT scans. *J. Acoust. Soc. Am.* 113, 85–93.
- Benkeser, P. J., Frizzel, L. A., Ocheltree, K. B. & Cain, C. A. (1987). A tapered phased array ultrasound transducer for hyperthermia treatment. *IEEE Trans. Ultrason. Ferroelec. Frequency Control.* 34, 446–453.
- Bihrlé, R., Foster, R. S., Sanghvi, N. T., Fry, F. J. & Donohue, J. P. (1994). High-intensity focused ultrasound in the treatment of prostatic tissue. *Urology.* 43, 21–26.
- Bobkova, S., Gavrilov, L., Khokhlova, V., Shaw, A., & Hand, J. (2010). Focusing of high intensity ultrasound through the rib cage using therapeutic random phased array. *Ultrasound in Med. and Biol.* 36, 6, 888-906.
- Borasi, G., Russo, G., Alongi, F., Nahum, A., Candiano, G. C., Stefano, A., Gilardi, M. C. & Messa, C. (2013). High-intensity focused ultrasound plus concomitant radiotherapy: a new weapon in oncology? *Journal of Therapeutic Ultrasound* 1, 6.
- Botros, Y. Y., Ebbini, E. S. & Volakis, J. L. (1998). Two-step hybrid virtual array-ray (VAR) technique for focusing through the rib cage. *IEEE Trans. Ultrason. Ferroelec. Freq. Ctrl.* 45, 4, 989–999.
- Brown, S. A, Greenbaum, L., Shtukmaster, S., Zadok, Y., Ben-Ezra, S. & Kushkuley, L. (2009). Characterization of non-thermal focused ultrasound for non-invasive selective fat cell disruption (lysis): Technical and pre-clinical assessment. *Plastic and Reconstructive Surgery*, 124, 92-101.
- Buchanan, M. T. & Hynynen, K. (1994). Design and experimental evaluation of an intracavitary ultrasound phased array system for hyperthermia. *IEEE Trans. Biomed. Eng.* 41, 12, 1178-1187.
- Cain, C. A. & Umemura, S. A. (1986). Concentric-ring and sector vortex phased array applicators for ultrasound hyperthermia therapy. *IEEE Trans. Microwave Theory Tech.* 34, 542–551.
- Chapman, A. & Ter Haar, G. (2007). Thermal ablation of uterine fibroids using MR-guided focused ultrasound—a truly non-invasive treatment modality. *Eur. Radiol.* 17, 10, 2505–2511.
- Civale, J., Clarke, R., Rivens, I. & ter Haar, G. (2006). The use of a segmented transducer for rib sparing in HIFU treatments. *Ultrasound in Med. and Biol.* 32, 11, 1753–1761.
- Clark, D., Sheirer, B., Manning, R. (2013). Curved ultrasonic HIFU transducer with air cooling passageway. *European Patent EP 2499636 B1*. Date of publication 04.09.2013 Bulletin 2013/36.
- Clement G. T. & Hynynen K. (2000). Criteria for the design and characterization of large-area arrays for transskull ultrasound surgery and therapy. *2000 IEEE Ultrasonics Symposium.* 1-4.
- Clement, G. T. & Hynynen, K. (2002). A non-invasive method for focusing ultrasound through the human skull. *Phys. Med. Biol.* 47, 8, 1219–1236.

- Clement, G. T., Sun, J., Giesecke, T. & Hynynen, K. (2000a). A hemisphere array for non invasive ultrasound surgery and therapy. *Phys. Med. Biol.* 45, 3707–3719.
- Clement, G. T., White, J. P. & Hynynen, K. (2000b). Investigation of a large area phased array for focused ultrasound surgery through the skull. *Phys. Med. Biol.* 45, 1071–1083.
- Clement, G. T., White, P. J., King, R. L., McDannold N. & Hynynen, K. (2005). A magnetic resonance imaging-compatible, large-scale array for transskull ultrasound surgery and therapy. *J. Ultrasound Med.* 24, 8, 1117–1125.
- Cline, H. E., Hynynen, K., Watkins, R. D., Adams, W. J., Schenck, J. F., Ettinger, R. H., Freund, W. R., Vetro, J. P. & Jolesz, F. A. (1995). Focused US system for MR imaging-guided tumor ablation. *Radiology.* 194, 3, 731-737.
- Cline, H. E., Hynynen, K., Hardy, C. J., Watkins, R. D., Schenck, J. F. & Jolesz, F. A. (1994). MR temperature mapping of focused ultrasound surgery. *Magn. Reson. Med.* 31, 6, 628-636.
- Cochard, E., Prada, C., Aubry, J. F. & Fink, M. (2009). Ultrasonic focusing through the ribs using the DORT method. *Med. Phys.* 36, 8, 3495-3503.
- Curiel, L., Chavrier, F., Souchon, R., Birer, A. & Chapelon, J. Y. (2002). 1.5-D High intensity focused ultrasound array for non-invasive prostate cancer surgery. *IEEE Trans. Ultrason. Ferroelectr. Freq. Control.* 49, 2, 231-242.
- Damianou, C. & Hynynen, K. (1993). Focal spacing and near-field heating during pulsed high temperature ultrasound hyperthermia treatment. *Ultrasound Med. Biol.*, 19, 777 - 787.
- Daum, D. R. & Hynynen K. (1998). Thermal dose optimization via temporal switching in ultrasound surgery. *IEEE Trans. Ultras. Ferroelec. Freq. Ctrl.* 45, 208-215.
- Daum, D. R., & Hynynen, K. (1999). A 256-element ultrasonic phased array system for the treatment of large volumes of deep seated tissue. *IEEE Trans. Ultras. Ferroelec. Freq. Ctrl.* 46, 5, 1254-1268.
- Daum, D. R., Smith, N. B., King, R. & Hynynen, K. (1999). *In vivo* demonstration of non-invasive, thermal surgery of the liver and kidney using an ultrasonic phased array. *Ultrasound in Med. and Biol.* 25, 7, 1087-1098.
- de Souza, N. M., Gilderdale, D. J., Puni, R., Coutts, G. A. & Young, I. R. (1996). A solid reusable endorectal receiver coil for magnetic resonance imaging of the prostate: design, use and comparison with an inflatable endorectal coil. *Journal Mag. Reson. Imaging.* 6, 5, 801-804.
- Diederich, C. J. & Hynynen, K. (1987). Induction of hyperthermia using an intracavitary ultrasonic applicator. *Proc. IEEE Ultrason. Symp.* 2, 871-874.
- Diederich, C. J. & Hynynen, K. (1989). Induction of hyperthermia using an intracavitary multi-element ultrasonic applicator. *IEEE Trans. Biomed. Eng.* 36, 432-438.
- Diederich, C. J. & Hynynen, K. (1990). The development of intracavitary ultrasonic applicators for hyperthermia: A design and experimental study. *Med. Phys.* 17, 626-634
- Diederich, C. J. & Hynynen, K. (1991). The feasibility of using electrically focused ultrasound arrays to induce deep hyperthermia via body cavities. *IEEE Trans. Ultrason. Ferroelect. Freq. Contr.* 38, 207-219.
- Diederich, C. J. & Hynynen, K. (1999). Ultrasound technology for hyperthermia. *Ultrasound in Med. and Biol.* 25, 6, 871-887.
- Duck, F. (1990). *Physical Properties of Tissue*. London: Academic Press. 346 P.
- Eames, M. D. C., Hanane, A., Snell, J. W, Kassell, N. F. & Aubry J. -F. (2013). Trans-cranial focused ultrasound without hair shaving: feasibility study in an ex vivo cadaver model. *Journal of Therapeutic Ultrasound.* 1, 24. <http://www.jtultrasound.com/content/1/1/24>
- Ebbini, E. S. & Cain, C. A. (1989). Multiple-focus ultrasound phased array pattern synthesis: Optimal driving signal distributions for hyperthermia. *IEEE Trans. Ultrason. Ferroelec. Freq. Contr.* 36, 5, 540–548.

- Ebbini, E. S. & Cain, C. A. (1991a). A spherical-section ultrasound phased-array applicator for deep localized hyperthermia. *IEEE Trans. Biomed. Eng.* 38, 7, 634–643.
- Ebbini, E. & Cain, C. A. (1991b). Optimization of the intensity gain of multiple focus phased array heating patterns. *Int. J. Hyperthermia.* 7, 951-973.
- Ebbini, E. S., Umemura, S. -I., Ibbini, M. & Cain C. A. (1988). A cylindrical-section ultrasound phased-array applicator for hyperthermia cancer therapy. *IEEE Trans. Ultrasonics Ferroelectr. Freq. Control.* 35, 5, 561-572.
- Elias, W.,J., Huss, D., Voss, T., Loomba, J., Khaled, M., Zadicario, E., Frysinger, R.,C., Sperling, S. A., Wylie, S., Monteith, S. J., Druzgalm J., Shahm B. B., Harrison, M. & Wintermark, M. (2013). A pilot study of focused ultrasound thalamotomy for essential tremor. *The New England Journal of Medicine.* 369, 7, 640-648.
- Ellens, N., Pulkkinen, A., Song, J. & Hynynen, K. (2011). The utility of sparse 2D fully electronically steerable focused ultrasound phased arrays for thermal surgery: a simulation study. *Phys. Med. Biol.* 56, 4913–4932.
- Fan, X. & Hynynen, K. (1995). Control of the necrosed tissue volume during noninvasive ultrasound surgery using a 16-element phasedarray. *Med. Phys.* 22, 297–306.
- Fan, X. & Hynynen, K. (1996a). Ultrasound surgery using multiple sonications - treatment time considerations. *Ultrasound Med. Biol.* 22, 471 – 482.
- Fan, X. & Hynynen, K. (1996b). A study of various parameters of spherically curved phased arrays for noninvasive ultrasound surgery. *Phys. Med. Biol.* 41, 4, 591-608.
- Fennessy, F. M. & Tempny, C. M. (2006). A review of magnetic resonance imaging-guided focused ultrasound surgery of uterine fibroids. *Top Magn Reson Imaging.* 17, 3, 173–179.
- Fennessy, F. M., Tempny, C. M., McDannold, N. J., So, M. J., Hesley, G., Gostout, B., Kim, H. S., Holland, G. A., Sarti, D. A., Hynynen, K., Jolesz, F. A. & Stewart, E. A. (2007). Uterine leiomyomas: MR imaging-guided focused ultrasound surgery - results of different treatment protocols. *Radiology.* 243, 3, 885-893.
- Filonenko, E. A., Khokhlova, V. A., Gavrilov, L. R. & Hand, J. W. (2004). **Heating of biological tissues by two-dimensional phased arrays with random and regular element distributions.** *Acoustical Physics.* 50, 2, 222-231.
- Fink, M. (1992). Time reversal of ultrasonic fields—Part I: Basic principles. *IEEE Trans. Ultrason. Ferroelect. Freq. Contr.* 39, 5, 555–566.
- Fjfield, T., Fan, X. & Hynynen, K. (1996). A parametric study of the concentric-ring transducer design for MRI guided ultrasound surgery. *J. Acoust. Soc. Am.* 100, 2, Pt. 1, 1220-1230.
- Fjfield, T., Sorrentino, V., Cline, H. & Hynynen K. (1997). Design and experimental verification of thin acoustic lenses for the coagulation of large tissue volumes. *Phys. Med. Biol.* 42, 2341-2354.
- Fjfield T., Silcox C. E. & K. Hynynen. (1999). Low-profile lenses for ultrasound surgery. *Phys. Med. Biol.* 44, 1803-1813.
- Foster R. S., Bihrlé R., Sanghvi N. T., Fry F. J. & Donohue J. P. (1993). High-intensity focused ultrasound in the treatment of prostatic disease. *Eur. Urol.* 23, (Suppl 1), 29-33.
- Fry W. J., Mosberg W., Barnard J. W. & Fry F. J. (1954). Production of focal destructive lesions in the central nervous system with ultrasound. *J. Neurosurgery,* 11, 471-478.
- Fry F. J. (1978). Intense focused ultrasound: Its production, effects and utilization. In F. J. Fry (Ed.) *Ultrasound: Its Applications in Medicine and Biology, Part II.* 689-736. New York: Elsevier.
- Funaki K. & Fukunishi H. (2006). The early effects of MRgFUS in treating uterine fibroids. *Therapeutic ultrasound. 5-th International Symposium on Therapeutic Ultrasound.* (Edited by G.T. Clement, N.J. McDannold, K. Hynynen). 513-517. Boston, USA: American Institute of Physics.

- Gao, J., Cochran, S., Huang, Z., Shi, L. & Volovick, A. (2011). Effect of focus splitting on ultrasound propagation through the rib cage in focused ultrasound surgery. *4th International Conference on Biomedical Engineering and Informatics (BMEI)*. 2327-2330.
- Gao J., Volovick A., Cao R., Nabi G., Cochran S., Melzer A. & Huang Z. (2012a). Optimizing sonication protocols for transthoracic focused ultrasound surgery. *AIP Conference Proceedings* 1503, 146; doi: 10.1063/1.4769933.
- Gao J., Volovick A., Pekelny Y., Huang Z. H., Cochran S. & Melzer A. (2012b). Focusing through the rib cage for MR-guided transcostal FUS. *AIP Conf. Proc.* 1481, 94.
- Gavrilov, L. R. (1974). Physical mechanism of the lesion of biological tissues by focused ultrasound. *Sov. Phys.-Acoust.* 20, 16-18.
- Gavrilov, L. R. (2003). Two-dimensional phased arrays for surgical application: Multiple foci generation and scanning. *Acoustical Physics.* 49, 5, 508-516.
- Gavrilov, L. R. (2008). The possibility of generating focal regions of complex configurations in application to the problems of stimulation of human receptor structures by focused ultrasound. *Acoustical Physics.* 54, 2, 315-326.
- Gavrilov, L. R. (2010). Evolution of high intensity focusing systems for different applications in medicine (Review). *Acoustical Physics.* 56, 6, 1097–1111.
- Gavrilov, L. R. (2014). Use of Focused Ultrasound for Stimulation of Various Neural Structures. New York: Nova Science Publishers.
- Gavrilov, L. R. & Hand, J. W. (1997). Development and investigation of ultrasound linear phased arrays for transrectal treatment of prostate. *Ultrasonics Sonochemistry.* 4, 2, 173-174.
- Gavrilov, L. R. & Hand, J. W. (2000a). A theoretical assessment of the relative performance of spherical phased arrays for ultrasound surgery. *IEEE Trans. Ultrason. Ferroelec. Freq. Contr.* 47, 1, 125–139.
- Gavrilov, L. R. & Hand, J. W. (2000b). Two-dimensional phased arrays for surgery: Movement of a single focus. *Acoustical Physics.* 46, 4, 390-399.
- Gavrilov, L. R. & Hand, J. W. (2000c). Design and experimental evaluation of an endocavitary linear phased array for ultrasound surgery of prostate. *Acoustical Physics.* 46, 2, 144-152.
- Gavrilov, L. R., Hand, J. W. & Abel, P. (1996). Ultrasound transrectal linear array for thermotherapy of prostatic diseases. In C. Franconi, G. Arcangeli & R. Cavaliere (Eds). *Hyperthermic Oncology* 1996, V. 2, 399-401. Rome: Tor Vergata University.
- Gavrilov, L. R., Hand, J. W., Abel, P. & Cain, C. A. (1997). A method of reducing grating lobes associated with an ultrasound linear phased array intended for transrectal thermotherapy of prostate. *IEEE Trans. Ultrason. Ferroelectr. Freq. Contr.* 44, 5, 1010-1017.
- Gavrilov, L. R., Hand, J. W. & Yushina, I. G. (2000). Two-dimensional phased arrays for application in surgery: Scanning of several foci. *Acoustical Physics.* 46, 5, 551-558.
- Gavrilov, L. R., Tsurulnikov, E. M. & Davies, I. ab I. (1996). Application of focused ultrasound for the stimulation of neural structures. *Ultrasound Med. Biol.* 22, 179-192.
- Gélat, P., ter Haar, G. & Saffari, N. (2011). Modelling of the acoustic field of a multi-element HIFU array scattered by human ribs. *Phys. Med. Biol.* 56, 5553-5581.
- Gélat, P., ter Haar, G. & Saffari, N. (2012). The optimization of acoustic fields for ablative therapies of tumours in the upper abdomen. *Phys. Med. Biol.* 57, 8471–8497.
- Gelet, A., Chapelon, J. Y., Bouvier, R., Pangaud, C. & Lasne Y. (1999). Local control of prostate cancer by transrectal high intensity focused ultrasound therapy: preliminary results. *J. Urol.* 161, 156–162.
- Gelet, A., Chapelon, J. Y., Margomari, J., Theillere, Y., Gorry F., Souchon, R. & Bouvier R. (1993). High-intensity focused ultrasound experimentation on human benign prostatic hypertrophy. *Eur. Urol.* 23, (Suppl 1), 44-47.

- Goland, V. I. & Kushkuley, L. (2009). Strongly focusing multielement therapeutic emitters for noninvasive ultrasonic ablation of adipose tissue. *Acoustical Physics*. 55, 4-5, 496-509.
- Goss, S. A., Frizell, L. A., Kouzmanoff, J. T., Barich, J. M., & Yang, J. M. (1996). Sparse random ultrasound phased array for focal surgery. *IEEE Trans. Ultras. Ferroelec. Freq. Ctrl.* 43, 6, 1111–1121.
- Hand J, W. (1998). Ultrasound hyperthermia and the prediction of heating. In F. A. Duck, A. C. Baker & H.C. Starritt (Eds). *Ultrasound in Medicine*. 151–176. Bristol, UK: IOP Publishing.
- Hand, J. W., Ebbini E., O'Keefe D., Israel D. & Mohammadttaghi S. (1993). An ultrasound linear array for use in intracavitary applicators for thermotherapy of prostatic diseases. *Proc. IEEE Ultrason. Symp.* 1993, 1225-1228.
- Hand, J. W. & Gavrilov, L. R. (2000). Great Britain Patent No. GB2347043 Ultrasound transducer arrays. (23 August 2000).
- Hand, J. W. & Gavrilov, L. R. (2002a). US patent 6488630 (03 December 2002) Array of quasi-randomly distributed ultrasound transducers.
- Hand, J. W. & Gavrilov, L. R. (2002b). Chinese patent CN 1340184 granted 16.08.2002. Ultrasound transducer arrays.
- Hand, J. W. & Gavrilov, L. R. (2002c). Hong Kong patent HK 1045015 granted 11.09.2002. Ultrasound transducer arrays.
- Hand, J. W., Shaw, A., Sathoo, N., Rajagopal, S., Dickinson, R. J. & Gavrilov, L. R. (2009). A random phased array device for delivery of high intensity focused ultrasound. *Phys. Med. Biol.*, 54, 5675-5693.
- Held, R. T., Zderic, V., Nguyen, T. N. & Vaezy, S. (2006). Annular phased-array high-intensity focused ultrasound device for image-guided therapy of uterine fibroids. *IEEE Trans. Ultras. Ferroelectr. Freq. Ctrl.* 53, 2, 335-348.
- Hertzberg, Y., Naor, O., Volovick, A. & Shoham, S. (2010a). Towards multifocal ultrasonic neural stimulation: pattern generation algorithms. *J. Neural Eng.*, 7, 5, 056002.
- Hertzberg, Y., Volovick, A., Zur, Y., Medan, Y., Vitek, S. & Navon, G. (2010b). Ultrasound focusing using magnetic resonance acoustic radiation force imaging: application to ultrasound transcranial therapy. *Med. Phys.* 37, 2934.
- Hill, C. R. & ter Haar, G. R. (1995). Review article: High intensity focused ultrasound - potential for cancer treatment. *Br. J. Radiology*. 68, 1296-1303.
- Hill, C. R., Bamber, J. C. & ter Haar, Gail R. (Editors). (2005). *Physical Principles of Medical Ultrasonics*. Chichester; Hoboken, NJ: John Wiley & Sons, 528 pp.
- Hindley, J., Gedroyc, W. M., Regan, L., Stewart, E., Tempny, C., Hynynen, K., McDannold, N., Inbar, Y., Itzchak, Y., Rabinovici, J., Kim, H. S., Geschwind, J. F., Hesley, G., Gostout, B., Ehrenstein, T., Hengst, S., Sklair-Levy, M., Shushan, A. & Jolesz, F. (2004). MRI guidance of focused ultrasound therapy of uterine fibroids: early results. *Am J Roentgenol*. 183(6), 1713-1719.
- Hölscher T., Raman R., Fisher D. J., Ahadi G., Zadicario E. & Voie A. (2013). Effects of varying duty cycle and pulse width on high-intensity focused ultrasound (HIFU)-induced transcranial thrombolysis. *Journal of Therapeutic Ultrasound* 1, 18.
- Hoshi, T. (2012). Handwriting transmission system using noncontact tactile display. *IEEE Haptics Symposium 2012, 4-7 March, Vancouver, BC, Canada*, 399-401.
- Hoshi, T., Iwamoto, T. & Shinoda, H. (2009). Non-contact tactile sensation synthesized by ultrasound transducers. In: *Proceedings of the World Haptics Conference*, 256–260.
- Hoshi, T., Takahashi, M.; Iwamoto, T. & Shinoda, H. (2010). Noncontact tactile display based on radiation pressure of airborne ultrasound, *IEEE Transactions on Haptics*, 3, 3, 155-165.

- Hurwitz, M.D., Ghanouni, P., Kanaev, S.V., Iozeffi, D., Gianfelice, D., Fennessy F.M., Kuten, A., Meyer J.E., LeBlang, S.D., Roberts, A., Choi, J., Lerner, J.M., Napoli, A., Turkevich, V.G., Inbar, Y., Tempany, C.M.C. @ Pfeffer, R.M. (2014) Magnetic resonance-guided focused ultrasound for patients with painful bone metastases: Phase II trial results. *JNCI J Natl. Cancer Inst.* 106, 5, 1-9; dju082 doi:10.1093/jnci/dju082.
- Hutchinson, E. B., Buchanan, M. T. & Hynynen, K. (1996). Design and optimization of an aperiodic ultrasound phased array for intracavitary prostate thermal therapies. *Med. Phys.* 23, 5, 767-776.
- Hutchinson, E. B. & Hynynen, K. (1996). Intracavitary ultrasound phased array for noninvasive prostate surgery. *IEEE Trans. Ultras. Ferroelec. Freq. Ctrl.* 43, 6, 1032-1042.
- Hutchinson, E. B. & Hynynen, K. (1998). Intracavitary ultrasound phased arrays for prostate thermal therapies: MRI compatibility and in vivo testing. *Medical Physics.* 25, 12, 2392-2399.
- Hynynen, K. (1991). The threshold for thermally significant cavitation in dog's thigh muscle *in vivo*. *Ultrasound in Med. and Biol.* 17, 2, 157-169.
- Hynynen, K., Dennie, J., Zimmer, J. E., Simmons, W., He, D., Marcus, F. & Aguirre, M. (1997). Cylindrical ultrasound transducers for cardiac catheter ablation. *IEEE Trans. Biomed. Eng.* 44, 144–151.
- Hynynen, K., Chung, A., Fjield, T., Buchanan, M., Daum, D., Colucci, V., Lopath, P. & Jolesz, F. A. (1996). Feasibility of using ultrasound phased arrays for MRI monitored noninvasive surgery. *IEEE Trans. Ultrason. Ferroelec. Freq. Contr.* 43, 6, 1043-1053.
- Hynynen, K., Clement, G. T., McDannold, N., Vykhodtseva, N., King, R., White, J., Vitek, S. & Jolesz, F. A. (2004). 500-Element ultrasound phased array system for noninvasive focal surgery of the brain: a preliminary rabbit study with ex vivo human skulls. *Magn. Reson. Med.* July, 52, 1, 100–107.
- Hynynen, K. & Jolesz F. A. (1998). Demonstration of potential noninvasive ultrasound brain therapy through an intact skull. *Ultrasound in Med. and Biol.* 24, 275-83.
- Hynynen, K., McDannold, N., Clement, G., Jolesz, F.A., Zadicario, E., Killiany, R. Moore, T. & Rosen D. (2006). Pre-clinical testing of a phased array ultrasound system for MRI-guided noninvasive surgery of the brain—A primate study. *European Journal of Radiology.* 59, 149–156.
- Hynynen, K. & Sun, J. (1999). Transskull ultrasound therapy: The feasibility of using image derived skull thickness information to correct the phase distortion. *IEEE Trans. Ultrason. Ferroelectr. Freq. Control.* 46, 3, 752–755.
- Hynynen, K. & Yin, J. (2009). Lateral mode coupling to reduce the electrical impedance of small elements required for high power ultrasound therapy phased array. *IEEE Trans. Ultrason. Ferroelectr. Freq. Control.* 56, 3, 564.
- Ibbini, M. S. & Cain, C.A. (1990). The concentric ring array for ultrasound hyperthermia: combined mechanical and electrical scanning. *Int. J. Hypertherm.* 6, 401-419.
- Ibbini, M. S., Ebbini, E. S. & Cain, C. A. (1990). N x N square-element ultrasound phased array applicator: simulated temperature distributions associated with directly synthesized heating patterns. *IEEE Trans. Ultrasonics Ferroelectr. Freq. Control.* 37, 491-500.
- Illing, R. & Emberton, M. (2006). Sonablate<sup>®</sup>-500: transrectal high-intensity focused ultrasound for the treatment of prostate cancer. *Expert Rev. Med. Devices* 3, 6, 717–729.
- Ilyin, S. A., Yuldashev, P. V., Bobkova, S. M., Gavrilov, L. R. & Khokhlova, V. A. (2011). The role of nonlinear propagation effects in ablation of soft tissue behind the rib cage using a HIFU phased array. *Proceedings of the XXIV Session of the Russian Acoustical Society, V. 3, 569-571, published at <http://ras.akin.ru>.*
- Ilyin, S. A., Yuldashev, P. V., Khokhlova, V. A., Gavrilov, L. R. & Sapozhnikov, O. A. (2012). Evaluation of quality of acoustic fields produced by multi-element phased arrays used in ultrasonic surgery during the focus steering. In: *Proceedings of the XXV Session of the*

- Russian Acoustical Society Session of the Scientific Council on Acoustics of the Russian Academy of Sciences (Taganrog, September 17-20, 2012), published at <http://ras.akin.ru>.*
- Ishida, K., Kubota, J., Mitake, T., Carlson, R. F., Seip, R., Sanghvi, N. T., Azuma, T., Sasaki, K., Kawabata, K. & Umemura S. -I. (2003). Development and animal experiment of variable focusing HIFU system for prostate cancer treatment. *3-rd International Symposium on Therapeutic Ultrasound*.
- Iwamoto, T., Maeda, T. & Shinoda, H. (2001). Focused ultrasound for tactile feeling display. In *Proceedings of the 2001 International Conference on Artificial Reality and Telexistence*, 121–126.
- Iwamoto, T. & Shinoda, H. (2005). Ultrasound tactile display for stress field reproduction - Examination of non-vibratory tactile apparent movement. *World Haptics. Italy, March 2005*, 220-228.
- Iwamoto, T. & Shinoda, H. (2006). Two-dimensional scanning tactile display using ultrasound radiation pressure. In *Proceedings of the Symposium on Haptic Interfaces for Virtual Environment and Teleoperator Systems (IEEE Haptics Symposium, 2006)*, 57–61.
- Iwamoto, T., Tatzono, M. & Shinoda, H. (2008). Non-contact method for producing tactile sensation using airborne ultrasound. In M. Ferre (Ed.), *Haptics: Perception, Devices and Scenarios: 6<sup>th</sup> International Conference, Eurohaptics 2008 Proceedings*, 504-513, Springer.
- Izumi, M., Ikeuchi, M., Kawasaki, M., Ushida, T., Morio, K., Namba, H., Graven-Nielsen, T., Ogawa, Y. & Tani, T. (2013). MR-guided focused ultrasound for the novel and innovative management of osteoarthritic knee pain. *BMC Musculoskeletal Disorders*, 14, 267.
- Jeanmonod, D., Werner, B., Morel, A., Michels, L., Zadicario, E., Schiff, G. & Martin, E. (2012). Transcranial magnetic resonance imaging–guided focused ultrasound: noninvasive central lateral thalamotomy for chronic neuropathic pain. *Neurosurg. Focus*. 32, 1, E1.
- Ji, X., Shen, G., Bai, J., Li, D., Yu, Y., Qiao, S. & Chen, Y. (2011). Multi-element ultrasound phased array applicator for the ablation of deep-seated tissue. *J. Shanghai Jiaotong Univ. (Sci.)*, 16, 1, 55-60.
- Jolesz, F. A. & McDannold, N. J. (2014). Magnetic resonance–guided focused ultrasound. A new technology for clinical neurosciences. *Neurol. Clin.* 32, 1, 253–269.
- Ju, K. -C., Chen, Y. -Y., Lin, W. -L. & Kuo, T. -S. (2003). One-dimensional phased array with mechanical motion for conformal ultrasound hyperthermia. *Phys. Med. Biol.* 48, 167–182.
- Khokhlova, V. A., Bobkova, S. M. & Gavrilov, L. R. (2010). Focus splitting associated with propagation of focused ultrasound through the rib cage. *Acoustical Physics*. 56, 5, 665–674.
- Khokhlova, V. A., Shmeleva, S. M., Gavrilov, L. R., Martin, E., Sathoo, N. & Shaw A. (2013). Infrared mapping of ultrasound fields generated by medical transducers: Feasibility of determining absolute intensity levels. *Journ. Acoust. Sos. America*. 134, 2, Pt. 2, 1586-1597.
- Kim, Y., Wan, T. -Y., Xu, Z. & Cain, C. A. (2011). Lesion generation through ribs using histotripsy therapy without aberration correction. *IEEE Trans. Ultras. Ferroelectr. Freq. Ctrl.* 58, 11, 2334-2343.
- Kluiwstra, J. -U. A., Tokano, T., Davis J., Strickberger, S. A. & Cain C. A. (1997). Real time image guided high intensity focused ultrasound for myocardial ablation. *In vivo* study. In *Proc. IEEE Ultrason. Symp.* 1327–1330.
- Kluiwstra, J. -U. A., Zhang, Y., Vanbaren, P., Strickberger S. A., Ebbini E. S. & Cain C. A. (1995). Ultrasound phased arrays for myocardial ablation: Initial studies. In *Proc. IEEE Ultrason. Symp.* 1605–1608.
- Kreider, W., Yuldashev, P. V., Sapozhnikov, O. A., Farr, N., Partanen, A., Bailey, M. R. & Khokhlova, V. A. (2013). Characterization of a multi-element clinical HIFU system using acoustic holography and nonlinear modeling. *IEEE Transactions on Ultrasonics, Ferroelectrics, and Frequency Control*. 60, 8, 1683-1698.

- Lalonde, R. J., Worthington, A. & Hunt, J. W. (1991). Field conjugate acoustic lenses for ultrasound hyperthermia. *1991 Ultrasonics Symposium*. 1339-1342.
- Lalonde, R. J., Worthington A. & Hunt J. W. (1993). Field conjugate lenses for ultrasound hyperthermia. *IEEE Trans. Ultras. Ferroelec. Freq. Ctrl.* 40, 592-602.
- Lee, H., Francischelli, D. & Smith, N. B. (2010). Design of focused ultrasound array for non-invasive transesophageal cardiac ablation. *The Open Medical Devices Journal*. 2, 51-60.
- Lindner, U., Ghai, S., Spensieri, P., Hlasny, E., Van der Kwast, T. H., McCluskey, S. A., Haider, M. A., Kucharczyk, W. & Trachtenberg, J. (2012). *Can. Urol. Assoc. J. December*; 6, 6, E283–E286.
- Li, F., Gong, X., Hu, K., Li, C. & Wang, Z. (2006). Effect of ribs in HIFU beam path on formation of coagulative necrosis in goat liver. *Therapeutic Ultrasound: 5th International Symposium on Therapeutic Ultrasound*. 477–480.
- Li, J. -L., Liu, X. -Zh., Zhang, D. & Gong X. -F. (2007). Influence of ribs on nonlinear sound field of therapeutic ultrasound. *Ultrasound in Med. and Biol.* 33, 9, 1413–1420.
- Lipsman, N., Schwartz, M. L., Huang, Y., Lee, L., Sankar, T., Chapman, M., Hynynen, K., & Lozano, A. M. (2013). MR-guided focused ultrasound thalamotomy for essential tremor a proof-of-concept study. *The Lancet Neurology*, 12, 5, 462 – 468.
- Liu, H. -Li, Chang, H., Chen, W. -S., Shih, T. -C., Hsiao, J. -K. & Lin W. -L. (2007). Feasibility of transrib focused ultrasound thermal ablation for liver tumors using a spherically curved 2D array: A numerical study. *Med. Phys.* 34, 9, 3436–3448.
- Liu, H. -L., Chen, H. -W., Kuo, Z. -H. & Huang, W. -C. (2008). Design and experimental evaluations of a low-frequency hemispherical ultrasound phased-array system for transcranial blood–brain barrier disruption. *IEEE Transactions on Biomedical Engineering*. 55, 10, 2407-2416.
- Lu, M., Wan, M., Xu, F., Wang, X. & Zhong, H. (2005). Focused beam control for ultrasound surgery with spherical-section phased array: Sound field calculation and genetic optimization algorithm. *IEEE Trans. Ultrasonics Ferroelectr. Freq. Control.* 52, 8, 1270-1290.
- Lu, M., Wan, M., Xu, F., Wang, X. & Zhong, H. (2006). Design and experiment of 256-element ultrasound phased array for noninvasive focused ultrasound surgery. *Ultrasonics*. 44, Suppl. 1, e325-e330.
- Lu, M., Wang, X., Wan, M., Feng, Y., Xu, F., Zhong, H. & Tan, J. (2008). Image-guided 256-element phased-array focused ultrasound surgery. *IEEE Engineering in Medicine and Biology Magazine*. Sept/Oct., 84-90.
- Marsac, L., Chauvet, D., Larrat, B., Pernot, M., Robert, B., Fink, M., Boch, A. L., Aubry, J. F. & Tanter M. (2012). MR-guided adaptive focusing of therapeutic ultrasound beams in the human head. *Medical Physics*. 39, 2, 1141-1150.
- Marquet, F., Aubry, J. F., Pernot, M., Fink, M. & Tanter M. (2011). Optimal transcostal high-intensity focused ultrasound with combined real-time 3D movement tracking and correction *Phys. Med. Biol.* 56, 7061–7080.
- Marquet, F., Boch, A. -L., Pernot, M., Montaldo, G., Seihean, D., Fink, M., Tanter, M. & Aubry, J. -F. (2013). Non-invasive ultrasonic surgery of the brain in non-human primates. *J. Acoust. Soc. Am.* 134, 2, Pt. 2, 1632-1639.
- Martin, E., Jeanmonod, D., Morel, A., Zadicario, E. & Werner, B. (2009). High-Intensity Focused Ultrasound for noninvasive functional neurosurgery. *Annals of Neurology*. 66, 6, 858-861.
- McDannold, N., Clement, G., Black, P. Jolesz, F. & Hynynen, K. (2010). Transcranial MRI-guided focused ultrasound surgery of brain tumors: Initial findings in three patients. *Neurosurgery*, 66, 2, 323–332.
- McDannold, N. & Maier, S. E. (2008). Magnetic resonance acoustic radiation force imaging. *Med. Phys.* 35, 3748.

- McDannold, N., Tempny, C., Jolesz, F. & Hynynen, K. (2006). Evaluation of referenceless thermometry in MRI-guided focused ultrasound surgery of uterine fibroids. *Therapeutic ultrasound. 5-th International Symposium on Therapeutic Ultrasound, Boston, USA*. G. T. Clement, N. J. McDannold, K. Hynynen (Eds.). American Institute of Physics. 156-160.
- McGough, R. J., Cindric, D. & Samulski, T. V. (2001). Shape calibration of a conformal ultrasound therapy array. *IEEE Trans. Ultrasonics Ferroelectr. Freq. Control*. 48, 2, 494-505.
- McGough, R. J., Kessler, M. L., Ebbini, E. S. & Cain, C. A. (1996). Treatment planning for hyperthermia with ultrasound phased arrays. *IEEE Trans. Ultras. Ferroelec. Freq. Ctrl*. 43, 6, 1074-1084.
- Medel, R., Monteith, S. J., Elias, W. J., Eames, M., Snell, J., Sheehan, J. P., Wintermark, M., Jolesz, F. A. & Kassell, N. F. (2012). Magnetic resonance-guided focused ultrasound surgery: Part 2: A review of current and future applications. *Neurosurgery*. 71, 4, 755-63.
- Melodelima, D., Lafon, C., Prat, F., Theillère, Y., Arefiev, A., & Cathignol, D. (2003). Transesophageal ultrasound applicator for sector-based thermal ablation: First *in vivo* experiments. *Ultrasound in Med. and Biol.* 29, 2, 285–291.
- Melodelima, D., Prat, F., Birer, A., Theillère, Y. & Cathignol, D. (2004). Comparison of two methods of treatment for intraluminal thermal ablation using an ultrasound cylindrical phased array. *Ultrasonics*. 42, 937–942.
- Menz, M. D., Oralkan, O., Khuri-Yakub, P. T., & Baccus, S. A. (2013). Precise neural stimulation in the retina using focused ultrasound. *The Journal of Neuroscience*, 33, 10, 4550–4560.
- Monteith, S. J., Harnof, S., Medel, R., Popp, B., Wintermark, M., Lopes, M. B., Kassell, N. F., Elias, W. J., Snell, J., Eames, M., Zadicario, E., Moldovan, K. & Sheehan, J. (2013a). Minimally invasive treatment of intracerebral hemorrhage with magnetic resonance-guided focused ultrasound. Laboratory investigation. *J. Neurosurg*. 118, 5, 1035–1045.
- Monteith, S., Sheehan, J., Medel, R., Wintermark, W., Eames, M., Snell, J., Kassell, N. F. & Elias, W. J. (2013b). Potential intracranial applications of magnetic resonance-guided focused ultrasound surgery. A review. *J. Neurosurg*. 118, 215–221.
- Monteith, S., Kassell, N. F., Goren, O. & Harnof, S. (2013c). Transcranial MR-guided focused ultrasound sonothrombolysis in the treatment of intracerebral hemorrhage. *Neurosurg Focus*. 34, 5, E14, 1-7.
- Monteith, S., Medel, R., Kassell, N. F., Wintermark, W., Eames M., Snell J., Zadicario, E., Grinfeld J., Sheehan J. P. & Elias W. J. (2013d). Transcranial magnetic resonance-guided focused ultrasound surgery for trigeminal neuralgia: a cadaveric and laboratory feasibility study. *Journal of Neurosurgery*, 118, 2, 319-328.
- Naor, O., Hertzberg, Y., Zemel, E., Kimmel, E. & Shoham, S. (2012). Towards multifocal ultrasonic neural stimulation II: Design considerations for an acoustic retinal prosthesis. *J. Neural Eng.*, 9, 026006.
- Napoli, A., Anzidei, M., De Nunzio, C., Cartocci, G., Panebianco, V., De Dominicis, C., Catalano, C., Petrucci, F. & Leonardo, C. (2013a). Real-time magnetic resonance-guided High-Intensity Focused Ultrasound focal therapy for localised prostate cancer: Preliminary experience. *European Urology*, 63, 2, 395-398.
- Napoli, A., Anzidei, M., Marincola, B. C, Brachetti, G., Ciolina, F., Cartocci, G., Marsecano, C., Zaccagna, F., Marchetti, L., Cortesi, E. & Catalano, C. (2013b). Primary pain palliation and local tumor control in bone metastases treated with magnetic resonance-guided focused ultrasound. *Invest Radiol*. 48, 6, 351-8.
- NCRP Report № 74. (1983). *Biological effects of ultrasound: mechanisms and clinical implications*. Prepared by Committee headed by W. Nyborg. Bethesda, MD: National Center for Radiological Protection. 266 pp.

- Ocheltree, K. B., Benkeser, P. J., Frizzell, L. A. & Cain, C. A. (1984). An ultrasonic phased array applicator for hyperthermia. *IEEE Trans. Sonics Ultrasonics*. 31, 526-31.
- Ocheltree K. & Frizzell L. (1989). Sound field calculations for rectangular sources. *IEEE Trans. Ultrason. Ferroelec. Freq. Ctrl.* 36, 242-248.
- O'Neil, H. T. (1949). Theory of Focusing Radiators. *J. Acoust. Soc. America*. 21, 5, 516-526.
- Pernot, M., Aubry, J. -F., Tanter, M., Thomas, J. -L., & Fink, M. (2003). High power transcranial beam steering for ultrasonic brain therapy. *Phys. Med. Biol.*, 48, 16, 2577–2589.
- Pernot, M., Aubry, J. -F., Tanter, M., Boch, A. L., Kujas, M. & Fink M. (2004a). Ultrasonic transcranial brain therapy: First *in vivo* clinical investigation on 22 sheep using adaptive focusing. *IEEE Ultrasonics Symposium*. 1013-1016.
- Pernot, M., Aubry, J. -F., Tanter, M., Boch, A. L., Kujas, M. & Fink M. (2005a). Adaptive focusing for ultrasonic transcranial brain therapy: First *in vivo* investigation on 22 sheep. *4-th International Symposium on Therapeutic Ultrasound, Kyoto, Japan*. Edited by G. R. ter Haar, I. Rivens. Mewill, New York: American Institute of Physics. 174-177.
- Pernot, M., Aubry, J. -F., Tanter, M. & Fink, M. (2004b). Prediction of the skull overheating during high intensity focused ultrasound transcranial brain therapy. *2004 IEEE Ultrasonics Symposium*. 1005-1008.
- Pernot, M., Aubry, J. -F., Tanter, M. & Fink, M. (2005b). Predicting and preventing skull overheating in non invasive brain HIFU treatment protocols. *4-th International Symposium on Therapeutic Ultrasound, Kyoto, Japan*. Edited by G.R. ter Haar, I. Rivens. Mewill, New York: American Institute of Physics. 147-150.
- Pernot, M., Aubry, J. -F., Tanter M., Marquet F., Montaldo G., Boch A. -L., Kujas M., Seilhean D. & Fink M. (2007). High power phased array prototype for clinical High Intensity Focused Ultrasound: Applications to transcostal and transcranial therapy. *Proc 29th IEEE EMBS Annual International Conference*. 234-237.
- Pinton, G., Aubry, J. -F., and Tanter, M. (2012). Direct phase projection and transcranial focusing of ultrasound for brain therapy. *IEEE Trans. Ultrason. Ferroelectr. Freq. Control*. 59, 1149–1159.
- Pulkkinen, A., Huang, Y., Song, J. & Hynynen, K. (2011). Simulations and measurements of transcranial low-frequency ultrasound therapy: skull-base heating and effective area of treatment. *Phys. Med. Biol.* 56, 15, 4661–4683.
- Qiao, S., Shen, G., Bai, J. & Chen Y. (2013). Transcostal high-intensity focused ultrasound treatment using phased array with geometric correction. *J. Acoust. Soc. Am.* 134 (2), Pt. 2, 1503-1514.
- Quesson, B., Merle, M., Kholer, M. O., Mougnot, C., Roujol, S., de Senneville, B. D. & Moonen, C. T. (2010). A method for MRI guidance of intercostal high intensity focused ultrasound ablation in the liver. *Med. Phys.* 37, 2533–40.
- Quinn, S. D., Vedelago, J., Regan, L. & Gedroyc, W. M. (2013). Safety and treatment volumes achieved following new developments of the magnetic resonance-guided focused ultrasound system in the treatment of uterine fibroids: a cohort study. *Journal of Therapeutic Ultrasound*. 1, 20.
- Rabinovici, J., Inbar, Y., Revel, A., Zalel, Y., Gomori, J. M., Itzhak, Y., Schiff, E. & Yagel, S. (2007). Clinical improvement and shrinkage of uterine fibroids after thermal ablation by magnetic resonance-guided focused ultrasound surgery. *Ultrasound Obstet. Gynecol.* 30, 771–777.
- Radar Handbook. (1970). Ed. by M. I. Skolnik. New York: McGraw-Hill.
- Raju, B. I., Hall, C. S. & Seip R. (2011). Ultrasound therapy transducers with space-filling non-periodic arrays. *IEEE Trans. Ultrason. Ferroelectr. Freq. Contr.* 58, 5, 944-954.
- Reverdy, F., Iturralde, G. & Dominguez N. (2012). Advanced ultrasonic 2D phased-array probes. *18th World Conference on Nondestructive Testing*, 16-20 April 2012, Durban, South A. 1-10.

- Rivens, I. H., Clarke, R. L. & ter Haar, G.R. (1996). Design of focused ultrasound surgery transducers. *IEEE Trans. Ultrason. Ferroelectr. Freq. Ctrl.* 43, 6, 1023-1031.
- Saleh, K. Y. & Smith, N. B. (2004). Two-dimensional ultrasound phased array design for tissue ablation for treatment of benign prostatic hyperplasia. *Int. J. Hyperthermia.* 20, 1, 7–31.
- Salgaonkar, V. A., Prakash, P., Plata, J., Holbrook, A., Rieke, V., Kurhanewicz, J., Hsu, I. -C. & Diederich, C. J. (2013). Targeted hyperthermia in prostate with an MR-guided endorectal ultrasound phased array: patient specific modeling and preliminary experiments. *Proc. SPIE 8584, Energy-based Treatment of Tissue and Assessment VII*, 85840U (February 26, 2013).
- Salomir, R., Palussiere, J., Vimeux, F. C., de Zwart, J. A., Quesson, B., Gauchet, M., Lelong, P., Pergrale, J., Grenier, N. & Moonen C. T. W. (2000). Local hyperthermia with MR-guided focused ultrasound: spiral trajectory of the focal point optimized for temperature uniformity in the target region. *J. Magn. Reson. Imaging.* 12, 571–583.
- Sanghvi, N. T., Foster, R. S., Bihrl, R., Casey, R., Uchida, T., Phillips, M. H., Syrus, J., Zaitsev, A. V., Marich, K. W. & Fry F. J. (1999). Noninvasive surgery of prostate tissue by high intensity focused ultrasound: an updated report. *Eur. J. Ultrasound.* 9, 19–29.
- Sapareto, S. A. & Dewey, W. C. (1984). Thermal dose determination in cancer therapy. *Int. J. Radiat. Oncol. Biol. Phys.*, 10, 787– 800.
- Seip, R., Chen, W., Carlson, R., Frizzell, L., Warren, G., Smith, N., Saleh, K., Gerber, G., Shung, K., Guo, H. & Sanghvi, N. T. (2005). Annular and cylindrical phased array geometries for transrectal high-intensity focused ultrasound (HIFU) using PZT and piezocomposite materials. *4-th International Symposium on Therapeutic Ultrasound, Kyoto, Japan*. Edited by G. R. ter Haar, I. Rivens. Mewill, New York: American Institute of Physics. 229-232.
- Sharifi, H. & Soltanian-Zadeh, H. (2001). New 2D ultrasound phased-array design for hyperthermia cancer therapy. *Proceedings of SPIE Medical Imaging 2001: Ultrasonic Imaging and Signal Processing Conference*, San Diego, CA, 17-22.
- Shaw A. (2008). A buoyancy method for the measurement of total ultrasound power generated by HIFU transducers. *Ultrasound Med Biol.* 34, 8, 1327-1342.
- Shaw, A., Bobkova, S. M., Khokhlova, V. A., Gavrilov, L. R. & Hand, J. W. (2011). Calibration of HIFU intensity fields measured using an infra-red camera. *Proceedings of the Conference AMUM 2010 Advanced Metrology for Ultrasound in Medicine, National Physical Laboratory, Teddington, UK*, 12-14 May 2010, *Journal of Physics: Conference series.* 279, 012019, 1-6. doi:10.1088/1742-6596/279/1/012019.
- Shinoda, H. (2010). Tactile interaction with 3D images. *IDW'10 (International Display Workshop)*, 1743-1746.
- Shmeleva, S. M., Khokhlova, V. A., Gavrilov, L. R., Martin, E., Sathoo, N. & Shaw, A. (2013). Feasibility of using infra-red system for absolute calibration of high intensity focused ultrasound fields. *J. Acoust. Soc. Am.* 134, 5, Pt. 2, 4154.
- Sinkus, R., Siegmann, K., Pernot, M., Athanasiou, A. & Fink M. (2008). Potential of MRI and ultrasound radiation force in elastography: Applications to diagnosis and therapy. *Proc. IEEE* 96, 490.
- Skolnik, M. I. (1962). *Introduction to Radar Systems*. New York, McGraw- Hill.
- Smith, N. B., Buchanan, M. T. & Hynynen, K. (1999). Transrectal ultrasound applicator for prostate heating monitored using MRI thermometry. *Int. Journ. of Radiat. Oncol. Biol. Physics.* 43, 1, 217-225.
- Smith, N. B. & Hynynen K. (1998). The feasibility of using focused ultrasound for transmyocardial revascularization. *Ultrasound in Med. and Biol.* 24, 7, 1045–1054.
- Smith, N. B., Merrilees, N. K., Dahleh, M. & Hynynen, K. (2001). Control system for an MRI compatible intracavitary ultrasound array for thermal treatment of prostate disease. *Int. J. Hyperthermia.* 17, 3, 271-282.

- Sokka, S. D. & Hynynen, K. H. (2000). The feasibility of MRI-guided whole prostate ablation with a linear aperiodic intracavitary ultrasound phased array. *Phys. Med. Biol.* *45*, 3373–3383.
- Song, J. & Hynynen, K. (2010). Feasibility of using lateral mode coupling method for a large scale ultrasound phased array for noninvasive transcranial therapy. *IEEE Trans Biomed Eng.* *57*, *1*, 124–133.
- Stephens, D.N., Kruse, D.E., Qin, S. & Ferrara K.W. (2011). Design aspects of focal beams from high-intensity arrays. *IEEE Transactions on Ultrasonics, Ferroelectrics, and Frequency Control*, *58*, *8*, 1590-1602.
- Stewart, E. A., Gostout, B., Rabinovici, J., Kim, H. S., Regan, L. & Tempny, C. M. (2007). Sustained relief of leiomyoma symptoms by using focused ultrasound surgery. *Obstet. Gynecol.* *110*, *2*, pt. 1, 279–287.
- Strickberger, S. A., Tokano, T., Kluiwstra, J. U. A, Morady, F. & Cain, C. (1999). Extracardiac ablation of the canine atrioventricular junction by use of high-intensity focused ultrasound. *Circulation.* *100*, *2*, 203-208.
- Sun, J. & Hynynen, K. (1998). Focusing of therapeutic ultrasound through a human skull: A numerical study. *J. Acoust. Soc. Am.* *104*, *3*, Pt 1, 1705–1715.
- Sun, J. & Hynynen, K. (1999). The potential of transskull ultrasound therapy and surgery using the maximum available skull surface area. *J. Acoust. Soc. Am.* *104*, *4*, 2519–2527.
- Tan, J. S., Frizzell, L. A., Sanghvi, N. T., Seip, R., Wu, J. S. & Kouzmanoff J. T. (2000). Design of focused ultrasound phased array for prostate treatment. *Proc. IEEE Ultrason. Symp.* 1247–1251.
- Tan, J. S., Frizzell, L. A., Sanghvi, N. T., Wu, J. S., Seip, R. & Kouzmanoff, J. T. (2001). Ultrasound phased array for prostate treatment. *J. Acoust. Soc. Am.* *109*, *6*, 3055-3064.
- Tan, N. & Raman S. S. (2013). Magnetic resonance-guided High-Intensity Focused Ultrasound: gynecological applications. In D. E. Dupuy et al. (Eds.), *Image-Guided Cancer Therapy*, New York: Springer Science+Business Media. 789-808.
- Tanter, M., Pernot, M., Aubry, J. -F., Montaldo, G., Marquet, F. & Fink, M. (2007). Compensating for bone interfaces and respiratory motion in high-intensity focused ultrasound. *Int. J. Hyperthermia.* *23*, *2*, 141–151.
- Tanter, M., Thomas, J. -L. & Fink, M. A. (1998). Focusing and steering through absorbing and aberrating layers: application to ultrasonic propagation through the skull. *J. Acoust. Soc. Am.* *103*, 2403–2410.
- Tanter, M., Thomas, J. -L. & Fink, M. A. (2000). Time reversal and the inverse filter. *J. Acoust. Soc. Am.* *108*, *1*, 223–234.
- Tavakkoli, J., Birer, A., Arefiev, A., Prat, F., Chapelon, J. -Y. & Cathignol, D. (1997). A piezocomposite shock wave generator with electronic focusing capability: application for producing cavitation-induced lesions in rabbit liver. *Ultrasound in Med. and Biol.* *23*, *1*, 107–115.
- Thomas, J. -L. & Fink M. A. (1996). Ultrasonic beam focusing through tissue inhomogeneities with a time reversal mirror: application to transskull therapy. *IEEE Trans. Ultrason. Ferroelectr. Freq. Contr.* *43*, 1122–1129.
- Trumm, C. G., Stahl, R., Clevert, D. A., Herzog, P., Mindjuk, I., Kornprobst, S., Schwarz, C., Hoffmann, R. T., Reiser, M. F. & Matzko, M. (2013). Magnetic resonance imaging-guided focused ultrasound treatment of symptomatic uterine fibroids: Impact of technology advancement on ablation volumes in 115 Patients. *Investigative Radiology.* *48*, *6*, 359-365. doi: 10.1097/RLI.0b013e3182806904.
- Umemura, S. & Cain, C. A. (1989). The sector-vortex phased array: acoustic field synthesis for hyperthermia. *IEEE Trans. Ultrasonics Ferroelectr. Freq. Control.* *36*, *2*, 249-257.
- Umemura, S. & Cain, C. A. (1992). Acoustical evaluation of a prototype sector-vortex phased array: applicator. *IEEE Trans. Ultrasonics Ferroelectr. Freq. Control.* *39*, *1*, 32-38.

- Umemura, S. -I., Holmes, K. R., Frizzell, L. A. & Cain C. A. (1992). Insonation of fixed porcine kidney by a prototype sector-vortex-phased array applicator. *Int. J. Hypertherm.* 831-842.
- Umemura, S., Sasaki, K., Kawabata, K., Azuma, T. & Sanghvi N. T. (1999). Coagulation of swine liver and canine prostate with a prototype split-focus transducer. *1999 IEEE Ultrasonics Symposium.*
- Wan H., VanBaren P., Ebbini E. S. & Cain C. A. (1996). Ultrasound surgery: comparison of strategies using phased array systems. *IEEE Trans. Ultras. Ferroelec. Freq. Ctrl.* 43, 1085-1097.
- Wang, H., Ebbini, E. & Cain, C. A. (1991). Effect of phase errors on field patterns generated by an ultrasound phased-array hyperthermia applicator. *IEEE Trans. Ultras. Ferroelectr. Freq. Ctrl.* 38, 5, 521-531.
- Werner, J., Park, E. -U., Lee, H., Francischelli, D. & Smith, N. B. (2010). Feasibility of *in vivo* transesophageal cardiac ablation using a phased ultrasound array. *Ultrasound in Med. and Biol.* 36, 5, 752-760.
- White, J., Clement, G. T. & Hynynen, K. (2005). Transcranial ultrasound focus reconstruction with phase and amplitude correction. *Trans. Ultrason. Ferroelectr. Freq. Control.* 52, 9, 1518-1522.
- White, J., Clement, G. T. & Hynynen, K. (2006a). Longitudinal and shear mode ultrasound propagation in human skull bone. *Ultrasound in Med. and Biol.* 32, 7, 1085-1096.
- Wintermark, M., Druzgal, J., Huss, D. S., Khaled, M. A., Monteith, S., Raghavan, P., Huerta, T., Schweickert, L. C., Burkholder, B., Loomba, J. J., Zadicario, E., Qiao, Y., Shah, B., Snell, J., Eames, M., Frysinger, R., Kassell, N. & Elias W. J. (2013). Imaging findings in MR imaging-guided focused ultrasound treatment for patients with essential tremor. *Am. J. Neuroradiol.* Originally published online on December 26, 2013.
- Wong, S. H., Scott, G. C., Conolly, S. M., Narayan, G. & Liang, D. H. (2006). Feasibility of noncontact intracardiac ultrasound ablation and imaging catheter for treatment of atrial fibrillation. *IEEE Trans. Ultras. Ferroelec. Freq. Ctrl.* 53, 12, 2394-2405.
- Wu, F., Zhi-Biao, W., Wen-Zhi, C., Hui, Z., Jin, B., Jian-Zhong, Z., Ke-Quan, L., Cheng-Bing, J., Fang-Lin, X. & Hai-Bing, S. (2004). Extracorporeal high intensity focused ultrasound ablation in the treatment of patients with large hepatocellular carcinoma. *Ann. Surg. Oncol.* 11, 1061-1069.
- Xu, Z., Ludomirsky, A., Eun, L. Y., Hall, T. L., Tran, B. C., Fowlkes, J. B. & Cain C. A. (2004). Controlled ultrasound tissue erosion. *IEEE Trans. Ultrason. Ferroelect. Freq. Contr.* 51, 6, 726-736.
- Yin, X., Epstein, L. M. & Hynynen K. (2004). Feasibility of noninvasive transesophageal cardiac thermal ablation using an ultrasound phased array. *2004 IEEE Ultrasonics Symposium.* 126-129.
- Yin, X., Epstein, L. M. & Hynynen K. (2006). Noninvasive transesophageal cardiac thermal ablation using a 2-D focused, ultrasound phased array: A simulation study. *IEEE Trans. Ultrason. Ferroelect. Freq. Contr.* 53, 6, 1138-1149.
- Yin, X. & Hynynen, K. (2005). A numerical study of transcranial focused ultrasound beam propagation at low frequency. *Phys. Med. Biol.* 50, 1821-1836.
- Yin, X. & Hynynen, K. (2006). A hemispherical sparse phased array design for low frequency transcranial focused ultrasound applications without skull-specific phase aberration correction. In: *Therapeutic Ultrasound: 5<sup>th</sup> International Symposium on Therapeutic Ultrasound.* G. T. Clement, N. J. McDannold & K. Hynynen (Eds). American Institute of Physics. 261-265.
- Yoon Y. J., Barthe P. G. & P. J. Benkeser. (1990). Variable-focus lens for ultrasound hyperthermia applications. *IEEE 1990 Ultrasonics Symposium Proceedings*, vol. 3 (Cat. No.90CH2938-9). New York: IEEE, 1661-1664.

- Yuldashev, P. V. & Khokhlova, V. A. (2011). Simulation of three-dimensional nonlinear fields of ultrasound therapeutic arrays. *Acoustical Physics*. 57, 3, 334-343.
- Yuldashev, P. V., Shmeleva, S. M., Ilyin, S. A., Sapozhnikov, O. A., Gavrilov, L. R. & Khokhlova V.A. (2013). The role of acoustic nonlinearity in tissue heating behind the rib cage using high intensity focused ultrasound phased array. *Phys. in Med. and Biol.* 58, 2537-2559.
- Zimmer, J. E., Hynynen, K., He, D. S. & Marcus F. (1995). The feasibility of using ultrasound for cardiac ablation. *IEEE Trans. Biomed. Eng.* 42, 9, 891–897.